

COMPARISON BETWEEN AIR DRYING AND STEAM DRYING  
IN A FLUIDIZED BED

by

Ernest F. Faber

Submitted in partial fulfilment of  
the requirements for the degree of  
Doctor of Philosophy  
in the  
Department of Chemical Engineering  
University of Natal

April 1991

### DECLARATION

I herewith declare that the whole thesis, unless specifically indicated to the contrary in the text, is my own original work.

---

Ernest F. Faber

## ACKNOWLEDGEMENTS

I wish to express my sincere gratitude to Prof. M.R. Judd for his encouraging support throughout the course of this work.

I would also like to thank my colleagues from the National Institute for Chemical Engineering Research for the stimulating working atmosphere. In particular I would like to mention Ed Hicks who gave me the necessary time for this study and showed great interest in its progress.

Furthermore I would like to thank Wolfgang Fischer and Peter Schout whose help was greatly appreciated during the experimental stage. David van Vuuren and Peter Knibbe were always available for discussions and suggestions and Mike Heydenrych gave his comments on the economic analysis. Beverlie Davies must be thanked for the professional editing of this thesis.

This work would not have been possible without the financial support of the Foundation for Research Development and the CSIR. It is gratefully acknowledged.

A special thank you goes to my wife Mariana, my children Nicoline, Mariani and Ann-Hélène for their patience during the completion of this thesis.

## TABLE OF CONTENTS

	<u>Page no.</u>
SYNOPSIS	(xx)
1. INTRODUCTION	1
2. SUPERHEATED-STEAM DRYING	3
2.1 Principle of superheated-steam drying	
2.2 Applications of steam drying	7
2.2.1 Kiln dryers	8
2.2.2 Spray dryers	9
2.2.3 Fluidized-bed dryers	10
2.2.4 Pneumatic conveying dryers	11
2.2.5 Impingement jet dryers	12
2.2.6 Other types of dryer	13
2.2.7 Product quality	14
2.3 Theory of drying kinetics in air and in steam	15
2.3.1 Heating-up period	20
2.3.2 Constant drying rate period	20
2.3.2.1 Fundamental mechanisms of drying in air and in steam	20
2.3.2.2 Convective heat transfer	23
2.3.2.3 Evaporation rates	27
2.3.2.4 Inversion temperature	30
2.3.3 Critical moisture content	32
2.3.4 Falling drying rate period	33
2.3.5 Evaporation of droplets	33
2.3.5.1 Droplets of pure water	34
2.3.5.2 Droplets of solutions	37
2.3.6 Drying theories	39
3. EXPERIMENTAL	46
3.1 Physical properties of the drying materials	46
3.2 Experimental equipment for measuring drying-rate curves in fluidized beds	48
3.2.1 Requirements for the drying equipment	48
3.2.2 Choice of a fluidized bed for determining drying rate curves	49
3.2.3 Description of the experimental equipment	50
3.2.4 Experimental procedure for measuring drying rate curves	53
3.2.5 Experimental programme	56
3.2.6 Data acquisition and processing	57

3.3	Experimental equipment for measuring gas-to-solid heat transfer coefficients in fluidized beds	61
3.3.1	Background to the development of the measuring equipment	61
3.3.2	Description of the experimental equipment for measuring heat transfer coefficients in fluidized beds	64
3.4	Experimental equipment for measuring sorption isotherms	65
3.4.1	Background to the development of the measuring equipment	65
3.4.2	Description of the experimental equipment for measuring sorption isotherms in steam	68
4.	DATA INTERPRETATION	74
4.1	Theoretical determination of the inversion temperature in a non-equilibrium system	76
4.1.1	Mathematical model for the determination of the inversion temperature in a non-equilibrium system	77
4.1.2	Explanation for the existence of the inversion temperature in a non-equilibrium system	81
4.2	Theoretical and experimental results for the inversion temperature in an equilibrium system	84
4.2.1	Mathematical model for the inversion temperature in an equilibrium system	85
4.2.2	Experimental results for the inversion temperature in an equilibrium system	86
4.3	Theoretical determination and experimental results of the gas-to-solid heat transfer coefficient in a fluidized bed	92
4.3.1	Theoretical determination of the gas-to-solid heat transfer coefficient in a fluidized bed	92
4.3.2	Experimental results of the gas-to-solid heat transfer coefficient in a fluidized bed	96
4.4	Comparison of the experimental drying rate curves recorded in a fluidized bed in air and in steam	98
4.4.1	Drying rate curves for alumina	98
4.4.2	Drying rate curves for molecular sieve	104

4.5	Development of theory necessary for interpreting data in the falling drying rate period	109
4.5.1	Normalization in a fluidized bed with respect to the inlet conditions of the drying medium	111
4.5.2	Normalization in a steam-operated fluidized bed	117
4.6	Comparison of the normalized drying rate curves in air and in steam	120
4.6.1	Normalized drying rate curves for alumina	
4.6.2	Normalized drying rate curves for molecular sieve	121
4.7	Mathematical model for the drying rate during the falling drying rate period	131
4.7.1	Mathematical model for air drying	131
4.7.2	Mathematical model for steam drying	136
4.7.3	Simulation of the drying of alumina	137
4.7.4	Simulation of the drying of molecular sieve	142
5.	ECONOMIC COMPARISON BETWEEN AIR DRYING AND STEAM DRYING IN A FLUIDIZED BED	146
5.1	Design of fluidized-bed dryers	147
5.2	Design method for steam fluidized-bed dryers	152
5.3	Results of the economic analysis	157
6.	CONCLUSIONS	171
7.	RECOMMENDATIONS	175
	APPENDICES	178
	Appendix A: Measurement errors	178
	Appendix B: Physical properties of the drying media and of the moisture	191
	Appendix C: Curve fitting for the sorption isotherm	192
	Appendix D: Influence of the system geometry and the mass flow rate of the drying medium on the locus of the inversion temperature	194

	<u>Page no.</u>
Appendix E: Heat transfer correlations for various geometrical configurations	202
Appendix F: Solution of differential equation 36 for the heat transfer coefficient	203
Appendix G: Comparison of the gas-to-solid heat transfer coefficient in a fluidized bed evaluated with drying and without drying	205
Appendix H: Normalization methods	208
Appendix I: Mathematical description of the heat and mass transfer mechanisms in capillary porous bodies	217
Appendix J: Conversion of experimentally recorded drying rate curves to design conditions	228
Appendix K	234
LITERATURE	241

## LIST OF FIGURES

Number	Title
1	Conventional air dryer
2	Superheated steam dryer
3	Convective superheated steam dryer with mechanical vapour compression
4	Conductive superheated steam dryer with mechanical vapour compression
5	Drying rate curves for clay in air and in steam
6	Drying rates of a droplet of coffee extract in air and in steam
7	Temperature evolution of a droplet of coffee extract during drying in air and in superheated steam
8	Driving forces in air drying
9	Driving forces in steam drying
10	Literature data of Colburn $j$ -factor for heat transfer in steam as function of Reynolds number
11	Effect of channel boundaries on flow pattern through ducts
12	Drying rates during evaporation of benzene into air and into superheated benzene
13	Drying rates during evaporation of water into air and into superheated steam
14	Inversion temperature
15	Temperature evolution of a droplet of water during drying in air and in superheated steam
16	Drying rates of a droplet of water in air and in steam
17	Drying periods for droplets of solutions
18	Experimental drying rig
19	Fluidized bed dryer
20	Diaphragm assembly
21	Damping of movements on diaphragms
22	Graphical representation of weight readings vs time
23	Smoothed weight readings as function of time



Number	Title
24	Experimental drying rate curve
25	Sorption isotherms for various materials
26	Division of moisture according to strength of bonding
27	Measuring equipment for sorption isotherms
28	Sorption isotherms for alumina
29	Sorption isotherms for molecular sieve
30	Temperature and humidity profile in a non-equilibrium system
31	Temperature and humidity profile in an equilibrium system
32	Theoretical modelling of experimental literature data for evaporation of water into humid air and steam
33	Normalized heat transfer for data of Yoshida [Y2]
34	Normalized temperature difference for data of Yoshida [Y2]
35	Experimental data for inversion temperature in a fluidized bed ( $\dot{M}_g = 16,70 \text{ kg h}^{-1}$ for alumina and $\dot{M}_g = 21,06 \text{ kg h}^{-1}$ for molecular sieve)
36	Experimental data for inversion temperature in a fluidized bed ( $\dot{M}_g = 19,27 \text{ kg h}^{-1}$ for alumina and $\dot{M}_g = 24,41 \text{ kg h}^{-1}$ for molecular sieve)
37	Experimental data for inversion temperature in a fluidized bed ( $\dot{M}_g = 22,76 \text{ kg h}^{-1}$ for alumina and $\dot{M}_g = 25,96 \text{ kg h}^{-1}$ for molecular sieve)
38	Outlet temperature in a fluidized bed as function of bypass mass flow
39	Literature data and own experimental data on heat transfer coefficients in a fluidized bed
40	Experimental data on air-to-solid heat transfer coefficient in a fluidized bed
41	Experimental data on steam-to-solid heat transfer coefficient in a fluidized bed
42	Experimental drying rates of alumina in air at an air flow rate of $16,70 \text{ kg h}^{-1}$
43	Experimental drying rates of alumina in steam at a steam flow rate of $16,70 \text{ kg h}^{-1}$

Number	Title
44	Experimental drying rates of alumina in air at an air flow rate of 19,27 kg h <sup>-1</sup>
45	Experimental drying rates of alumina in steam at a steam flow rate of 19,27 kg h <sup>-1</sup>
46	Experimental drying rates of alumina in air at an air flow rate of 22,76 kg h <sup>-1</sup>
47	Experimental drying rates of alumina in steam at a steam flow rate of 22,76 kg h <sup>-1</sup>
48	Experimental drying rates of alumina in air and in steam at various temperatures (mass flow rate of 19,27 kg h <sup>-1</sup> )
49	Experimental drying rates of alumina in air at various air flow rates
50	Experimental drying rates of alumina in steam at various steam flow rates
51	Experimental drying rates of molecular sieve in air at an air flow rate of 21,06 kg h <sup>-1</sup>
52	Experimental drying rates of molecular sieve in steam at a steam flow rate of 21,06 kg h <sup>-1</sup>
53	Experimental drying rates of molecular sieve in air at an air flow rate of 24,41 kg h <sup>-1</sup>
54	Experimental drying rates of molecular sieve in steam at a steam flow rate of 24,41 kg h <sup>-1</sup>
55	Experimental drying rates of molecular sieve in air at an air flow rate of 25,96 kg h <sup>-1</sup>
56	Experimental drying rates of molecular sieve in steam at a steam flow rate of 25,96 kg h <sup>-1</sup>
57	Experimental drying rates of molecular sieve in air and in steam at various temperatures (mass flow rate of 24,41 kg h <sup>-1</sup> )
58	Experimental drying rates of molecular sieve in air at various air flow rates
59	Experimental drying rates of molecular sieve in steam at various steam flow rates

Number	Title
60	Normalized drying rates of alumina in air at an air flow rate of 16,70 kg h <sup>-1</sup>
61	Normalized drying rates of alumina in steam at a steam flow rate of 16,70 kg h <sup>-1</sup>
62	Normalized drying rates of alumina in air at an air flow rate of 19,27 kg h <sup>-1</sup>
63	Normalized drying rates of alumina in steam at a steam flow rate of 19,27 kg h <sup>-1</sup>
64	Normalized drying rates of alumina in air at an air flow rate of 22,76 kg h <sup>-1</sup>
65	Normalized drying rates of alumina in steam at a steam flow rate of 22,76 kg h <sup>-1</sup>
66	Normalized drying rates of alumina in air and in steam at various temperatures (mass flow rate of 19,27 kg h <sup>-1</sup> )
67	Normalized drying rates of molecular sieve in air at an air flow rate of 21,06 kg h <sup>-1</sup>
68	Normalized drying rates of molecular sieve in steam at a steam flow rate of 21,06 kg h <sup>-1</sup>
69	Normalized drying rates of molecular sieve in air at an air flow rate of 24,41 kg h <sup>-1</sup>
70	Normalized drying rates of molecular sieve in steam at a steam flow rate of 24,41 kg h <sup>-1</sup>
71	Normalized drying rates of molecular sieve in air at an air flow rate of 25,96 kg h <sup>-1</sup>
72	Normalized drying rates of molecular sieve in steam at a steam flow rate of 25,96 kg h <sup>-1</sup>
73	Normalized drying rates of molecular sieve in air and in steam at various temperatures (mass flow rate of 24,41 kg h <sup>-1</sup> )
74	Simulation of the normalized drying rates of alumina in air at an air flow rate of 16,70 kg h <sup>-1</sup>
75	Simulation of the normalized drying rates of alumina in steam at a steam flow rate of 16,70 kg h <sup>-1</sup>
76	Simulation of the normalized drying rates of alumina in air at an air flow rate of 19,27 kg h <sup>-1</sup>

Number	Title
77	Simulation of the normalized drying rates of alumina in steam at a steam flow rate of $19,27 \text{ kg h}^{-1}$
78	Simulation of the normalized drying rates of alumina in air at an air flow rate of $22,76 \text{ kg h}^{-1}$
79	Simulation of the normalized drying rates of alumina in steam at a steam flow rate of $22,76 \text{ kg h}^{-1}$
80	Simulation of the normalized drying rates of molecular sieve in air at an air flow rate of $21,06 \text{ kg h}^{-1}$
81	Simulation of the normalized drying rates of molecular sieve in steam at a steam flow rate of $21,06 \text{ kg h}^{-1}$
82	Simulation of the normalized drying rates of molecular sieve in air at an air flow rate of $24,41 \text{ kg h}^{-1}$
83	Simulation of the normalized drying rates of molecular sieve in steam at a steam flow rate of $24,41 \text{ kg h}^{-1}$
84	Simulation of the normalized drying rates of molecular sieve in air at an air flow rate of $25,96 \text{ kg h}^{-1}$
85	Simulation of the normalized drying rates of molecular sieve in steam at a steam flow rate of $25,96 \text{ kg h}^{-1}$
86	Schematic procedure for the economic analysis
87	Algorithm for the economic analysis
88	Drying system for the economic analysis
89	Comparison of the capital costs of an air-drying system and a steam-drying system for alumina as function of the inlet temperature into the dryer
90	Comparison of the capital costs of an air drying system and a steam drying system for molecular sieve as function of the inlet temperature into the dryer
91	Comparison of the running costs of an air drying system and a steam drying system for alumina as function of the inlet temperature into the dryer
92	Comparison of the running costs of an air drying system and a steam drying system for molecular sieve as function of the inlet temperature into the dryer

Number	Title
93	Normalized costs for a drying system for alumina as function of the inlet temperature into the dryer
94	Normalized costs for a drying system for molecular sieve as function of the inlet temperature into the dryer
95	Comparison of the capital costs of an air-drying system and a steam-drying system for alumina as function of the product moisture content
96	Comparison of the capital costs of an air-drying system and a steam-drying system for molecular sieve as function of the product moisture content
97	Comparison of the running costs of an air-drying system and a steam-drying system for alumina as function of the product moisture content
98	Comparison of the running costs of an air-drying system and a steam-drying system for molecular sieve as function of the product moisture content
99	Normalized costs for a drying system for alumina as function of the product moisture content
100	Normalized costs for a drying system for molecular sieve as function of the product moisture content
101	Comparison of the capital costs of an air-drying system and a steam-drying system for alumina as function of the product flow rate
102	Comparison of the capital costs of an air-drying system and a steam-drying system for molecular sieve as function of the product flow rate
103	Comparison of the running costs of an air-drying system and a steam-drying system for alumina as function of the product flow rate
104	Comparison of the running costs of an air-drying system and a steam-drying system for molecular sieve as function of the product flow rate
105	Normalized costs for a drying system for alumina as function of the product flow rate

Number	Title
106	Normalized costs for a drying system for molecular sieve as function of the product flow rate
107	Thermocouple assembly
108	Measuring tip of a thermocouple
109	Comparison of the normalized drying rate curves with respect to the averaged drying rate with normalization over mass transfer and over heat transfer
110	Inversion temperature for a plate ( $l = 0,2 \text{ m}$ )
111	Inversion temperature for a tube ( $l = 1 \text{ m}$ ; $d = 0,0288 \text{ m}$ )
112	Inversion temperature for a sphere ( $d = 0,001 \text{ m}$ )
113	Normalized heat transfer coefficient for various configurations
114	Normalized heat transfer coefficient of a plate as function of temperature for various mass flow rates
115	Normalized heat transfer coefficient of a tube as function of temperature for various mass flow rates
116	Normalized heat transfer coefficient of a sphere as function of temperature for various mass flow rates
117	Heat transfer coefficient in a fluidized bed evaluated without drying
118	Heat transfer coefficient in a fluidized bed evaluated with drying
119	Normalization methods
120	Drying rate conversion over temperature for molecular sieve in air
121	Drying rate conversion over temperature for molecular sieve in steam
122	Drying rate conversion over mass flow rate for molecular sieve in air
123	Drying rate conversion over mass flow rate for molecular sieve in air
124	Forces acting on the flow of gas in a fluidized bed
125	Forces acting on the fluidized bed

## LIST OF TABLES

Table 1	Heat energy requirements in Megajoules for drying of 29 338 kg of southern yellow pine from 105 % to 10 % moisture content (dry basis) [M4]
Table 2	Correlation of drying data in terms of the Colburn j-factor
Table 3	Physical properties of the test materials
Table 4	Experimental programme
Table 5	Inversion temperature of an equilibrium system as function of the by-pass mass fraction (fbp)
Table 6	Bubble volume fraction in air and in steam for alumina at a mass flow rate of 19,27 kg h <sup>-1</sup>
Table 7	Bubble volume fraction in air and in steam for molecular sieve at a mass flow rate of 24,41 kg h <sup>-1</sup>
Table 8	Dimensionless humidity/temperature potential as a function of the dimensionless height
Table 9	Error in the heat transfer coefficients by ignoring measurement errors in the gas temperature
Table 10	Normalized physical properties for various temperatures
Table 11	Comparison of the transfer coefficients in air and in steam
Table 12	Evaluation of the time variable forces at the beginning and at the end of a drying test
Table 13	Error in the drying rate due to the change of gas weight with time

## NOMENCLATURE

Symbols	Dimension	Description
Alphabetic		
A	$m^2$	Surface area of particles
a	$m^2 m^{-3}$	Specific surface area
B	$s m^{-1}$	Transfer coefficient
$c_p$	$J kg^{-1} K^{-1}$	Specific heat
$C_i$	-	Constant ( $i=1\dots n$ )
d	m	Diameter
f	-	Function
H	$J kg^{-1}$	Enthalpy
$\dot{H}$	W	Enthalpy flow
h	$W m^{-2} K^{-1}$	Heat transfer coefficient
L	m	Height of the dryer
M	kg	Mass
$\dot{M}$	$kg s^{-1}$	Mass flow rate
$\tilde{M}$	$kg mol^{-1}$	Molecular weight
$\dot{m}$	$kg m^{-2} s^{-1}$	Specific mass flow rate
n	-	Constant
p	Pa	Pressure
$\dot{q}$	$W m^{-2}$	Heat flow
R	m	Radius
r	m	Axis
T	K	Temperature
t	s	Time
u	$m s^{-1}$	Velocity
W	kg	Weight reading
X	$kg kg^{-1}$	Moisture content of solid material
Y	$kg kg^{-1}$	Humidity of drying medium
y	$mol mol^{-1}$	Humidity of drying medium



Symbols	Dimension	Description
Greek		
$\rho$	$\text{kg m}^{-3}$	Density
$\eta$	$\text{Pa s}$	Dynamic viscosity
$v$	-	Normalized drying rate
$\nu_i$	$\text{m}^2 \text{s}^{-1}$	Kinematic viscosity
$\Delta h_v$	$\text{J kg}^{-1}$	Latent heat
$\xi$	-	Dimensionless transfer potential
$\tau$	-	Dimensionless time
$\zeta$	-	Dimensionless height
$\Phi$	$\text{m}^2$	Area of the dryer
$\beta$	$\text{m s}^{-1}$	Mass transfer coefficient
$\lambda$	$\text{W m}^{-1} \text{K}^{-1}$	Thermal conductivity
$\chi$	-	Flow resistance
$\delta$	-	Volume fraction of bubbles in a fluidized bed
$\mu$	-	Diffusion resistance factor
$\Psi$	-	Ratio of free area to total area
	-	Error
Special		
$d$	-	Total differential
$\partial$	-	Partial differential
$z$	-	Height-axis
$\Delta$	-	Difference

Symbols	Dimension	Description
---------	-----------	-------------

---

## Subscripts

a	Air
b	Boiling
bc	Bubble crowd
bp	Bypass
br	Rising bubble
c	Correction
d	Dryer
dp	Dry particle
e	External
eq	Equivalent
ev	Evaporate
f	Fluidization
g	Gas
i	Inversion
in	Inlet of the dryer
l	Liquid
mf	Minimum fluidization
n	Index
no	Normal
o	Surface
out	Outlet of the dryer
p	Particle
s	Steam
t	Total
u	Evaporative interface
v	Vapour
w	Water
wa	Wet air
wb	Wet-bulb
1	Case 1
2	Case 2
I	Constant drying rate period
$\infty$	Bulk

Symbols	Dimension	Description
---------	-----------	-------------

---

## Superscripts

*	Equilibrium
'	Falling drying rate period
°	Mass transfer
•	Heat transfer

## Dimensionless numbers

Re	Reynolds number
Pr	Prandtl number
Nu	Nusselt number
Le	Lewis number
Gz	Graetz number
Kn	Knudsen number

Definition of dimensionless numbers used in Section 4.5

Dimensionless humidity potential

$$\xi_g^\circ = \frac{(Y_p^\star - Y_g)}{(Y_p^\star - Y_{g,in})}$$

dimensionless humidity potential for the falling drying rate period

$$\xi_g' = \frac{(Y_p - Y_g)}{(Y_p - Y_{g,in})}$$

dimensionless humidity potential of the particles

$$\xi_p^\circ = \frac{(Y_p^\star - Y_p)}{(Y_p^\star - Y_{g,in})}$$

dimensionless height for mass transfer

$$\zeta^{\circ} = \frac{\rho_g \beta A z}{M_g L}$$

dimensionless temperature potential

$$\xi_g^{\circ} = \frac{(T_g - T_{p,I})}{(T_{g,in} - T_{p,I})}$$

dimensionless temperature potential for the falling drying rate period

$$\xi_g^{\circ'} = \frac{(T_g - T_p)}{(T_{g,in} - T_p)}$$

dimensionless temperature potential of the particles

$$\xi_p^{\circ} = \frac{(T_p - T_{p,I})}{(T_{g,in} - T_{p,I})}$$

dimensionless height for the heat transfer

$$\zeta^{\circ} = \frac{h A}{M_g c_{pg}} \frac{z}{L}$$

dimensionless time

$$\tau^{\circ} = \frac{h A}{M_p c_{pp}} t$$

Meaning of symbols used in Section 4.4, 4.6 and 4.7

⊙  $T = 75^{\circ}\text{C}$

□  $T = 100^{\circ}\text{C}$

◇  $T = 125^{\circ}\text{C}$

▷  $T = 150^{\circ}\text{C}$










⬡  $T = 175^{\circ}\text{C}$

●  $T = 200^{\circ}\text{C}$










■  $T = 225^{\circ}\text{C}$

◆  $T = 250^{\circ}\text{C}$

Meaning of symbols used in Section 4.4, 4.6 and 4.7

	T = 75 °C
	T = 100 °C
	T = 125 °C
	T = 150 °C
	T = 175 °C
	T = 200 °C
	T = 225 °C
	T = 250 °C
	T = 275 °C

Meaning of symbols used in Section 4.4, 4.6 and 4.7

	T = 75 °C
	T = 100 °C
	T = 125 °C
	T = 150 °C
	T = 175 °C
	T = 200 °C
	T = 225 °C
	T = 250 °C
	T = 275 °C

## SYNOPSIS

Drying is a unit operation that enjoys wide application in the chemical processing industry. The drying process itself, however, is grossly energy-inefficient with typical efficiencies ranging between 20 and 50 %. Superheated-steam drying has been advocated as one of the means for reducing energy consumption in the drying process, but only a few results have been reported as to its economic viability. Without a sound economic basis, however, steam drying will not be accepted by the processing industry.

The reason for the scarceness of economic data on steam drying is the lack of suitable equipment for determining drying data in steam and the lack of knowledge to use these data in the design of industrial dryers. In this thesis laboratory drying equipment and data interpretation procedures are developed to compare air drying and steam drying in fluidized beds. Even though such equipment and procedures are available for air drying, they cannot be applied to steam drying.

Novel equipment was developed to measure the drying kinetics of materials in fluidized beds. The drying equipment consists of a laboratory-scale fluidized bed that rests freely on a balance. The balance is connected to a data-acquisition system that records the weight loss of the drying material with time. The tests were carried out at various inlet temperatures and at various mass flow rates of the drying medium. Two capillary porous materials, namely a weakly hygroscopic alumina and a highly hygroscopic molecular sieve, were investigated.

The recorded drying rate curves are used to study the differences in drying rates between air drying and steam drying. Separate comparisons are made for the constant and the falling drying rate periods.

For the constant drying rate period, literature data indicate the existence of an inversion temperature. Below this temperature, drying rates are higher in air than in steam, whereas above it, drying rates are higher in steam. Even though the inversion temperature was already found before, no comprehensive explanation was put forward for its existence. In this thesis, the existence of the inversion temperature is proved for equilibrium systems and non-equilibrium systems by mathematical modelling of the drying behaviour in the constant drying rate period. The results of this modelling are verified on own experimental data and on literature data.

For the falling drying rate period, steam drying was found to have a greater kinetic advantage for the hygroscopic molecular sieve than for the non-hygroscopic alumina. Due to the higher drying rates during the falling drying rate period, the total drying time of molecular sieve in steam was notably shorter than in air, even at temperatures below the inversion temperature.

For a better comparison of the drying rates in the falling drying rate period, the drying rates are normalized with respect to the constant drying conditions at the inlet into the dryer. This normalization procedure was introduced by Zabeschek [Z1] for non-equilibrium systems in air. In the present thesis this procedure was extended to equilibrium systems in air and in steam. This normalization procedure makes it possible to record drying rate curves of a material in fluidized beds and use them in the design of other drying equipment. The normalized drying rate curve was described by mathematical modelling. The model avoids the use of sophisticated computer hardware and software and yet describes the drying behaviour qualitatively well.

The recorded drying rate curves are used as input data for the economic analysis. The design of the fluidized bed dryer is the first step of the economic analysis. No design data for steam-operated fluidized beds could be found in the literature. A design procedure applicable to both air and steam dryers was developed. The procedure dimensions the dryer on the basis of heat transfer expressions as opposed to mass transfer expressions that are used in conventional design procedures.

The design method is incorporated into a computer program that dimensions fluidized bed dryers for a given duty and determines the energy costs and capital costs of the drying system. In steam drying, energy costs are around 40 % lower than in air drying, whereas capital costs are roughly 20 % higher. The economic advantage of steam drying is, however, more apparent for the highly hygroscopic molecular sieve than for the weakly hygroscopic alumina.



## 1. INTRODUCTION

Drying is one of the most important unit operations in the chemical processing industry. Virtually all products require to be dried during some stage of their manufacture. In South Africa, about R300 million is spent annually on drying [C5], which makes it the most expensive operation in the chemical processing industry. In many industrialized countries, drying competes with distillation for consuming the greatest amount of energy. Unlike distillation, however, drying is often grossly energy-inefficient, with 50 % to 80 % of the energy supplied being wasted, mainly with the exhaust gas [B11,B12, M10]. Widespread promotion of energy-efficient dryers is therefore advocated as a means of realizing significant energy savings.

Several ways of saving energy in drying may be considered [B1]:

- Heat recovery from the dryer exhaust by means of a heat exchanger
- Closed-cycle heat pumps
- Open-cycle heat pumps (superheated-steam drying)
- Better control and instrumentation of dryers
- Optimization of dryer design and operation
- Improved dewatering of dryer feedstocks
- Alternative drying technologies, for example microwave drying

Of these options, the open-cycle heat pump or superheated-steam dryer has the highest potential for saving energy. Other advantages of drying in superheated steam include its inert atmosphere, enhanced drying rates, improved product quality, and easier drying control [A1,B2-4,C7-9,F5,G1,H10,K1,K4,L1,M4,M8,P4,R2,S7,T2,V6,W3,Y1-2]. Disadvantages are limited essentially to the need for a more complex drying system and condensation problems. In particular, temperature-sensitive materials must be dried under vacuum to prevent degradation. An excellent review of the merits of superheated-vapour drying has been presented by Beeby and Potter [B3].

In practice, cost will be an important factor in selecting a drying system. Therefore an economic comparison of a superheated-steam drying system and an air-drying system must be performed. Cost-optimized drying systems must be designed for air and for steam and the running and investment costs in the two drying media must be compared.

A dryer can only be designed if drying data on the material to be dried are available. The most important drying data are the drying rate curve, which indicates how quickly a material dries, and the sorption isotherm, which indicates to what remaining moisture content a material can be dried. These data cannot be obtained theoretically but must be determined experimentally for each material. In conventional testing equipment, drying rate curves and sorption isotherms can only be measured in air. Therefore special equipment must be designed to determine these data in both air and steam.

With the help of mathematical models, the recorded drying data can then be extrapolated to conditions different from those used in the experiment. In general, mathematical drying models are very complex and are of limited practical interest to the processing industry. Furthermore, the available models were developed for air drying and cannot be used directly for steam drying as the mechanisms of moisture movement are different in these two drying media. Therefore it is useful to develop a simple model that takes into account the differences between moisture movement in air and in steam and that does not require extensive computer software and hardware for its solution. This model must then be verified on the experimental drying rate curves.

Finally, the recorded data and the findings must be incorporated into an economic study of air and steam drying. The comparison should be done for optimized drying systems in air and in steam. The influence of the operating conditions on the running costs and investment costs of the two systems should be studied.

## 2. SUPERHEATED-STEAM DRYING

The concept of superheated-steam drying is not new. It dates back to the beginning of this century [B3,F5] and was arose out of the need for greater energy efficiency and faster drying. In the following chapters a literature review of theoretical studies and practical applications of steam drying is presented and discussed.

### 2.1 Principle of superheated-steam drying

The principle of steam drying is best understood by comparing it with conventional air drying. In a conventional air dryer such as that shown in Figure 1, ambient air is drawn into the system by a blower, passes through a heater where it is heated up to the inlet temperature, and then enters the dryer itself. Wet feed is introduced into the dryer and comes into contact with the hot dry air; dry product and cold humid air leave the dryer.

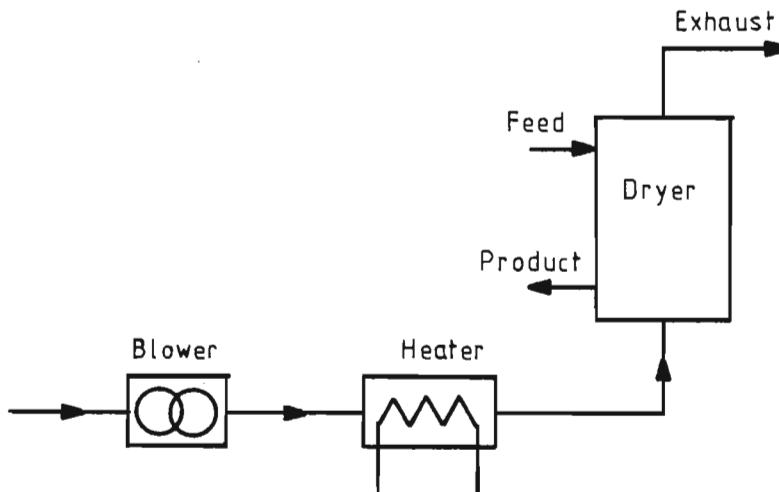


Figure 1: Conventional air dryer

In a conventional convective dryer, roughly 50 % of the energy supplied is used for evaporation, and more than 30 % is lost as sensible heat with the exhaust [B4]. Some of the sensible heat may be recovered by partial recirculation or by heat exchange with the incoming air. Large, expensive exchangers are required to heat the incoming air to a temperature approaching that of the exhaust air. The largest

energy content in the exhaust gas is the latent heat of the evaporated moisture, and, to recover this, the exhaust has to be cooled down to below the dew-point (typically below 60 °C). Even then, the latent heat can never be recovered completely.

A schematic diagram of steam drying is shown in Figure 2. The dryer operates in a closed cycle. Steam that is circulated by a blower passes through a heater where it is brought up to the inlet temperature and then enters the dryer. At the outlet of the dryer, the exhaust is split into two streams. The circulating steam is fed back to the blower, and an amount of steam equivalent to that arising from the evaporation of the moisture is split off from the system. This split-off stream consists of pure steam and can be used for heating purposes either inside or outside the drying system. The energy of this steam is set free at a low temperature (boiling point) and as such cannot be used satisfactorily inside the drying system. If the energy is required inside the drying system, expensive equipment is needed to raise the temperature level at which the energy is set free. If the split-off steam can be used without raising the temperature level at which the energy is set free, for instance outside the drying system to heat water or to preheat process streams, then the use of expensive heat-exchanging equipment can be avoided. Which route should be followed is, in the end, a decision based on economics.

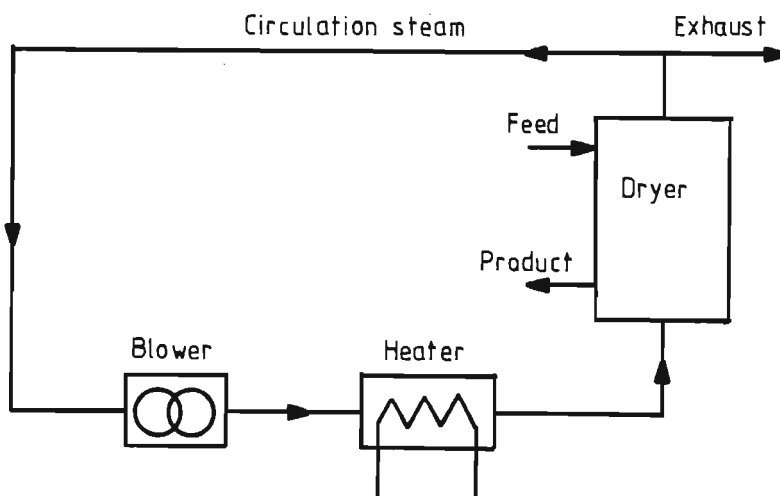


Figure 2: Superheated-steam dryer

Inside the drying system, the energy of the split-off steam may be recovered by compressing the exhaust steam and subsequently condensing it. The condensation temperature of the exhaust steam is above that of the recirculating steam, so an additional heat source is not needed. The high-pressure steam leaving the compressor may be used to heat the recirculating steam in a direct-contact dryer (convective dryer) as shown in Figure 3, or to heat the wet particles by means of internal heating elements in an indirect-contact dryer (conductive dryer) as shown in Figure 4.

In the direct-contact system, all the heat necessary for evaporation is supplied by the circulating steam. The amount of heat obtainable from a unit mass of steam is determined by its temperature drop as it passes through the dryer. The exit temperature cannot be reduced below the condensation point, so the inlet temperature of the steam has to be high (often above 170 °C) in order to supply adequate heat at an economical steam flow rate. Consequently the heating steam must condense at a correspondingly high pressure (800 kPa to 1 000 kPa), and this places high demands on the compressor.

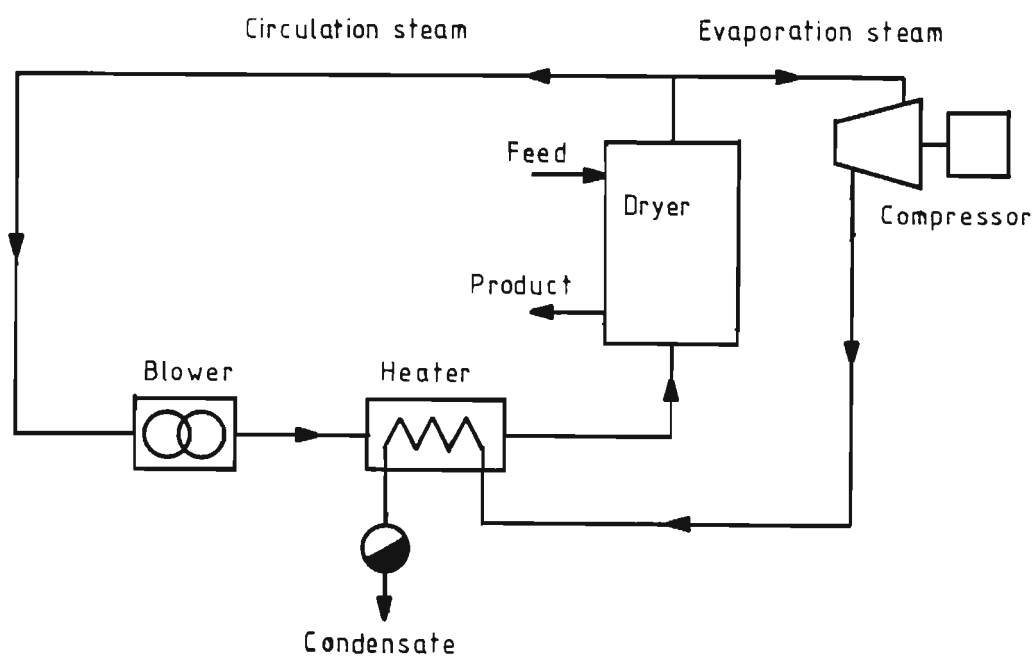


Figure 3: Convective superheated-steam dryer with mechanical vapour compression

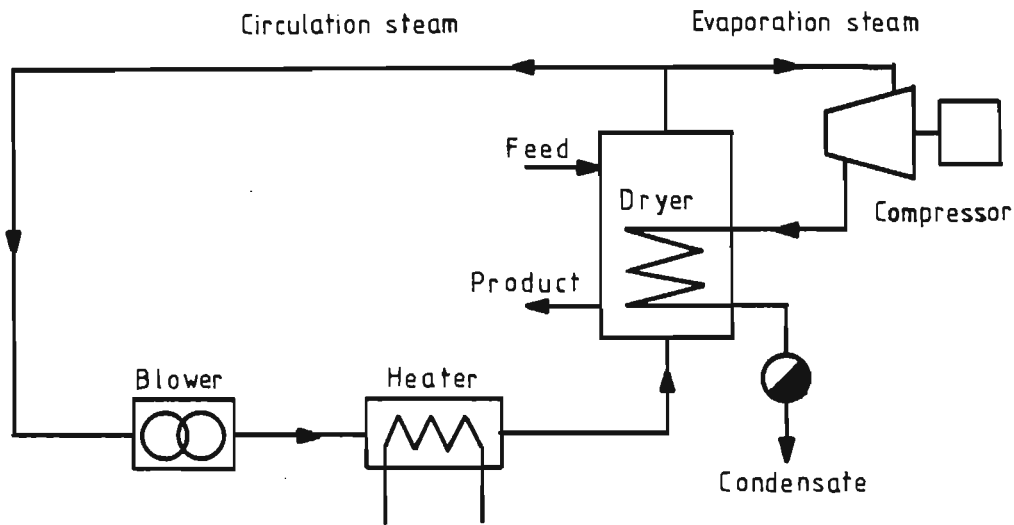


Figure 4: Conductive superheated-steam dryer with mechanical vapour compression

In the indirect-contact system, the heat necessary for evaporation is supplied by the compressed steam condensing in heating elements inside the dryer. High heat transfer coefficients may be obtained, so low temperature driving forces are acceptable, and the heating steam may be at a low pressure (200 kPa to 400 kPa).

Because conductive dryers are generally more efficient than convective dryers and make fewer demands on the compressor, the second route is to be preferred. The major problems with this route are:

#### Condensation of the circulating steam in the pipes

Condensation occurs at any cold spots.

#### Fouling of the heat transfer surfaces inside the dryer

If the dryer is operated with sticky material, the danger of fouling is increased.

### Steam superheating after compression

The steam leaves the compressor highly superheated. These high temperatures can damage the compressor and lead to poor heat transfer coefficients in the heating elements. This is avoided in systems in which the cooling water is injected directly into the compression chamber.

In summary, drying in superheated steam provides the opportunity of recovering both the sensible and the latent heat that is normally wasted in the exhaust from conventional dryers.

## 2.2 Applications of steam drying

Superheated-steam drying was first mentioned by Hausbrand [H5] at the beginning of the century. Industrial applications of this drying method were confined to the timber industry. Due to unsuitable equipment and lack of knowledge of superheated-steam drying, this drying method was forgotten and it was only in the 1950s that interest in superheated-steam drying revived with a series of theoretical investigations [C7-9,M8,T3,W3]. The main objective was to compare the relative rates of drying in air and in steam. Even though these investigations shed some light on superheated-steam drying, confusion resulted from the divergences in the results obtained. In 1970 Yoshida and Hyodo [Y2] found the explanation for the contradictory results experimentally and introduced the term 'inversion temperature'. Below this temperature drying is faster in air than in steam; above this temperature drying is faster in steam than in air.

Up to this time commercial applications had been limited due to the lack of incentive for more energy-efficient drying methods and for tighter air pollution control. After the energy crisis of 1973, there was an ever-increasing interest in superheated-steam drying. This interest has continued and has resulted in a large number of theoretical and experimental investigations [B3,C7,C10,C12,F2,F4-5,G1,H8,K4,K7,M4,P4,S7,V6]. Today superheated-steam drying is being applied in a number of industries. Conventional dryers and newly developed dryers

have been used with steam. In the following subsections, the applications of steam drying are divided into different groups, depending on the type of dryer that is used.

### 2.2.1 Kiln dryers

The first kiln dryers employing superheated steam as the drying medium were used in the timber industry as early as 1908 [M4]. In general, timber can be dried faster in steam than in humid air. Rosen [R2] carried out steam-drying tests under pressure on a variety of timber boards. He found a reduction in drying time for green-yellow poplar timber (from a moisture content of 110 % down to 10 %) from five to seven days down to 30 hours, and for red oak (18 % to 6 % moisture content) from five to ten days down to 24 hours. The dried timber showed some discoloration but the structure of the wood was intact and only a little internal stress was present.

Rosen [R2] found the capital and operating costs of drying in steam to be lower than those for drying in air. The cost of a pressurized steam-drying system was 5 % less than that of a conventional dryer. The heat input into the system (0,82 kWh per kg of water evaporated) was considerably less than the heat requirements of conventional dryers.

Miller [M4] evaluated the economics of three drying processes in the timber industry:

- conventional air drying
- high-temperature air drying, and
- superheated-steam drying with vapour compression.

Theoretical heat balances for drying southern yellow pine from a moisture content of 105 % to 10 % were made. The heat needed to evaporate moisture is compared with the total energy needed (to raise the temperature of the wood, raise the temperature of the kiln and compensate for heat losses) in Table 1.



Table 1: Heat energy requirements in Megajoules for  
drying of 29 338 kg of southern yellow pine  
from 105 % to 10 % moisture content (dry basis) [M4]

Heat energy	Conventional drying	High-temperature drying	Vapour compression drying
Energy to remove moisture	65,3	65,0	63,5
Total energy consumption	101,5	102,9	39,7
Efficiency	0,64	0,63	1,6

In the case of the vapour compressor, the steam is compressed to 700 kPa and leaves the compressor highly superheated at 405 °C. This high temperature requires a specially designed compressor. In addition, the compressor has to accommodate a varying steam flow rate while maintaining a constant outlet pressure. The compressed steam is fed into heating coils, condensed and used to heat the circulating steam inside the drying kiln. The extractives and preservatives from the timber that are dissolved in the steam may damage the compressor and foul the heating coils.

### 2.2.2 Spray dryers

Benstead [B4] has presented a mathematical model of a circulating superheated-steam drying system. The excess steam produced by evaporation is split off and compressed and is then condensed in a heat exchanger and used to heat the circulating steam. The model can be used to determine the necessary sizes of the compressor, fan, flash chamber and heat exchanger. The compression pressure is selected such that the condensation temperature will exceed the temperature of the inlet steam. Water injection into the compressor is useful for controlling the degree of superheating and for improving compression efficiency. The mathematical model shows that the performance of the dryer is most sensitive to steam leakages, dryer inlet temperature and compressor efficiency. Leakages should be less than 10 % of the drying rate.

Experimental runs were made on a spray dryer with a bone nutrient product, paracetamol and dairy products [B4]. Some problems arose. Because of the lower dynamic viscosity of steam, droplets travel 60 % further in steam than in air. Deposition problems on the walls of spray dryers can occur unless the atomizer is modified. Further, the high temperature of the droplets in steam drying may lead to degradation of heat-sensitive products. Difficulties in transporting the product out of the dryer were also experienced.

The lower density of steam results in higher relative velocities in steam drying, so higher Reynolds numbers are achieved which favours heat transfer. Benstead estimated a 40 % saving in running costs.

Gauvin and Costin [G1] developed a mathematical model for dimensioning spray dryers. The aim of their study was to compare operating and capital costs for steam and air drying. Costs were determined for industrial-size spray dryers designed to dry solutions of sodium nitrate in air and in superheated steam. The designs were optimized. Capital costs for steam drying were 33 % lower and operating costs 21,5 % lower than those for air drying.

### 2.2.3 Fluidized-bed dryers

In 1962 Basel and Gray [B2] reported on a fluidized-bed dryer in which polypropylene was dried in a superheated-vapour mixture of hexane and isopropylalcohol. The evaporated solvent was then recovered from the exhaust by condensation. In conventional propylene production, an intermediate product is formed that is wet with solvent and alcohol. This material is then washed with water, yielding a water/alcohol solution that must be fractionated to recover the solvent, and a water-wet product that must be dried. Drying of the wet polymer with the superheated solvent eliminates the water-washing and fractionating step and, in addition, provides an economical drying system with considerable heat economy because of the much lower latent heat of the solvent.

In 1960, a full-scale facility was commissioned. The authors [B2] report that the system went on stream with a minimum of operational

difficulties and rapidly reached design capacity. The boiling point of the solvent vapour is 62 °C, so, compared with superheated steam, condensation was not a significant problem.

Keogh and Potter [K4] described a drying system for coal using a fluidized bed with internal heating elements. The system consists of a battery of multiple-effect dryers. Coal is fed separately into a high-pressure, a medium-pressure and a low-pressure stage. The dried coal leaves each dryer at the corresponding pressure. The heating elements of the high-pressure dryer are operated with steam supplied from a boiler. The dryer exhaust is split into two parts: one part is recirculated to the fluidized bed; the other part is fed into the heating elements of the medium-pressure dryer where it condenses and releases its latent heat for drying. This pattern is repeated in the second stage. The condensate from the heating elements of the low-pressure stage may be used as feed water to the boiler. This system is designed to be used in a power station.

Potter *et al.* [P4] used a pilot plant to dry 0,25 t h<sup>-1</sup> of brown coal with a 66 % moisture content. The system worked well, with heat transfer coefficients of 340 W m<sup>-2</sup> K<sup>-1</sup> being obtained for operation at atmospheric pressure. Operation at 1 300 kPa was expected to double this value.

#### 2.2.4 Pneumatic conveying dryers

A superheated-steam dryer based on the principle of pneumatic conveying is described by Svensson [S7] and by Frame *et al.* [F5]. The dryer consists of a closed pressurized system, in which the material to be dried is exposed to indirectly heated steam. Superheated steam circulates inside the dryer at a pressure of 300 kPa to 600 kPa and serves as transport gas for the wet material. This flows through a cascade of heat exchangers and conveying pipes. The dried product is extracted in a cyclone and the steam is recirculated. The heat exchangers are heated with high-pressure steam from an external source. Operating parameters have to be chosen in such a way as to limit fouling of the heat-exchanging surfaces and to prevent clogging of the equipment. The heat transfer coefficients were found to be three

to four times those of air drying ( $965 \text{ W m}^{-2} \text{ K}^{-1}$  to  $1\,136 \text{ W m}^{-2} \text{ K}^{-1}$ ), and the average drying rates were two to three times higher than in air drying.

This system may be used for pulp and paper, and for industrial and agricultural wastes. The first commercial-size steam dryer for 50 000 metric tons of pulp per year was erected in Sweden in 1981. This equipment uses 62 % less energy than a conventional flash dryer.

In a later study, Hilmar and Gren [H8] used this equipment successfully for the drying of wood residues. They studied specifically the heat transfer coefficients from the tubes to the material and found them to be in accordance with theoretically estimated data. Fouling occurred on the heat-exchanging tubes. By increasing the temperature of the superheated steam at the inlet into the dryer, fouling was reduced.

#### 2.2.5 Impingement jet dryers

Steam drying can be applied for the drying of paper [C12] or printed matter [K7] on an impingement jet dryer.

Cui *et al.* [C12] present a mathematical model for determining the constant drying rate and the energy requirements of drying in superheated steam. They validated their model on an experimental unit. Energy requirements are predicted to be as low as  $640 \text{ kJ kg}^{-1}$  of water evaporated. Typical energy consumptions in conventional air dryers are between 5 020 and 7 100  $\text{kJ kg}^{-1}$  of water evaporated. The effect of jet pressure, jet temperature and jet velocity on the energy requirements is discussed. Further tests to evaluate the product quality more closely are recommended.

Klemm *et al.* [K7] investigated the use of an impingement jet dryer for the drying of heatset inks. In air-drying equipment, the equilibrium moisture content of the printing paper is strongly reduced during this drying process. Subsequent interaction with moisture in the air causes waves in the paper which reduce the optical quality of the printed products. In steam drying, the equilibrium moisture con-

tent of the printing paper can be maintained and the formation of waves in the paper can be prevented. A further advantage of using superheated steam as the drying medium is the higher evaporation rates of the solvents that are used for the printing inks. Evaporation rates were found to be 15 to 25 % higher in steam. The solvents could be recovered by condensing the steam and separating the oily phase from the water phase. There was only a slight loss in the glossy quality of the paper due to the steam.

#### 2.2.6 Other types of dryer

Akao *et al.* [A1] designed a steam dryer for soy sauce cake. Because of its high protein content, soy sauce cake is an excellent animal feed and fertilizer mix; however, objectionable odours must be removed before it can be marketed. Superheated-steam drying proved to be effective for this task. Tests were done on a pilot-plant fluidized-bed dryer. Various problems, including erosion, corrosion and fires, frequently occurred due to oil condensation and dust accumulation. It was consequently decided to choose an indirectly heated dryer for commercial application. A cylindrical-tube dryer equipped with a rotating high-speed agitator, having 30 impellers inside, was selected. Saturated steam at a temperature of 176 °C was injected into the heating jacket. Superheated steam in the temperature range 200 °C to 250 °C was introduced directly into the dryer. The wet soy sauce cake at 12 % moisture content was pulverized and then fed into the dryer. The dried product left at a moisture content below 5 %. The 2,2 t h<sup>-1</sup> commercial plant has been in operation since December 1980.

Theoretical and practical studies were carried out at EDF (Electricité de France) [F4,M2] on a steam-drying system incorporating mechanical vapour compression. The system is applied for the drying of beetroot pulp and lucerne. The energy performance of the steam-drying system was compared with that of existing air dryers. For the conversion of the existing drying systems to steam dryers, a payback period of between two and three years was found. Pilot plant studies on a rotating kiln dryer and a belt dryer were successful. Problems were only experienced at start-up due to decompression of the dryer when the compressor was switched on.

An application of superheated-steam drying in the filtration field is described by Emmett and Dahlstrom [E1]. They found that, by blowing steam through the filter cake during the filtration operation, the remaining moisture content of the filter cake could be reduced to such an extent as to eliminate a possible subsequent drying step completely. This system was tried on a pilot-plant basis for iron ore concentrates with a reduction of the moisture content from 15 to 10 %, for salt with a reduction of 27 % in energy requirements and for an intermediate organic product with an increase of 67 % in production rate. Applications were tested on disk, drum and horizontal belt filters.

#### 2.2.7 Product quality

The above review of the basic research into superheated-steam drying has shown that its advantages over conventional air drying include higher overall drying rates, shorter total drying times and energy savings. Other advantages can arise with certain materials and when specific product quality characteristics are required. For example, oxidizable materials have to be dried in an inert atmosphere. Steam is non-reactive with many substances, does not contain the pollutants often present in flue gases, and is generally cheaper than a nitrogen supply.

Foods are particularly sensitive to oxidation. In experiments with potato slices, Yoshida and Hyodo [Y1] found that the browning that occurred in air drying was eliminated by drying in steam. More importantly, the vitamin C content of the product increased from 3,4 % to 5,5 % when drying in steam as a result of less oxidation of the vitamin. For these reasons, and because of the absence of pollutants, steam is considered to be an attractive drying medium for the food industry.

When drying in steam, the final moisture content of the product can be controlled by selecting a suitable steam temperature. The higher the degree of superheating, the lower the final equilibrium moisture content. For example, Potter *et al.* [P4] found that when drying Victorian brown coal in steam at 110 °C, the final moisture content

was 17 % by mass. By increasing the temperature to 170 °C, the moisture content could be decreased to 3 %. These data also indicate that drying to low moisture contents with steam is feasible.

When drying in air, the final moisture content can also be decreased by increasing the air temperature. In tests with wood pulp, Svensson [S7] found that, for the same temperature, the moisture content in air was lower than in steam over the entire temperature range studied. This was considered a positive attribute because the chances of overdrying are reduced. The same applies to the drying of heatset inks described by Klemm et al [K7]. In steam drying the equilibrium moisture content of printed matter is maintained and the optical quality of the product improved.

The porosity of the product can be affected by the choice of drying medium. Because boiling occurs internally when drying in steam, increased porosity of non-rigid materials can be obtained [W3]. The opposite effect may be obtained when solutions are dried. Because the solution is at a higher temperature when drying in steam, the crystallization period is delayed and the dried product is generally more compact [M8].

### 2.3 Theory of drying kinetics in air and in steam

The drying kinetics of a material determine the size of the drying system needed and are of prime importance for the design of the dryer. Drying kinetics are often discussed in terms of the drying rate curve which gives the rate of drying as a function of the moisture content of the material. For different materials the drying rate curve shows different shapes. It is widely accepted practice to simplify the drying rate curve by dividing it into four distinct regions:

- heating-up period,
- constant drying rate period,
- first falling drying rate period and
- second falling drying rate period.

Not all materials exhibit all four of these drying regimes, but such a division is a good basis for discussing the drying behaviour in air and in steam.

At the start of drying, the material is generally cold. During the heating-up period, heat is transferred to the material and is used partly to evaporate moisture and partly to heat up the material. The temperature of the material increases until a point is reached where all the heat that is transferred to the material is being used for evaporating moisture. The temperature of the material does not increase any further but remains constant. This is the beginning of the constant drying rate period.

During the constant drying rate period, evaporation takes place from the surface of the solid. The drying rate remains constant for as long as the moisture in the interior of the solid arrives fast enough to keep the surface above the maximum hygroscopic moisture content. The vapour that is released must be transported to the bulk of the drying medium. The drying rate is therefore controlled largely by the external heat and mass transfer, as governed by the physical properties of the medium, its velocity and its temperature.

As drying progresses, the mean moisture content of the wet material drops linearly with time until it reaches a point called the upper critical moisture content. At this point the rate of moisture transfer from the interior of the solid is no longer sufficient to keep the surface above the maximum hygroscopic moisture content and the rate of drying starts to decrease. The value of the upper critical moisture content depends on the ease of moisture movement through the solid.

During the first falling drying rate period, the surface dries out in patches and its temperature starts to rise above the wet-bulb temperature. The drying rate decreases because of the lower temperature difference between the surface and the medium, and also because part of the evaporative surface is already dry. Nevertheless, the drying rate continues to be influenced by the external conditions because most evaporation takes place from the surface. Eventually, when the surface of the solid is completely dried out, evaporation begins to



take place within the pores of the material. This marks the start of the second falling drying rate period; the moisture content at this stage is called the lower critical moisture content.

During the second falling drying rate period, the rate of drying is controlled by the rate of moisture (liquid and vapour) transfer inside the solid, and not by external conditions. The surface temperature continues to rise until it reaches the temperature of the drying medium (dry-bulb temperature).

Drying stops when the moisture content reaches the equilibrium moisture content, which is the lowest moisture content to which a material can be dried under specific conditions of temperature and humidity. At the equilibrium moisture content, moisture is trapped in interstices and pores or adsorbed on surfaces and exhibits a vapour pressure that is lower than that of the pure liquid at the same temperature.

Typical drying rate curves for the drying of clay in steam and in air [H10] are shown in Figure 5. The curves clearly show a constant drying rate period and a falling drying rate period for both media. Under the prevailing conditions ( $T_g = 300\text{ }^{\circ}\text{C}$ ;  $\dot{m} = 4\,500\text{ kg m}^{-2}\text{ h}^{-1}$ ), the drying rate in steam is higher than that in air except during the last stages of drying when the moisture content is very low. In addition, the critical moisture content is lower when drying in steam. This means that the constant drying rate period - during which drying rates are high - is prolonged. As a consequence the total drying time in steam is significantly shorter.

The effect of temperature is further illustrated by the data of Trommelen and Crosby [T2] who investigated the drying of droplets of solutions suspended in a gas stream. Their results for a solution of coffee extract are presented in Figures 6 and 7. The ratio of the actual to the initial moisture content is recorded as a function of time. (The results cannot be presented in the form of a drying rate as a function of time because the decrease of the surface area of the droplet with time was not recorded.)

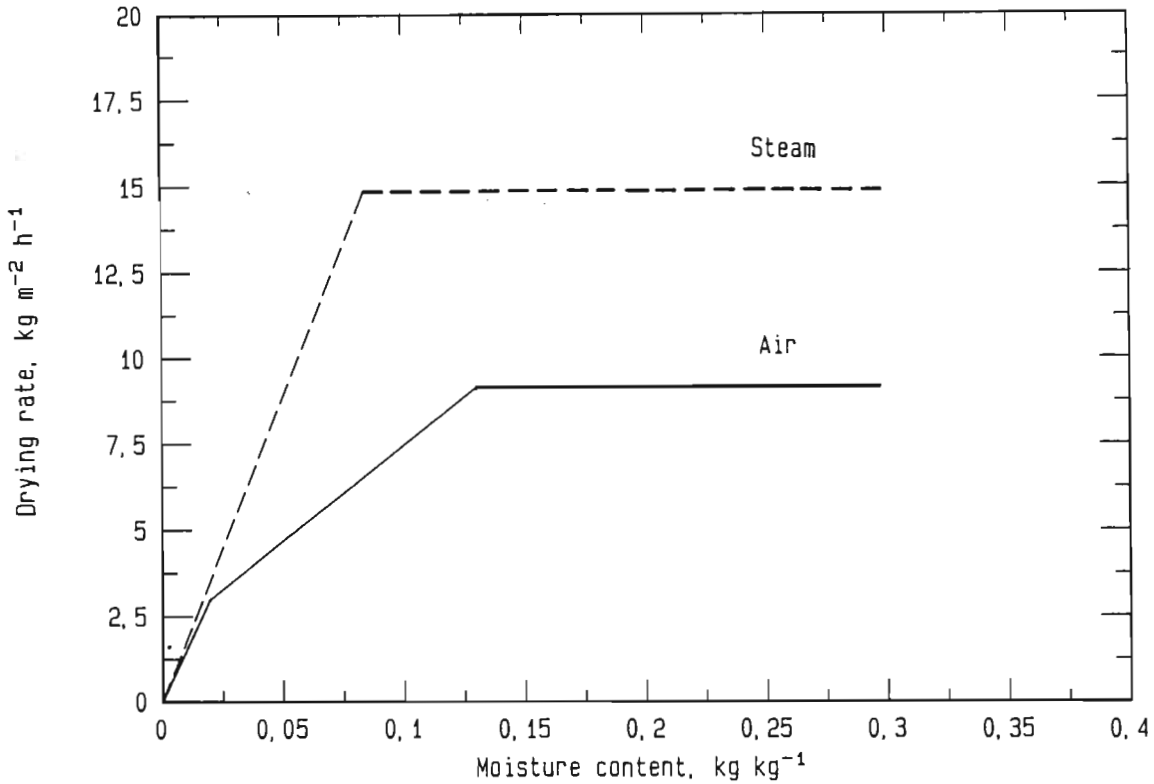


Figure 5: Drying rate curves for clay in air and in steam [H10]

At 145 °C, drying in air occurs faster than in steam. The time required for total drying is 40 % shorter in air. Qualitatively, one can see that, in this case, drying is faster during the constant drying rate period. For the later stages of drying, no conclusions can be drawn from these figures. At a temperature of 250 °C, drying occurs faster in steam than in air. The total drying time is shorter by 25 % and the drying rate during the constant drying rate period is higher in steam.

The above two examples clearly illustrate the dependence of the relative drying rates in steam and air on the operating conditions. The data also indicate other differences in behaviour during the constant and falling drying rate periods. It is therefore useful to investigate the drying characteristics in each drying regime separately.

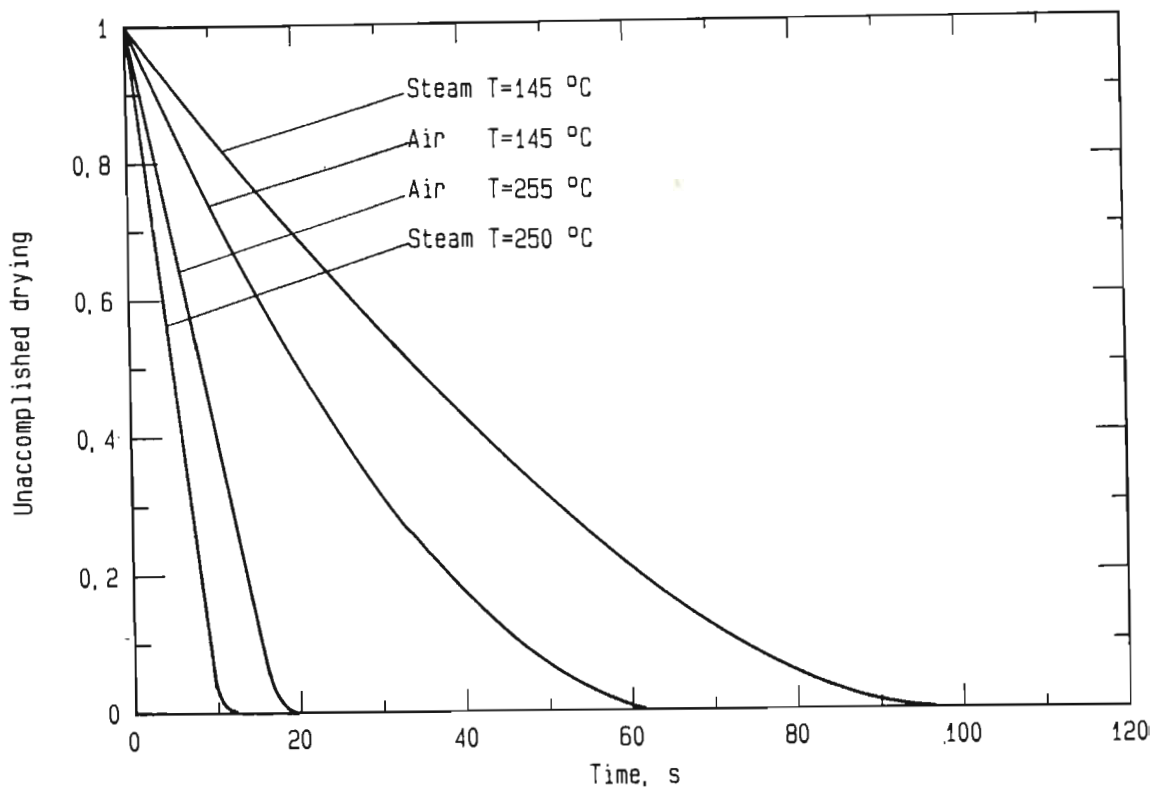


Figure 6: Drying rates of a droplet of coffee extract  
in air and in steam [T2]

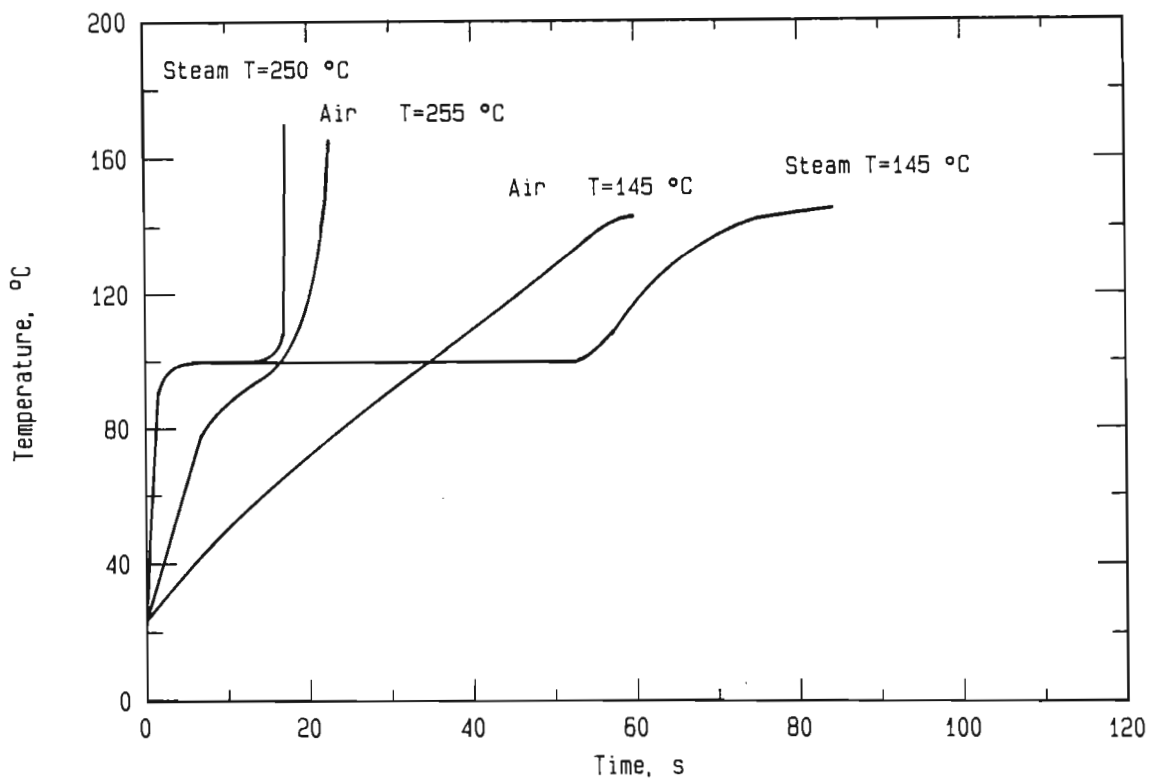


Figure 7: Temperature evolution of a droplet of coffee extract  
during drying in air and in superheated steam [T2]

### 2.3.1 Heating-up period

In steam drying, the material is heated up by condensation of steam on the surface of the material. The amount of condensation depends on the superheating of the drying steam, on the physical properties of the material and on its moisture content. The steam that condenses increases the moisture content of the material and must again be removed during the course of drying. As condensation occurs on the surface of the material, it is generally easily removed and is not seen as a drawback to steam drying. Furthermore the condensation keeps the surface wet and prevents case hardening, a situation that often occurs with organic materials and in which the outer surface of the material closes and so prevents the moisture inside from reaching the surface. This considerably reduces the kinetics of drying. In order to prevent excessive condensation in steam, the material must be preheated.

In air drying, condensation does not occur unless the humidity of the drying air is close to saturation, a case that does not occur in practice.

### 2.3.2 Constant drying rate period

As mentioned before, the drying rate during the constant drying rate period is governed by external processes of heat and mass transfer, the mechanisms of which are discussed below. Furthermore, in this section, literature data from experimentally determined drying rates are discussed to illustrate important differences in heat and mass transfer characteristics that must be considered when choosing between drying in air and drying in superheated steam. Before these rates of drying are discussed, the data are examined in terms of semi-empirical correlations of transfer coefficients.

#### *2.3.2.1 Fundamental mechanisms of drying in air and in steam*

The fundamental difference between air drying and steam drying during the constant drying rate period lies in the mechanisms by which these

drying processes take place. In air, drying takes place by evaporation, whereas in steam, drying takes place by boiling.

Evaporation means that drying can occur at temperatures below the boiling point. The vapour pressure of the liquid is below the system pressure. The speed of drying is governed by two driving forces, as represented in Figure 8. The first one is based on mass transfer from the evaporative surface to the bulk of the drying medium, and the second one on heat transfer from the drying medium to the evaporative surface.

The drying medium of air is unsaturated and hence not in equilibrium with the evaporating moisture. In its effort to reach equilibrium, the air absorbs the evaporating moisture and increases its humidity.

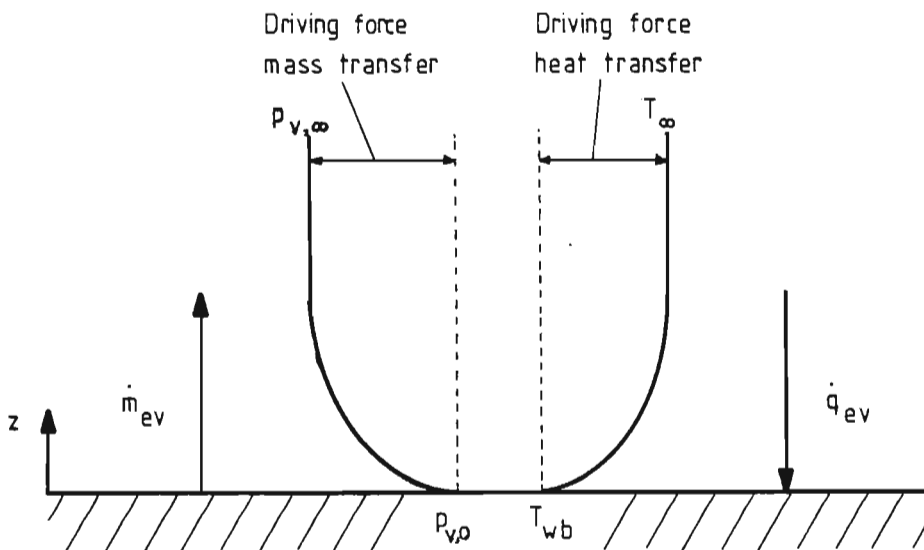


Figure 8: Driving forces in air drying

Heat must be supplied to the liquid moisture to enable it to change into vapour. This heat is drawn from the drying medium. A kinetic equilibrium is reached when the heat supplied by the drying medium is equal to the energy required for evaporation. The driving force for heat transfer is the temperature difference between the air and the evaporative surface. The driving force for mass transfer is the difference in saturation between the evaporative surface and the bulk of the drying medium. If one assumes that the air at the surface is

saturated, then its humidity is determined solely by its temperature. The higher the temperature, the higher the humidity and the greater the driving force for mass transfer, but the lower the driving force for heat transfer. For given air conditions (temperature, humidity) there is one temperature at which kinetic equilibrium is reached. This is called the wet-bulb temperature and it is dependent on the humidity and the temperature of the air. The higher the humidity or the temperature, the higher the wet-bulb temperature.

In Figure 9 temperature and pressure profiles are presented for steam drying. The vapour pressure of the liquid moisture is equal to the system pressure and drying occurs by boiling. The drying rate is governed by one mechanism only, that is heat transfer from the steam to the drying surface. There is no resistance to mass transfer and all the heat that is supplied to the surface is used for drying. The boiling point is independent of the steam conditions and is a function of the system pressure alone.

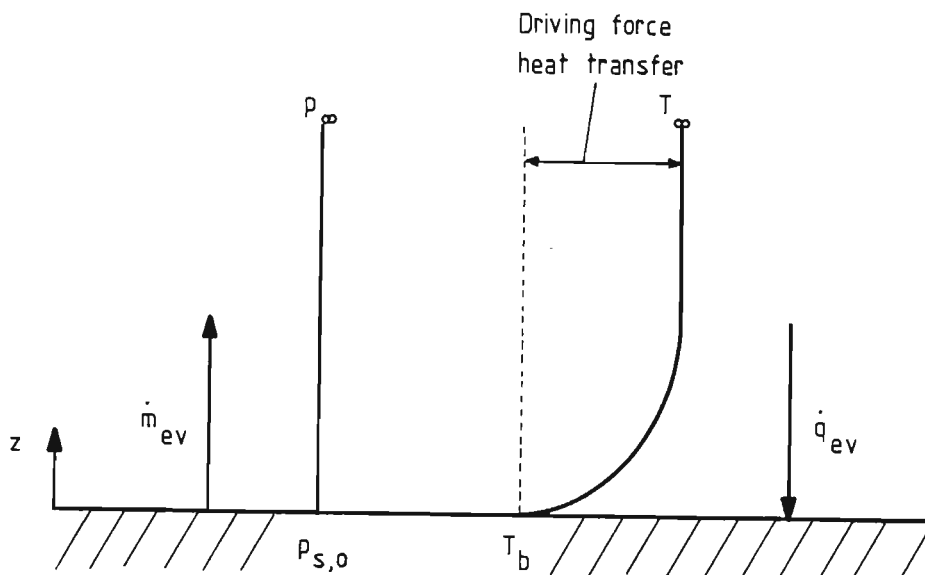


Figure 9: Driving forces in steam drying

### 2.3.2.2 Convective heat transfer

Drying rates are often determined experimentally by using either pan dryers or suspended droplets. In pan drying, the sample rests in a pan placed in the centre of a duct through which the drying medium is blown by a fan. Evaporation can be determined by measuring the mass loss of the sample or the humidity increase of the drying medium.

In the suspended droplet dryer, a droplet is produced at the tip of a tube and is dried in a vapour stream. The mass loss of the droplet and its temperature are recorded as functions of time.

Hyodo and Yoshida [H10] have correlated the data of a number of authors in terms of the Colburn  $j$ -factor. The data are shown in Figure 10 and the correlations are summarized in Table 2.

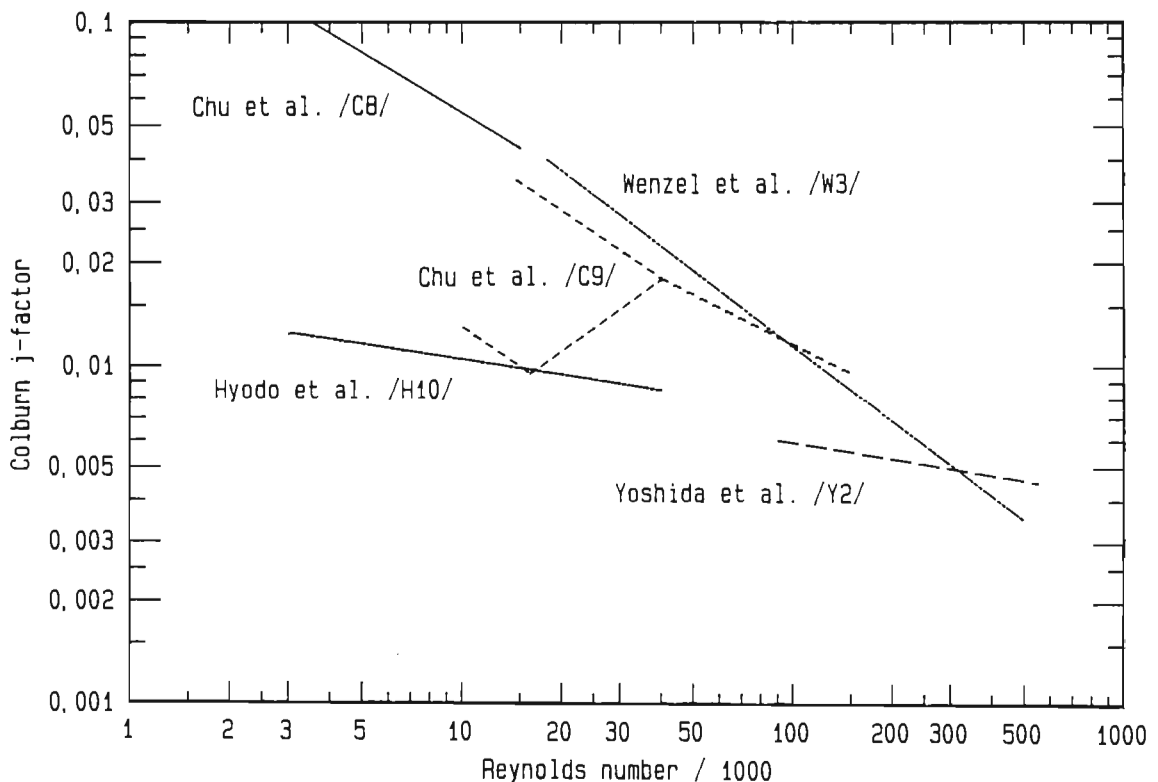


Figure 10: Literature data of Colburn  $j$ -factor for heat transfer in steam as function of Reynolds number

Table 2: Correlation of drying data in terms of the Colburn j-factor

Author	Correlation for j-factor
Wenzel and White [W3]	$18,8 \text{ Re}^{-0,57}$
Chu <i>et al.</i> [C8]	$10,5 \text{ Re}^{-0,65}$
Chu <i>et al.</i> [C9]	$19,6 \text{ Re}^{-0,46}$
Hyodo and Yoshida [H10]	$0,0673 \text{ Re}^{-0,2}$

Published results differ considerably, especially at low Reynolds numbers. Chu *et al.* [C9] showed that a long calming section upstream of the pan is essential to create laminar or transitional flow of the drying medium over the pan. In tests without the calming section, the experimental results fall on a line that represents an extension of the turbulent flow line. In tests in which the calming section was much longer than the length of the pan, a distinct transition region was found. This shows that if the calming section is too short, a pseudo-turbulent flow is obtained; even though the Reynolds number indicates laminar flow, the flow pattern is turbulent.

In forced convective heat transfer, a laminar flow layer is formed at the beginning of the pan. This layer increases in thickness along the length of the pan and collapses after a certain length to generate a turbulent flow layer. For Reynolds numbers lower than the critical Reynolds number, the laminar layer exists over the whole length of the pan. For above-critical Reynolds numbers, the laminar layer exists over the first part of the pan and is then replaced by a turbulent layer. It is impossible to specify the value of the critical Reynolds number, as this depends strongly on the shape of the pan's edge, the roughness of the sample being dried and the ratio of the height of the duct to the depth of the sample [W3]. The effect of the channel boundaries on the flow of vapour around the pan is shown in Figure 11.

At turbulent Reynolds numbers, the experimental data do not show such a wide discrepancy. This indicates that in a turbulent regime the data are less dependent on the geometry of the experimental system.



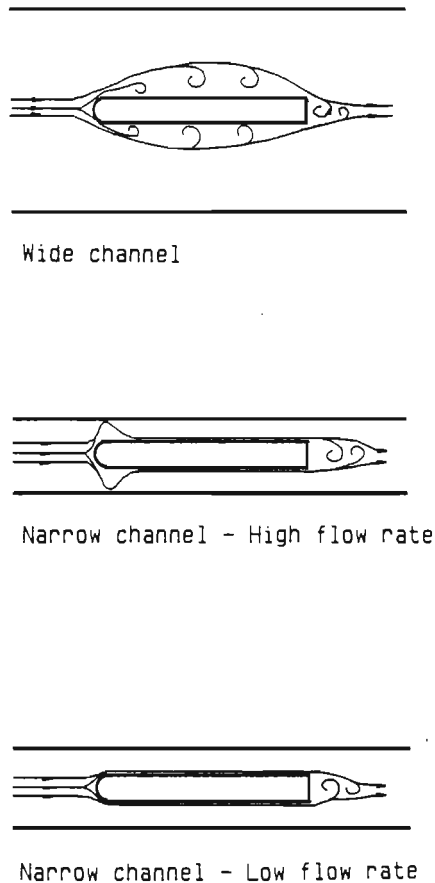


Figure 11: Effect of channel boundaries on flow pattern through ducts [W3]

In suspended-droplet investigations, there is better agreement. The heat transfer coefficients are normally correlated in terms of the Nusselt number and the Reynolds number. The general equation, called the Ranz and Marshall equation, may be written as follows:

$$Nu = C_1 + C_2 Re^{0,5} pr^{0,33} \quad (1)$$

The constant  $C_1$  represents the Nusselt number at zero flow and for spheres has a value of 2. The constant  $C_2$  is determined experimentally.

Toei *et al.* [T1] investigated the evaporation of water drops into superheated steam and into mixtures of steam and air for flows in the range  $9 < Re < 120$ . They obtained a value of 0,65 for  $C_2$ .

Trommelen and Crosby [T2] carried out an extensive study of the evaporation of various aqueous suspensions and solutions into air and steam. They recommend a value of 0,6 for  $C_2$ .

In the Reynolds number range for which the above correlations are valid ( $9 < Re < 120$ ), the calculated Nusselt numbers for  $C_2 = 0,6$  and  $C_2 = 0,65$  vary by a maximum of 6 %. This variation is within the limits of experimental error, so the difference in the reported values for  $C_2$  is considered to be insignificant.

Lee and Ryley [L2] studied the evaporation of non-spherical droplets of water into superheated steam. They reported a value of 0,74 for  $C_2$ . This correlation is applicable only to non-spherical droplets and should not be compared with those for spheres, because the flow profile around the droplet is different.

In the above examples, heat transfer coefficients and flows have been represented by dimensionless groups. This practice serves to eliminate differences in transfer rates resulting from differences in physical properties and flow geometries. For example, at the same mass flux  $\dot{m}$ , where

$$\dot{m} = \rho u \quad (2)$$

the Reynolds numbers ( $Re = u d \rho \eta^{-1}$ ) in air and steam are different. We have:

$$\dot{m}_s = \dot{m}_a \quad (3)$$

or

$$\rho_s u_s = \rho_a u_a \quad (4)$$

The ratio of the Reynolds numbers in the two media is then:

$$\begin{aligned} \frac{Re_s}{Re_a} &= \left( \frac{\rho_s u_s}{\eta_s} \right) \left( \frac{\eta_a}{\rho_a u_a} \right) \\ &= \frac{\eta_a}{\eta_s} \end{aligned} \quad (5)$$

Because the dynamic viscosity of steam is lower than that of air at the same temperature and pressure (150 °C; 100 kPa;  $\eta_a/\eta_s = 1,68$ ), the Reynolds number for steam is higher. It is possible therefore that at the same mass flux, heat transfer in steam may take place in the turbulent regime, and in air in the laminar regime.

#### 2.3.2.3 Evaporation rates

Several investigators have compared the kinetics of evaporation in air and in superheated steam for the constant drying rate period. Flat pans [C8-9,W3], wetted wall columns [Y2] and suspended droplets [M8,T3] were used. For flat pans and wetted wall columns, higher drying rates were generally found in superheated steam. Only for low temperatures were drying rates higher in air. For suspended droplets, steam drying rates were higher above 220 °C.

Chu *et al.* [C9] investigated the drying of sand in several superheated-steam/air mixtures. The authors correlated the drying rates during the constant rate period with the mass flow rate of the gas over a range of temperatures. At mass flow rates above 1,22 kg m<sup>-2</sup> s<sup>-1</sup> drying rates for superheated steam were higher than those for air even at low temperatures (air, 138 °C; steam, 121 °C).

More data were reported by Wenzel and White [W3] who investigated the drying of sand in pan dryers during the constant drying rate period. They used superheated steam over a range of temperatures, mass flow rates and pressures. They compared their results with those for the evaporation of water.

Evaporation rates for the drying of sand were found to be 20 % higher than those for evaporation from a pan of water. This was explained in terms of the roughness of the sand surface which both promotes turbulence and has a larger evaporative interphase compared with a flat surface. Nevertheless the drying rate curves for evaporation of water and drying of sand follow the same pattern during the constant rate period. This is to be expected because drying rates during the constant rate period are governed by external conditions of heat and mass transfer. The temperature of the drying surface is constant and

equal to the temperature of a liquid surface under the same conditions. It is therefore concluded that evaporation from a liquid surface can be used to simulate drying during the constant drying rate period.

Wenzel and White [W3] found the evaporation of water to be faster in steam than in air. In both media heat is transferred by convection from the gas to the water surface and to the outer surface of the pan. The heat transferred to the water surface is immediately used to vaporize the water. In steam drying the temperature of the water is at the boiling point. The heat transferred to the walls of the pan vaporizes the water close to it. The evaporated water rises in the form of bubbles. The boiling heat transfer coefficient is very high and consequently the heat transfer resistance is very low.

In air drying, the water is at the wet-bulb temperature (i.e. below the boiling point) and the heat that is conducted through the pan walls must be transferred through the water to the surface before evaporation can take place. This resistance to heat transfer is not negligible. The higher evaporation rates in steam can therefore be attributed to the higher heat transfer through the pan walls. Wenzel and White [W3] did additional experiments with well-insulated pans but again found higher evaporation rates in steam.

Chu *et al.* [C8] investigated the evaporation rates of water, 1-butanol and benzene. The evaporation rates of these liquids into their superheated vapours were compared with data for the evaporation of the same liquids into air obtained by other authors. It was again found that the relative drying rates were temperature-dependent. For example, the evaporation of water into steam was faster than into air only for temperatures of the drying medium higher than 125 °C; for temperatures higher than 100 °C, the evaporation of benzene into its superheated vapour was faster in steam than in air. The results are presented in Figures 12 and 13.

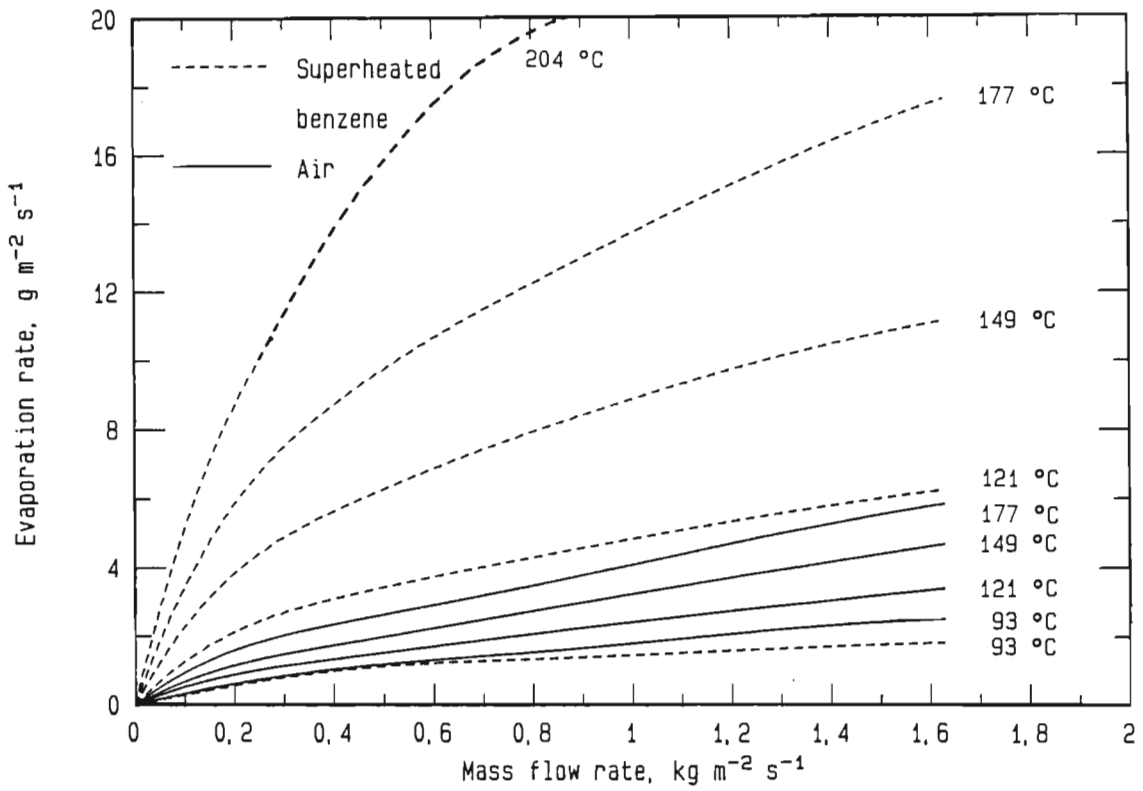


Figure 12: Drying rates during evaporation of benzene into air and into superheated benzene [C8]

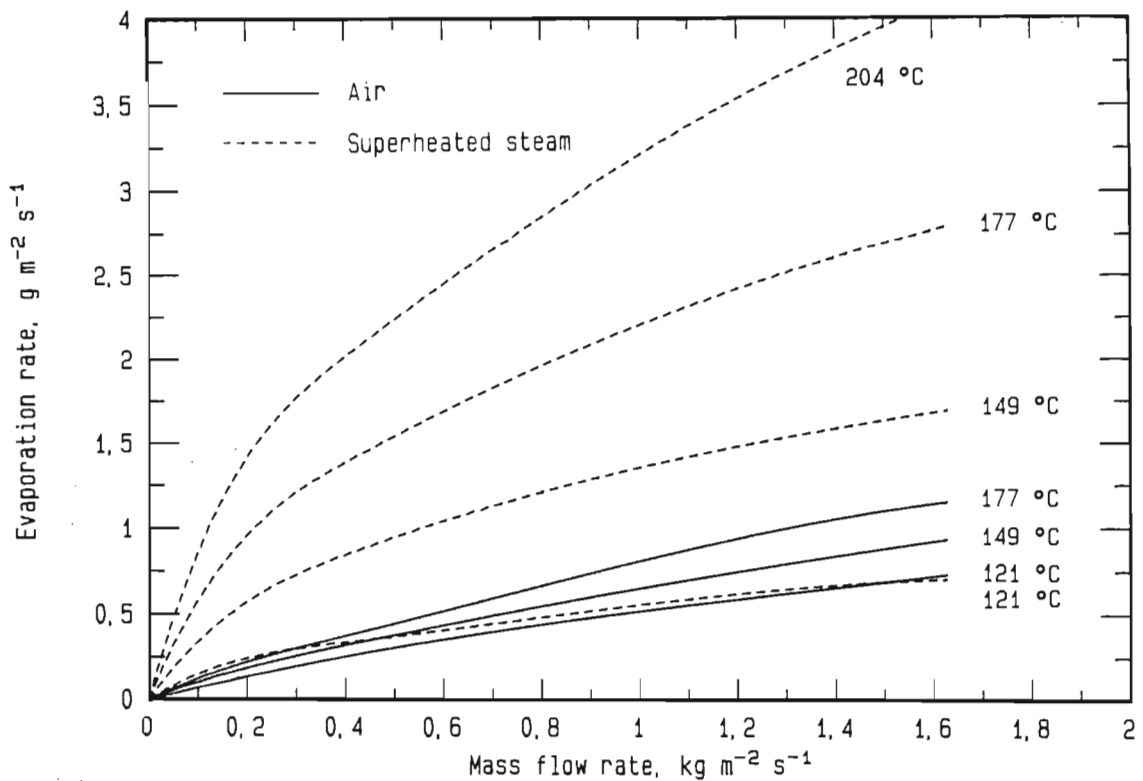


Figure 13: Drying rates during evaporation of water into air and into superheated steam [C8]

#### 2.3.2.4 Inversion temperature

The experimental studies have indicated that the relative rate of evaporation in air and in steam is dependent on gas temperature and velocity. In an attempt to quantify this phenomenon, Yoshida and Hyodo [Y2] measured the evaporation rate of water into air, humid air and superheated steam. The tests were done on a wetted wall column in which the convective heat transferred to the water could easily be measured and where errors due to radiative and conductive heat transfer were negligible. The inlet temperature, flow rate and humidity of the gases were varied. The results are qualitatively presented in Figure 14.

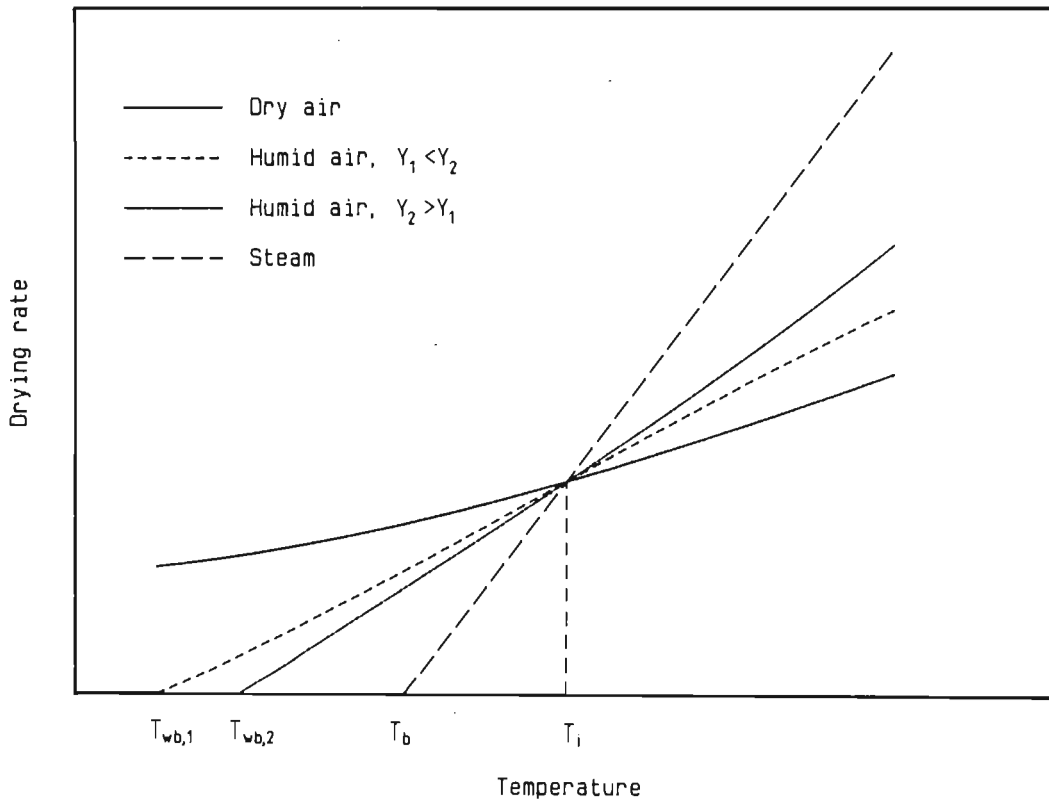


Figure 14: Inversion temperature

The diagram can be divided into two regions. At low temperatures, evaporation takes place faster in dry air than in superheated steam; the higher the humidity of the air, the lower the drying rate. As the temperature is increased, however, the drying rates in steam and in humid air increase relative to that in dry air. Eventually a temperature - called the inversion temperature - is reached at which the drying rates are the same, independent of the humidity. Above the inversion temperature, drying occurs faster in steam than in air. The

value of the inversion temperature was found to vary with the flow rate of the drying medium; the higher the flow rate, the lower the inversion temperature. Yoshida and Hyodo [Y2] give values of 160 °C and 176 °C for gas velocities of 15 m s<sup>-1</sup> and 5 m s<sup>-1</sup> respectively. The inversion point may also be influenced by surface conditions of the evaporating liquid and is dependent on the properties of the material being dried.

A theoretical explanation of the inversion temperature was not given in the paper. However, the Ranz and Marshall equation (Equation 1) predicts higher heat transfer coefficients in steam than in air. Another important parameter in determining the evaporation rate is the driving force for evaporation, that is, the temperature difference between gas and liquid. At low temperatures, close to the boiling point, the driving force for superheated steam drying is significantly lower than for air drying. This is because the temperature of the drying surface is at the wet-bulb temperature for air drying and at the boiling point for superheated-steam drying. The higher the temperature of the drying medium, the smaller the difference in driving force becomes.

The evaporation rate during the constant rate period can be represented as the product of the heat transfer coefficient and the temperature driving force:

$$\dot{m}_{ev} = \frac{h \Delta T}{\Delta h_v} \quad (6)$$

Because the temperature difference between drying medium and product is lower in steam than in air, the evaporation rate in steam is lower than indicated by the ratio of heat transfer coefficients.

Danilov and Leonchik [D1] compared the drying rates in air and in steam on a theoretical basis. He expressed the evaporation rate by the difference in chemical potential between the evaporative surface and the bulk of the drying medium. His approach was based entirely on the mass transfer and did not take into account the heat transfer. The wet-bulb temperature of air was fixed at 60 °C. Danilov found an inversion temperature at which the driving force in steam becomes

greater than the driving force in air. However, for a complete theoretical explanation of the inversion temperature, heat and mass transfer must be considered simultaneously, as these processes determine the wet-bulb temperature.

Nomura [N1] presents a mathematical model to determine the inversion temperature for the evaporation from a horizontal plate. If heat effects due to radiation are neglected, then the locus of the inversion temperature does not change with the mass flow rate of the drying medium. If radiation is considered, the locus of the inversion temperature is shifted to lower temperatures when the mass flow rate is increased. The theoretical results were confirmed by experimental use of a closed-circuit dryer.

If a dryer is operated at temperatures below the inversion temperature, the rate of recirculation of the humid exhaust air is limited because the drying rate decreases as the humidity increases [Y2]. This is not a constraint above the inversion temperature, because the drying rate is then higher in humid air than in dry air.

### 2.3.3 Critical moisture content

The first (upper) critical moisture content that marks the end of the constant drying rate period is not only a function of the drying material, but also a function of the drying rate during the constant rate period.

During the constant rate period, liquid transferred through the body of the material is evaporated from the surface. As long as the surface remains wet, the drying rate stays constant. Because the internal moisture concentration decreases as drying progresses, the rate of moisture transfer decreases. At some stage, a point is reached where the transfer rate is insufficient to keep the surface above the maximum hygroscopic moisture content. The surface then dries out in patches and the drying rate decreases.

If drying is slow, the liquid has more time to diffuse to the surface, which remains above the hygroscopic moisture content even when



the material has a low mean moisture content. If drying is fast, the surface starts drying out at higher mean moisture contents, and the critical moisture content is consequently also higher. In other words, the higher the drying rate, the higher the critical moisture content.

The mobility of the liquid inside the sample also has an important effect on the critical moisture content. In superheated-steam drying, the surface is at the boiling point of water; in air drying it is close to the wet-bulb temperature. The higher temperature in steam drying promotes the mobility of the liquid and so the critical moisture content is lower [L5]. Therefore the constant rate period is extended in steam drying, and the total drying time is shorter than in air.

#### 2.3.4 Falling drying rate period

Not many experimental data suitable for comparing steam and air drying are available for the falling rate period.

In tests with clay, Yoshida and Hyodo [Y2] found that the second falling rate period did not occur in steam drying, whereas distinct first and second falling drying rate periods were detected when drying in air. A comparison of the rates of drying in steam and in air can be made with the reported data only for a temperature of 300 °C. At this temperature, the drying rate during the falling rate period is distinctly higher in steam drying. This supports the argument that the higher particle temperature in steam drying promotes the mobility of moisture inside the material. Note that during the second falling drying rate period, the drying rate is completely governed by the moisture mobility inside the material. The differences between air drying and steam drying in the falling drying rate period will be discussed in more detail in Sections 4.4 to 4.7.

#### 2.3.5 Evaporation of droplets

The evaporation of droplets is discussed separately, as there the

drying circumstances are different from those in the evaporation from flat surfaces and from wetted wall columns.

#### 2.3.5.1 Droplets of pure water

Trommelen and Crosby [T2] investigated the evaporation of droplets of water in air and in superheated steam to simulate conditions in a spray dryer. For both drying media, the evaporation was described as taking place in two distinct periods:

- an induction period
- a constant temperature period.

The constant temperature period is equivalent to the constant rate period for particle drying. In the case of droplets, however, the rate is not constant as the surface area and diameter are continually changing; this affects both the area available for evaporation and the transfer characteristics between the droplet and the gas phase.

According to Equation 7, the ratio of the heat transfer coefficients for droplets of different diameters is equal to the inverse of the square root of the ratio of the droplet diameters.

$$\frac{h_1}{h_2} = \left( \frac{d_2}{d_1} \right)^{0,5} \quad (7)$$

As the droplet dries, the drying rate (expressed in  $\text{kg s}^{-1}$ ) diminishes because the evaporative interface diminishes. However, because the heat transfer coefficient increases with decreasing diameter, the specific drying rate (expressed in  $\text{kg m}^{-2} \text{s}^{-1}$ ) increases as the droplet dries. This means that a constant drying rate period does not occur for the evaporation of droplets.

During the induction period, the temperature of the droplets rose from the initial temperature to the equilibrium temperature of the system at which it stayed during the constant temperature period. As shown in Figure 15, the equilibrium temperature in superheated steam corresponds to the boiling point of water at the pressure of the system. In air drying this temperature is close to the wet-bulb

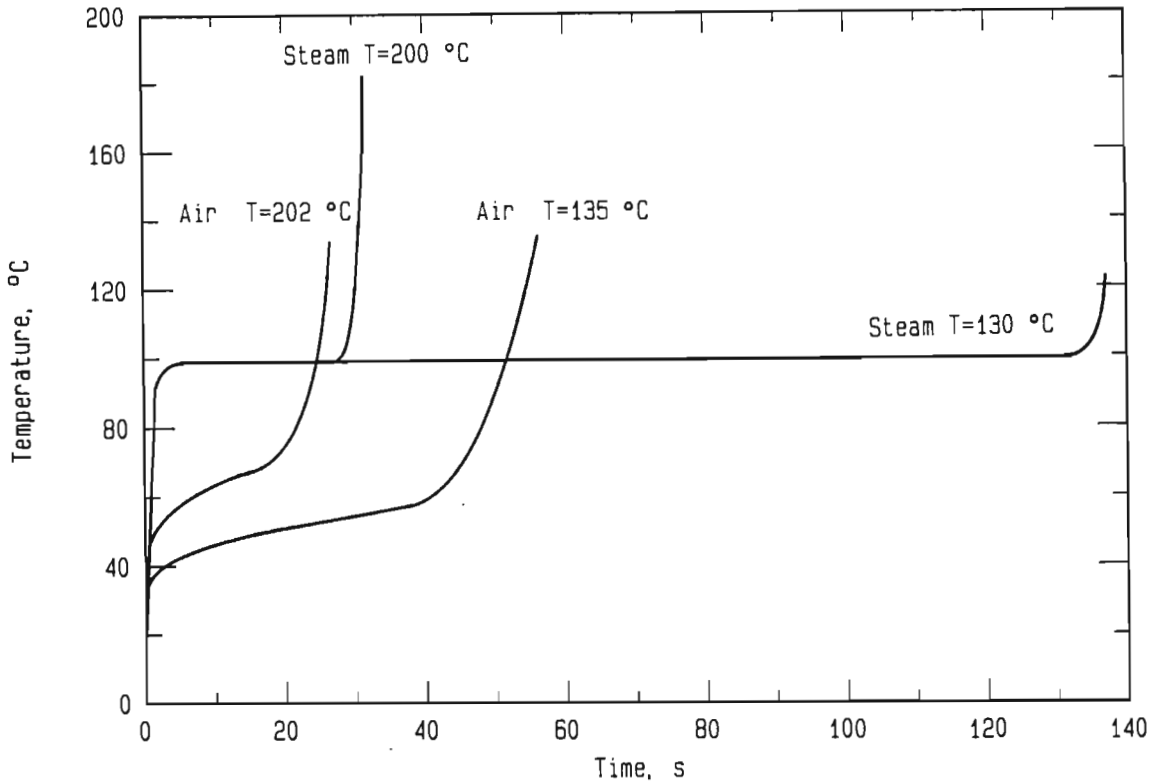


Figure 15: Temperature evolution of a droplet of water during drying in air and in superheated steam [T2]

temperature. The difference between droplet temperature and wet-bulb temperature results from the radiative and conductive heat transfer to the droplet.

The evaporation rates increased from their initial value to a maximum at the beginning of the constant temperature period. As the droplet dries, it gets smaller and the evaporative surface shrinks. Therefore, during the constant temperature period the rate of evaporation continually decreased. The evaporation data are shown in Figure 16.

For both drying media, evaporation increased with the velocity and temperature of the drying medium. The difference in evaporation rates between air and steam decreased with increasing temperature. The highest temperature used in the investigations by Trommelen and Crosby [T2] was 200 °C. Even at this temperature, the evaporation rate remained higher for air than for steam.

In the tests by Trommelen and Crosby, the temperature of the drying medium was kept constant. In a spray dryer, however, the droplet is

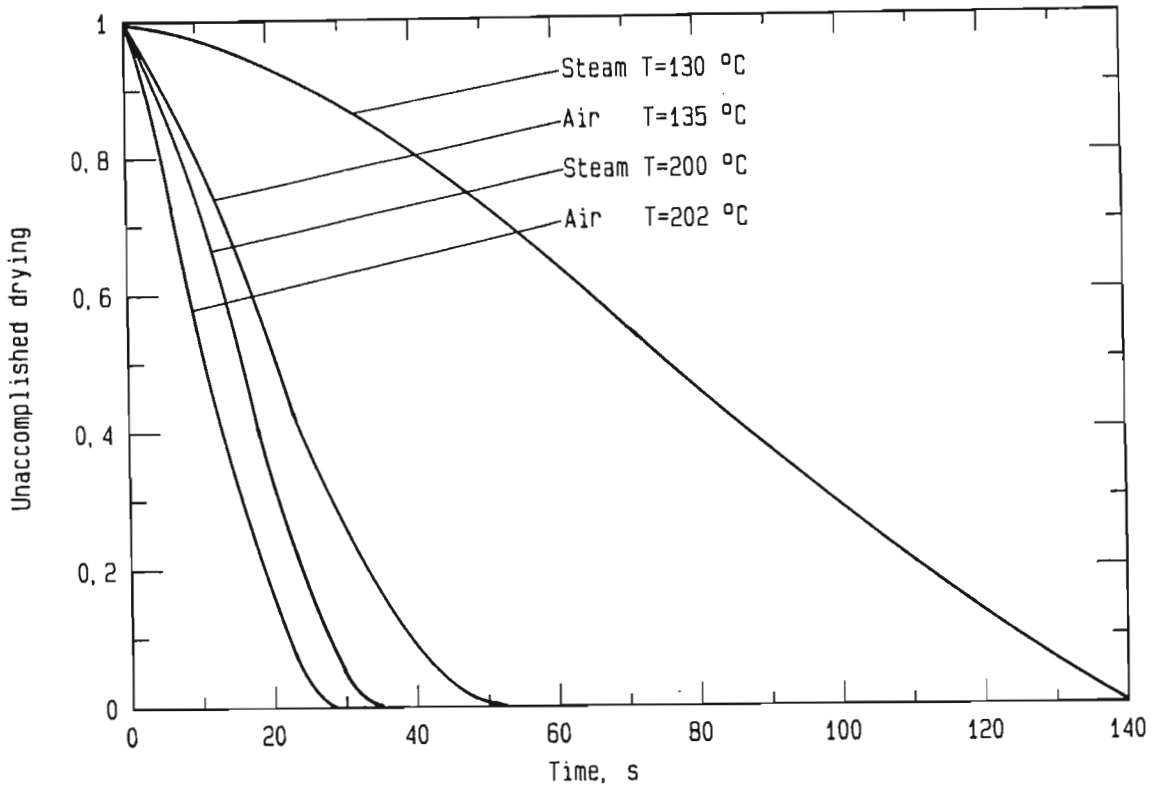


Figure 16: Drying rates of a droplet of water in air and in superheated steam [T2]

exposed to a descending temperature as it moves through the dryer. Crowe *et al.* [C10] developed a mathematical model to study this phenomenon in air and in steam. They found that for droplets of an initial diameter of 200  $\mu\text{m}$  and an inlet temperature of the drying medium of 200 °C, drying times were 75 % shorter in air than in steam. The explanation for this was found by studying the temperature evolution of both droplet and drying medium during their contact period. The temperature of the droplet during the constant drying rate period is at the boiling point (100 °C at 100 kPa) in steam drying as compared to the wet-bulb temperature (for most drying operations around 50 °C) in air drying. The energy for heating the droplets up and for evaporating the moisture is delivered by the drying medium. Due to this thermal coupling, the temperature of the drying medium decreases. Because the heat capacity of steam is higher (roughly double) than that of air, the temperature of the steam decreases less than that of air for the same mass flux. Crowe *et al.* calculated that the temperature of steam would fall to 150 °C and that of air to 90 °C. This means that the temperature difference between drying

medium and droplet is similar in air drying and in steam drying. Because of higher heat transfer coefficients in steam, the drying rates are higher.

In superheated-steam drying, a certain amount of condensation occurs on the droplet during the induction period. The amount of condensation depends on the degree of superheating and on the initial temperature of the droplet. An unsupported droplet initially at 30 °C will experience a maximum increase in weight of about 12,5 % when exposed to steam at 150 °C at atmospheric pressure [M8]. This means that the initial moisture content of the droplet is increased before drying starts. The steam that condenses on the drop during the induction period has to be evaporated again during the course of drying.

#### *2.3.5.2 Droplets of solutions*

Such evaporation is of interest, as it offers additional insight into the differences between drying in air and in steam.

In his study of the evaporation of solutions, Moyers [M8] divided the drying cycle into four parts:

- induction period,
- evaporation period,
- evaporation/crystallization period, and
- heating-up period.

These periods are discussed in terms of the temperature of the core of the droplet, as shown in Figure 17.

#### Induction period

The drying behaviour of the solutions during the induction period is the same as that of pure water droplets.

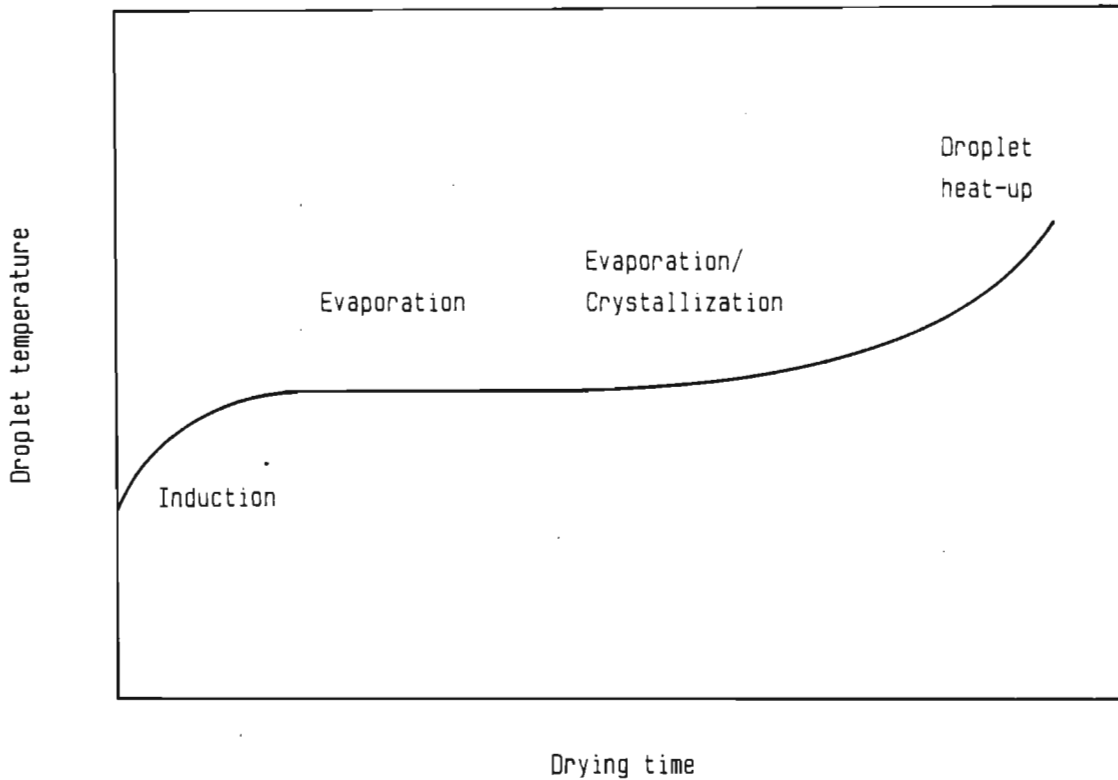


Figure 17: Drying periods for droplets of solution

#### Evaporation period

Solutions do not exhibit a constant temperature period; instead, the temperature rises throughout the drying period. This is because as the droplet dries, the solids concentration increases and the water vapour pressure decreases. In superheated steam, the temperature rise is less than in air drying, and is equivalent to the change in the boiling point elevation as the droplet becomes more concentrated.

#### Evaporation/crystallization period

A solid crust is formed around the liquid core of the droplet. The liquid part of the droplet stays at a constant temperature during this period, because its concentration is constant. The crust develops a resistance to heat and mass transfer and the evaporation rate decreases. The droplet temperature in steam drying is higher than in air drying. As solubility generally increases with temperature, the

crystallization period is retarded and the evaporation period extended. Although evaporation was normally faster in air during the evaporation period, complete drying was sometimes faster in steam. The reasons are firstly the extension of the evaporation period, and, secondly, the greater permeability of the crust when formed in steam. Around 200 °C and for the same linear velocity of the drying medium, the evaporation rates are the same.

#### Heating-up period

During the heating-up period the particle, now dry, quickly reaches the gas temperature.

#### 2.3.6 Drying theories

The constant drying rate period can be modelled relatively easily, as the processes of heat and mass transfer from gases to solids are well known. A drying model that covers the falling drying rate period as well is more difficult to develop. Indeed, the mechanisms of heat and mass transfer inside the porous body must be described by physical formulas. The inner pore structure of a rigid capillary porous body consists of a complex net of capillaries that change in diameter and shape, and are interlinked and very tortuous. Therefore it is understandable that the modelling of the flow of heat and mass through such a matrix is not an easy task.

The moisture transfer inside the porous material can be attributed to different mechanisms [K3]:

- Vapour diffusion through the inert gas in the pores
- capillarity flow in the liquid phase through the pores
- Flow caused by a pressure gradient in the liquid and vapour phases
- Flow caused by a vaporization-condensation sequence
- Flow caused by gravity (mainly in coarse-pored particles)
- Flow caused by shrinkage
- Flow caused by an electrical potential (electro-osmosis)
- Flow caused by a temperature gradient (thermodiffusion)

Although more than one of these mechanisms of flow may be effective at one time, only one predominates in a solid at any given time during drying. However, a different mechanism may predominate at a different time during the drying process. These mechanisms have been included partially in the drying theories. The drying models can be divided into several categories according to the principles they are based on:

- Liquid diffusion theory
- Capillarity theory
- Theory of combined vapour diffusion and liquid capillarity motion
- Theory embodying the principles of irreversible processes
- Evaporation-condensation theory
- Theory of evaporation from a front withdrawing into the body

Some of the theories may be applied to the whole drying process, whereas others are applicable only to very distinct periods in the drying process [K3].

#### Liquid diffusion theory

This theory was first proposed by Sherwood [S6] who postulated that the mass transfer rate is proportional to the gradient in moisture content. The advantage of this assumption is the convenience of employing the analogy in heat and mass transfer and the availability of mathematical solutions for the equations [C3]. The gravitational forces and capillary forces are neglected. Unfortunately it was not possible to fit the theoretically predicted moisture profiles to the measured values if a constant diffusivity was assumed. The diffusional theory describes the movement of moisture from a high to a low moisture content. However, it has been shown [C3] that, when the right differences in pore space exist, moisture can flow from a low concentration to a high concentration. So it became obvious that if Sherwood's diffusion theory fits experimental data, this is generally accidental [B7].



### Capillarity theory

This theory was first proposed by Buckingham in 1907 [B10]. He introduced the concept of capillary potential and postulated the mechanism of unsaturated capillary flow. Liquid moisture is moved to the evaporative interface by forces based on the surface tension. The model was of the same form as Darcy's law for fluid flow through porous media, but the hydraulic conductivity was found to be a function of the moisture content of the solid [N3]. In the later stages of drying, when the capillary forces cease to act, this theory fails, unless the hydraulic conductivity is changed accordingly. It is however not useful to describe a phenomenon using wrong assumptions, even though the end-result may be correct.

### Theory of combined vapour diffusion and liquid capillary motion

This theory was introduced independently by Krischer [K9] in engineering and by Phillip and de Vries [P2] in soil science. Liquid moves by capillarity through the pores of the solid, while vapour flows by diffusion through the empty pores. This theory is more plausible than the simple capillary theory, as in the later stages of drying the capillary motion of the liquid is strongly reduced and the moisture movement occurs mainly in the vapour phase. The two phases, liquid and gas, are treated separately, so that two sets of conductivities have to be determined. These conductivities depend strongly on the moisture content, the temperature and the nature of the solid.

### Theory embodying the principles of irreversible processes

This theory was developed by Luikov [L5] and is based on the application of the methods of the thermodynamics of irreversible processes to the case of internal heat and moisture transfer during drying. Liquid and vapour moisture move on the basis of the same driving forces, namely moisture content gradient, pressure gradient and temperature gradient. Luikov stresses the importance of the influence of the temperature gradient on the moisture movement and shows that moisture can flow against the moisture content gradient if the appropriate temperature gradient exists.

### Evaporation-condensation theory

In the evaporation-condensation theory, the migration of moisture takes place entirely in the gaseous phase. This theory can definitely only be applied to the later stages of drying, as it excludes the mechanism of capillary motion [H4].

### Theory of evaporation from a front withdrawing into a body

This theory is based on the assumption of evaporation from an internal interface parallel to the surface. The evaporating plane retreats into the porous material as drying proceeds. The region above this plane contains dry solids and vapour, whereas the region below contains solid, liquid and vapour. Each region is characterized by an effective thermal conductivity and molar diffusivity. There is evidence of the existence of such an interphase, even though the limits of this interphase are not all that strict, but the jump in moisture content takes place over a limited distance.

As Keey [K3] points out, none of the mechanisms of moisture transfer can be used alone in order to describe the drying of porous solids. Depending on the drying stage, different mechanisms prevail. Therefore theories that are built on a single mechanism cannot describe the whole drying cycle, unless the transfer coefficients are allowed to vary drastically with moisture content. The drying process is then being described by a mechanism that is not acting and the purpose of investigating the mechanisms involved in drying is defeated.

The early theories neglected the influence of the heat transfer on the mass transfer and treated the phenomenon of drying isothermally. Today, however, it is accepted that the heat transfer cannot be neglected in the description of the drying process. The inclusion of the heat transfer phenomenon in the drying model increases the degree of difficulty of the solution drastically.

Work was and is being done by many researchers to investigate the influence of a temperature gradient on the mass transfer [C2,K13,L3,P2,P5]. The difficulty in determining suitable transfer coefficients

still limits the incorporation of this phenomenon into practical drying models.

It has also been found that the mechanisms that govern the drying process depend on the drying conditions. In gentle drying at low temperatures, the pressure inside the particle can be assumed to be constant and no pressure gradient exists inside the material. If the drying process is speeded up, moisture evaporates faster inside the material than it can be transported to the outer surface. This creates a pressure buildup, which helps to evacuate the moisture. This phenomenon is dealt with by Krischer and Kröll [K9] and Luikov [L5] but, in general, when the drying theories should be tested on experimental data, this phenomenon was neglected. The importance of moisture transport on basis of a total pressure gradient is shown by Moyne and Degiovanni [M9].

In the drying models, little is taken into account about the transfer of heat through the material. Heat is transferred by conduction, by convection and by evaporation and condensation sequences. The convective component can generally be neglected, as was shown by Luikov [L5]. The heat conductivity is strongly dependent on the moisture content of the body. A study of this was done by Moench [M6]. In general, the heat conductivity is assumed to be constant throughout the body or to vary according to an empirical relation.

The development of a drying model that describes the process as accurately as possible leads to a set of partial differential equations. These equations are highly non-linear and require sophisticated computer hardware and software. Therefore the solution of such models was hampered until fairly recently [T4]. In the past, simplifications were made to the models to put them into a solvable form. Obviously these simplifications also placed a limitation to the models.

Berger and Pei [B5] investigated Krischer's theory assuming constant transfer coefficients. It is obvious that this approach cannot lead to a satisfactory solution, but it gives an indication of the importance of the different transfer mechanisms.

Novak and Coulman [N3] solved their model by taking into account the temperature and moisture content dependence of the transfer coefficients. They tested their model on the drying of sand. The movement of moisture vapour was assumed to take place only by diffusion. As the drying of sand was carried out at low temperatures, this assumption proved to be satisfactory. A more universal model requires the inclusion of transfer effects due to total pressure gradients.

Imakoma *et al.* [I1] developed an isothermal model, in which no parameters need to be determined by drying experiments. Moisture moves in the liquid phase on the basis of capillary pressure gradient, total pressure gradient and by surface flow. Most theories neglect the effect of a total pressure gradient on the flow of liquid moisture and often try to include the movement of adsorbed water in the coefficient for capillary motion. Moisture moves in the vapour by diffusion and by viscous flow. Imakoma *et al.* verified their model by doing drying tests of alumina at relatively low temperatures (81,5 °C). They found that the moisture transfer in the vapour phase is only of secondary importance. During the beginning stages of drying, most of the moisture moves in the liquid phase by capillarity and during the later stages of drying, the adsorbed water flow is predominant. This theory is attractive in so far as the transfer mechanisms are related to fundamental principles of mass transfer. The major drawback is the exclusion of heat transfer effects and of moisture movement by temperature gradient.

Moyne and Degiovanni [M9] developed a model taking into account moisture movement on the basis of a temperature gradient. They tested their model by means of drying tests on a Ytong slab and found that moisture movement on the basis of temperature gradients was negligible. The transfer coefficients that were used were determined theoretically. This theory was also extended to drying in superheated steam by modifying the boundary conditions.

Most of the drying models assume equilibrium between the vapour in the gas phase and the liquid moisture in the pores. Hadley [H2] presents a theory that does not need such an assumption. In the so-called non-equilibrium model, a mass transfer coefficient must be

determined for the local evaporation of moisture. If the moisture content of a material falls far below the critical moisture content, the assumption of equilibrium is no longer valid [B6].

Van Brakel [B7] gives a critical review of the drying models. He states that basically the same type of description is used in all the drying models. The differences arise from the transfer mechanisms that are used to describe the drying process.

The more universal a drying model, the more complex it becomes. As a result, a large number of parameters have to be determined. Transfer coefficients can be determined from purely theoretical considerations, theoretical considerations corrected by empirical functions or from purely empirical functions adapted to measured data. Another problem that arises from complex models is the difficulty in solving a system of partial differential equations (PDE). Even though powerful computer hardware and software are available, standard procedures for solving PDEs cannot be used in the solution. The solution programs have to be 'custom made' and require an extensive mathematical knowledge of the problem. Even then the processing time of these models is very long and they remain of little practical value. This does not mean that these models are of no use at all. They further the knowledge of the mechanisms involved in the drying process and provide the means for simulating the drying process, so that few experimental tests are required.

In this thesis, a model is developed to describe the differences in drying behaviour in air and in steam. The model is based on the principal transfer mechanisms that act during drying. These mechanisms are different in air and in steam. The use of extensive computer hardware and software for the solution of the model was avoided.

### 3. EXPERIMENTAL

Standard equipment for determining drying characteristics in steam is not available. Therefore new equipment and procedures had to be developed. These are described below.

#### 3.1 Physical properties of the drying materials

The material used in the experimental drying tests was selected according to following criteria:

##### Easy fluidization

This study focuses on fluidized bed drying. Therefore the experimental drying material should be easily fluidizable.

##### Sphericity

The drying rates and gas-to-solid heat transfer coefficients will be modelled mathematically. In order to test the models on the experimental data, the external surface of the particles must be determined. This is much easier to do for spherical particles than for angular particles.

##### Narrow size distribution

As mentioned, the external surface of the particles must be measured as accurately as possible. This is most easily done for spherical particles with a narrow size distribution.

##### Diameter around 2 mm

In this study, the gas-to-solid heat transfer coefficient will be measured. The method for calculating it is based on the determination of the temperature profile in the fluidized bed. If the particles are

too small, the temperature profile cannot be measured accurately. Furthermore, for particles larger than 500  $\mu\text{m}$ , a large amount of literature data is available for comparing with the experimental results.

#### High moisture absorption and exhibition of a constant drying rate period

The drying rate curves that will be recorded should cover both the constant and falling drying rate periods. At the temperatures that will be used (up to 275 °C), the drying rates are high and consequently the drying times are short. For the evaluation of the drying data it is desirable that the drying time should be at least a few minutes. After a heating-up period the material should exhibit a constant drying rate period, which is necessary to determine the gas-to-solid heat transfer coefficients. Therefore a material should be chosen that has a high moisture absorption (to give a reasonable drying time) and has an adequate hygroscopicity (so that a constant drying rate period and a falling drying rate period are recorded).

#### Abrasion resistance and temperature resistance up to 275 °C

For an accurate measurement of the drying rates, the material must not degrade at operating temperatures.

#### Rewettability

If the material is rewettable, the amount that is needed for the experimental program can be kept small.

#### Rigidity

The mathematical modelling of the drying process is simplified by choosing a material that does not exhibit any geometric changes during drying.



The selection criteria made it difficult to find suitable materials. Finally alumina and molecular sieve were selected as the most appropriate materials. The physical properties of the materials, as communicated by the manufacturers and as measured, are given in Table 3.

Table 3: Physical properties of the test materials

Property	Alumina	Molecular sieve
Particle diameter, mm	1,63	2,2
Particle density, kg m <sup>-3</sup> *	640,00	1 240,0
Skeletal density, kg m <sup>-3</sup>	3 083,00	2 124,0
Pore volume, cm <sup>3</sup> g <sup>-1</sup>	0,8137	0,2575
Mean pore diameter, nm	11,9	1,5

\*Manufacturer's data

Alumina has fairly large pores and is a non-hygroscopic material. On the other hand, molecular sieve has fairly narrow pores and is a hygroscopic material. Hygroscopic and non-hygroscopic materials represent the two extremes in the shape of the drying rate curves of granular porous materials. Therefore alumina and molecular sieve are the ideal materials for comparing the drying kinetics of the different materials in air and in steam.

### 3.2 Experimental equipment for measuring drying rate curves in fluidized beds

In conventional equipment for measuring drying rate curves in fluidized beds, the drying rate is measured indirectly from the humidity uptake of the drying medium. In steam drying this technique is obviously not applicable. Special equipment had to be developed to study the drying kinetics in steam drying.

#### 3.2.1 Requirements for the drying equipment

For a meaningful comparison between air and steam drying, the drying rate curves in steam and in air should be determined in the same equipment. Furthermore the variation of the drying kinetics with



drying conditions must be investigated. Therefore the equipment must operate according to following criteria:

- Drying rate curves must be measurable in air and in steam.
- The inlet temperature of the drying medium must be variable over a large temperature range.
- The inlet temperature of the drying medium must be accurately controllable.
- The flow rate of the drying medium must be able to be varied.
- A large amount of materials must be able to be processed.

### 3.2.2 Choice of a fluidized bed for determining drying rate curves

The design of any type of dryer requires knowledge of the drying kinetics of the material to be dried. In principle this information can be obtained in two different ways:

- 1) Determination of drying rate curves in the type of dryer that should be designed.

In drying equipment (tray dryer, fixed-bed dryer, etc.) the state of the drying medium, as well as the state of the material to be dried, changes with its location in the dryer. This means that a drying rate curve is linked to the apparatus in which it is measured. Therefore a drying rate curve that is recorded in a certain type of equipment can be used to design only this type of equipment; for example, a drying rate curve recorded in a tray dryer can, strictly speaking, only be used to design a tray dryer.

- 2) Determination of the drying characteristics of a representative sample of the material (slab, single particle, etc.) under various drying conditions

In this case the drying kinetics of a small sample of the material are determined. This information cannot be used directly in the design of the dryer but must be linked to a

model describing the temperature and humidity profiles of the material and the drying medium inside the dryer. This approach is more universal, as any type of dryer can be designed on the basis of the measured drying characteristics. However, the use of drying models introduces some degree of inaccuracy, the magnitude of which depends on the type of dryer to be designed.

The drying rate that is measured in a fluidized bed is the average of the drying rates of all the particles. Due to the well-mixed behaviour of the material in the fluidized bed, the drying rate of a single particle at the inlet conditions into the dryer can be determined after some mathematical transformation of the recorded drying rate of the total bed mass (as will be shown in Section 4.5.2). The inlet conditions of the drying medium into the dryer (temperature, flow rate) are kept constant during one experimental run. After completion of the experimental programme, drying characteristics of a single particle are available for a number of different drying conditions. This information can then be used to design other drying equipment. In addition, fluidized-bed dryers can be designed directly on the basis of the measured drying rate curves. This is why a fluidized-bed dryer was chosen for recording the drying rate curves.

### 3.2.3 Description of the experimental equipment

A schematic diagram of the drying rig is shown in Figure 18. The main part of the rig consists of a fluidized-bed dryer that rests freely on a balance. The dimensions and shape of the dryer can be seen on Figure 19. The bed is connected via two flexible diaphragms to the steam and air supply lines. The incoming gas stream is divided and enters the base of the dryer horizontally and from opposite sides. In this way the horizontal components of the impulse forces counterbalance each other, so that they exert no tilting force on the dryer. The effect of the change of momentum of the flowing gas and the change of buoyancy during drying on the balance reading is negligible. An in-depth discussion of the influences of the flowing gas on the balance reading is presented in Appendix K. The effectiveness of the diaphragms is discussed later in this chapter.

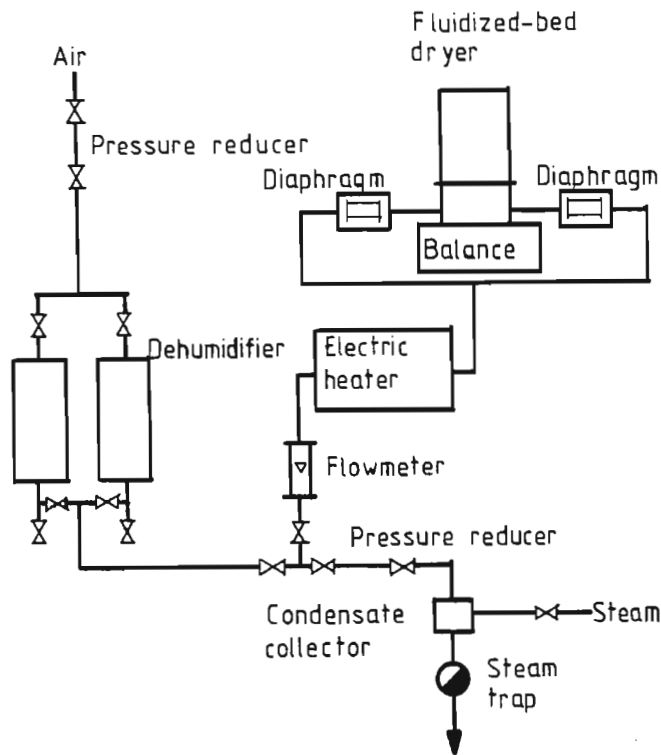


Figure 18: Experimental drying rig

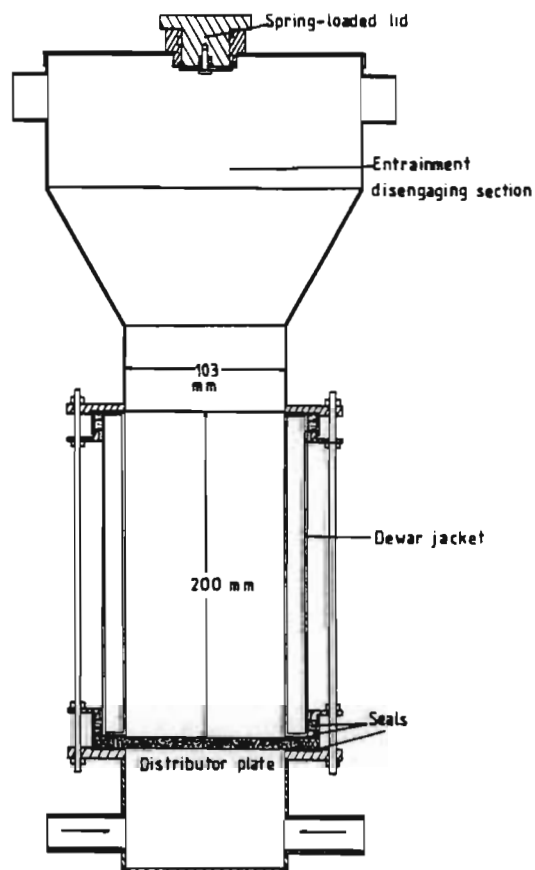


Figure 19: Fluidized-bed dryer

Either air or steam can be supplied as the drying medium. For air operation, compressed air flows via a pressure regulator to a dehumidification unit. The dried air is metered in a rotameter and is heated before it enters the dryer. Temperatures of up to 350 °C can be attained in the electric heater. All pipes downstream of the heater are wrapped with heating tape and are lagged. The temperatures of the gas entering the dryer and leaving the dryer are monitored by thermocouples. Furthermore the temperature of the gas at various heights above the distributor plate is measured. All of these temperatures are recorded at regular intervals. The exhaust gas is blown to atmosphere. For steam operation, moisture is removed in a condensate collector before the steam is metered and heated.

The dryer is a Dewar jacket consisting of a double-walled Pyrex-glass vessel that is evacuated and covered with a silver deposit on the inside. This deposit contains a window 5 mm wide through which the fluidization can be observed. On top of the dryer is an opening through which the material can be fed in. This opening can be closed with a spring-loaded lid. The inlet and outlet sections of the vessel are wrapped in heating tape, which is insulated and regulated by an on/off temperature controller. This design ensures that heat losses are virtually eliminated and that condensation does not occur within the bed. The inner diameter of the jacket is 103 mm and its height is 200 mm, allowing operation with a bed height of up to 100 mm. The upper part of the vessel is conical, so as to eliminate particle entrainment. A screen, made of a fine wire mesh, is used to prevent fines that may be present in the bed material from escaping and being recorded as weight loss. The distributor plate for the fluidized bed consists of a 6-mm-high layer of small glass beads that are sandwiched between two screens.

The balance is a commercial Mettler balance, type PE-16. The maximum mass that can be measured is 16 kg, and it is accurate to within 0,1 g.

The diaphragms that connect the drying vessel to the supply plumbing are shown in Figure 20. Each diaphragm consists of two brass sheets 0,3 mm thick joined with a brass tube. One sheet is fixed to the rigidly supported supply plumbing, and the other to the fluidized

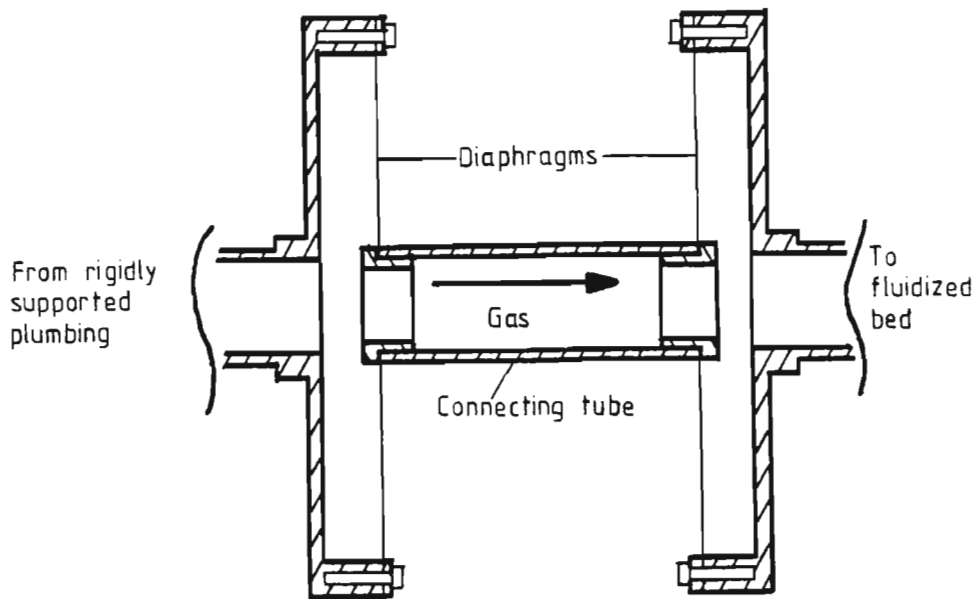
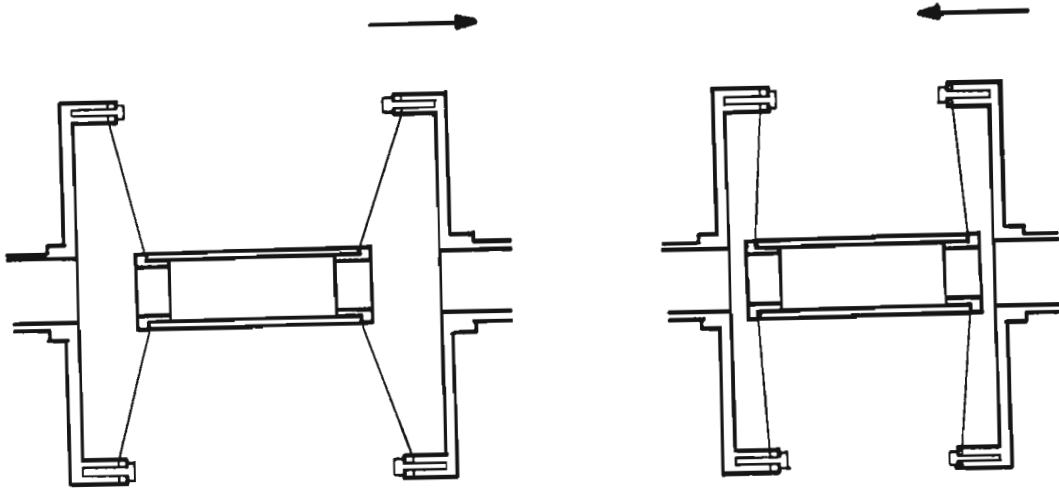


Figure 20: Diaphragm assembly

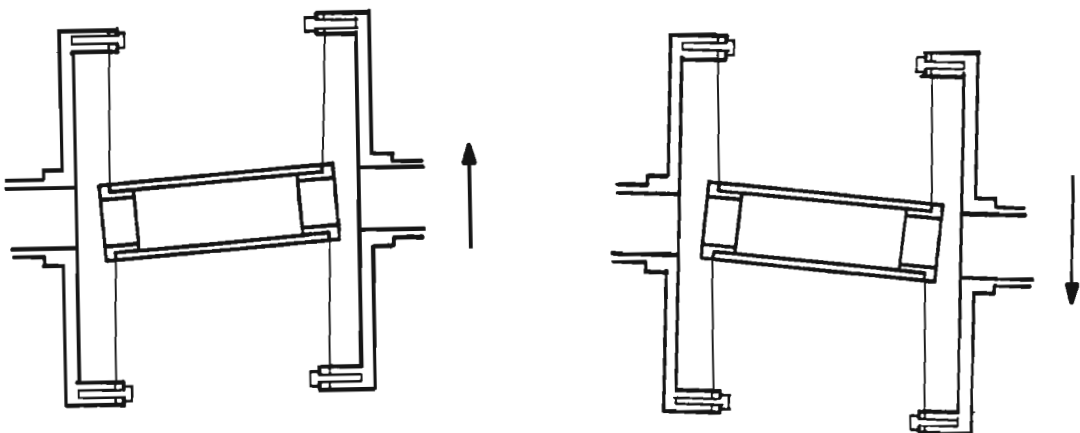
bed. Horizontal and vertical movements of the dryer are dampened by the flexible brass sheets as shown in Figure 21. The effectiveness of the diaphragms was tested in preliminary tests. Dry material was fluidized in the equipment and the balance was tared. Different weights (100 g, 150 g and 200 g) were put on top of the fluidized bed. They were measured with an accuracy better than 0,6 %. The diaphragms have the added advantage of damping vibrations originating from the supply plumbing. A bursting test showed that the diaphragms can withstand an over-pressure of 70 kPa.

#### 3.2.4 Experimental procedure for measuring drying rate curves

Before the experimental run, the material must be wetted. This is done in a commercial laboratory fluidized bed made by BUCHI. This fluidized bed is equipped with a pneumatic nozzle for spraying liquids onto the fluidizing material. Distilled water is fed by a peristaltic pump into the nozzle, where it is atomized by compressed air and sprayed onto the testing material. A preweighed amount of dry material, corresponding to one experimental run, is fluidized in the BUCHI equipment at ambient conditions and wetted with a preweighed amount of distilled water. The wetting conditions (flow rate of the fluidizing air) are kept identical for all the wetting tests. This ensures that the resulting moisture content of the material is always



a) Damping of horizontal movement



b) Damping of vertical movement

Figure 21: Damping of movements on diaphragms

the same. The wetted material is removed from the fluidized bed and is stored in a sealed glass container, where it is kept for 24 hours before use. This allows the material to absorb the moisture evenly.

For the drying tests, the flow rate and the inlet temperature of the drying medium are set. The fluidized bed is empty. After the drying conditions have been reached and have remained constant for 15 minutes, the data acquisition program is readied and the actual test can begin. The flow of drying medium is stopped. The material to be tested is quickly added to the dryer via the opening in the lid. A funnel is used to prevent spillage. After this the opening is closed with a spring-loaded stopper. The flow of drying medium is switched on again, the balance is zeroed and the data acquisition program is started. This operation takes around 15 seconds.

The data that are gathered by the data acquisition system are stored on floppy disk and are also displayed on the screen of the PC, so that the drying process can be monitored. Depending on the drying conditions and the material, the tests last between 15 and 60 minutes. The balance reading decreases during drying and when it has stayed constant for 5 minutes, the drying test is finished and the data acquisition program is stopped.

The shutdown procedure differs in steam and in air operation. With steam operation, the steam flow is slowly turned down, while the air flow is slowly opened. The air flow is used to purge the dryer of all remaining steam. The procedure is done in such a way that condensation of the steam is prevented. When the steam valve is completely closed, air is left blowing through the material for a short time before it is switched off. With air operation, this is not necessary. After a drying test, the air flow is switched off immediately.

The material is sucked out of the dryer with a small vacuum cleaner. The operating conditions for the next test can then be set.

In preliminary tests it was shown that the material is completely dried after a drying test. The material was weighed and dried in a vacuum oven for 12 hours. The resulting weight loss was negligible. This is understandable, as temperatures over 100 °C are used.

### 3.2.5 Experimental programme

Table 4 shows the experimental drying programme. "A" indicates that the test was performed with air and "S" that the test was performed with steam.

Table 4 Experimental programme

Temperature °C	Mass flow rate of drying medium, kg h <sup>-1</sup>					
	Alumina			Molecular sieve		
	16,70	19,27	22,76	21,06	24,41	25,96
75	A	A	A	A	A	A
100	A	A	A	A	A	A
125	A/S	A/S	A/S	A/S	A/S	A/S
150	A/S	A/S	A/S	A/S	A/S	A/S
175	A/S	A/S	A/S	A/S	A/S	A/S
200	A/S	A/S	A/S	A/S	A/S	A/S
225	A/S	A/S	A/S	A/S	A/S	A/S
250	A/S	A/S	A/S	A/S	A/S	A/S
275	A/S	A/S	A/S	A/S	A/S	A/S

For each material three mass flow rates of the drying medium were chosen. The mass flow rates were selected in such a way that when the material was wet, it still fluidized at the lowest mass flow rate and when it was dried, it was not entrained at the highest flow rate. Therefore the selected mass flow rates for alumina and for molecular sieve are different. For the comparison between air drying and steam drying, the same mass flow rate of the drying medium was chosen. Therefore the mass flow rate of the drying medium was the same in air as in steam.



The temperatures were varied in 25 °C-steps from 75 to 275 °C. Higher temperatures could not be used because of the limited conversion range of the A/D-converter chips. At the two lowest temperatures (75 and 100 °C) steam tests could not be performed for obvious reasons.

The bed height was fixed at 60 mm for all the tests.

### 3.2.6 Date acquisition and processing

The weight readings of the balance appear on a liquid crystal display, but can also be read via a digital output on the balance. This output is fed directly into a microcomputer where it is collected and processed by a data-acquisition program. It is subsequently stored on floppy disk and displayed on the screen of the PC. The frequency of the data transmission is fixed by the hardware to five readings per second. In preliminary tests it was shown that such a high frequency is not necessary for the determination of the drying rate curve. As the data are stored on floppy disks, these would be filled up very quickly if the high transmission frequency were to be maintained. For these reasons, the data-acquisition software averages the weight readings over an interval of 10 seconds (corresponding to 50 readings) for drying tests below 200 °C and over an interval of 5 seconds (corresponding to 25 readings) for tests above 200 °C. The averaged value is then stored on floppy disk.

The weight readings are not smooth, but fluctuate. The reason for this fluctuation can be found in the fluidization process itself. During fluidization, the level of the fluidizing mass in the dryer is not stable. This is due to bubbles that are generated at the distributor plate. These bubbles rise through the bed and lift the material above them. At the surface of the bed, these bubbles burst. The material is thrown upwards and then falls back into the bed. The level of the bed fluctuates around a mean value. When the bed height has reached its lowest point, the particles are, on average, accelerated upwards. As the bed height passes through the mean value, the particles decelerate in their upwards movement. The bed height then passes the maximum value and, during the downwards movement, the particles accelerate again. If the positive direction for acceleration is con-

sidered to be upwards, then the particles experience a negative acceleration or a deceleration. After passing through the mean bed height, the particles decelerate on their downwards movement, which corresponds to an upward-directed acceleration. After that the cycle begins anew.

In summary, the particles decelerate when the bed height is above the mean and accelerate when the bed height is below the mean. During acceleration, a downward-directed reaction force is pushing on the balance and the balance shows a higher weight than average. During deceleration, an upward-directed reaction force causes the balance to show a lower weight than average. As the bed height passes through the average value, the balance indicates the average weight. This description is based on the assumption that the acceleration and deceleration forces, as well as the wall friction during acceleration and deceleration are equal in magnitude. It is however not important whether the fluctuations occur around a mean value or not, as one is not interested in the absolute value of the balance reading, but only in the decrease of the readings with time.

A BASIC program was written for further processing of the data. The program reads the stored weight readings from the floppy disk into the internal memory of the PC. The data are then displayed in graphical form on the screen as is shown in Figure 22.

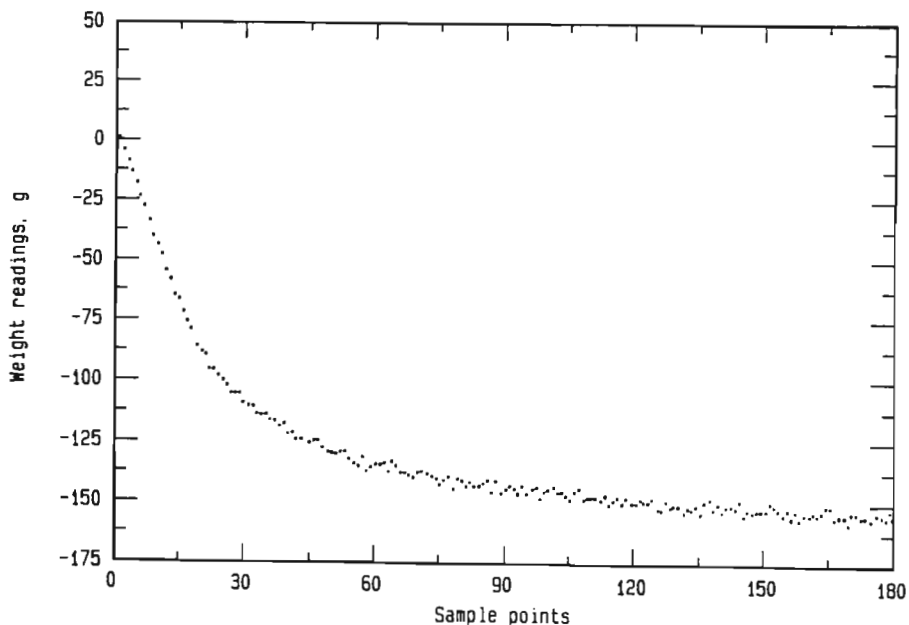


Figure 22: Graphical representation of weight readings vs time

The X-axis represents the number of sample points, which is a measure for the drying time, and the Y-axis represents the recorded weight. As the balance is zeroed before the start of the tests and as the weight of the material decreases during drying, the recorded balance reading is negative.

The fluctuations in the balance readings are smoothed by using a filtering technique based on a three-point moving average algorithm. This technique is widely accepted for the processing of data by computer because of its simplicity and its speed [N4]. High-frequency and low-frequency noises are removed from the drying rate curve. Each point of the graph is corrected by using following formula:

$$W_{\text{new},n} = 0,25 W_{\text{old},n-1} + 0,5 W_{\text{old},n} + 0,25 W_{\text{old},n+1} \quad (8)$$

Where W is the weight reading and n is the n-th point in time.

The smoothing algorithm is applied several times to the curve. After each smoothing the result is displayed in graphical form, so that the smoothing process can be followed. After 10 to 12 repetitions, the curve stabilizes and the smoothing process is stopped. A typical result is shown in Figure 23.

The drying rate curve of the material must be determined from this graph. The drying rate is defined as the loss of moisture from the material per unit of time. Therefore the slope of the curve determines the drying rate. The slope is calculated by fitting a straight line (linear regression) through three consecutive points (e.g. points 1,2 and 3). The slope of this line then represents the drying rate at the moisture content of the medium point. After that the three points are shifted on by one point in time (e.g. to points 2,3 and 4). This procedure is repeated until the whole drying rate curve has been formed. By a mass balance calculation, the scale representing the drying time is changed into a scale representing the moisture content of the material. The result is again displayed graphically on the screen and stored on floppy disk. A typical drying rate curve is presented in Figure 24.

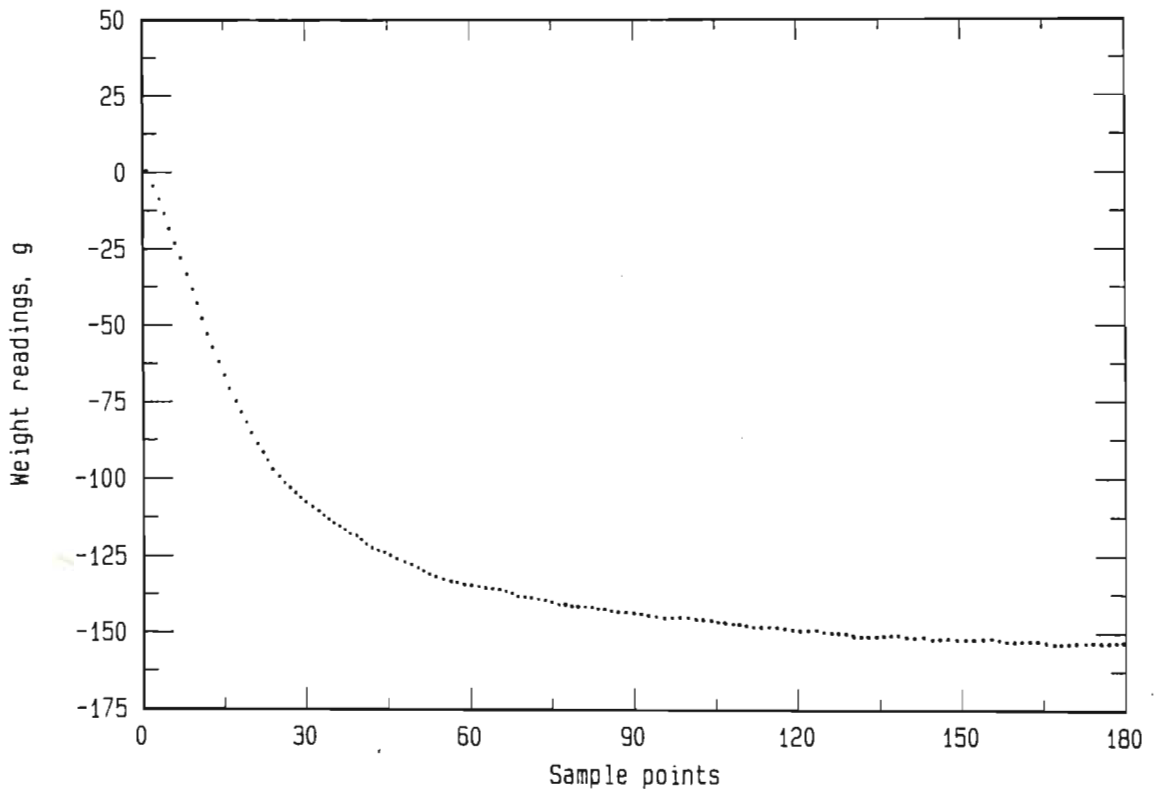


Figure 23: Smoothed weight readings as function of time

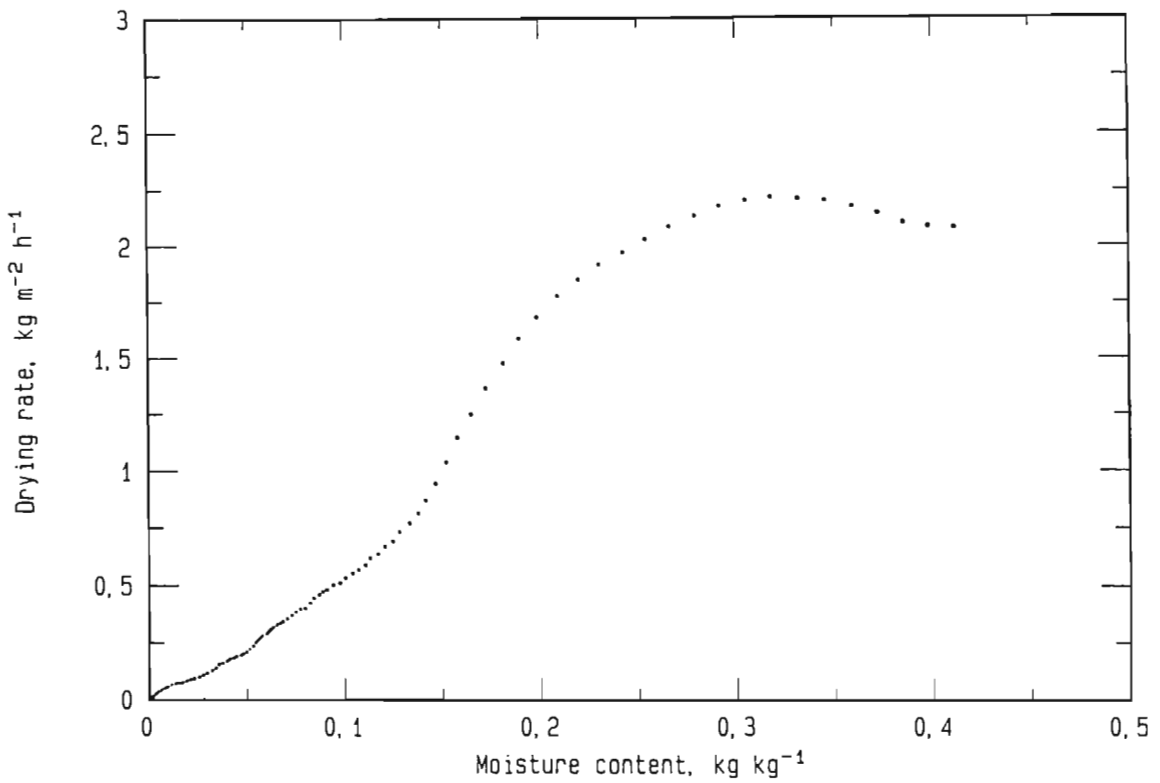


Figure 24: Experimental drying rate curve

During the constant drying rate period, the slope of the weight loss versus time is constant. This slope decreases at the critical moisture content. For an accurate determination of the critical moisture content, it is necessary that the linear regression be done with the minimum number of points possible. Indeed, if the number of points used in the linear regression is too large, the slope of the linear fit already starts decreasing for moisture contents above the critical moisture content. On the other hand, if the number of points is too small, the slope fluctuates too widely. It was found that the best results were obtained using three points.

### 3.3 Experimental equipment for measuring gas-to-solid heat transfer coefficients in fluidized beds

The gas-to-solid heat transfer coefficient is an important parameter in the design of fluidized beds. Furthermore it will be used in this thesis for transforming the measured drying rate curves into a normalized drying rate curve. No data were found in the literature for steam fluidized beds and the gas-to-solid heat transfer coefficient had to be determined experimentally.

#### 3.3.1 Background to the development of the measuring equipment

Two techniques are used for measuring the gas-to-solid heat transfer coefficient in fluidized beds, namely a steady state technique and an unsteady state technique.

##### Steady state technique

In the steady state technique, the temperature of the fluidized bed is kept constant by either evaporating moisture from the material, by heat exchange with a surface, or by replacing hot solids with a fresh cool solid [K12]. By measuring and recording the temperature profile of the fluidizing gas, the heat transfer coefficient can be determined.

The temperature of the fluidizing gas approaches the temperature of the solids within a very narrow layer (a few mm) above the distributor plate. Therefore it is very difficult to measure this profile accurately. Even though thermocouples can be made very small, it is difficult to say at exactly what height above the distributor plate the temperature was measured. Especially for small particles, in which temperature equilibrium between gas and solids is reached very quickly, this technique is not appropriate.

#### Unsteady state technique

In the unsteady state technique, the temperature of the bed is not constant but changes with time. The gas-to-solid heat transfer coefficient is determined from the time-evolution of the exit gas temperature.

Both techniques require the measurement of gas temperatures and solids temperatures for the determination of the heat transfer coefficient. The inlet and outlet temperatures of the fluidizing gas can be measured by bare thermocouples. The temperature of the gas inside the fluidized bed is, however, more difficult to measure. Some investigators took it to be the temperature read by a bare thermocouple, and others took it as that read by a suction thermocouple. It was shown by Walton *et al.* [W1] that the suction thermocouple reading is equal to or higher than the bare thermocouple reading. The reason lies in the fluidizing behaviour of the material. The fluidizing gas flows through the fluidized bed in the form of emulsion gas and bubble gas. The temperature of the emulsion gas is closer to the solids temperature than is the temperature of the bubble gas. A suction thermocouple only samples and measures the temperature of the gas. Therefore the temperature reading of a suction thermocouple lies between the temperatures of the emulsion gas and the bubble gas. Furthermore, the temperature of the suction thermocouple varies depending on the sampling velocity, as discussed by Kunii and Levenspiel [K12]. If there is a large pressure drop over the probe, a temperature close to the bare thermocouple reading will be measured. If the pressure drop is small, then a temperature close to that of the bubble gas will be measured. It is generally accepted that the

temperature measured by a bare thermocouple lies in between the gas temperature and the solids temperature [H9].

In the relevant literature, the temperature of the solids was taken to be the same as either the temperature of the exit gas, or the temperature in the main portion of the bed, or the temperature of the collapsed bed. If thermal equilibrium is assumed between solids and gas, the temperature of the solids and of the exit gas will be equal. It was however found by some investigators [H9] that even for relatively high beds, thermal equilibrium was not reached. One reason for this can be found in the bubbling behaviour of the bed. Even though the emulsion gas is in thermal equilibrium with the solids, the bubble gas is not. This bubble gas then mixes with the emulsion gas at the exit of the bed and the exit gas temperature will differ from the solids temperature.

To determine the heat transfer coefficients from the measured temperatures, certain assumptions must be made with regard to the flow of the gas through the fluidized bed. In early investigations, the fluidized bed was assumed to be a homogeneous system. The flow pattern of the fluidizing gas was assumed to be plug flow or well-mixed flow. The influence of bubbles was ignored. In later investigations, Kunii and Levenspiel [K12] included bubble behaviour in their interpretation of the measured data. The bubble diameter was assumed to be constant over the bed height. Kunii and Levenspiel had to choose a very small bubble diameter to fit the literature data. In practice the bubble behaviour can also be included by assuming a by-pass mass flow or by assuming longitudinal mixing of the fluidizing gas [M1].

Another influence, which is often neglected, is the heat that the particles exchange with the surfaces of the fluidized bed. Heat exchange with the walls of the fluidized bed can be minimized by proper insulation. Heat exchange with the distributor plate, however, cannot be eliminated as easily. Heertjes *et al.* [H6] found that the temperature drop across the distributor plate can be considerable compared with the temperature drop across the bed. The distributor plate is at a higher temperature than the solids in the bed and the surface-to-solids heat exchange in fluidized beds is extremely good, so that the heat exchange between distributor plate and solids can be considerable.



Most investigations have been done for particle Reynolds numbers smaller than 100. In this region, the corresponding Nusselt numbers lie far below the Nusselt number for a single sphere. The reason is that in this region the assumption of plug flow of the fluidizing medium is not valid any more and the uneven distribution of the flow has a negative effect on the heat transfer from gas to solids [S3]. The available literature data show a wide scatter. The proposed correlations are in very poor agreement, even from a qualitative point of view [H9]. The reason for this discrepancy lies partly in the different measurement techniques used, the theoretical assumptions made and the fluidization behaviour of the different materials.

For Reynolds numbers higher than 100, better agreement is found in the experimental data. As shown by Martin [M1], the Nusselt number can then be determined from the Nusselt number of a single sphere at free-falling velocity. The Nusselt number for the fluidized-bed system does not vary much between minimum fluidization velocity and entrainment velocity.

### 3.3.2 Description of the experimental equipment for measuring heat transfer coefficients in fluidized beds

A steady state technique was chosen to determine the gas-to-solid heat transfer coefficient. During the constant drying rate period, the temperature of the material is constant. The temperature profile of the fluidizing medium is measured by six thermocouples inserted into the bed at different heights above the distributor plate. A figure of the experimental assembly is presented in Appendix A.2 together with a discussion of the errors in the determination of the heat transfer coefficient. The thermocouples are soldered into the lid of the dryer and are automatically inserted in the fluidized bed when the lid is closed. The thermocouples are of type K and are protected by a 1/16-inch stainless steel sheath that is open at the bottom, so that the measuring tip of the thermocouple wires is in direct contact with the fluidizing medium. The distances above the distributor plate are 0,5; 2,5; 5; 7,5; 11,5 and 24 mm. With these distances, the temperature profile can be measured for most drying conditions.



The analog signals of the thermocouples are filtered and sent to an A/D-converter with built-in cold-junction compensation. The resulting digital signal is then fed to a microcomputer that stores the temperature data on floppy disk. These data are stored at the same frequency as the weight readings, i.e. every 10 seconds for tests below 200 °C and every 5 seconds for tests above 200 °C.

A BASIC program was written for further evaluation of the temperature readings. The program reads the data from the disk into the internal memory of the PC and displays them on the screen in graphical form. The temperatures are displayed on the Y-axis, and the time is displayed on the X-axis. There are six curves on the graph, each representing the temperature evolution with time of one thermocouple. During the early stages of the test (constant drying rate period), each thermocouple indicates a constant temperature. These data can then be used for determining the temperature profile over the height of the dryer.

### 3.4 Experimental equipment for measuring sorption isotherms

The sorption isotherms of materials are used in the mathematical modelling of the drying process. Furthermore, they indicate to what extent the material can be dried under specific conditions. This is useful for selecting the correct drying conditions and also for preventing overdrying.

#### 3.4.1 Background to the development of the measuring equipment

The sorption isotherm or moisture isotherm of a material relates the equilibrium moisture content of this material to the relative humidity of the drying agent at a fixed temperature. Figure 25 shows sorption isotherms for various materials. The sorption isotherm is dependent on the nature of the material and is an indication of the strength of the bonding of the moisture to the solid matrix. Materials can be divided into non-hygroscopic and hygroscopic. In non-hygroscopic materials, liquid moisture is not bound to the solid skeleton and the moisture exerts a vapour pressure equal to the satu-

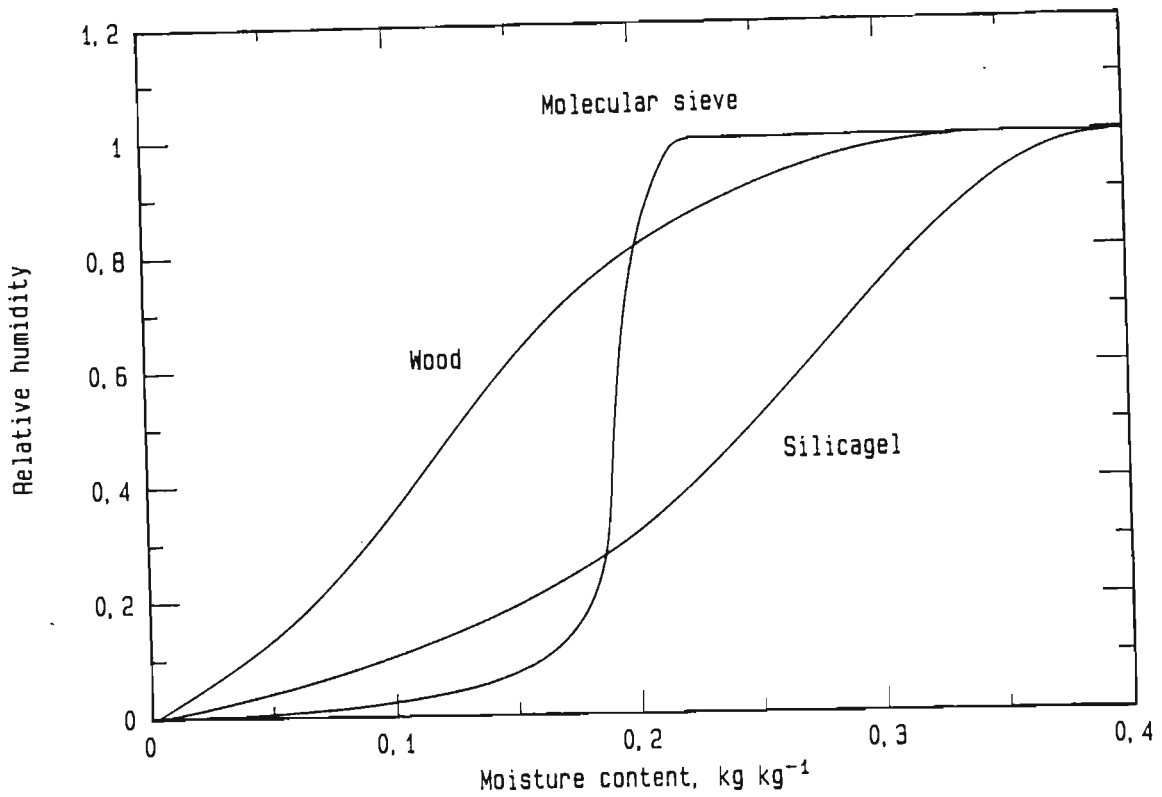


Figure 25: Sorption isotherms for various materials [K3,L5]

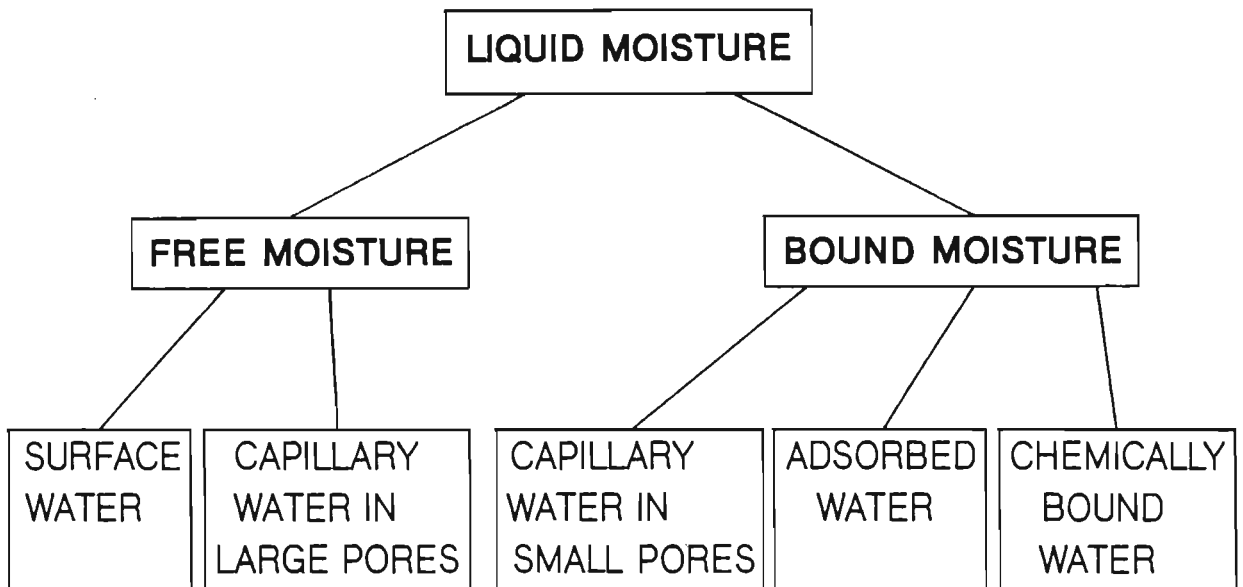


Figure 26: Division of moisture according to strength of bonding

ration pressure at the same temperature. In hygroscopic materials, moisture is bound to the solid skeleton and exerts a vapour pressure that is lower than the saturation pressure.

The liquid moisture of materials can be divided into free water and bound water as represented in Figure 26.

The free water is the liquid moisture that exerts a vapour pressure equal to that of a flat surface of water. This is the water that is easily removed from the solid. The bonding force can be considered to be negligible. The free water can then be divided into surface water and capillary water in the larger pores. The surface water is the water in a film around the particle. This is the water that is removed during the constant drying rate period. In the larger pores, the capillary water exerts full vapour pressure, as the curvature of the liquid surface is not yet pronounced.

The bound moisture is the liquid moisture exerting a vapour pressure below the vapour pressure of a flat surface of water and is made up of the condensed capillary water in the smaller pores, the physically bound or adsorbed water and the chemically bound water.

The condensed capillary water in the smaller pores (in general smaller than  $10^{-7}$  m) exerts a vapour pressure below that of a flat surface. In order to remove this water, the temperature inside the body has to be higher than the boiling temperature of a flat surface. The smaller the pores, the higher the temperature must be.

The physically bound water is adsorbed on the walls of the pores by physical forces. This water can be removed at higher temperatures.

The chemically bound water is present in the form of hydroxyl ions and crystal water. The chemical bond is the strongest bond keeping the liquid moisture bound to the solid matrix. In general chemically bound water can be removed only at temperatures that are not applied in drying operations.

The equilibrium moisture content depends on the way in which it is reached, either by drying (desorption) or by wetting (adsorption). No

universal explanation has been put forward for this phenomenon of hysteresis [L5]. In the context of this thesis, the terms sorption isotherm and desorption isotherm are treated as synonymous.

Sorption isotherms are also strongly temperature-dependent. Data are available for a large number of materials [K1-2,K9,L5], but are generally limited to low temperatures ( $<60^{\circ}\text{C}$ ). Data for high temperatures are available for only very few materials (timber, building materials, paper). In steam drying, temperatures higher than the boiling point are reached by the material. It is therefore of special interest to know the sorption isotherms of the materials being tested at these high temperatures.

In principle there are two ways of measuring sorption isotherms, namely a static method and a dynamic method. In the static method, a weighed amount of material is exposed to a quiescent air atmosphere of a certain humidity. This method generally gives very accurate results, but requires a long time (several days) before the material is in equilibrium with its surroundings. The humidity of the air is set by using salt solutions. This method is therefore limited to lower temperatures. In the dynamic method, air with a set humidity is blown over a weighed amount of material. Equilibrium is reached faster (a matter of hours), but the results are not as accurate. In this method it is difficult to set the humidity of the air accurately.

#### 3.4.2 Description of the experimental equipment for measuring sorption isotherms in steam

For this thesis, the static method was chosen because of the simpler experimental equipment involved. The measuring technique is however different from standard methods in that the environment of the material is not humid air, but pure steam [A2]. The measuring equipment is shown in Figure 27 and is described below together with the measuring procedure.

A sample of roughly 300 g of material is wetted with distilled water using the same wetting procedure as in the drying tests described in

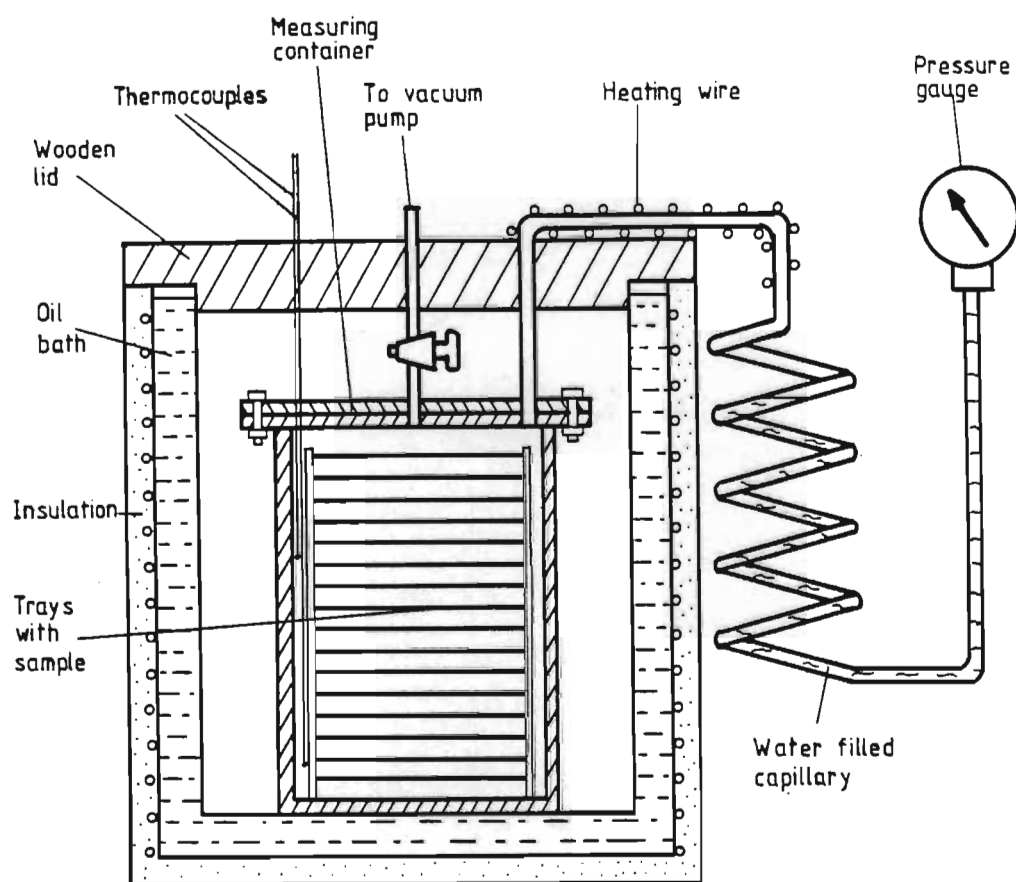


Figure 27: Measuring equipment for sorption isotherms

Section 3.2.4. The wetted material is then placed in a cylindrical stainless steel container, referred to as the measuring container. The material is spread in single particle layers onto 15 stacked glass trays. This provides good contact between the material and the steam environment and speeds up the achievement of equilibrium. Distilled water is added at the bottom of the container. The container is then sealed and placed in a heating jacket. The temperature in the measuring container is measured with two calibrated thermocouples inserted at different levels. The pressure inside the measuring container is measured by a Bourdon pressure gauge, which is linked via a water-filled capillary to the measuring container. The heating jacket is a double-walled, stainless steel cylindrical pot, closed at the bottom and open at the top. The top can be closed with a 70 mm thick wooden lid to prevent heat losses. The space in between the double walls of the container is filled with heating oil. The oil is heated by a heating tape wrapped around the outside wall of the jacket. Fibreglass insulation around the jacket prevents heat losses. The heat input into the heating tape is controlled by an on/off temperature controller. This creates temperature fluctuations of  $\pm 3^{\circ}\text{C}$  on

the outside wall of the heating jacket. The oil inside the jacket dampens these fluctuations down to  $\pm 0,4$  °C on the inside wall of the heating jacket. In the measuring container these fluctuations are further dampened down to  $\pm 0,1$  °C by the air surrounding the measuring container.

The measuring container is then heated to the set temperature. When this temperature is reached, the air inside the measuring container is sucked out by a water-jet pump. The pressure in the container falls to 5 kPa. The suction is maintained for half an hour. The distilled water in the bottom of the measuring container evaporates and this helps to get rid of all the air inside the container. By weighing the assembly from time to time, the evaporation process can be monitored. As evaporation proceeds, the temperature inside the container decreases and the rate of evaporation slows down. The evacuation process is then stopped and the container is left to reach the set temperature again. The evacuation procedure is then repeated three to four times until all the distilled water in the container has evaporated. At this point there is no air left in the container. This can be checked by measuring the temperature and the total pressure in the container. If the pressure is equal to the saturation pressure at the given temperature, the container is air-free. If the pressure is higher than saturation pressure, a certain amount of air is still present. This may be caused by a leak in the container. If the pressure is equal to saturation pressure then the container is left at the set temperature for two days. If after that time the pressure is still the same, the container is well sealed.

To determine the sorption isotherm, the total steam pressure inside the container and the moisture content of the sample must be measured.

The pressure inside the container is measured by a Bourdon pressure gauge connected via a capillary to the container. The capillary is heated at the outlet from the container to prevent condensation. On the gauge side, the capillary is filled with distilled water, so that the meniscus lies outside the heated zone on the container side.

The moisture content of the material is measured by weighing the container with its contents on a balance. The balance is a commercial

Mettler balance with an accuracy of 0,1 g. If the weight of the empty container and of the dry material are known, the moisture content of the material can be calculated. The weight of the dry material is determined at the end of the run by drying the sample in a vacuum oven.

The temperature inside the container is measured by two thermocouples that are inserted at different heights. It was found that the temperature over the height of the container is uniform to within 0,6 °C.

In order to record the sorption isotherm of the material, measuring points must be available at different moisture contents of the material. The moisture content of the material is reduced by sucking steam out of the container for a certain amount of time. The material is then left to reach equilibrium again. The pressure and the moisture content are recorded twice a day. When these data cease to change, equilibrium has been reached. This takes two to three days. In order to control the decline in moisture content of the material, the container is placed on the balance before the vacuum pump is connected and the steam atmosphere is evacuated from the container until a certain weight loss has occurred.

The principle of the pressure measurement will now be explained. As long as the material is above the critical moisture content, the pressure that is recorded is equal to the saturation pressure of water at the set temperature. This pressure is also equal to the pressure at the liquid meniscus in the capillary. When the moisture content of the material falls below the critical moisture content, the pressure that is recorded is below the saturation pressure. The pressure at the liquid surface in the capillary must be equal to the pressure inside the container. As the capillary is heated at its top and not at its bottom, a temperature gradient exists along the height of the capillary. Therefore, if the pressure drops inside the container, water is evaporated from the liquid column until the level has dropped to a point where the saturation pressure corresponding to the temperature of the liquid level in the capillary is equal to the pressure in the container. The indication on the Bourdon pressure gauge is determined from the difference between the pressure exerted on the Bourdon spiral and the ambient pressure. At the beginning of each run, the zero point, where equilibrium exists between the out-



side and inside pressures in the gauge, is recorded together with the barometric pressure. The pressure inside the Bourdon spiral consists of the pressure inside the container plus the pressure exerted by the water column. If the height of the water column decreases, then the pressure on the inside of the Bourdon tube will decrease. The capillary is therefore rolled into a spiral to limit the decrease of the water level.

Between ten and fifteen measuring points were recorded for one sorption isotherm. The operating temperature was limited to 95 °C. At higher temperatures, sealing problems occurred with the valve leading to the vacuum pump. In principle, however, this measuring technique can be used at higher temperatures.

In Figures 28 and 29 the sorption isotherms for alumina and molecular sieve are presented. The symbols represent the measured data and the continuous lines the curve fitting. The data at 20 °C were recorded according to the standard static method using desiccators and salt solutions, because the low vapour pressure of water at 20 °C did not allow an accurate measurement using the previously described method. The relative pressure is the ratio between the pressure exerted by the moisture inside the material and the saturation pressure. It is equivalent to the relative humidity.

For alumina and molecular sieve the sorption isotherm shows the characteristic shape of capillary porous materials. For high moisture contents, the relative pressure is close to one and continues to fall, the lower the moisture content becomes. With an increase in temperature, the sorption isotherm is shifted upwards to higher values of the relative pressure. For alumina, the slope of the sorption isotherm is flatter than for molecular sieve and the relative pressure is already below one for relatively high moisture contents ( $> 0,35 \text{ kg kg}^{-1}$ ). For molecular sieve, the relative pressure is unity for all temperatures down to a moisture content of  $0,2 \text{ kg kg}^{-1}$  and then falls steeply.

To allow use of the measured sorption isotherm in the mathematical modelling of the drying process, curve fitting had to be undertaken to put the data into a mathematical form. The curve fitting procedure is described in Appendix C.



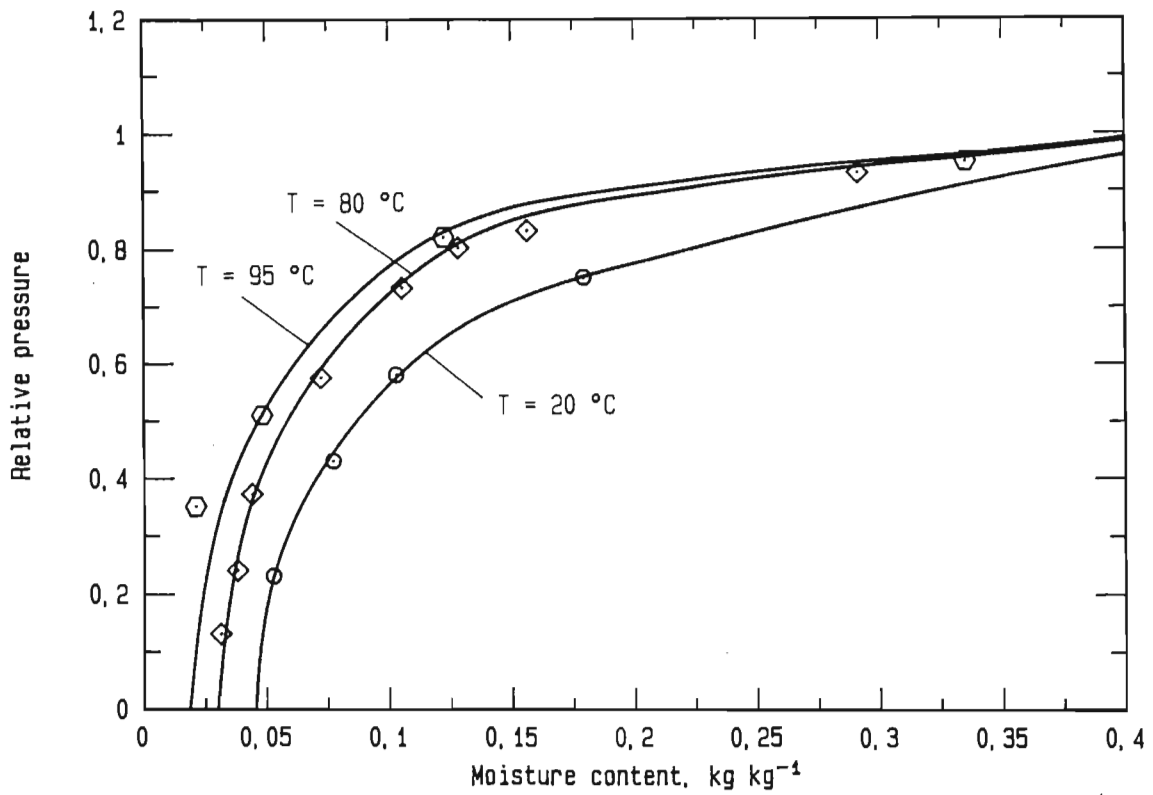


Figure 28: Sorption isotherms for alumina

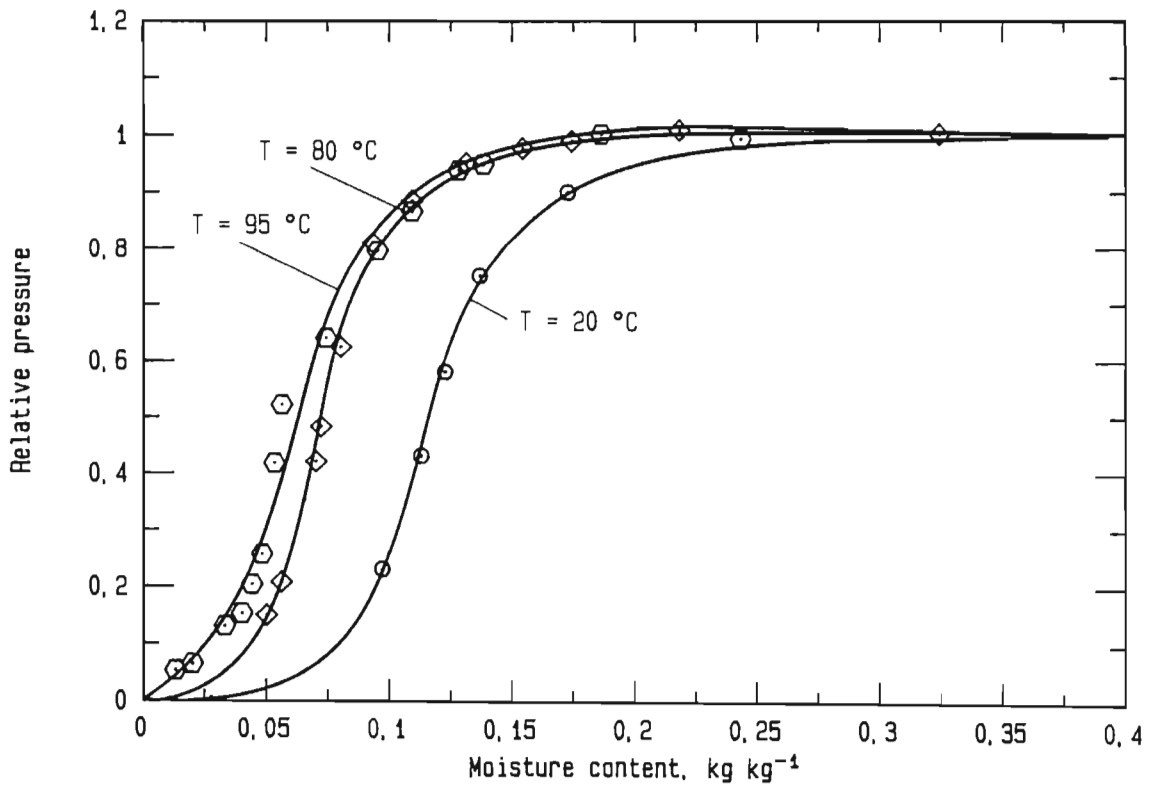


Figure 29: Sorption isotherms for molecular sieve

#### 4. DATA INTERPRETATION

In this chapter, the measured experimental data are evaluated and a comparison is made between the drying behaviour in air and in steam. For this comparison, the drying process is divided into the constant drying rate period and the falling drying rate period. These two periods are investigated separately.

For the constant drying rate period, the drying kinetics and the heat transfer coefficients are compared. The drying systems are divided into two categories:

- non-equilibrium systems and
- equilibrium systems.

In a non-equilibrium system, the drying medium that leaves the dryer is not in equilibrium with the wet material (Figure 30). There is a temperature difference and a humidity difference between the evaporative surface and the bulk of the drying medium. In an equilibrium

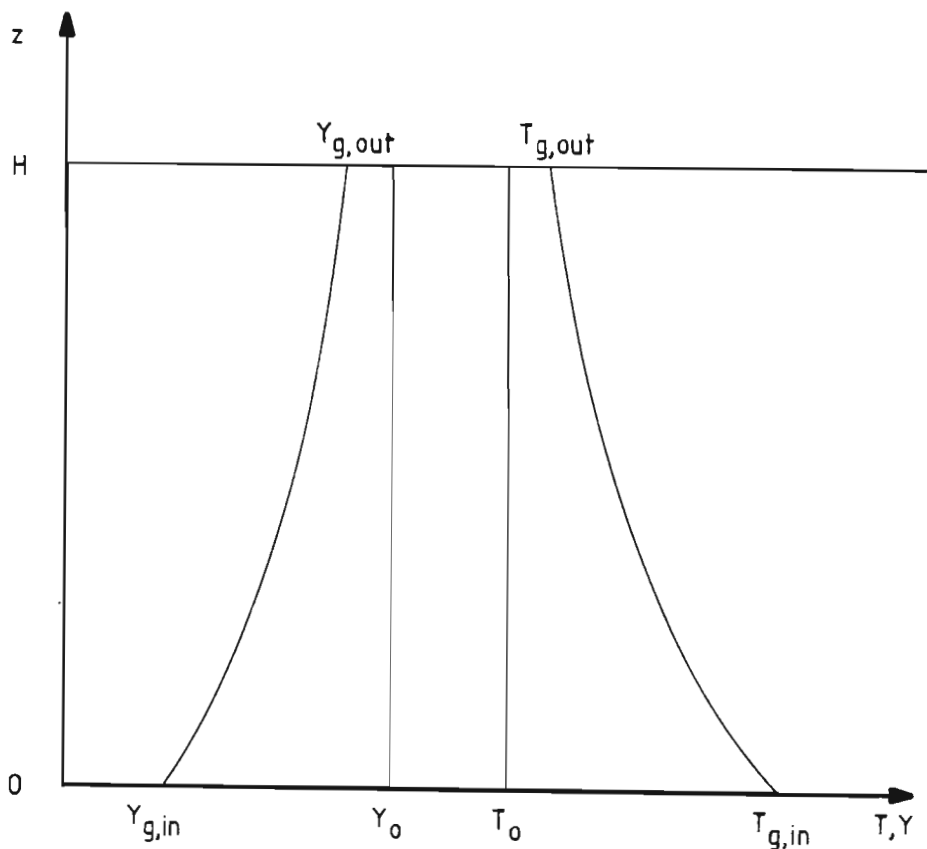


Figure 30: Temperature and humidity profile in a non-equilibrium system

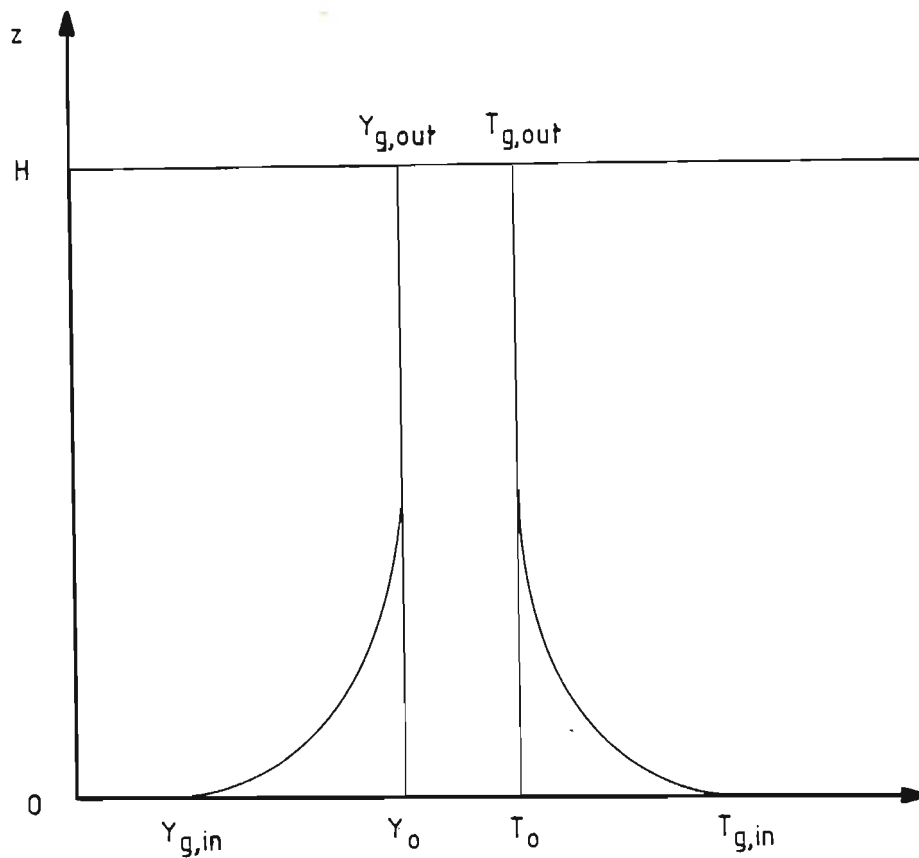


Figure 31: Temperature and humidity profile  
in an equilibrium system

system, however, the temperature and humidity of the drying medium are in equilibrium with the wet material (Figure 31).

In general, fluidized-bed systems are operated under equilibrium conditions. This is also the case in the experimental fluidized-bed drying tests that were performed in the context of this thesis. Most of the dryers that are commonly used in industry (tray dryers, rotary dryers, belt dryers etc.) fall into the category of non-equilibrium systems. Therefore, for the sake of completeness, the case of non-equilibrium systems is presented on a theoretical basis. These theoretical results are compared with literature data wherever possible.

The comparison of the drying rates in air and in steam is made for the same mass flow rates of the drying media. Other possible comparisons could be based on the same volumetric flow rate or on the same Reynolds number. The same mass flow rate was chosen for following reasons:

- (i) The term 'inversion temperature' was originally introduced by Yoshida and Hyodo [Y2] for the same mass flow rate of the drying medium.
- (ii) Experimental drying data that are based on the same mass flow rate of the drying medium are available in the literature.
- (iii) The present experiments were carried out in a fluidized-bed system. The lower limit for the velocity of the fluidizing medium is the minimum fluidizing velocity. This is higher in steam than in air because of the lower density and lower dynamic viscosity of steam. A further consequence of the lower density in steam is that the material starts fluidizing in the two media at roughly the same mass flow rate.

For the falling drying rate period, the drying kinetics are discussed on basis of the recorded drying rate curves. During this period, the material properties are important, and separate comparisons are made for the two types of drying material (hygroscopic molecular sieve and non-hygroscopic alumina).

For a better understanding of the drying mechanisms inside the material the drying rate curves are normalized with respect to the constant conditions at the inlet into the dryer. By doing this the drying process is uncoupled from the drying equipment that it is recorded. Therefore this normalized drying curve is well suited for the modelling of the drying process in the inside of the material. In this thesis a mathematical model was developed based on a shrinking core model. This model avoids the use of sophisticated computer hardware and software and is used to simulate the drying of the investigated materials.

#### 4.1 Theoretical determination of the inversion temperature in a non-equilibrium system

In a non-equilibrium system, the inversion temperature is determined by the kinetics of heat and mass transfer. Theoretical expressions for the heat and mass transfer rates must be available.

#### 4.1.1 Mathematical model for the determination of the inversion temperature in a non-equilibrium system

At the inversion temperature, the drying rates in air and in steam are equal. This can be expressed by Equation 9:

$$\dot{m}_{ev,a} = \dot{m}_{ev,s} \quad (9)$$

For both media, the evaporation rate can be determined from an energy balance:

$$\dot{q} = \dot{m}_{ev} \Delta h_v \quad (10)$$

The heat that is brought to the material is used for the evaporation of moisture. The kinetic expression for the heat transfer can be written as:

$$\dot{q} = h (T_\infty - T_p) \quad (11)$$

In steam drying, the particle is at the boiling point  $T_b$ , and in air drying at the wet-bulb temperature  $T_{wb}$ . Given all this information, Equation 9 can now be written as follows:

$$\frac{h_a (T_i - T_{wb})}{\Delta h_v(T_{wb})} = \frac{h_s (T_i - T_b)}{\Delta h_v(T_b)} \quad (12)$$

The temperature that is indicated in the special brackets behind the evaporation enthalpy,  $\Delta h_v$ , is the temperature at which the evaporation enthalpy must be determined. By rearranging this equation, the inversion temperature can be expressed by:

$$T_i = \frac{T_b - \frac{h_a \Delta h_v(T_b)}{h_s \Delta h_v(T_{wb})} T_{wb}}{1 - \frac{h_a \Delta h_v(T_b)}{h_s \Delta h_v(T_{wb})}} \quad (13)$$

The only unknown in this equation is the wet-bulb temperature. For completely dry air, the wet-bulb temperature is a function of only the inlet temperature of the drying medium. The relation between

inlet temperature and wet-bulb temperature can be determined by replacing in Equation 10 the heat flux  $q$  and the mass flux  $\dot{m}_{ev}$  by their respective kinetic expressions. This leads to:

$$h_a (T_{in} - T_{wb}) = \rho_a \beta_a (Y^*(T_{wb}) - Y_{\infty}) \Delta h_v(T_{wb}) \quad (14)$$

From this equation the wet-bulb temperature can be determined by iteration. The heat transfer coefficient  $h_a$  is determined from standard correlations [V5]. In Appendix E, these correlations are listed for the various flow regimes (laminar, turbulent, intermediate) and the various geometries of drying equipment and material (plate, tube, sphere).

The mass transfer coefficient  $\beta_a$  is determined from the similarity between heat and mass transfer (Lewis's law):

$$\beta_a = \frac{h_a}{\rho_a c_{pa} Le^n} \quad (15)$$

The exponent  $n$  of the Lewis number was chosen as 0,66 [S2]. The expressions for the physical properties of the drying medium are listed in Appendix B.

Equation 14 establishes a relation between  $T_{in}$  and  $T_{wb}$ . The inversion temperature can be determined iteratively from Equation 13 ( $T_i = T_{in}$ ).

Another interesting items of information that can be obtained from Equation 10 are the evaporation rates in dry air, humid air and pure steam. From Equations 10 and 11 one gets for dry air and humid air:

$$\dot{m}_{ev,a} = \frac{h_a (T_{\infty} - T_{wb})}{\Delta h_v(T_{wb})} \quad (16)$$

and for steam

$$\dot{m}_{ev,s} = \frac{h_s (T_{\infty} - T_b)}{\Delta h_v(T_b)} \quad (17)$$

In air, the wet-bulb temperature is determined by Equation 14. The heat and mass transfer coefficients are calculated for the desired conditions of flow rate, temperature etc. The wet-bulb temperature depends on the degree of humidity and on the inlet temperature of the air.

In steam, the boiling point is fixed for a given pressure of the system. Therefore Equation 17 can be used directly to calculate the evaporation rate. The heat transfer coefficient  $h_s$  is determined by the same correlation as in air, but by using the physical properties of steam.

Yoshida and Hyodo [Y2] determined experimentally the inversion temperature and the evaporation rate of water into dry air, humid air and steam by using a wetted wall column. The information that they gave on their experimental system was sufficient to allow the author to simulate their tests. Evaporation rates were calculated for air at various degrees of humidity by using Equation 16 and for pure steam by using Equation 17. As Yoshida and Hyodo used a cylindrical device, heat transfer coefficients were determined according to a correlation for flow through a tube proposed by the VDI [V5]. This correlation can be found in Appendix E.

The calculated evaporation rates agreed to within 15 % with the experimental results given by Yoshida. One peculiarity was that the calculated evaporation rates for dry air always exceeded the measured ones, whereas the calculated evaporation rates for steam were always lower. There is evidence in the literature that the humidity of the air influences the heat transfer correlation [C1,C7,K11,V7,W2]. Unfortunately there is no agreement on the extent of this influence. It was however shown experimentally by Wenzel and White [W3] that higher heat transfer coefficients than predicted by standard heat transfer correlations are found in steam. One reason for the higher heat transfer coefficients in steam could be the gas radiative heat transfer from the drying medium to the material. Air is composed of symmetrical molecules and has no gas radiative heat transfer component. Steam is composed of non-symmetrical molecules and can transfer heat by gas radiation.

As the air humidity influences the heat transfer and as higher heat transfer coefficients than are predicted by standard heat transfer correlations were found in steam, it was proposed to multiply the heat transfer coefficient in Equation 16 by a correction function that is humidity-dependent. For simplicity, a linear correction function was used.

$$f_c = C_1 y + C_2 \quad (18)$$

$y$  is the molar fraction of water vapour in the air expressed in moles of water vapour per moles of humid air. For dry air,  $y = 0$  and  $f_c = C_2$ . For steam  $y = 1$  and  $f_c = C_1 + C_2$ . The constants  $C_1$  and  $C_2$  were determined by calculating the corrected evaporation rates in air and in steam and by changing  $C_1$  and  $C_2$  until the calculated results were close to those obtained by Yoshida. The following values were found for the correction factors:  $C_1 = 0,204$  and  $C_2 = 0,935$ .

After correction, the calculated evaporation rates differed by a maximum of only 7 % from the experimental values obtained by Yoshida.

The calculated evaporation rates using Equations 16 and 17 with corrected heat transfer coefficients and the experimental data of Yoshida are represented in Figure 32. The calculated data fit the experimental results well for temperatures below 300 °C. At 300 °C a difference is found between calculated and experimental data. This may be due to radiative heat transfer components that normally have significance at higher temperatures. In the present calculations, heat transfer by radiation was neglected.

By using Equation 13 to determine the inversion temperature, a temperature of 172,7 °C is found. The inversion temperature given by Yoshida is 170 °C. The difference between predicted inversion temperature and experimentally determined inversion temperature is very small and can easily be explained by measuring inaccuracies.



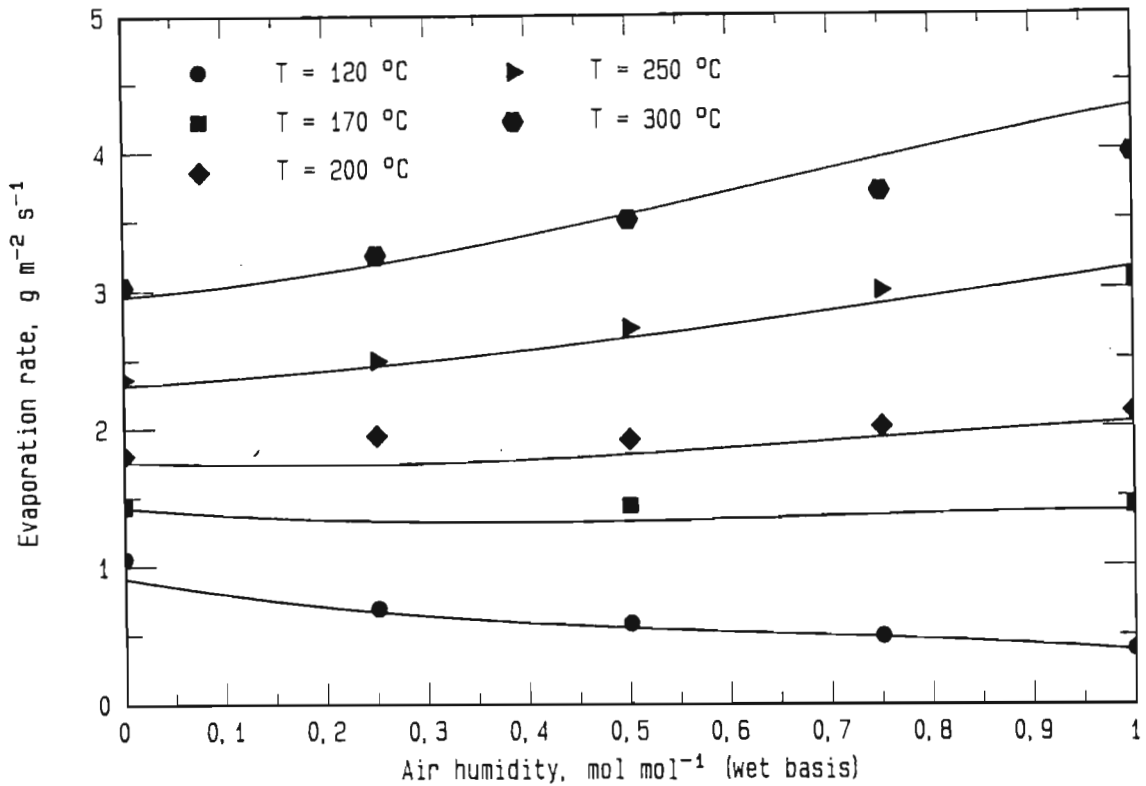


Figure 32: Theoretical modelling of experimental literature data [Y2] for evaporation of water into humid air and steam

#### 4.1.2 Explanation for the existence of the inversion temperature in a non-equilibrium system

In the previous section it was shown that the evaporation rates in air and in steam can be predicted by using Equations 16 and 17 and that the inversion temperature can be predicted by using Equation 13. The reason for the existence of the inversion temperature, however, has not yet been given. This is done below. The numerical results have been calculated for the experimental system of Yoshida.

To explain the existence of the inversion temperature, it is necessary to introduce the term of 'normalized evaporation rate'. The normalized evaporation rate is defined as the evaporation rate in humid air (or in steam) divided by the evaporation rate in dry air at

the same temperature and mass flow rate of the drying medium. By using Equations 16 and 17, the normalized evaporation rate for steam can be written as:

$$\frac{\dot{m}_{ev,s}}{\dot{m}_{ev,a}} = \frac{h_s}{h_a} \frac{(T_\infty - T_b)}{(T_\infty - T_{wb})} \frac{\Delta h_v(T_{wb})}{\Delta h_v(T_b)} \quad (19)$$

If the concept of normalized coefficients is extended to Equation 19, then the normalized evaporation rate is obtained from the product of the normalized heat transfer coefficient and the normalized temperature driving force divided by the normalized latent heat. These normalized coefficients will now be investigated separately.

In Figure 33, the normalized heat transfer coefficients are represented as a function of the humidity for various temperatures.

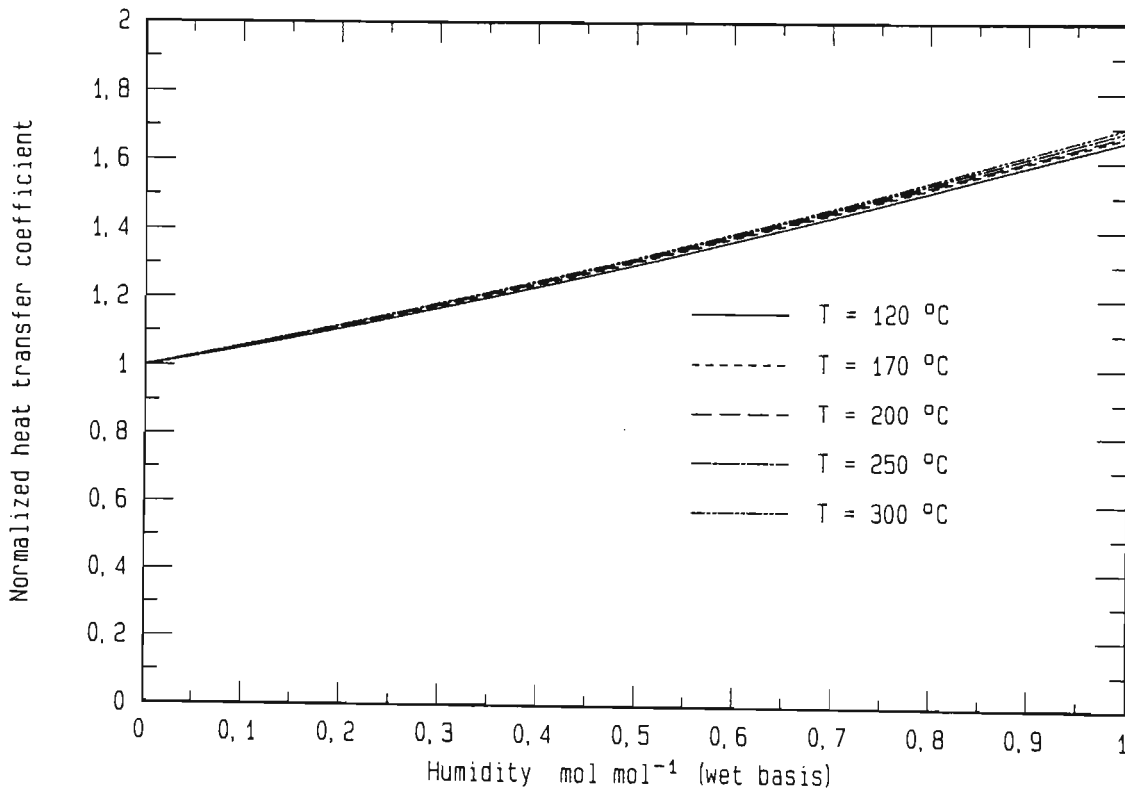


Figure 33: Normalized heat transfer for data of Yoshida [Y2]

By definition, the normalized heat transfer coefficient for dry air is unity. For all temperatures the normalized heat transfer coefficient increases with increasing humidity. At high temperatures, the normalized heat transfer coefficient increases only slightly more sharply than at lower temperatures. For steam, the normalized heat transfer coefficient is between 65 and 70 % higher than for dry air.

The normalized temperature driving force is defined as the temperature difference between drying medium and particle in wet air (or steam) divided by the temperature difference between drying medium and particle in dry air. In Figure 34 the normalized temperature driving forces are represented as a function of the humidity for various temperatures.

Again, by definition the normalized temperature driving force for dry air is unity. It decreases with increasing humidity. The extent of the decrease becomes smaller with an increase in temperature. For a temperature of 120 °C, the normalized temperature driving force in steam is only 22 % of the normalized driving force in air, whereas at a temperature of 300 °C it is 80 %.

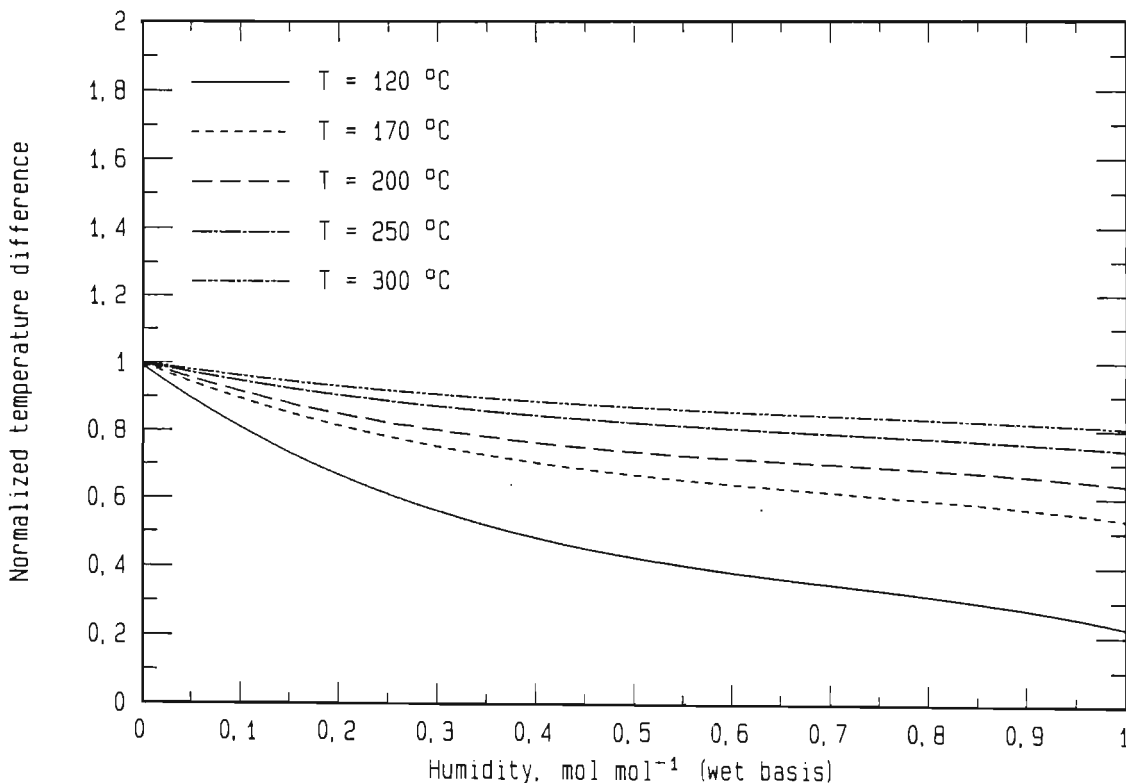


Figure 34: Normalized temperature difference for data of Yoshida [Y2]

The normalized latent heat is defined as the latent heat in steam drying divided by the latent heat in air drying. In air the material is at the wet-bulb temperature and in steam at the boiling point. As the latent heat decreases with temperature, the normalized latent heat is always smaller than unity. For a gas temperature of 100 °C the normalized latent heat has a value of 0,93 and for a temperature of 300 °C a value of 0,95. This change with temperature is small and the influence of the temperature change of the normalized latent heat on the normalized evaporation rate is therefore neglected.

At temperatures below the inversion temperature, the higher temperature driving force in air dominates. With an increase in temperature, this advantage of air is eroded, and the higher heat transfer coefficient in steam becomes dominant. This means that the root cause of the inversion temperature is the reduction in the normalized temperature driving force with increasing temperature.

In Section 4.1.1, a mathematical model was presented to determine the inversion temperature. This model was tested on the experimental data of Yoshida and Hyodo [Y2] and the existence of the inversion temperature was explained on the basis of normalized coefficients. One question that remains is whether or not the inversion temperature is unique, i.e. independent of the system geometry and the mass flow rate of the drying medium. A discussion of this topic in the main part of this thesis would lead too far. Therefore this question is addressed in Appendix D.

#### 4.2 Theoretical and experimental results for the inversion temperature in an equilibrium system

In an equilibrium system, the inversion temperature is determined by a total energy balance around the drying system. The kinetics of heat and mass transfer play a role only in so far as they determine the temperature at which the drying medium (air) leaves the drying system (i.e. the wet-bulb temperature).

#### 4.2.1 Mathematical model for the inversion temperature in an equilibrium system

The inversion temperature is determined by expressing the drying rate in air and in steam over the total energy that the drying medium transmits to the wet material.

In the case of air, the material is at the wet-bulb temperature. Therefore the drying rate can be expressed by:

$$\dot{m}_{ev,a,I} = \frac{\dot{m}_a c_{pa} (T_{in} - T_{wb})}{\Delta h_v + T_{wb} t} \quad (20)$$

In the case of steam, the material is at the boiling point and the drying rate can be written as:

$$\dot{m}_{ev,s,I} = \frac{\dot{m}_s c_{ps} (T_{in} - T_b)}{\Delta h_v + T_b t} \quad (21)$$

At the inversion temperature, the drying rate in air and in steam is equal. If, furthermore, air and steam pass at the same mass flow rate over the material, the inversion temperature can be iteratively determined over the following equation:

$$T_i = \frac{T_b - \frac{c_{pa}}{c_{ps}} \frac{\Delta h_v + T_b t}{\Delta h_v + T_{wb} t} T_{wb}}{1 - \frac{c_{pa}}{c_{ps}} \frac{\Delta h_v + T_b t}{\Delta h_v + T_{wb} t}} \quad (22)$$

This form of the inversion temperature is formally analogous to the inversion temperature in the non-equilibrium case (Equation 13). The heat transfer coefficients expressing the kinetics of heat transfer have been replaced by the specific heat capacities expressing the heat storage capacity of the drying media.

The wet-bulb temperature that is used in Equations 20 and 22 needs still to be determined from the kinetic equilibrium between heat and mass transfer, analogous to the non-equilibrium case (Equation 14).

#### 4.2.2 Experimental results for the inversion temperature in an equilibrium system

The fluidized-bed drying tests were run under conditions at which equilibrium between the drying medium and the material should be reached. Therefore these drying tests were taken to be indicative of the inversion temperature in an equilibrium system.

In Figures 35 to 37 the drying rate during the constant drying rate period is plotted for air and for steam as a function of the inlet temperature into the dryer. The inversion temperature lies between 163 °C and 172 °C. For an equilibrium system at a pressure of 87 kPa (a pressure corresponding to the altitude of Pretoria (1 370 m above sea level)), Equation 22 predicts an inversion temperature of 154,2 °C. The experimental results gave an inversion temperature above the theoretically expected inversion temperature.

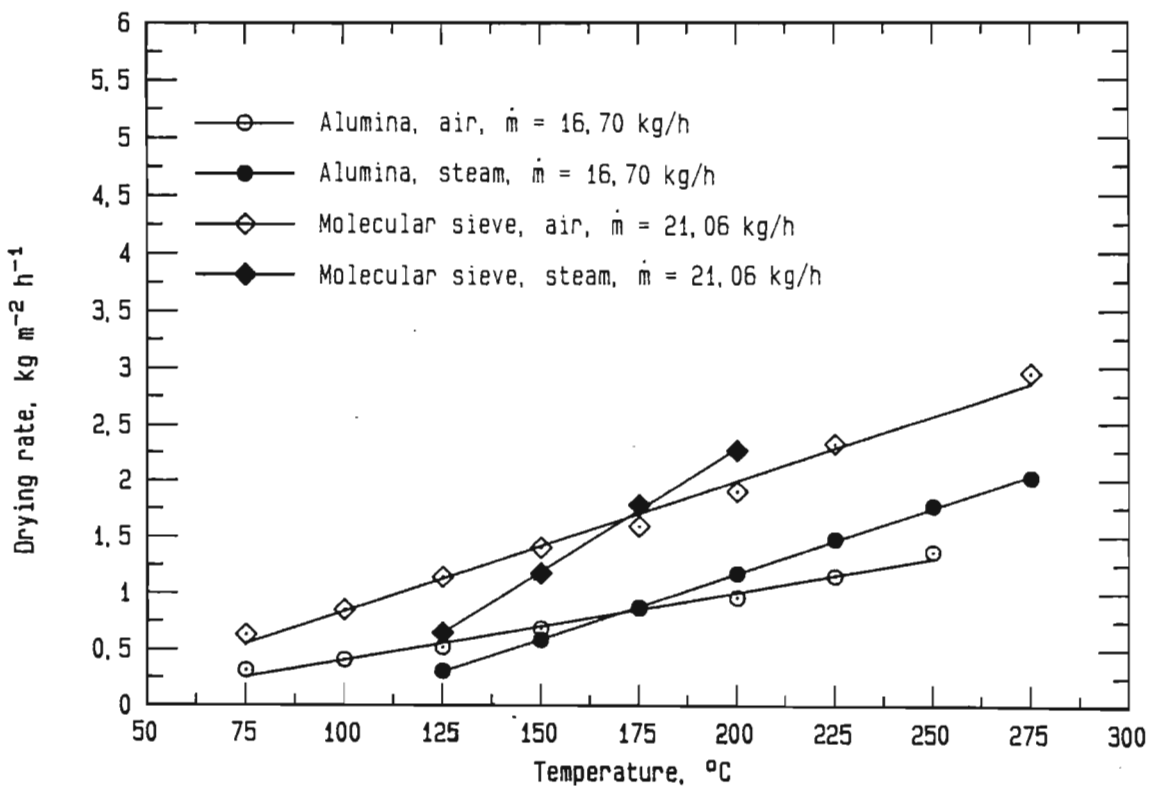


Figure 35: Experimental data for inversion temperature in a fluidized bed ( $\dot{m}_g = 16,70$  kg h<sup>-1</sup> for alumina and  $\dot{m}_g = 21,06$  kg h<sup>-1</sup> for molecular sieve)

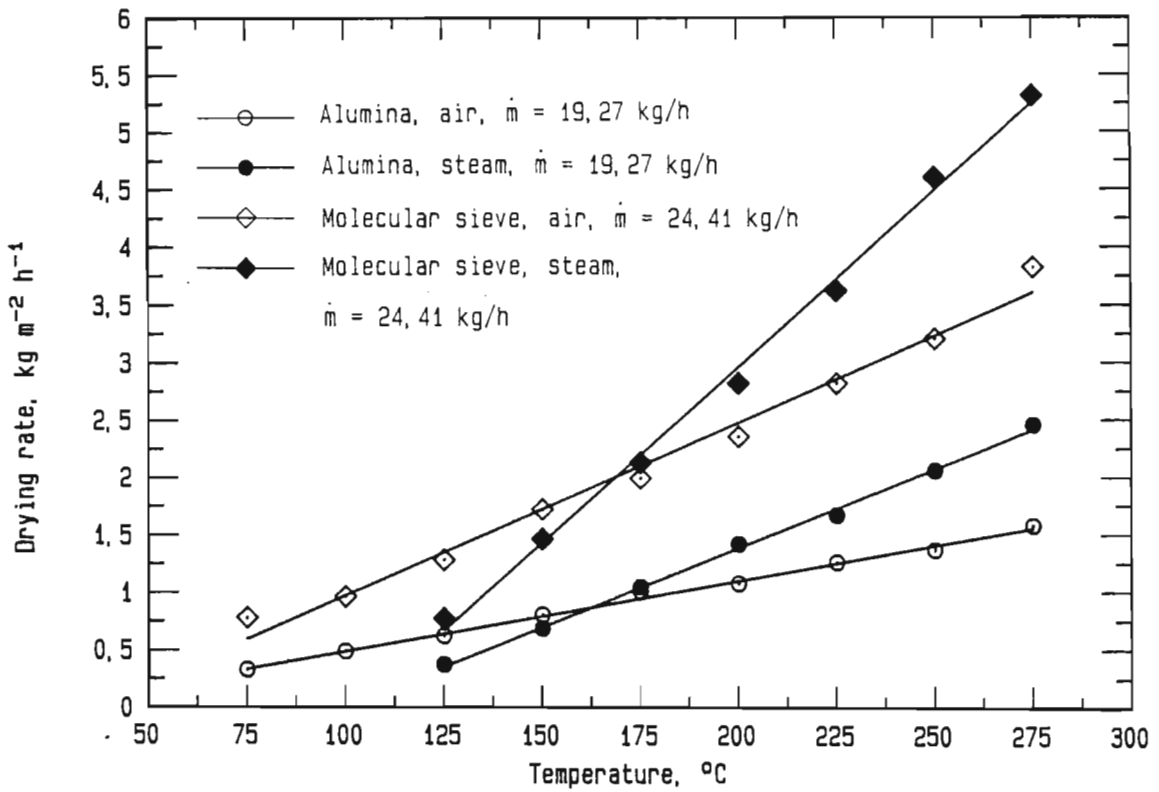


Figure 36: Experimental data for inversion temperature in a fluidized bed ( $\dot{m}_g = 19,27$  kg h<sup>-1</sup> for alumina and  $\dot{m}_g = 24,41$  kg h<sup>-1</sup> for molecular sieve)

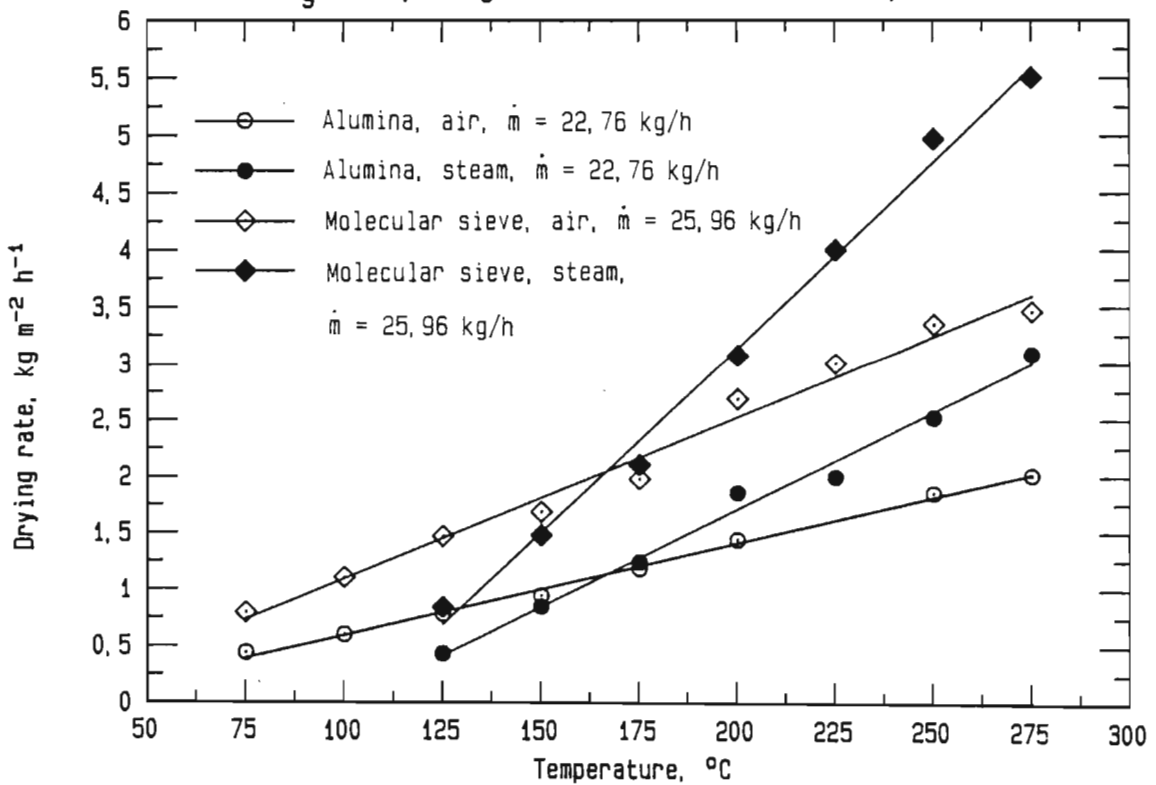


Figure 37: Experimental data for inversion temperature in a fluidized bed ( $\dot{m}_g = 22,76$  kg h<sup>-1</sup> for alumina and  $\dot{m}_g = 25,96$  kg h<sup>-1</sup> for molecular sieve)

An explanation for this may be found in the by-pass mass flow rate of the drying medium in fluidized beds. One part of the drying medium flows through the dryer in the form of bubbles. These bubbles do not take part fully in the mass and heat transfer. This phenomenon can be described by the by-pass volume of drying medium. It has been found by various authors [P1,Z1] that in a fluidized bed the by-pass volume is of the order of 5 to 10 %. The exact by-pass volume depends on the type of distributor plate, on the type of fluidizing material, on the dimensions and shape of the fluidized bed and on the operating conditions (temperature, mass flow rates, etc.). As a result of this by-pass flow, the exit temperature from the dryer lies above the wet-bulb temperature. Indeed, at the outlet of the dryer, the by-pass drying medium is at conditions close to those of the inlet. After leaving the bed, it mixes with the bulk of the drying medium that took part in the drying process and attained equilibrium with the material (i.e. is at the wet-bulb temperature and saturation humidity). After mixing, the resulting exhaust stream is no longer in equilibrium with the material. This means that the present fluidized bed dryer is not an ideal equilibrium system.

In Table 5 the theoretical inversion temperature is presented for various by-pass mass fractions of air and steam.

Table 5: Inversion temperature of an equilibrium system  
as a function of the by-pass mass fraction (fbp)

fbp,a	fbp,s	0,000	0,025	0,050	0,075
0,000		154,2	157,0	160,1	163,2
0,025		151,7	154,2	157,0	160,1
0,050		149,2	151,7	154,2	157,0
0,075		147,0	149,2	151,7	154,2

One can see that it is not the total amount of by-pass mass flow that determines the inversion temperature, but the difference between the by-pass flow in air and in steam. The by-pass mass flow in steam must be more than 7,5 % higher than that in air to explain the results in Figures 35 to 37. The by-pass mass fractions of air and of steam are discussed below.



In order to determine the by-pass mass fraction in air, the difference between the measured outlet temperature and the theoretical equilibrium temperature (wet-bulb temperature) is plotted against the inlet temperature in Figure 38.

The continuous lines represent the theoretically calculated values for various by-pass mass fractions. The temperature of the exhaust stream is calculated from the following equation:

$$T_{out} = (1-f_{bp}) T_{wb} + f_{bp} T_{in} \quad (23)$$

Here  $f_{bp}$  is the mass fraction of by-pass flow of the drying medium.

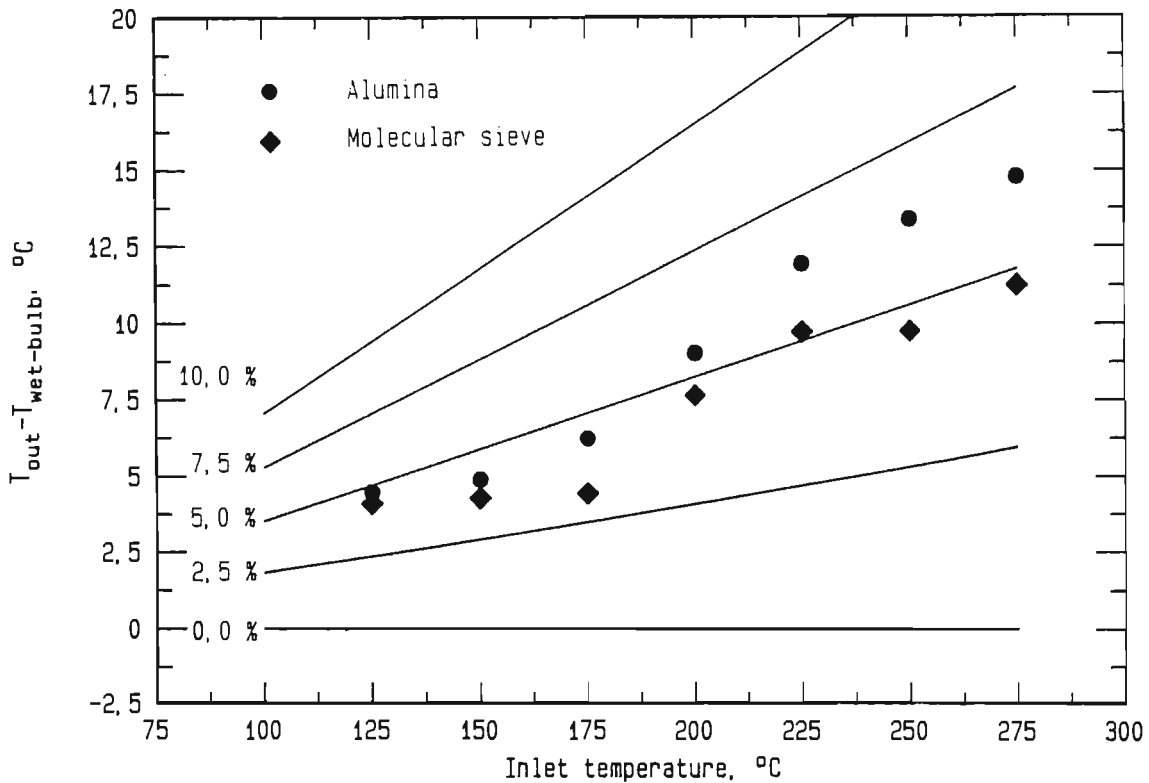


Figure 38: Outlet temperature in a fluidized bed as function of by-pass mass flow

The by-pass mass fraction is of the order of 5 %, an amount that has been found by other authors [P1]. It is higher for the higher temperatures and lower for the lower temperatures. Furthermore, the by-pass mass fraction is lower for molecular sieve and higher for alumina. An explanation for this behaviour may be found in the difference between the sizes of the bubbles that flow through the

beds of molecular sieve and alumina. However, these results will not be investigated in more detail, as an indication of the by-pass mass fraction is sufficient.

No indication could be obtained for the by-pass mass fraction in steam, because condensation took place on the thermocouple measuring the outlet temperature of the steam. As a result, the thermocouple registered boiling point throughout the constant drying rate period.

The by-pass mass fractions in air and in steam were evaluated theoretically. According to Palancz [P1], the volume fraction of bubbles in the bed can be calculated from the following ratio:

$$\delta = \frac{u_f - u_{mf}}{u_{bc}} \quad (24)$$

Here  $u_f$  is the fluidizing velocity,  $u_{mf}$  is the minimum fluidizing velocity and  $u_{bc}$  is the absolute velocity of a crowd of bubbles in the bed.

$u_{bc}$  is determined from the following formula:

$$u_{bc} = u_f - u_{mf} + u_{br} \quad (25)$$

$u_{br}$  is the rising velocity of a single bubble relative to the emulsion phase and can be written, according to Davidson and Harrison [D2], as:

$$u_{br} = 0,711 (g d_b)^{0,5} \quad (26)$$

Using Equations 24 to 26, the volume fraction of bubbles in the bed can be calculated for air and for steam for bubbles of different diameter. The results are presented in Tables 6 and 7.

For the same mass flow rate of drying medium the amount of bubble gas is always higher in steam than in air. This is due to the higher excess velocity that occurs in steam, the excess velocity being the difference between the actual fluidizing velocity and the minimum fluidizing velocity. The bubble gas is, however, not identical to the

Table 6: Bubble volume fraction in air and in steam for alumina at a mass flow rate of  $19,27 \text{ kg h}^{-1}$

$T_{in}, ^\circ\text{C}$	Bubble diameter, m					
	0,01		0,025		0,05	
	$\delta_{air}$	$\delta_{steam}$	$\delta_{air}$	$\delta_{steam}$	$\delta_{air}$	$\delta_{steam}$
125	0,49	0,67	0,38	0,56	0,30	0,47
150	0,54	0,70	0,43	0,60	0,34	0,52
175	0,59	0,74	0,47	0,64	0,39	0,55
200	0,62	0,76	0,51	0,67	0,42	0,59
225	0,65	0,78	0,54	0,69	0,45	0,62
250	0,68	0,80	0,57	0,71	0,48	0,64
275	0,70	0,81	0,59	0,74	0,51	0,66

Table 7: Bubble volume fraction in air and in steam for molecular sieve at a mass flow rate of  $24,41 \text{ kg h}^{-1}$

$T_{in}, ^\circ\text{C}$	Bubble diameter, m					
	0,01		0,025		0,05	
	$\delta_{air}$	$\delta_{steam}$	$\delta_{air}$	$\delta_{steam}$	$\delta_{air}$	$\delta_{steam}$
125	0,59	0,74	0,48	0,64	0,39	0,56
150	0,64	0,77	0,52	0,68	0,44	0,60
175	0,67	0,79	0,56	0,71	0,47	0,63
200	0,70	0,81	0,59	0,73	0,51	0,66
225	0,72	0,82	0,62	0,75	0,54	0,69
250	0,75	0,83	0,65	0,77	0,56	0,71
275	0,76	0,84	0,67	0,78	0,59	0,72

by-pass gas. The difference is that the bubble gas participates to a certain extent in the heat and mass transfer, whereas the by-pass gas is a theoretical concept and does not participate at all in the heat and mass transfer processes. The amount of bubble gas is, however, an indication of the amount of by-pass gas. From the results in Tables 6 and 7, one would therefore expect an inversion temperature that is higher than that of an ideal equilibrium case. This is also what is found in Figures 35 to 37.

#### 4.3 Theoretical determination and experimental results of the gas-to-solid heat transfer coefficient in a fluidized bed

The same tests that are used to determine the drying kinetics are also used to determine the gas-to-solid heat transfer coefficient in a fluidized bed. During the constant drying rate period, the temperature of the material is constant. Therefore the steady state technique is used to determine the gas-to-solid heat transfer coefficient.

The experimental data are evaluated using the following assumptions:

- plug flow for the fluidizing medium, and
- well-mixed flow for the solids.

##### 4.3.1 Theoretical determination of the gas-to-solid heat transfer coefficient in a fluidized bed

The following evaluation is done for air, but the evaluation for steam is analogous. The energy balance over a differential volume of the fluidized bed can be written as follows:

$$\frac{d\dot{H}}{dz} + d\dot{q} = 0 \quad (27)$$

The kinetic expression for the differential heat transfer,  $dq$ , can be written as follows:

$$d\dot{q} = h (T_a - T_p) \quad (28)$$

The enthalpy flow of the fluidizing medium can be written as follows:

$$\dot{H} = \dot{M}_a c_{pa} T_a + \dot{M}_a Y c_{ps} T_a \quad (29)$$

The derivative of the enthalpy with respect to height can then be expressed as follows:

$$\frac{d\dot{H}}{dz} = \dot{M}_a (c_{pa} + Y c_{ps}) \frac{dT_a}{dz} + \dot{M}_a c_{ps} T_a \frac{dY}{dz} \quad (30)$$

The specific heat capacities of the drying medium,  $c_{pa}$ , and of the vapour,  $c_{ps}$ , are considered to be independent of temperature and are determined at the arithmetic mean temperature between inlet and outlet of the dryer.

In general, the humidity increase of the drying medium with the height in the fluidized bed is neglected in the literature. In this thesis the moisture change of the drying medium with height in the dryer is taken into account. In Appendix G, the consequences of this are discussed.

The humidity profile in the bed can be derived by a mass balance. The mass balance over a differential volume of fluidized bed is written as follows:

$$\dot{M}_a \frac{dY}{dz} - d\dot{m}_{ev} = 0 \quad (31)$$

During the constant drying rate period, all the heat that is transmitted to the material is used for drying. Therefore the mass transfer can be expressed by the heat transfer according to following expression:

$$d\dot{m}_{ev} = \frac{d\dot{q}}{(\Delta h_v + c_{ps} (T_a - T_p))} \quad (32)$$

In this expression the superheating of the moisture after evaporation is taken into account. Because of the well-mixed behaviour of the particles in the fluidized bed, the particle temperature is constant over the height of the dryer. The latent heat is calculated at the particle temperature.

Using Equations 28, 31 and 32, the following expression for the humidity profile is obtained:

$$\dot{M}_a \frac{dY}{dz} = \frac{h (T_a - T_p) a \Phi}{\Delta h_v + c_{ps} (T_a - T_p)} \quad (33)$$

With Equations 28, 30 and 33, Equation 27 can be written as follows:

$$\dot{M}_a (c_{pa} + Y c_{ps}) \frac{dT_a}{dz} + h a \Phi (T_a - T_p) \left(1 + \frac{c_{ps} T_a}{\Delta h_v + c_{ps} (T_a - T_p)}\right) = 0 \quad (34)$$

The temperature gradient of the fluidizing medium can then be expressed by:

$$\frac{dT_a}{dz} = - h a \Phi (T_a - T_p) \frac{\left(1 + \frac{c_{ps} T_a}{\Delta h_v + c_{ps} (T_a - T_p)}\right)}{\dot{M}_a (c_{pa} + Y c_{ps})} \quad (35)$$

By separating the variables, one gets following expression:

$$\frac{dT_a}{(T_a - T_p) \left(1 + \frac{c_{ps} T_a}{\Delta h_v + c_{ps} (T_a - T_p)}\right)} = - \frac{h a \Phi}{\dot{M}_a (c_{pa} + Y c_{ps})} dz \quad (36)$$

By integrating Equation 36, the temperature of the drying medium is determined as a function of the height in the dryer. The integration of this temperature function is given in full in the Appendix F.

The only unknown is the heat transfer coefficient. In the present experiments the temperature of the drying medium was measured at five different levels in the dryer. For each measuring point the heat transfer coefficient was determined. Only temperature readings that differed by more than 2 °C from the outlet temperature were considered, as otherwise the measuring inaccuracies led to erroneous results. The arithmetic average of the results considered gave the heat transfer coefficient.

For the steam case, the derivation of Equation 36 is analogous. The expression  $\dot{M}_a (c_{pa} + Y c_{ps})$  is replaced by the expression  $\dot{M}_s c_{ps}$ .

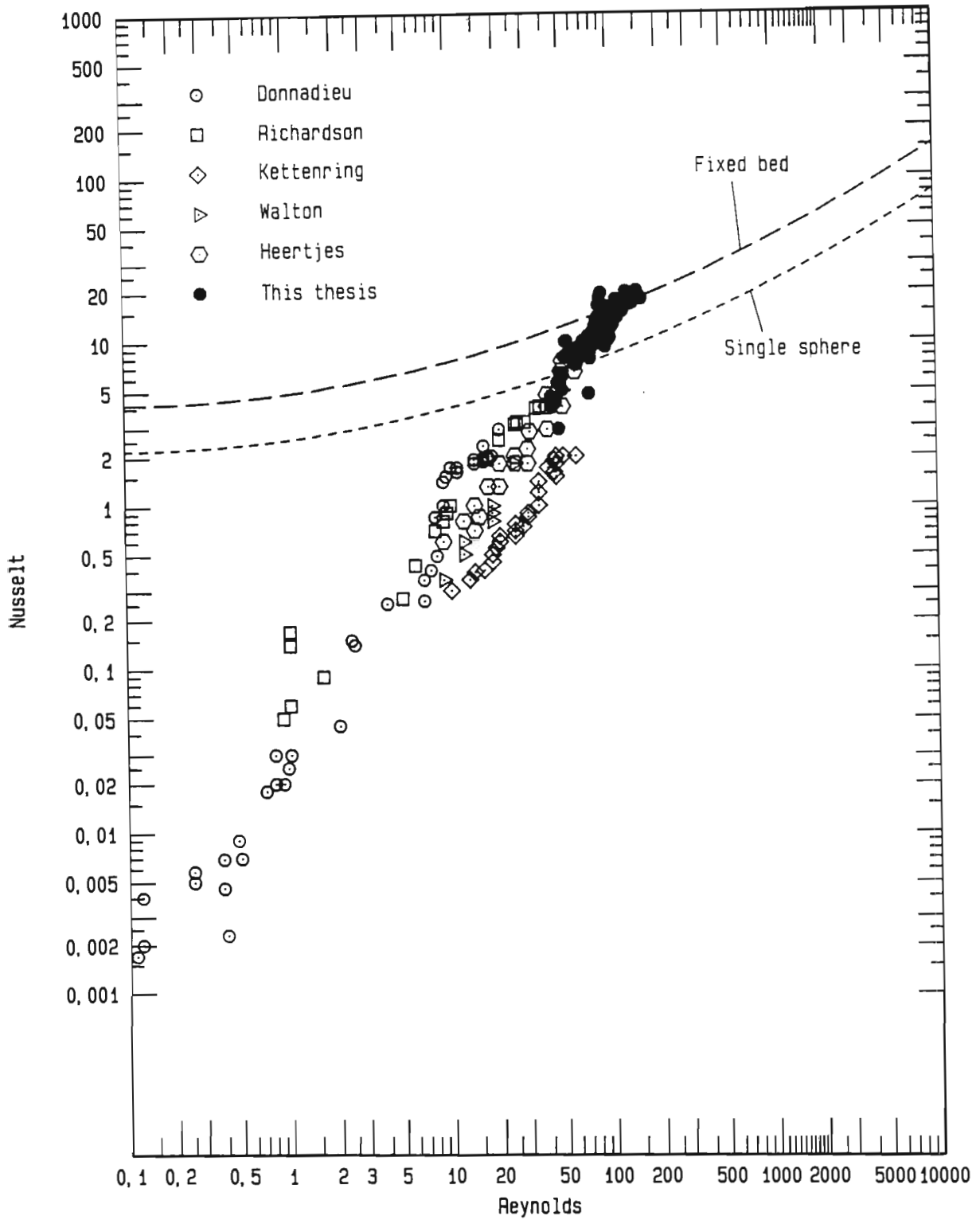


Figure 39: Literature data and own experimental data on heat transfer coefficients in a fluidized bed

#### 4.3.2 Experimental results of the gas-to-solid heat transfer coefficient in a fluidized bed

In Figure 39 the present data are compared with literature data from various authors. The data are presented in the form of dimensionless numbers as Nusselt number versus Reynolds number. The Reynolds number was calculated using the mean diameter of the particles and the free linear velocity at the inlet into the dryer. The Reynolds number was not corrected for the porosity of the bed. The continuous line represents Equation 37 proposed by Kothari [K14] for heat transfer in fluidized beds:

$$Nu = 0,03 Re^{1,3} \quad (37)$$

The Reynolds number range that was investigated (42,3 to 155,6) lies around 100. The literature data [K12,M1,M7] indicate that a Reynolds number of 100 is critical for the correlation of heat transfer data in a fluidized bed. The present data are at the high end of the Reynolds number range and agree well with the data of the other authors. For higher Reynolds numbers, no heat transfer data that could be used directly in this figure were found in the literature.

The data for air and for steam are now compared. In Figure 40 the data are presented for air and in Figure 41 for steam. In both figures the continuous line represents Equation 37. The data for steam are not as widely scattered and they agree well with Equation 37. The data for air are more scattered and lie, on average, above Equation 37. Because of the higher heat capacity of steam, the temperature profile of steam extends to higher bed heights than the temperature profile of air. The temperatures  $T_{az}$  that are measured and used in Equation 36 to calculate the heat transfer coefficient in steam differ more from the particle temperature than those measured in air. This gives a higher accuracy of the calculated values.

In summary one can say that the heat transfer correlation given by Equation 37 can be used to determine the gas-to solid heat transfer coefficient in a fluidized bed both in air and in steam.



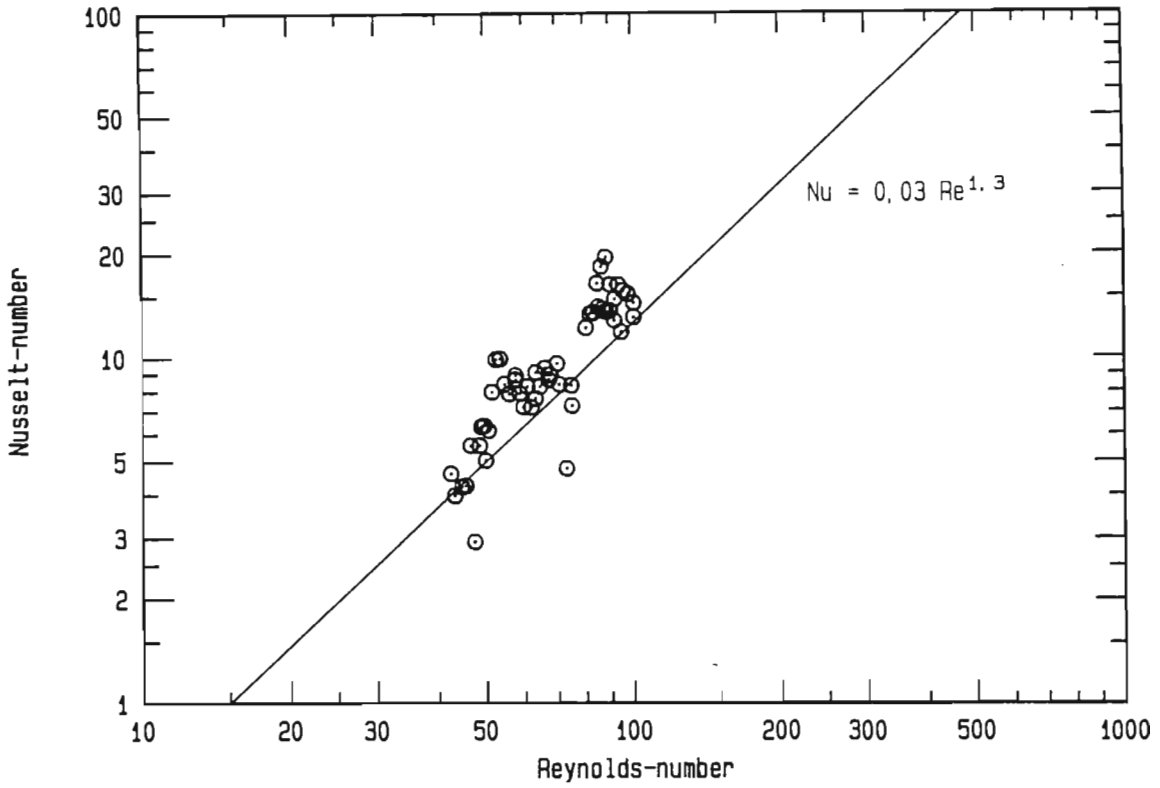


Figure 40: Experimental data on air-to-solid heat transfer coefficient in a fluidized bed

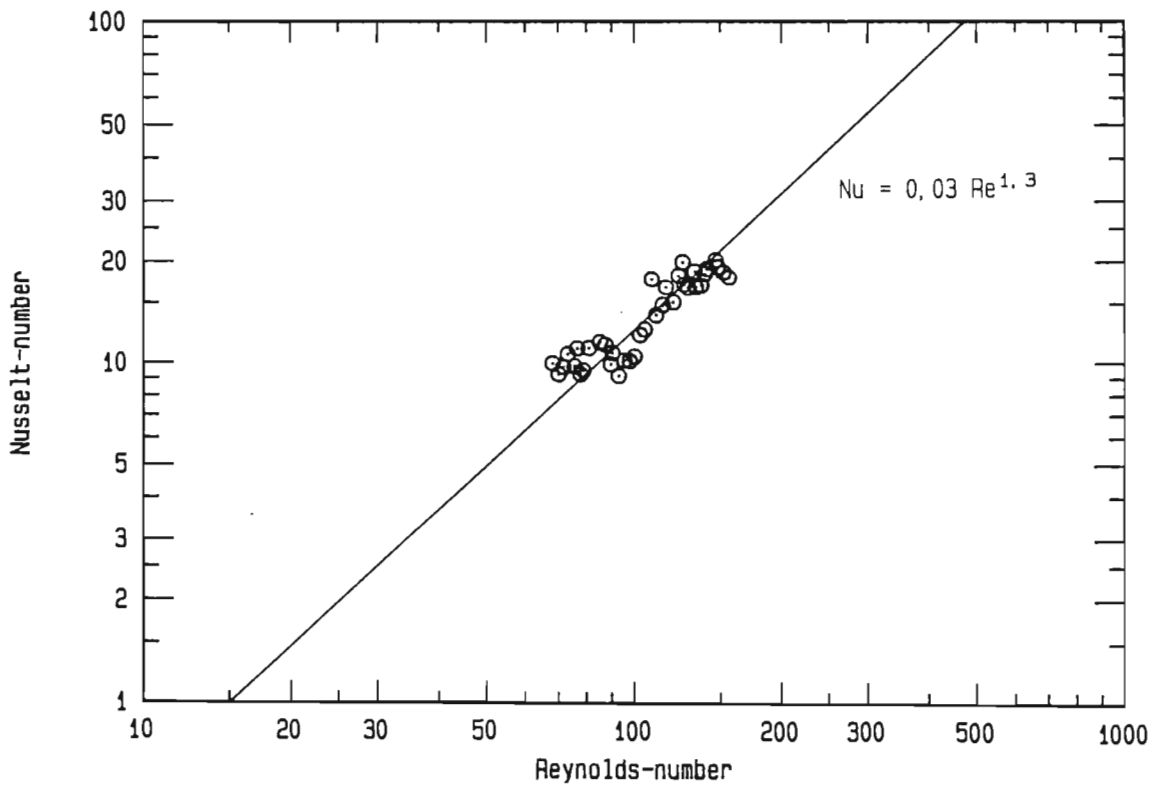


Figure 41: Experimental data on steam-to-solid heat transfer coefficient in a fluidized bed

#### 4.4 Comparison of the experimental drying rate curves recorded in a fluidized bed in air and in steam

As was mentioned earlier, the shape of the drying rate curve is strongly dependent on the material to be dried. The drying rate curves for alumina and molecular sieve are therefore discussed separately.

##### 4.4.1 Drying rate curves for alumina

In Figures 42 to 47 the drying rate curves for alumina in air and in steam are plotted as a function of the gas inlet temperature into the dryer. For easier comparison, the x and y-scales are the same in all the figures. Between two curves, the inlet temperature of the drying medium was raised by 25 °C. For air, the lowest temperature is 75 °C and for steam, 125 °C. For both drying media, the highest temperature is 275 °C. Not all the measured points are plotted in the figures, as otherwise they would be overloaded.

The shape of the drying rate curves are similar in air and in steam and one can clearly see a constant drying rate and a falling drying rate period. During the constant drying rate period, the drying rate in steam increases more sharply with an increase in temperature (this phenomenon was discussed in Section 4.2). The drying rate curves for steam are therefore more widely spaced. The beginning of the falling drying rate period is not marked by a sharp decrease, but by a smooth decline of the drying rate. Therefore the critical moisture content cannot be clearly determined from Figures 42 to 47. However, one can see that the critical moisture content for air and for steam is similar. The falling drying rate period is convexly shaped outwards. Because of the high temperatures that were used in the steam tests and because the air tests were carried out with completely dry air, the equilibrium moisture content was assumed to be zero.

For a direct comparison, the drying rate curves in air and in steam are plotted at three different temperatures (125 °C, 175 °C, 225 °C) in Figure 48.

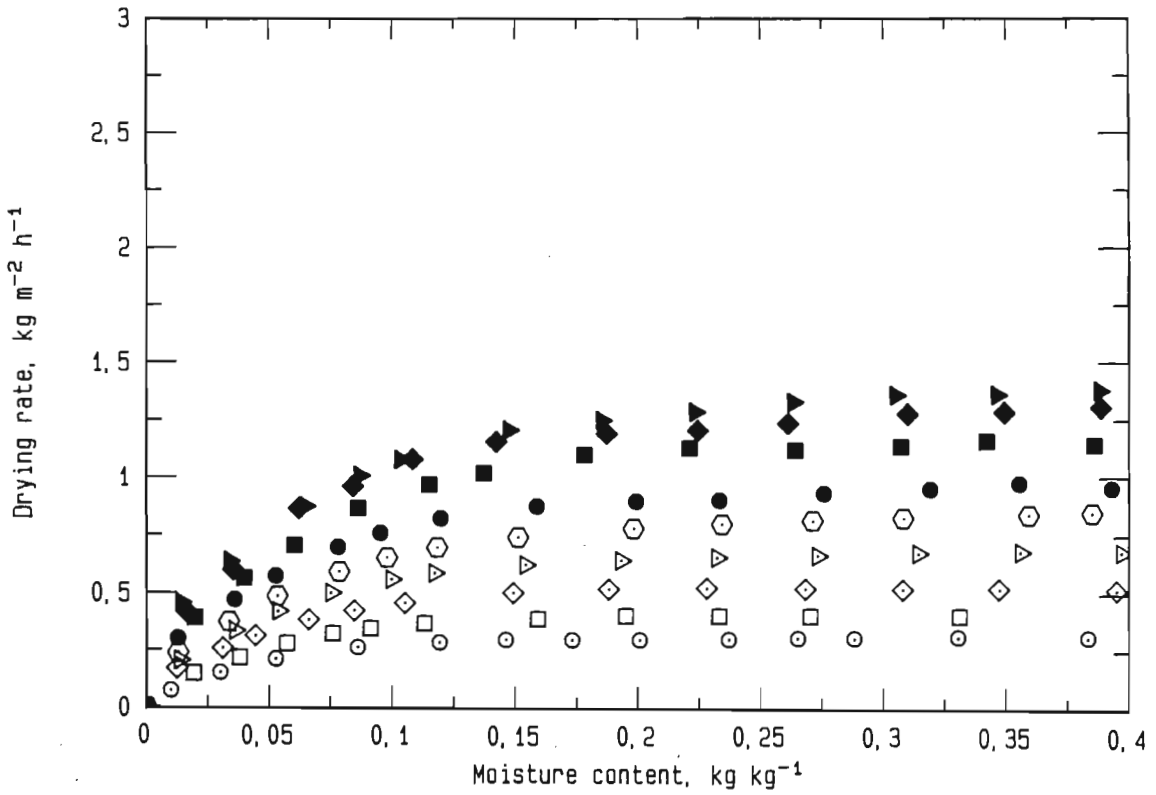


Figure 42: Experimental drying rates of alumina in air  
at an air flow rate of  $16,70 \text{ kg h}^{-1}$   
(see Nomenclature for symbols)

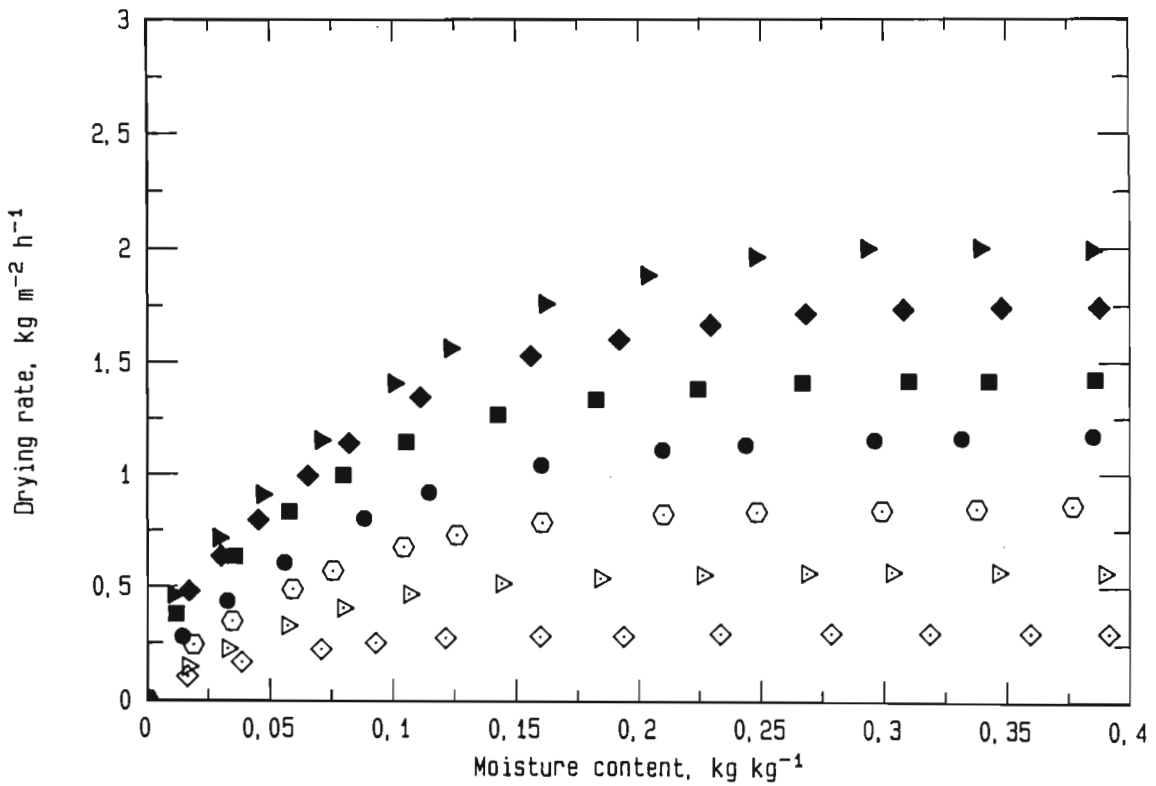


Figure 43: Experimental drying rates of alumina in steam  
at a steam flow rate of  $16,70 \text{ kg h}^{-1}$   
(see Nomenclature for symbols)

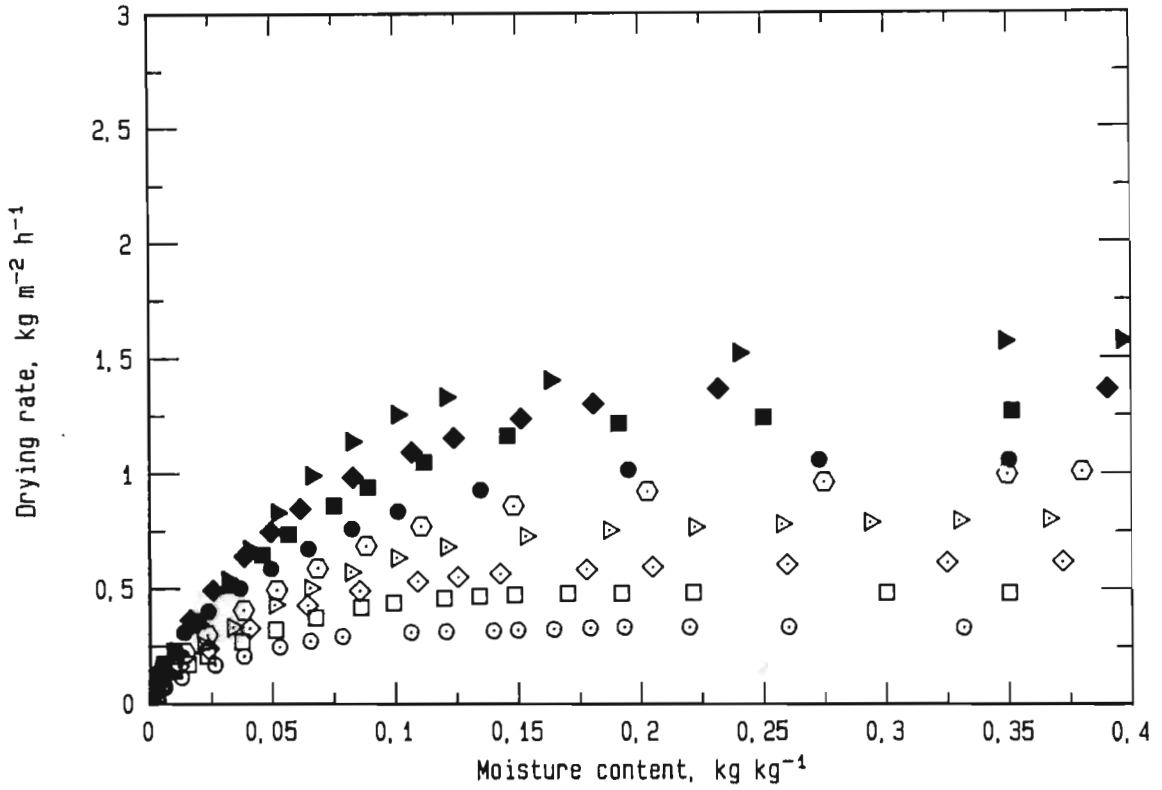


Figure 44: Experimental drying rates of alumina in air  
at an air flow rate of  $19,27 \text{ kg h}^{-1}$   
(see Nomenclature for symbols)

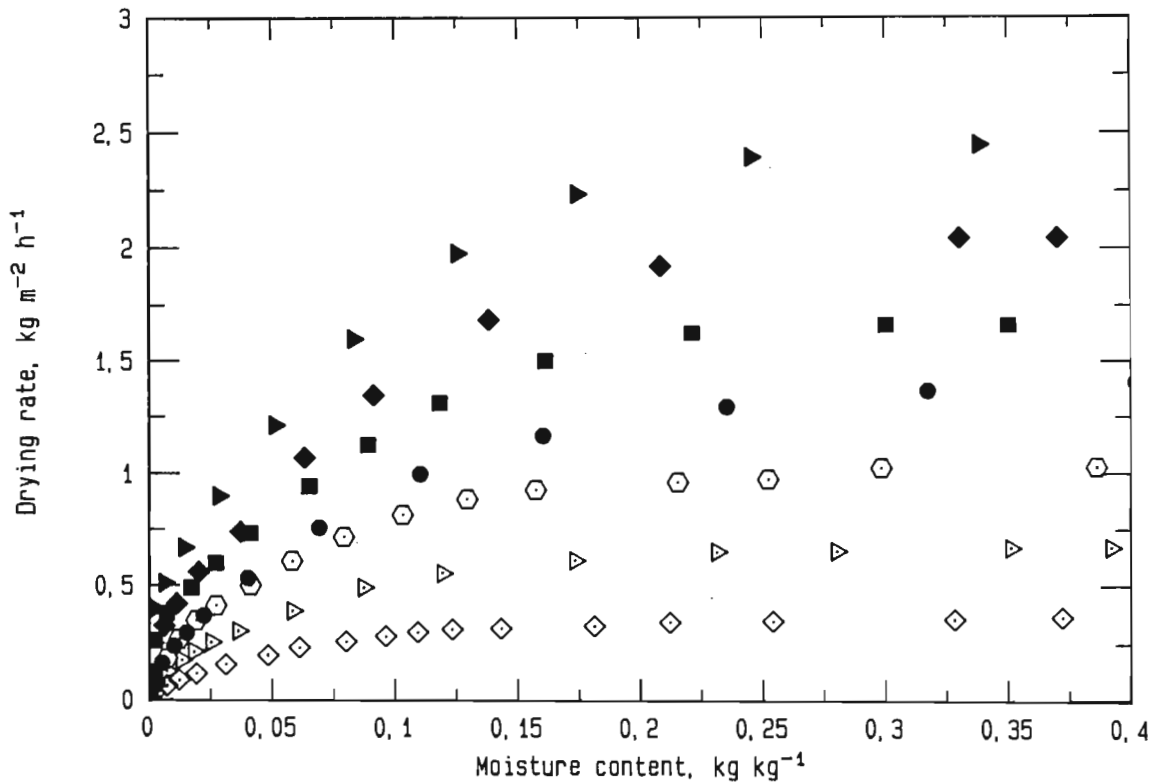


Figure 45: Experimental drying rates of alumina in steam  
at a steam flow rate of  $19,27 \text{ kg h}^{-1}$   
(see Nomenclature for symbols)

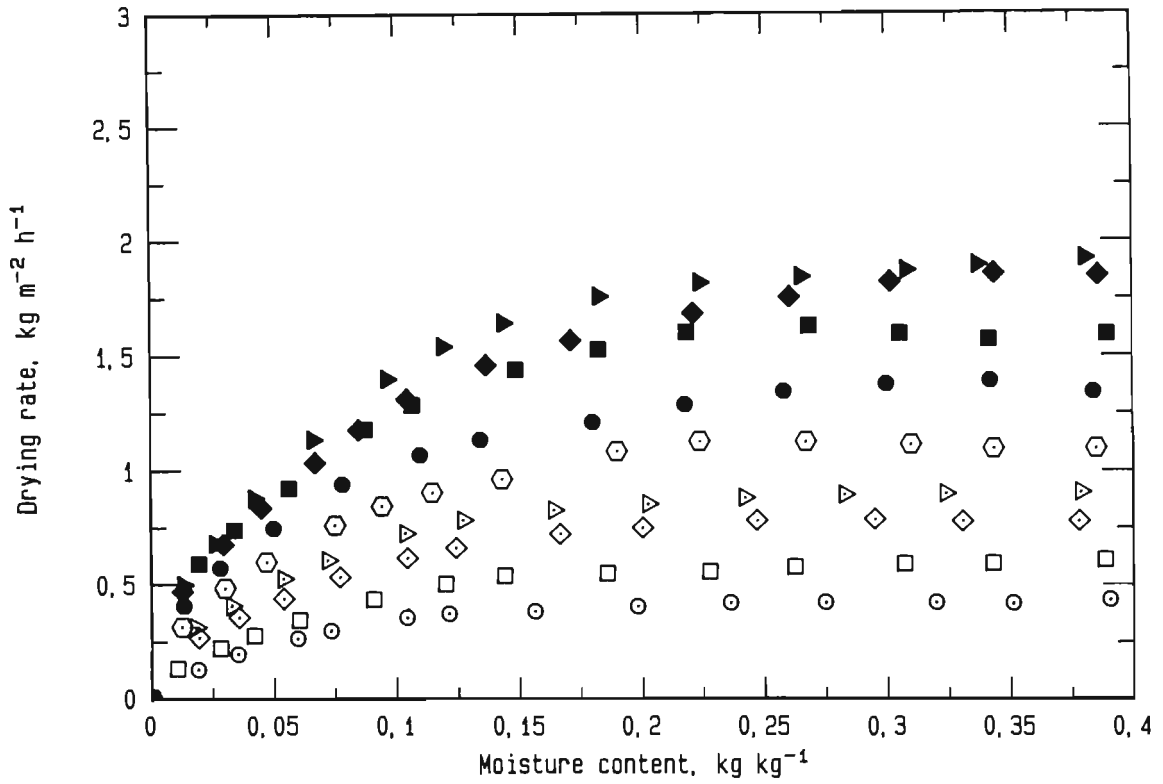


Figure 46: Experimental drying rates of alumina in air  
at an air flow rate of  $22,76 \text{ kg h}^{-1}$   
(see Nomenclature for symbols)

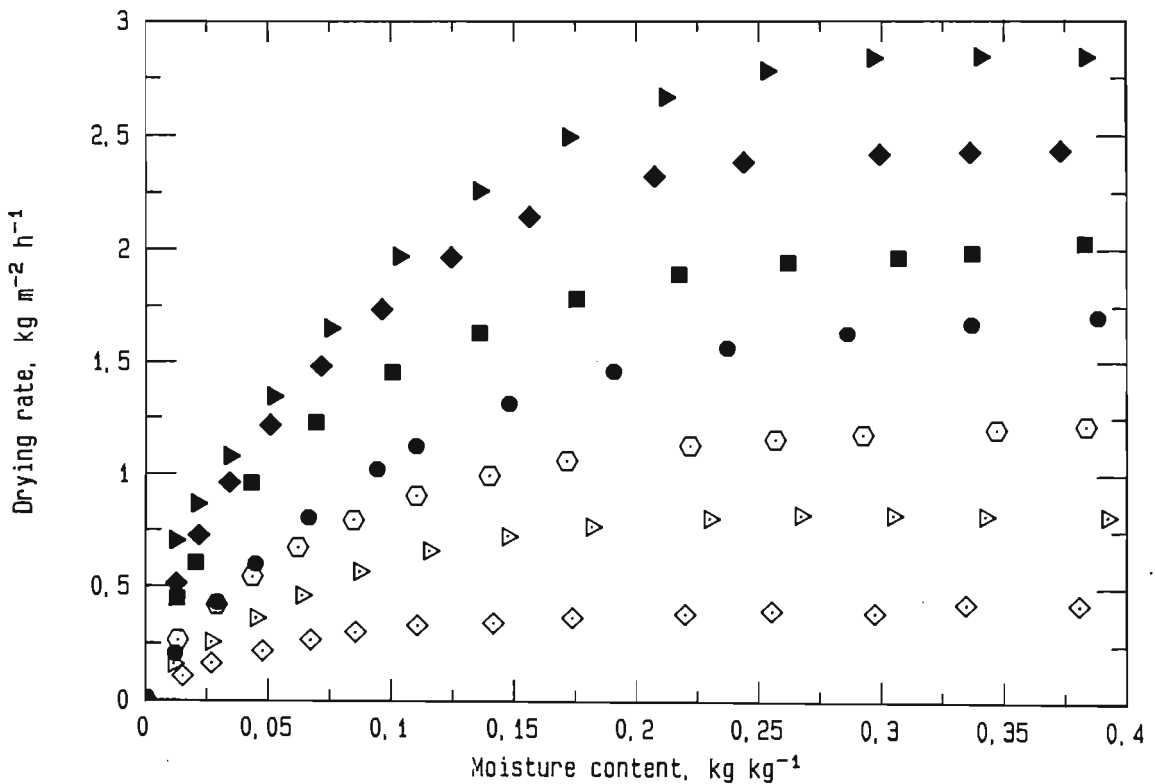


Figure 47: Experimental drying rates of alumina in steam  
at a steam flow rate of  $22,76 \text{ kg h}^{-1}$   
(see Nomenclature for symbols)

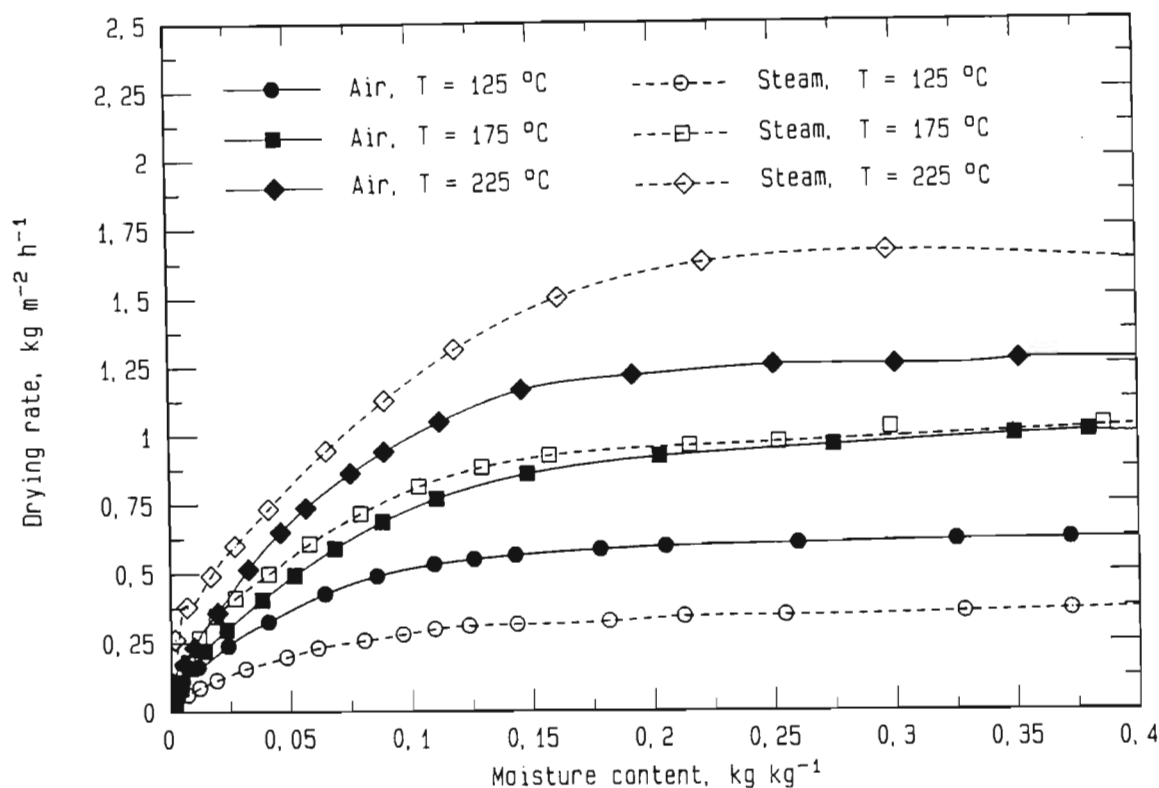


Figure 48: Experimental drying rates of alumina in air and in steam at various temperatures (mass flow rate of 19,27 kg h<sup>-1</sup>)

At the low temperature (125 °C) the drying rate of steam lies below the drying rate of air. This is to be expected, as 125 °C lies below the inversion temperature. One can also clearly see the similarity in the shape of the drying rate curves. This similarity becomes even more apparent at the medium temperature of 175 °C. The two curves are virtually identical, with only a slight advantage on the steam side. This is because the temperature is slightly higher than the inversion temperature. This kinetic advantage also prevails during the falling drying rate period. At the high temperature of 225 °C, the drying rate curve of steam lies far above the drying rate curve of air.

In Figure 49, the drying rates of alumina in air are plotted at different mass flow rates of the drying medium for two temperatures (125 °C and 200 °C). In Figure 50, the rates are plotted for steam. One can clearly see the increase in the drying rate with increases in the mass flow rate.

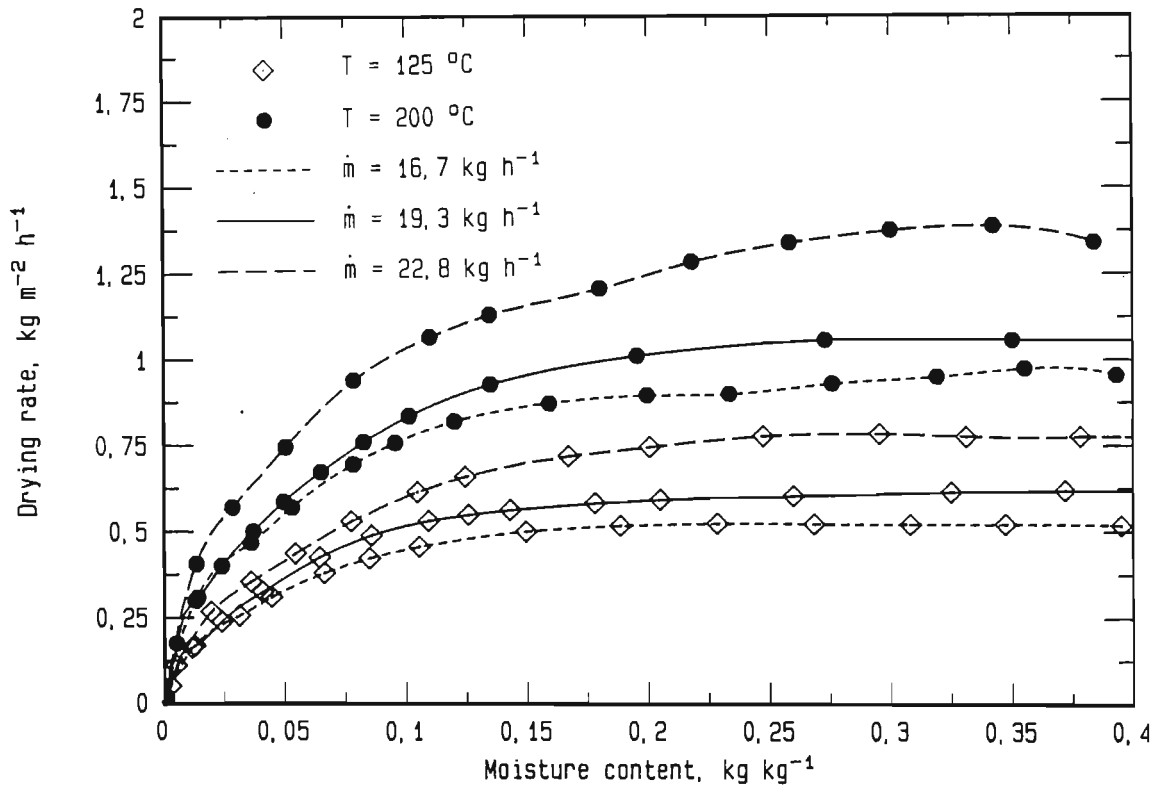


Figure 49: Experimental drying rates of alumina in air  
at various air flow rates

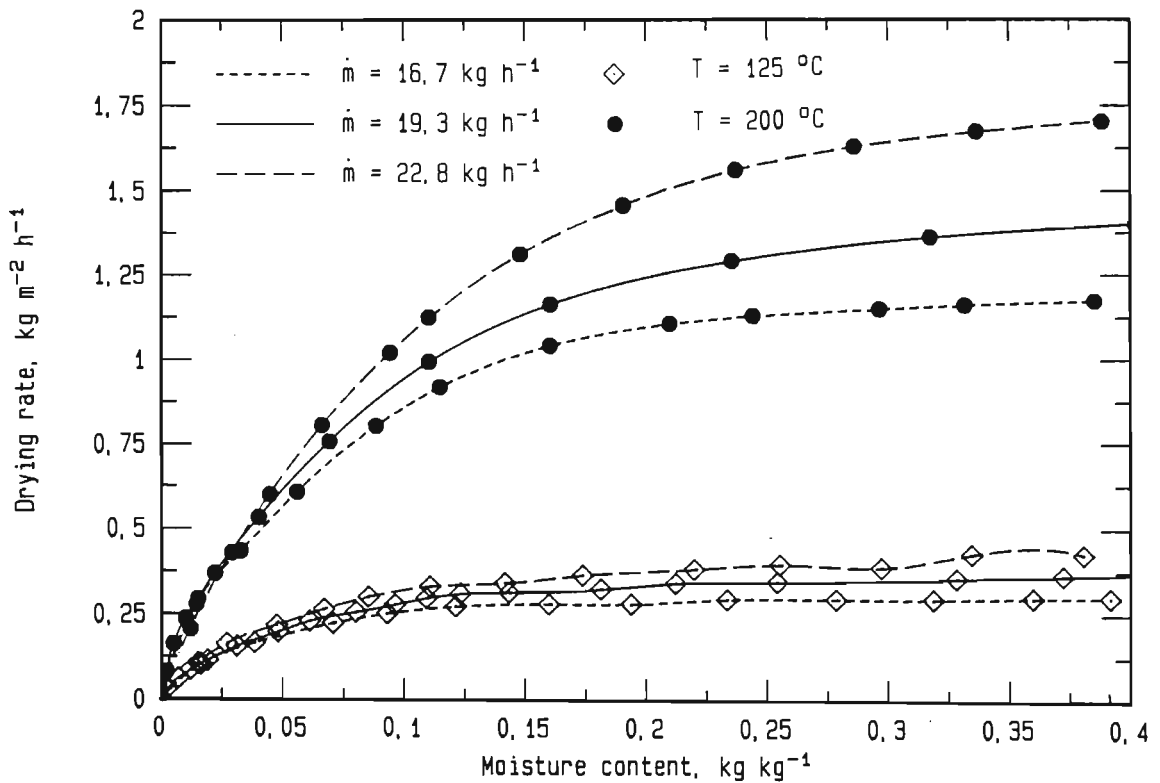


Figure 50: Experimental drying rates of alumina in steam  
at various steam flow rates

#### 4.4.2 Drying rate curves for molecular sieve

In Figures 51 to 56 the drying rate curves for molecular sieve in air and in steam are plotted as a function of the gas inlet temperature into the dryer.

For both drying media, one can clearly see a constant and a falling drying rate period. The shape of the drying rate curve however, is different. In steam the constant drying rate period is extended and the critical moisture content is shifted to lower values. This is a result of the higher particle temperature in steam and consequently of the higher moisture mobility inside the material. This difference was not found for the drying of alumina. The reason is that the pore structure of molecular sieve is finer than that of alumina, and therefore the resistance to moisture movement inside the solid matrix is higher and the influence of this resistance on the drying rate more pronounced. As a consequence, the change in particle temperature (or moisture mobility) between air and steam has a greater impact on the drying rate of molecular sieve than on that of alumina. During the constant drying rate period, the same observations are valid as for alumina. At the beginning of the falling drying rate period, the drying rate drops sharply, but then levels then off and approaches zero. This behaviour can be seen more clearly for air, as here the falling drying rate period is longer, but this also applies, to a lesser extent, to steam. The equilibrium moisture content was assumed to be zero.

For a direct comparison of the drying rate curves in air and in steam, the drying rate curves of molecular sieve in air and in steam are plotted for three different temperatures in Figure 57.

During the constant drying rate period, the behaviour is as expected, with the drying rate in air dominating at low temperatures and the drying rate in steam dominating at high temperatures. Because of the extension of the constant drying rate period in steam, molecular sieve is an interesting material for comparing drying rate curves in the different media.



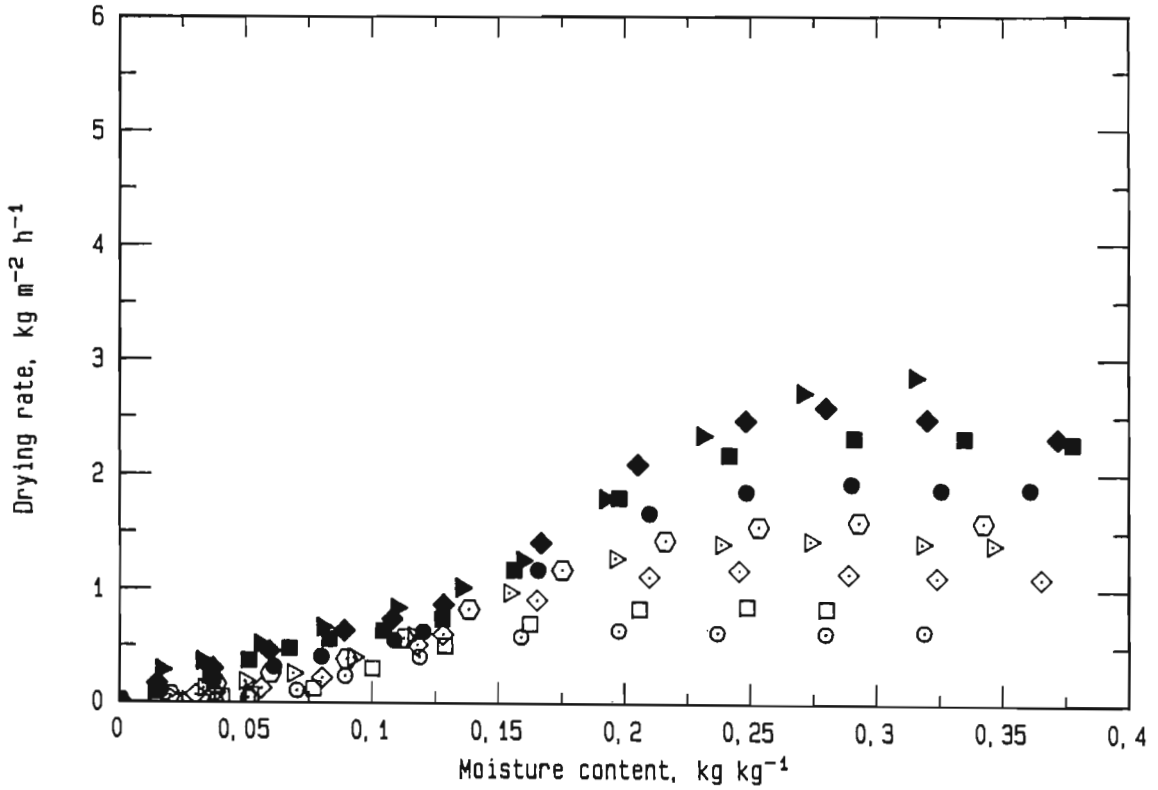


Figure 51: Experimental drying rates of molecular sieve in air  
at an air flow rate of  $21,06 \text{ kg h}^{-1}$   
(see Nomenclature for symbols)

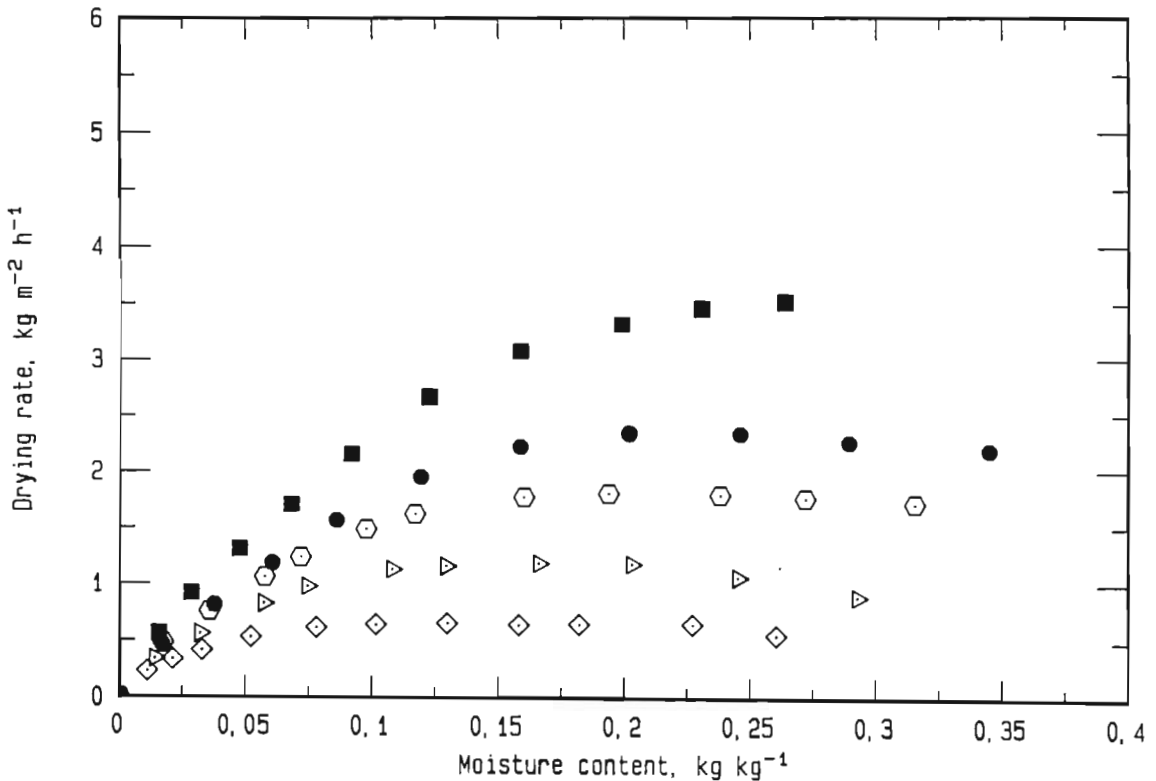


Figure 52: Experimental drying rates of molecular sieve in steam  
at a steam flow rate of  $21,06 \text{ kg h}^{-1}$   
(see Nomenclature for symbols)

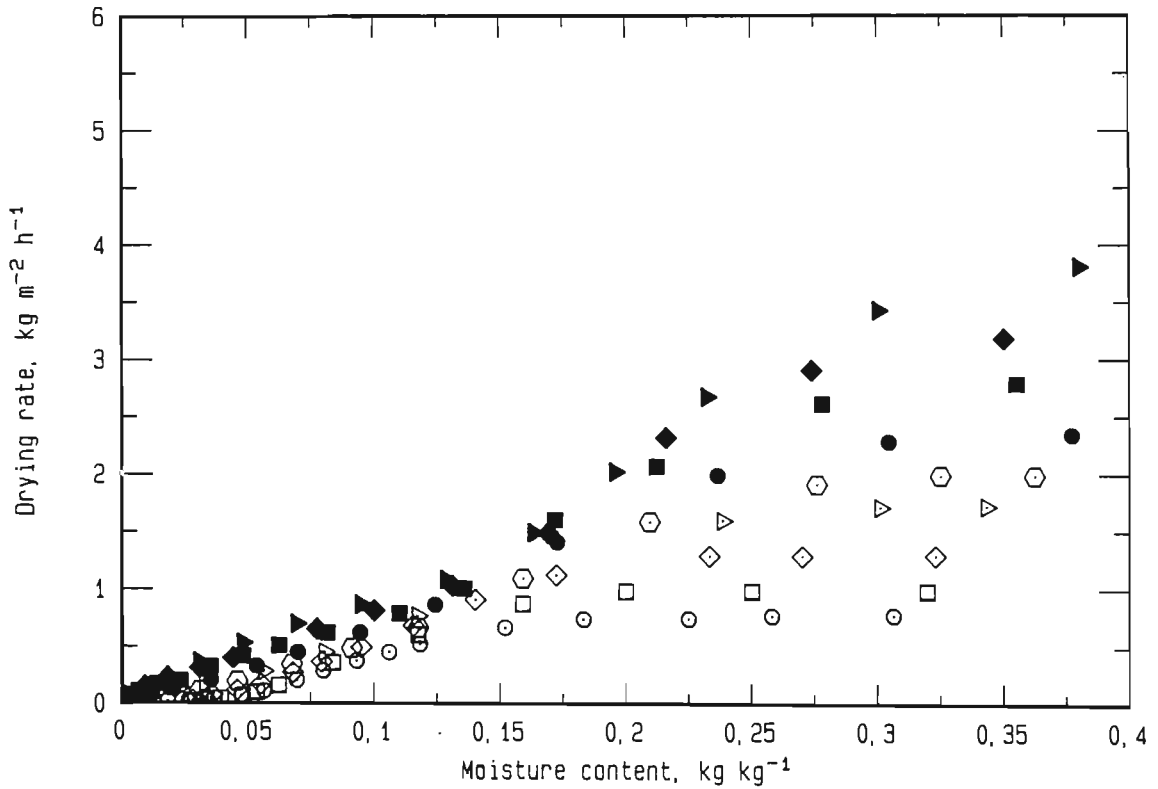


Figure 53: Experimental drying rates of molecular sieve in air  
at an air flow rate of  $24,41 \text{ kg h}^{-1}$   
(see Nomenclature for symbols)

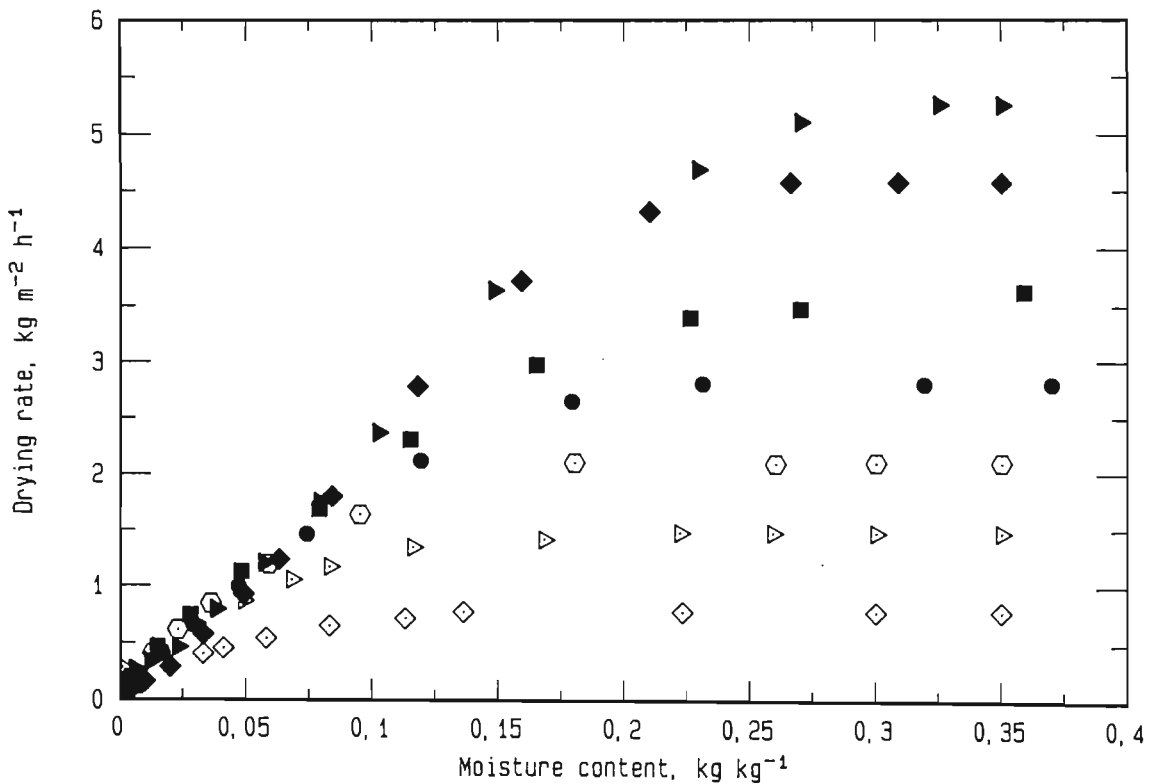


Figure 54: Experimental drying rates of molecular sieve in steam  
at a steam flow rate of  $24,41 \text{ kg h}^{-1}$   
(see Nomenclature for symbols)

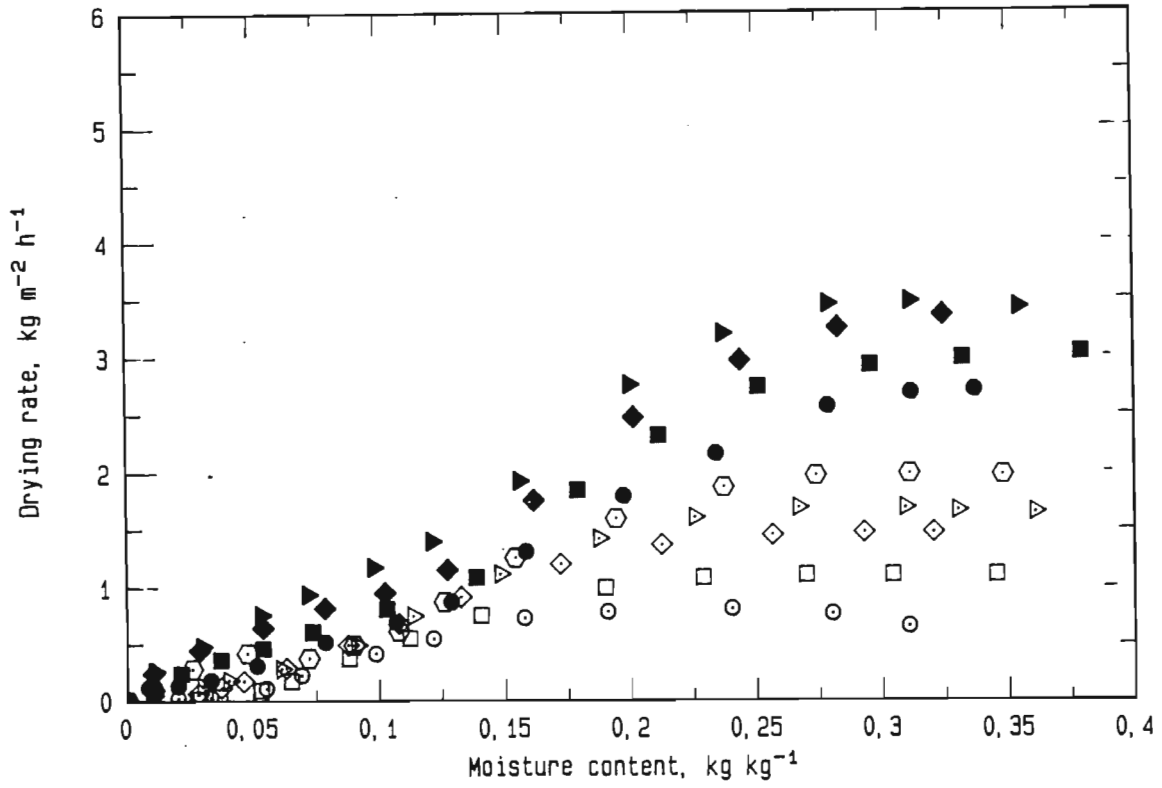


Figure 55: Experimental drying rates of molecular sieve in air  
at an air flow rate of  $25,96 \text{ kg h}^{-1}$   
(see Nomenclature for symbols)

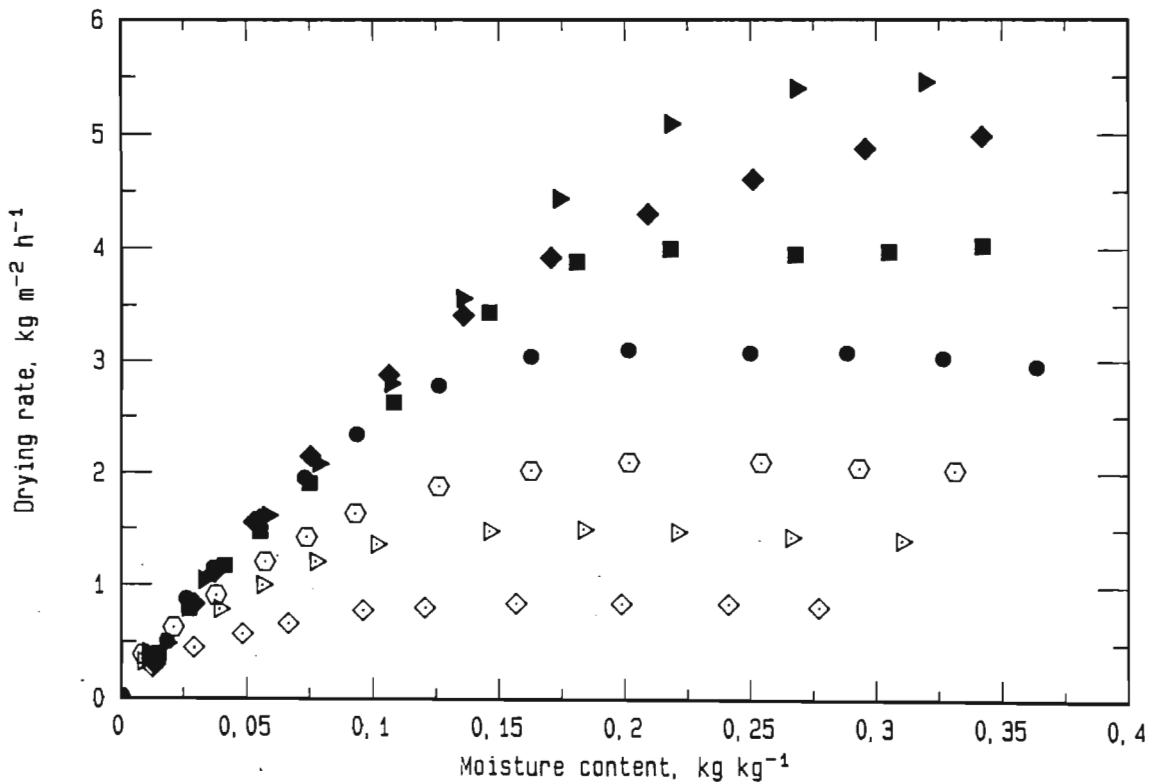


Figure 56: Experimental drying rates of molecular sieve in steam  
at a steam flow rate of  $25,96 \text{ kg h}^{-1}$   
(see Nomenclature for symbols)

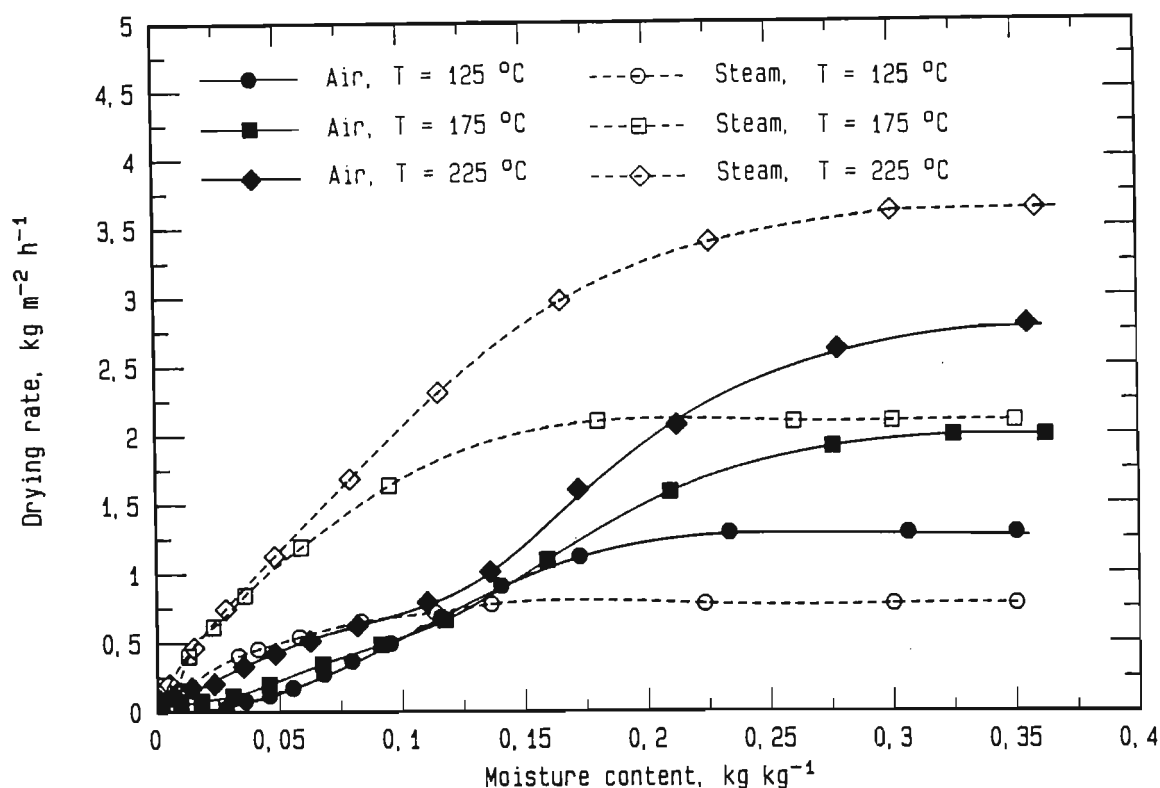


Figure 57: Experimental drying rates of molecular sieve in air and in steam at various temperatures (mass flow rate of 24,41 kg h<sup>-1</sup>)

At the low temperature of 125 °C, an interesting phenomenon occurs. The drying rate in steam is lower during the constant drying rate period. As the drying rate curve in air starts falling at higher moisture contents than in steam, there is a cross-over point. Below this cross-over point, the drying rate in steam is higher than the drying rate in air. As a consequence, drying conditions can be such that the total drying time in steam is shorter, even though the dryer is operated below the inversion temperature. Therefore, from a kinetic point of view, steam drying is especially interesting for materials with a long falling drying rate period.

At the medium temperature of 175 °C, the drying rates during the constant drying rate period are similar, with a slight advantage for steam. Because of the extension of the constant drying rate period in steam, the drying rates during the falling drying rate period are much higher in steam than in air.

At the high temperature of 225 °C, the drying rate curve in steam lies far above the drying rate curve in air.

In Figure 58, the drying rates of molecular sieve in air are plotted for various mass flow rates of the drying medium at two temperatures (125 °C and 200 °C). In Figure 59, the rates are plotted for steam. One can clearly see an increase in the drying rate with increases in the mass flow rate.

#### 4.5 Development of theory necessary for interpreting data in the falling drying rate period

For a direct comparison of the drying rate curves recorded under different external drying conditions, the curves are put into a normalized form. With the help of these normalized drying curves, the drying time of the material can be determined, with certain assumptions, for any type of dryer [S4,Z1]. One condition is, however, that the normalized drying rate curve must be determined for constant conditions (temperature, humidity, flow rate, etc.) of the drying medium. In fluidized beds, this condition is not fulfilled. The temperature of the drying medium falls in a very narrow layer above the distributor plate to the temperature of the particles. Consequently the particles that are close to the distributor plate are exposed to a high temperature and experience a high drying rate, while the particles higher up in the bed are exposed to a lower temperature and experience a lower drying rate. Above a certain height in the bed, the temperature of the drying medium and of the particles is equal, so that no drying occurs. The drying rate that is measured is the average of the drying rates of all the particles. Therefore the measured drying rate must first be modified to a theoretical drying rate under constant conditions of the drying medium. This modification was first described by Zabeschek [Z1]. He normalized the drying rate curve with respect to the constant conditions at the inlet into the drying system. This normalized drying rate is equivalent to the normalized drying rate of a single particle exposed to the constant drying conditions at the inlet of the dryer. The resulting normalized drying rate curve is uncoupled from the drying equipment that it is recorded in and can be used in the design of any type of dryer.

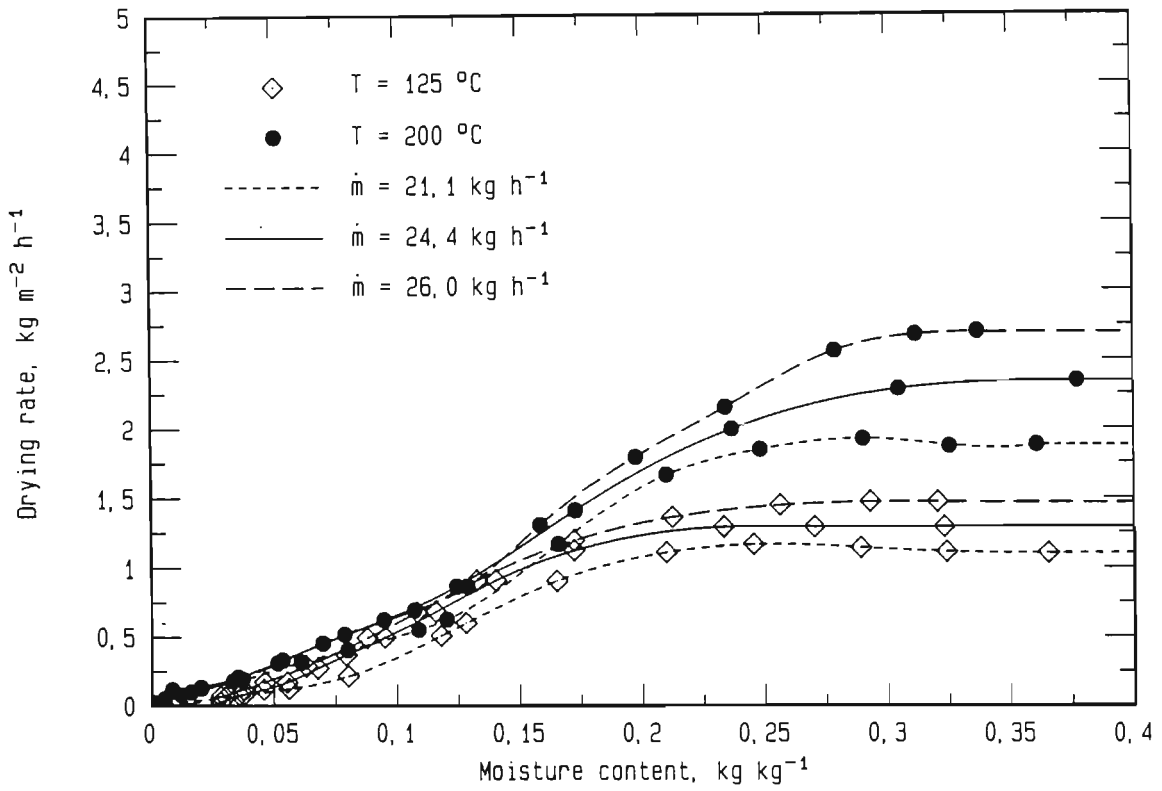


Figure 58: Experimental drying rates of molecular sieve in air at various air flow rates

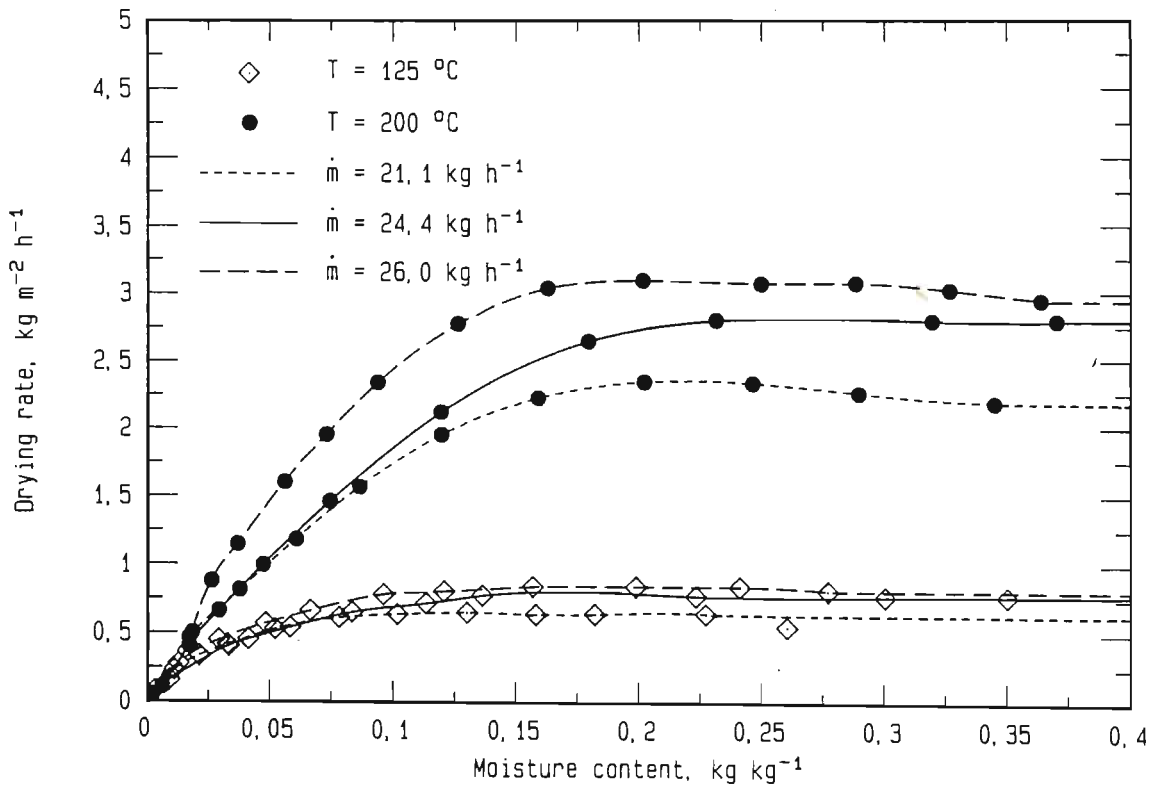


Figure 59: Experimental drying rates of molecular sieve in steam at various steam flow rates

Zabeschek's derivation is limited to non-equilibrium systems. Furthermore his method cannot be applied to steam drying, as it is based on the measurement of the humidity change of the drying medium between inlet and outlet (mass transfer) of the dryer. This measurement cannot be done in steam.

The fluidized-bed dryer that was used in this thesis was essentially an equilibrium system and Zabeschek's normalization method could not be applied. Therefore a new normalization method was developed for equilibrium systems. This method uses heat transfer expressions for the normalization in steam.

In Appendix H a review is given of all possible normalization methods. In general the normalization of drying rate curves is done with respect to the average drying rate in the constant drying rate period. In this case, however, the resulting normalized drying rate curve is dependent on the drying equipment it was recorded in and cannot be used in such a universal way as the normalized drying rate curve with respect to the constant conditions at the inlet into the dryer. The dryers are divided into non-equilibrium and equilibrium systems. The normalization is presented with respect to the averaged drying rate in the constant drying rate period and with respect to the constant drying conditions at the inlet into the drying system. For each case the normalization is presented using mass transfer expressions and using heat transfer expressions.

#### 4.5.1 Normalization in a fluidized bed with respect to the inlet conditions of the drying medium

Firstly the normalization method of Zabeschek for non-equilibrium systems is presented to understand the principle of the normalization procedure with respect to the constant conditions at the inlet into the dryer. Then this normalization procedure is extended to equilibrium systems. The flow of the drying medium through the bed and the flow of the particles in the bed must be modelled. In this thesis, plug flow of the drying medium and well-mixed flow of the fluidized particles was assumed, in accordance with the assumptions made for the determination of the gas-to-solid heat transfer coefficient in Section 4.3.1.

According to Zabescek [Z1], the normalized drying rate with respect to the inlet conditions can be determined by integrating the differential mass balance over the height of the dryer.

The differential mass balance can be written as follows:

$$- \dot{M}_g \frac{\partial Y_g}{\partial z} dz + d\dot{m}_{ev} A \frac{dz}{L} = 0 \quad (38)$$

The differential evaporation rate can be written as follows:

$$d\dot{m}_{ev} = v d\dot{m}_{ev,I} \quad (39)$$

During the constant drying rate period, the differential mass balance is:

$$d\dot{m}_{ev,I} = \rho_g \beta (Y_p^* - Y_g) \quad (40)$$

With Equations 39 and 40, Equation 38 can be written as follows:

$$- \dot{M}_g \frac{\partial Y_g}{\partial z} dz + v \rho_g \beta (Y_p^* - Y_g) A \frac{dz}{L} = 0 \quad (41)$$

By introducing the following dimensionless numbers the equations can be written in a simpler form. These dimensionless numbers are frequently used in the drying literature [H3,P3,S4,Z1]. All of the dimensionless numbers that will be used during this section are introduced here, even though not all will be used immediately.

The dimensionless numbers are the following:

Dimensionless humidity potential

$$\xi_g^o = \frac{(Y_p^* - Y_g)}{(Y_p^* - Y_{g,in})} \quad (42)$$

dimensionless humidity potential for the falling drying rate period



$$\xi_g' = \frac{(Y_p - Y_g)}{(Y_p - Y_{g,in})} \quad (43)$$

Dimensionless humidity potential of the particles

$$\xi_p^\circ = \frac{(Y_p^* - Y_p)}{(Y_p^* - Y_{g,in})} \quad (44)$$

and the dimensionless height

$$\zeta^\circ = \frac{\rho_g \beta A z}{\dot{M}_g L} \quad (45)$$

Using the dimensionless humidity potential and the dimensionless height, the differential mass balance of Equation 41 can be written as follows:

$$\frac{d\xi_g^\circ}{\xi_g^\circ} = -v d\zeta^\circ \quad (46)$$

If this differential equation is integrated over the height of the bed, this leads to:

$$v = - \frac{\ln(\xi_{g,out}^\circ)}{\zeta_{out}^\circ} \quad (47)$$

This form represents the normalized drying rate with respect to the inlet conditions into the bed, i.e. the normalized drying rate of a single particle exposed to the constant drying conditions at the inlet to the fluidized-bed dryer. To apply Equation 47, the difference between the humidity of the gas at the surface of the particles,  $Y_p^*$ , and the humidity of the gas leaving the dryer,  $Y_{g,out}$ , must be known as a function of time.  $Y_{g,out}$  can be measured by IR-absorption and  $Y_p^*$  can be calculated from the temperature of the material during the constant drying rate period.

Due to the assumption of plug flow, an exponential humidity profile is developed. In the constant drying rate period the humidity potential at the outlet of the dryer can be determined by integrating the differential mass balance (Equation 38) over the height of the dryer.

The dimensionless form of the integrated equation looks as follows:

$$\xi_{g,out}^{\circ} = \exp(-\zeta_{out}^{\circ}) \quad (48)$$

Equation 48 gives a relation between the humidity potential in the constant drying rate period and the dimensionless height of the dryer.

In Table 8 the dimensionless humidity potential is given as a function of the dimensionless height.

Table 8: Dimensionless humidity potential as a function of the dimensionless height

$\xi_{g,out}$	$\zeta_{out}$
0,9048	0,1
0,6065	0,5
0,3679	1,0
0,04979	3,0
0,00674	5,0
0,000045	10,0
0,000000002	20,0

Because of the exponential profile, the exhaust humidity can never be identical to the humidity at the surface of the drying material. For large values of  $\zeta_{out}^{\circ}$  (i.e. large bed heights, low fluidizing velocities, small diameter particles), the humidity potential assumes very low values. The difference between air humidity at the surface of the particles and at the outlet of the dryer cannot be determined by measuring the two values separately, as the required measuring accuracy cannot be achieved by any instrument.

In Zabeschek's experiments,  $\zeta_{out}^{\circ}$ -values around 1 were calculated and Equation 47 could be applied to determine the normalized drying rate. In the present tests, however,  $\zeta_{out}^{\circ}$ -values larger than 20 were found and Equation 47 could not be used for the determination of the normalized drying rate, at least not for values of the moisture content close to the critical moisture content. For experiments with large  $\zeta_{out}^{\circ}$ -values, the air humidity at the outlet of the dryer must be determined theoretically from the air

humidity at the surface of the particles. The normalization procedure for this case is presented below.

The normalized drying rate is determined by the total mass balance around the dryer:

$$\dot{M}_g (Y_{g,out} - Y_{g,in}) = \int_0^L v \rho_g \beta A (Y_p^* - Y_g) \frac{dz}{L} \quad (49)$$

The right hand of Equation 49 contains the integral of the differential evaporative mass transfer over the height of the dryer. The evaporative mass transfer is expressed by the mass transfer in the constant drying rate period corrected by the normalized drying rate. Little error is done to the total evaporation rate by assuming that the outlet humidity of the drying medium is equal to the humidity on the surface of the particles:

$$Y_{g,out} = Y_p \quad (50)$$

With the dimensionless humidity potential of the particles, Equation 49 can be written as follows:

$$1 = v \int_0^{\xi_{out}^0} \frac{\xi_g^0}{(1 - \xi_p^0)} d\xi^0 \quad (51)$$

The humidity potential,  $\xi_g^0$ , is a function of the dimensionless height,  $\xi^0$ , and before Equation 51 can be integrated,  $\xi_g^0$  must be expressed by  $\xi^0$ . For the falling drying rate period, the mass balance over a differential element of the dryer is as follows:

$$- \dot{M}_g \frac{\partial Y_g}{\partial z} dz + \rho_g \beta (Y_p - Y_g) A \frac{dz}{L} = 0 \quad (52)$$

$Y_p$  is the humidity at the surface of the material and for the falling drying rate period is different from the saturation humidity  $Y_p^*$ .  $Y_p$  is a function of the moisture content and the temperature of the particles and therefore not dependent on the bed height. Rearrangement of Equation 52 leads to:

$$\frac{dY_g}{(Y_p - Y_g)} = \frac{\rho_g \beta A}{M_g} \frac{dz}{L} \quad (53)$$

With the dimensionless humidity potential for the falling drying rate period, Equation 53 can be written after integration in the dimensionless form as:

$$\xi_p^{\circ'} = \exp(-\zeta^{\circ}) \quad (54)$$

By a mathematical rearrangement, the humidity potential in the falling drying rate period can be expressed by the humidity potential in the constant drying rate,  $\xi_g^{\circ}$ , and the humidity potential of the particles,  $\xi_p^{\circ}$ :

$$\xi_g^{\circ'} = \frac{\frac{Y_p^* - Y_g - Y_p^* + Y_p}{Y_p^* - Y_{g,in}}}{\frac{Y_p^* - Y_{in} - Y_p^* + Y_p}{Y_p^* - Y_{g,in}}} \quad (55)$$

$$= \frac{\xi_g^{\circ} - \xi_p^{\circ}}{1 - \xi_p^{\circ}} \quad (56)$$

or

$$\xi_g^{\circ} = (1 - \xi_p^{\circ}) \xi_g^{\circ'} + \xi_p^{\circ} \quad (57)$$

With Equation 54 integrated into Equation 57, the dimensionless humidity potential is expressed as a function of the dimensionless height and the dimensionless humidity potential of the particles:

$$\xi_g^{\circ} = (1 - \xi_p^{\circ}) \exp(-\zeta^{\circ}) + \xi_p^{\circ} \quad (58)$$

The dimensionless humidity potential of the particles is determined by the humidity at the surface of the particles in the constant drying rate period,  $Y_p^*$ , and in the falling drying rate period,  $Y_p$ . In the constant drying rate period the humidity at the surface of the particles is determined solely by the particle temperature. In the falling rate period the humidity at the surface of the particles is determined by measuring the humidity of the drying medium at the outlet of the dryer (e.g. by IR-absorption).

Using Equation 58 in Equation 51 and integrating leads to:

$$v = \frac{(1 - \xi_p^o)}{1 - \xi_p^o + \xi_p^o z_{g,out}^o - (1 - \xi_p^o) \exp(-z_{g,out}^o)} \quad (59)$$

Equation 59 represents the normalized drying rate with respect to the constant conditions at the inlet of the dryer for an equilibrium system. In general fluidized beds can be treated as equilibrium systems as the drying medium leaves the dryer in moisture and thermal equilibrium with the particles in the bed. Only when the mass flow rates of the drying medium are high and the exchanging surface of the particles is small, will the exiting drying medium not be in equilibrium with the particles. This is normally only the case for large particles (> 3 mm).

#### 4.5.2 Normalization in a steam-operated fluidized-bed dryer

For steam-operated fluidized beds, Equation 59 cannot be used for the normalization as the humidity of the drying medium is unity at any time of the drying process and any location in the dryer. Therefore, for steam-operated fluidized beds the normalization of the drying rate must be done by heat transfer expressions.

The total energy balance around the drying system can be written as follows:

$$\dot{M}_g c_{pg} (T_{g,in} - T_{g,out}) = \int_0^L \dot{m}_{ev} \Delta h_v A \frac{dz}{L} + M_p c_{pp} \frac{\partial T_p}{\partial t} \quad (60)$$

With

$$\dot{m}_{ev} = v \dot{m}_{ev,I} \quad (61)$$

and

$$\dot{m}_{ev,I} = \frac{h (T_g - T_{p,I})}{\Delta h_v} \quad (62)$$

Equation 60 can be written as follows:

$$\dot{M}_g c_{pg} (T_{g,in} - T_{g,out}) = \int_0^L v h A (T_g - T_{p,I}) \frac{dz}{L} + \dot{M}_p c_{pp} \frac{\partial T_p}{\partial t} \quad (63)$$

The energy that the drying medium gives to the particles is used for evaporating moisture and to heat up the particles. The part of the energy that is used for evaporation is expressed by the heat transferred to the particles in the constant drying rate period corrected by the normalized drying rate.

For the equilibrium case, the outlet temperature of the drying medium is identical to the temperature of the particles.

$$T_{g,out} = T_p \quad (64)$$

At this stage a certain number of dimensionless numbers are introduced. They are the corresponding heat transfer expressions of the dimensionless numbers for the mass transfer. To illustrate this the dimensionless number for the heat transfer has the same symbol, only the superscript  $\circ$  is blackened  $\bullet$ .

Dimensionless temperature potential

$$\xi_g^\bullet = \frac{(T_g - T_{p,I})}{(T_{g,in} - T_{p,I})} \quad (65)$$

dimensionless temperature potential for the falling drying rate period

$$\xi_g^{\bullet'} = \frac{(T_g - T_p)}{(T_{g,in} - T_p)} \quad (66)$$

dimensionless temperature potential of the particles

$$\xi_p^* = \frac{(T_p - T_{p,I})}{(T_{g,in} - T_{p,I})} \quad (67)$$

and the dimensionless height

$$\zeta^* = \frac{h A}{\dot{M}_g c_{pg}} \frac{z}{L} \quad (68)$$

A new dimensionless number that is introduced here is the dimensionless time:

$$\tau^* = \frac{h A}{\dot{M}_p c_{pp}} t \quad (69)$$

With these dimensionless numbers Equation 63 can be written as follows:

$$1 = v \int_0^{\zeta_{out}^*} \frac{\xi_g^*}{1 - \xi_p^*} d\zeta^* - \zeta_{out}^* \frac{d\xi_p^*}{d\tau^*} \quad (70)$$

The temperature potential must be expressed as a function of the height before Equation 70 can be integrated. The temperature profile in the fluidized bed can be determined by integrating the following differential equation for the energy transfer from the drying medium to the particles:

$$\dot{M}_g c_{pg} \frac{\partial T_g}{\partial z} dz + h A (T_g - T_p) \frac{dz}{L} + \dot{M}_p c_{pp} \frac{\partial T_p}{\partial t} = 0 \quad (71)$$

If the temperature change of the particles with time is neglected, Equation 71 can be written after integration in the dimensionless form as:

$$\xi_g^* = \exp(-\zeta^*) \quad (72)$$

With

$$\xi_g^{\bullet'} = \frac{\xi_g^{\bullet} - \xi_p^{\bullet}}{1 - \xi_p^{\bullet}} \quad (73)$$

the temperature potential can be expressed as follows:

$$\xi_g^{\bullet} = (1 - \xi_p^{\bullet}) \exp(-\tau^{\bullet}) + \xi_p^{\bullet} \quad (74)$$

With Equation 74, Equation 70 can be written in the integrated form as follows:

$$v = \frac{1 - \xi_p^{\bullet} + (1 - \xi_p^{\bullet}) \tau_{out}^{\bullet} \frac{\partial \xi_p^{\bullet}}{\partial \tau^{\bullet}}}{1 - \xi_p^{\bullet} + \xi_p^{\bullet} \tau_{out}^{\bullet} - (1 - \xi_p^{\bullet}) \exp(-\tau_{out}^{\bullet})} \quad (75)$$

This is the normalized form of the drying rate curve in the equilibrium system.  $\xi_p^{\bullet}$  is determined by measuring the temperature of the particles as a function of time during the drying process. The normalization of the drying rate curve using heat transfer expressions is also valid for air drying. Equation 75 was used for all the normalizations of the drying rate curve presented in this thesis. The normalization over heat transfer expressions has the advantage that it is easier to measure a temperature than a humidity.

#### 4.6 Comparison of the normalized drying rate curves in air and in steam

The drying rates during the falling drying rate period can best be evaluated in their normalized form. The normalization with respect to the constant conditions at the inlet into the dryer is used. The temperature and the mass flow rate of the drying medium are the same in air and in steam. Therefore this type of normalization shows the differences in the drying kinetics resulting from the transfer mechanisms inside the material. The results are presented as normalized drying rate as function of the normalized moisture content. The nor-



malized moisture content being the ratio of the actual moisture content to the critical moisture content. (At the high temperatures that were used in the experiments, the equilibrium moisture content can be assumed to be zero).

#### 4.6.1 Normalized drying rate curves for alumina

In Figures 60 to 65, the normalized drying rate for alumina is plotted against the normalized moisture content for different temperatures and mass flow rates.

For air and for steam, the normalized drying rate increases with an increase in temperature. At low temperatures (75 °C and 125 °C), the drying rates decrease very quickly below the critical moisture content and then level off as the material reaches complete dryness. This results in a concavely shaped normalized drying rate curve. At high temperatures (275 °C), the normalized drying rates do not drop that sharply after the critical moisture content and the result is a convexly shaped normalized drying rate curve. This means that, with an increase in the external temperature, the moisture transfer inside the material increases relatively more than the moisture transfer outside the material. The reason for this may be a strong temperature dependence of the moisture transfer coefficients inside the material, or additional moisture transfer mechanisms that become apparent only at higher temperatures (i.e. moisture movement in the vapour phase and in the liquid phase on the basis of total pressure gradients, thermal diffusion etc.).

The shape of the normalized drying rate curves in air and in steam is similar, and so is their magnitude. This indicates that similar mechanisms must be acting in air and in steam, or that the temperature-dependence of the mechanisms involved in air drying and steam drying is similar.

In Figure 66, the normalized drying rates for alumina are plotted for air and for steam at two temperatures (125 °C and 275 °C). The normalized drying rate in steam lies below the normalized drying rate in

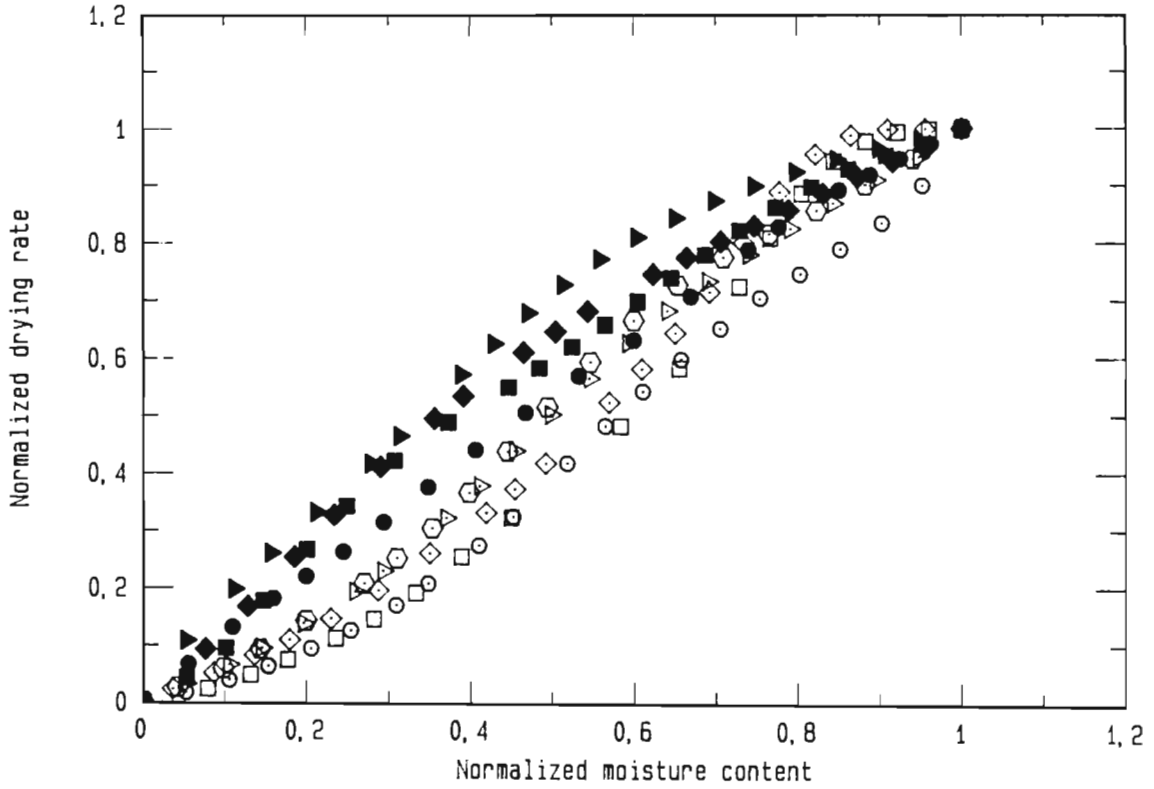


Figure 60: Normalized drying rates of alumina in air  
at an air flow rate of  $16,70 \text{ kg h}^{-1}$   
(see Nomenclature for symbols)

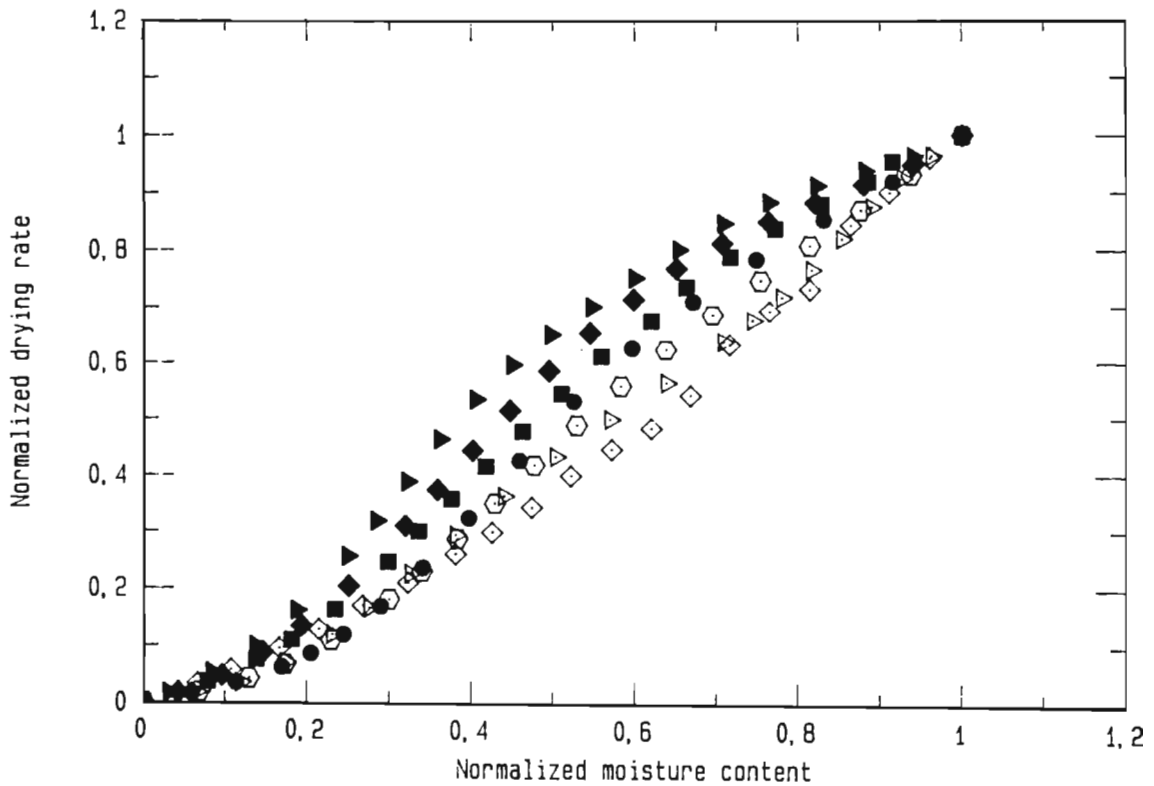


Figure 61: Normalized drying rates of alumina in steam  
at a steam flow rate of  $16,70 \text{ kg h}^{-1}$   
(see Nomenclature for symbols)

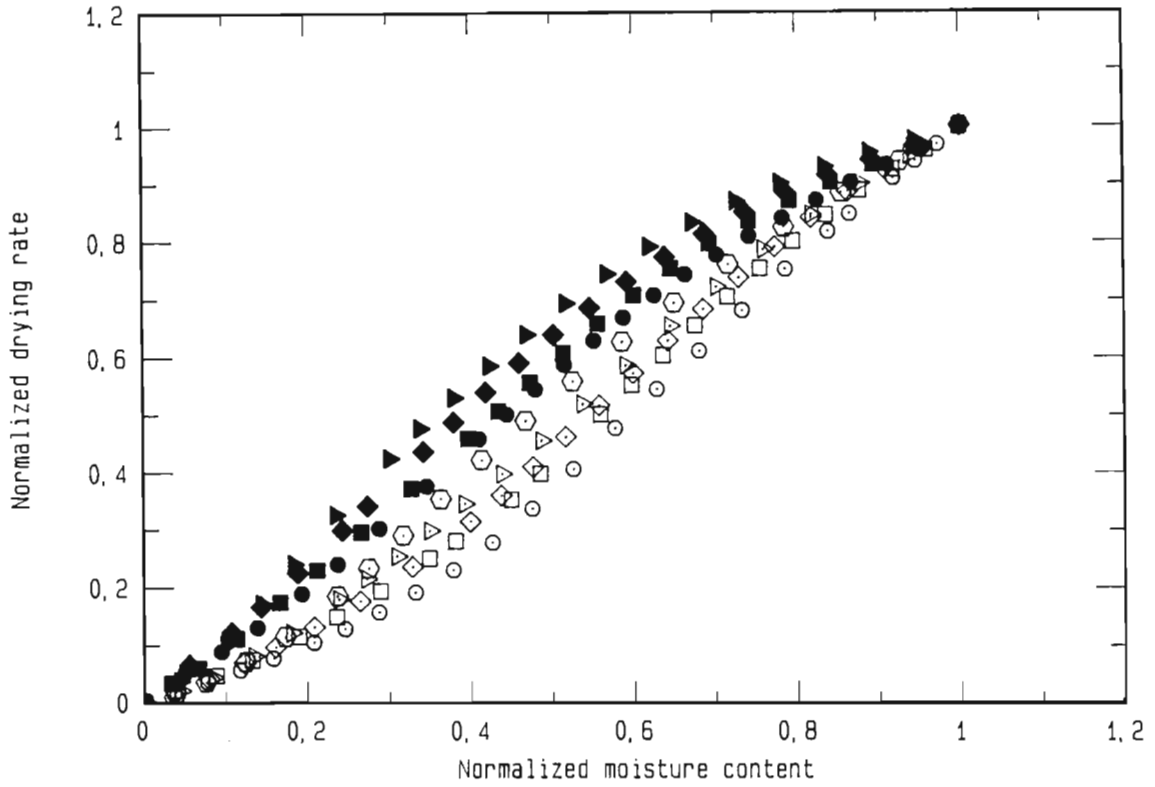


Figure 62: Normalized drying rates of alumina in air  
at an air flow rate of  $19,27 \text{ kg h}^{-1}$   
(see Nomenclature for symbols)

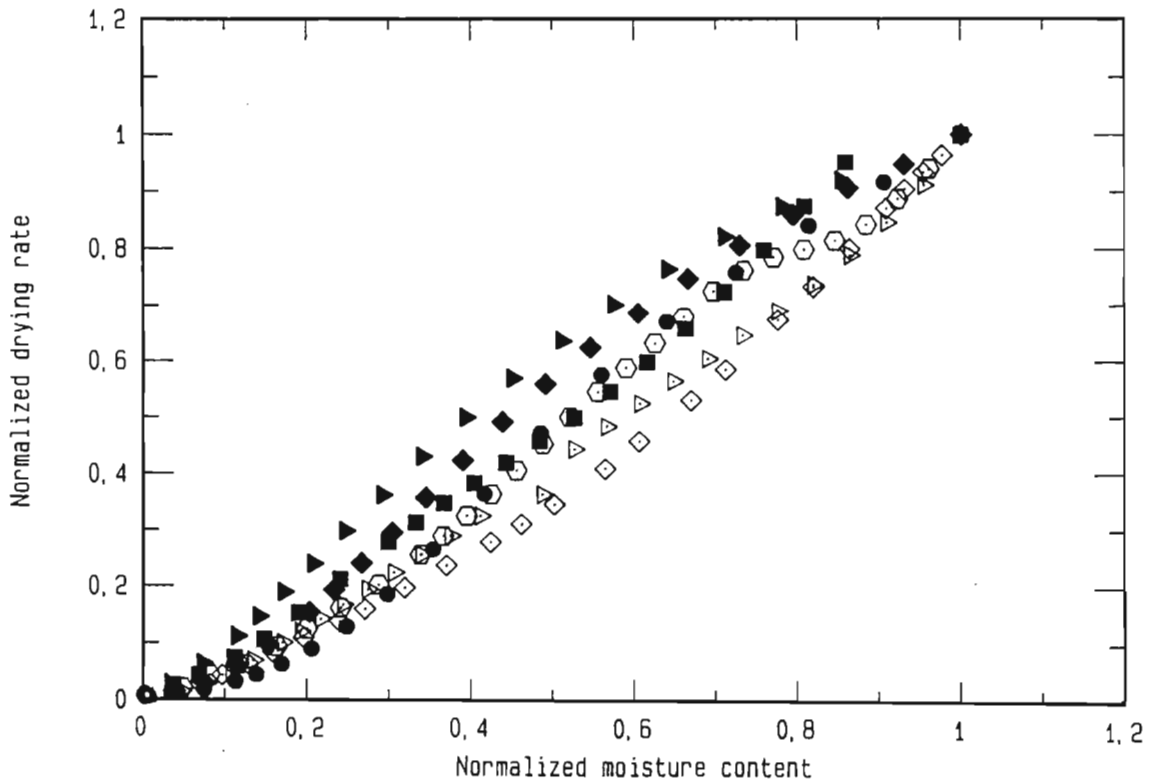


Figure 63: Normalized drying rates of alumina in steam  
at a steam flow rate of  $19,27 \text{ kg h}^{-1}$   
(see Nomenclature for symbols)

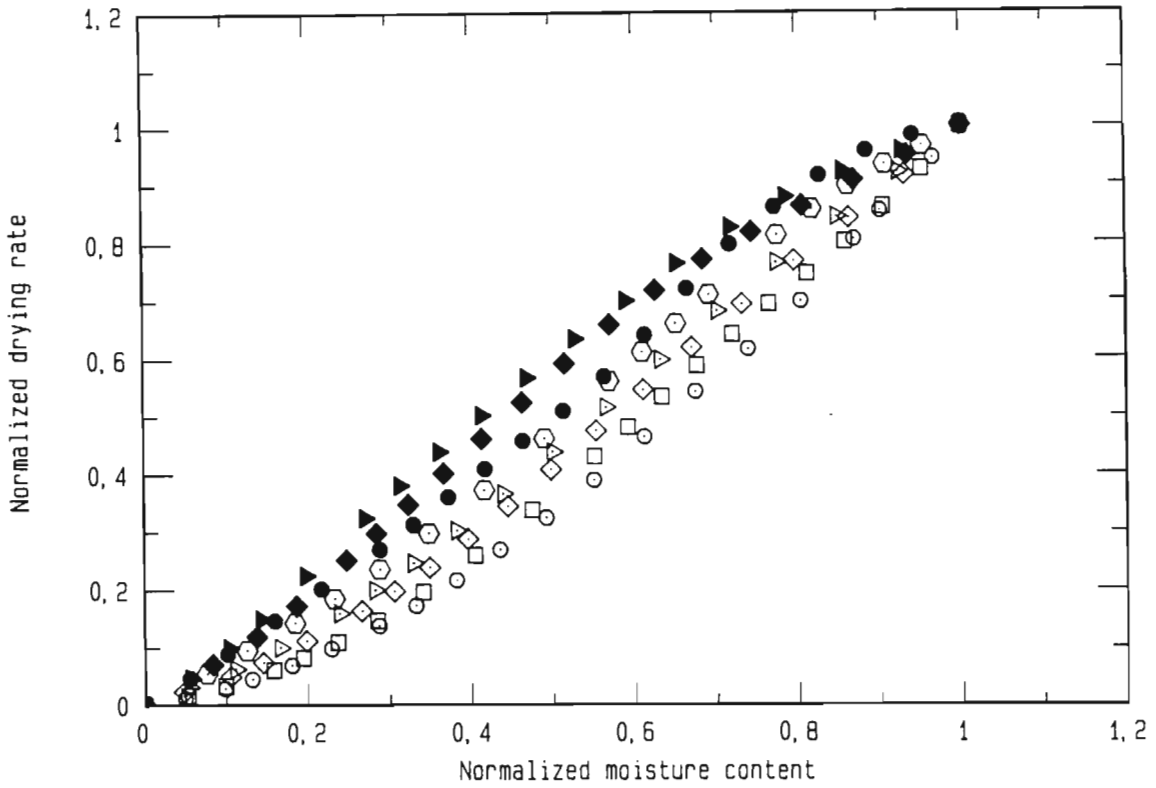


Figure 64: Normalized drying rates of alumina in air  
at an air flow rate of  $22,76 \text{ kg h}^{-1}$   
(see Nomenclature for symbols)

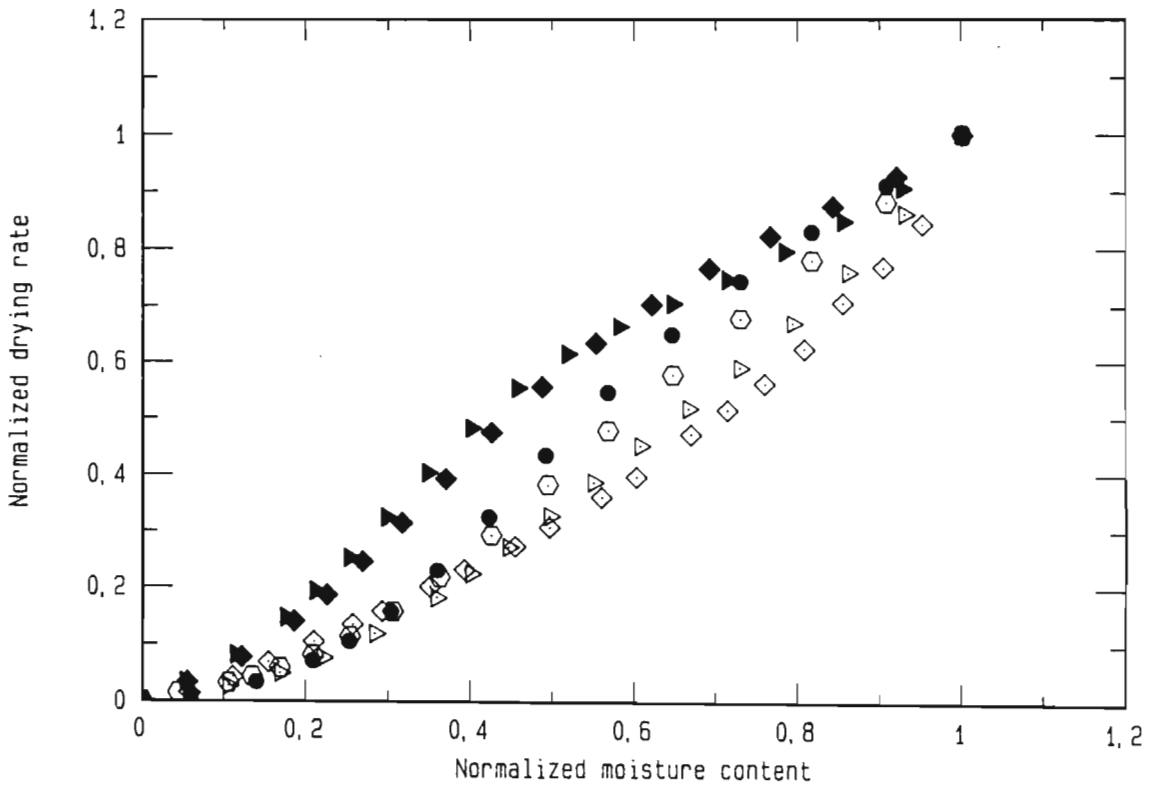


Figure 65: Normalized drying rates of alumina in steam  
at a steam flow rate of  $22,76 \text{ kg h}^{-1}$   
(see Nomenclature for symbols)

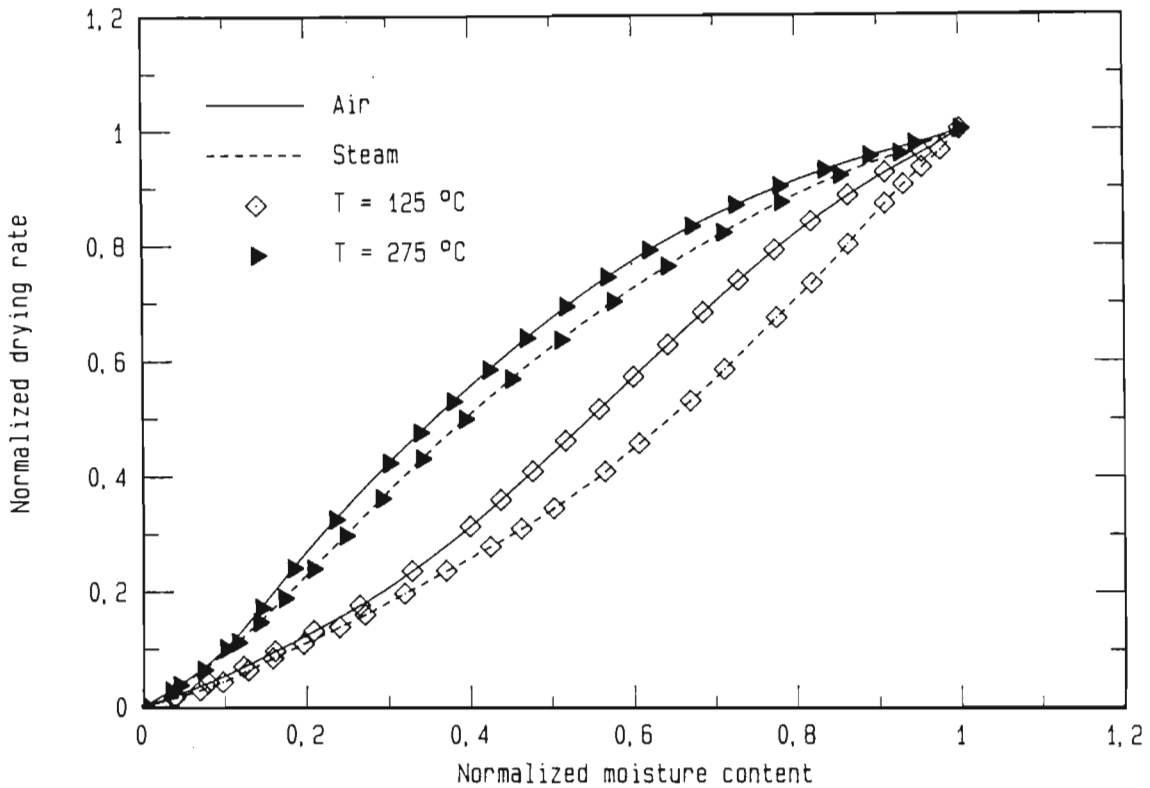


Figure 66: Normalized drying rates of alumina in air and in steam at various temperatures (mass flow rate of  $19,27\text{ kg h}^{-1}$ )

air. This seems to indicate that the relative kinetics, which are defined here as the kinetics of the external drying processes compared to the internal ones, are higher in steam than in air.

The difference between the normalized drying rates is higher at the low temperature and smaller at the high temperature. This means that with an increase in temperature, the relative kinetics increase faster in steam than in air. This can be due to an additional internal transfer mechanism that becomes only active in steam and only at higher temperatures. One example of such a transfer mechanism is the

moisture transfer in the liquid phase on basis of a total vapour pressure gradient. This mechanism can be expected to be more pronounced in steam than in air, because in steam such a total pressure gradient must exist to evacuate the vapour from the inside of the material, whereas in air vapour can move by diffusion and this movement does not require a total pressure gradient. At the higher temperatures, drying is very fast and a high pressure gradient is needed in steam drying to evacuate the produced vapour. This pressure gradient helps also the transfer of liquid moisture. This is why the relative kinetics increase faster in steam than in air with an increase in temperature.

#### 4.6.2 Normalized drying rate curves for molecular sieve

In Figures 67 to 72, the normalized drying rate for molecular sieve is plotted against the normalized moisture content for different temperatures.

In air drying, the normalized drying rates fall sharply down to a normalized moisture content of about 0,6. From here on, they approach zero very slowly. The influence of temperature on the normalized drying rate curve is not as pronounced as for alumina. For normalized moisture contents above 0,6, no temperature influence is apparent. For lower normalized moisture contents, the normalized drying rate increases with an increase in temperature.

In steam drying, the normalized drying rate does not fall as quickly as in air drying and for normalized moisture contents bigger than 0,6 the normalized drying rates lie higher than in air. For small normalized moisture contents (below 0,4), the normalized drying rate curves in steam level off and slowly approach zero. Over the whole moisture range, a temperature-dependence of the normalized drying rate is not clearly apparent.

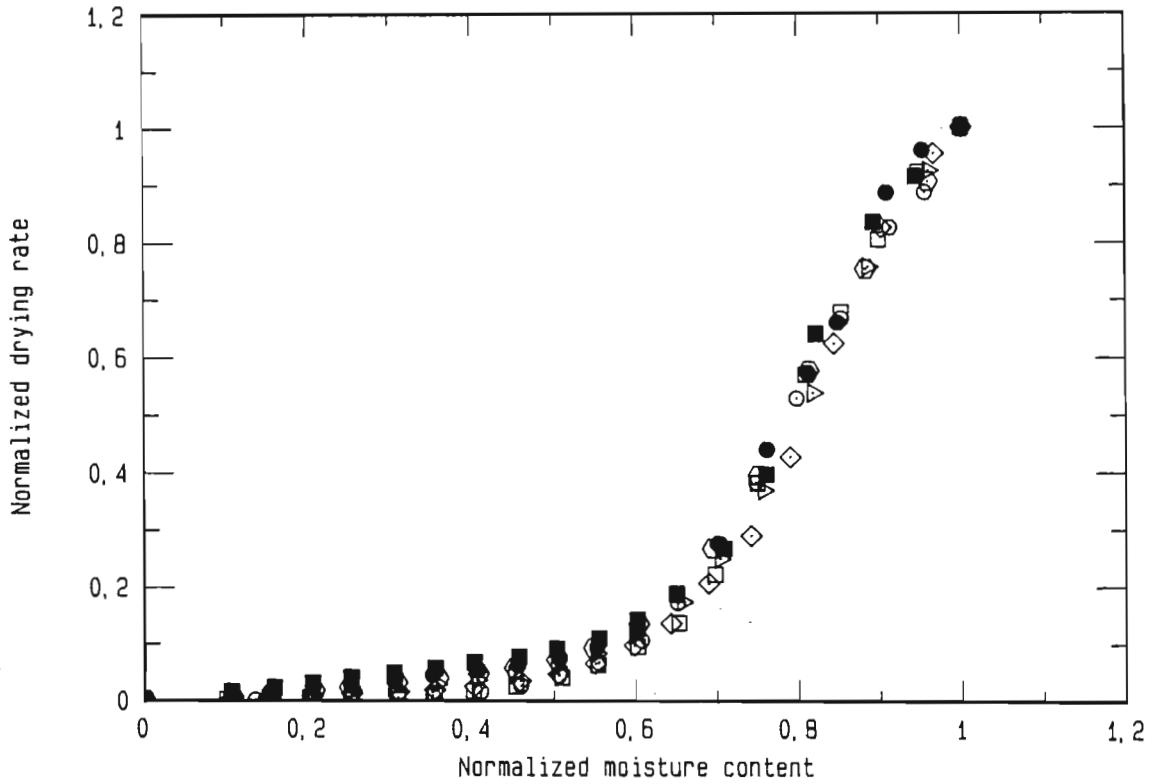


Figure 67: Normalized drying rates of molecular sieve in air  
at an air flow rate of  $21,06 \text{ kg h}^{-1}$   
(see Nomenclature for symbols)

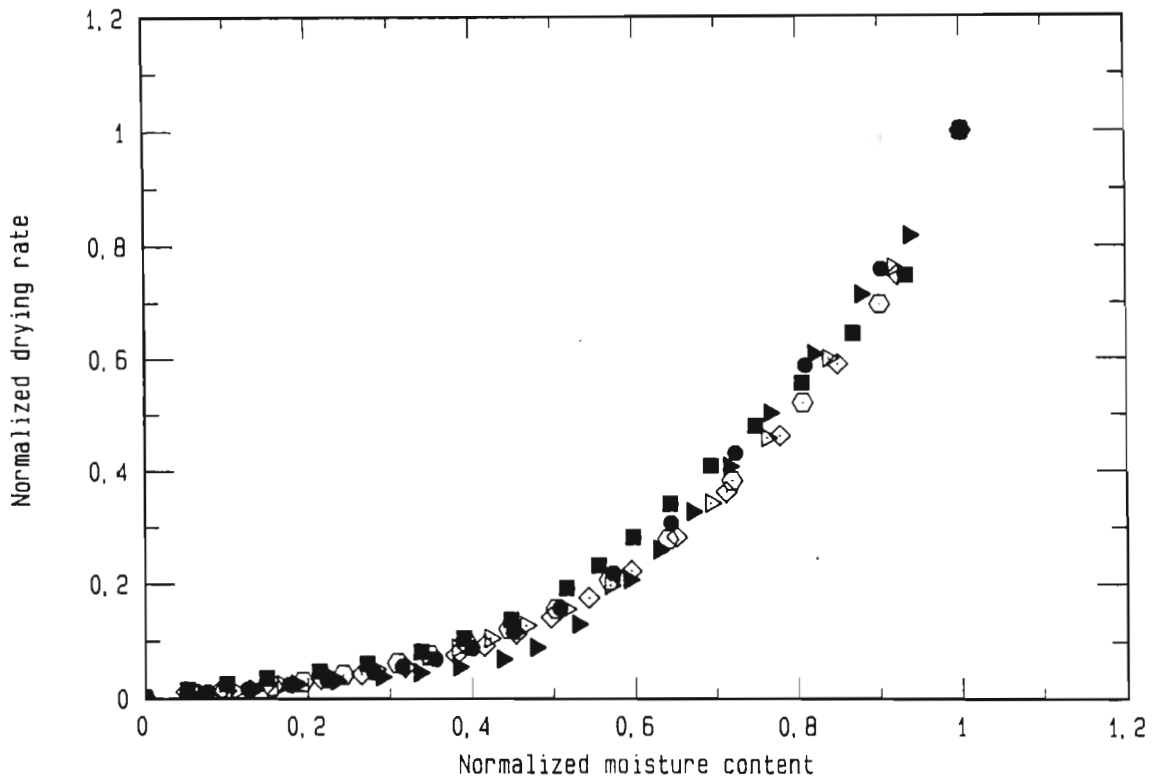


Figure 68: Normalized drying rates of molecular sieve in steam  
at a steam flow rate of  $21,06 \text{ kg h}^{-1}$   
(see Nomenclature for symbols)

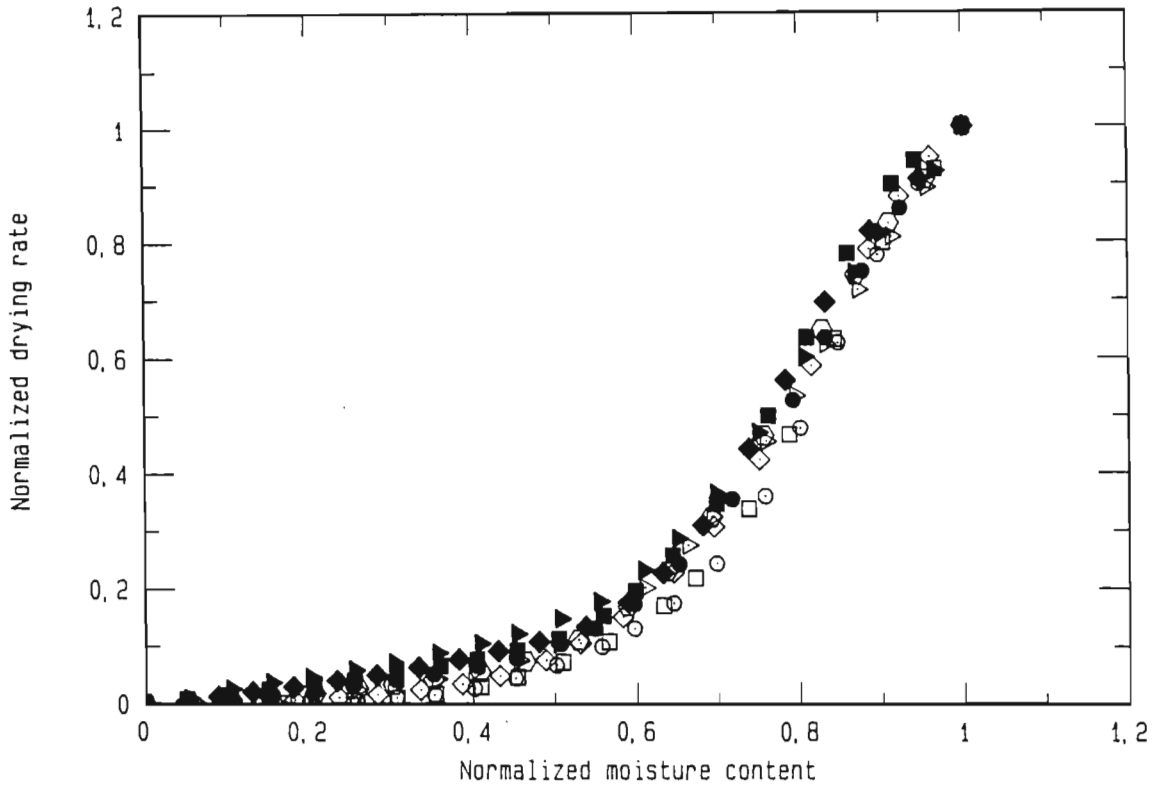


Figure 69: Normalized drying rates of molecular sieve in air  
at an air flow rate of 24,41 kg h<sup>-1</sup>  
(see Nomenclature for symbols)

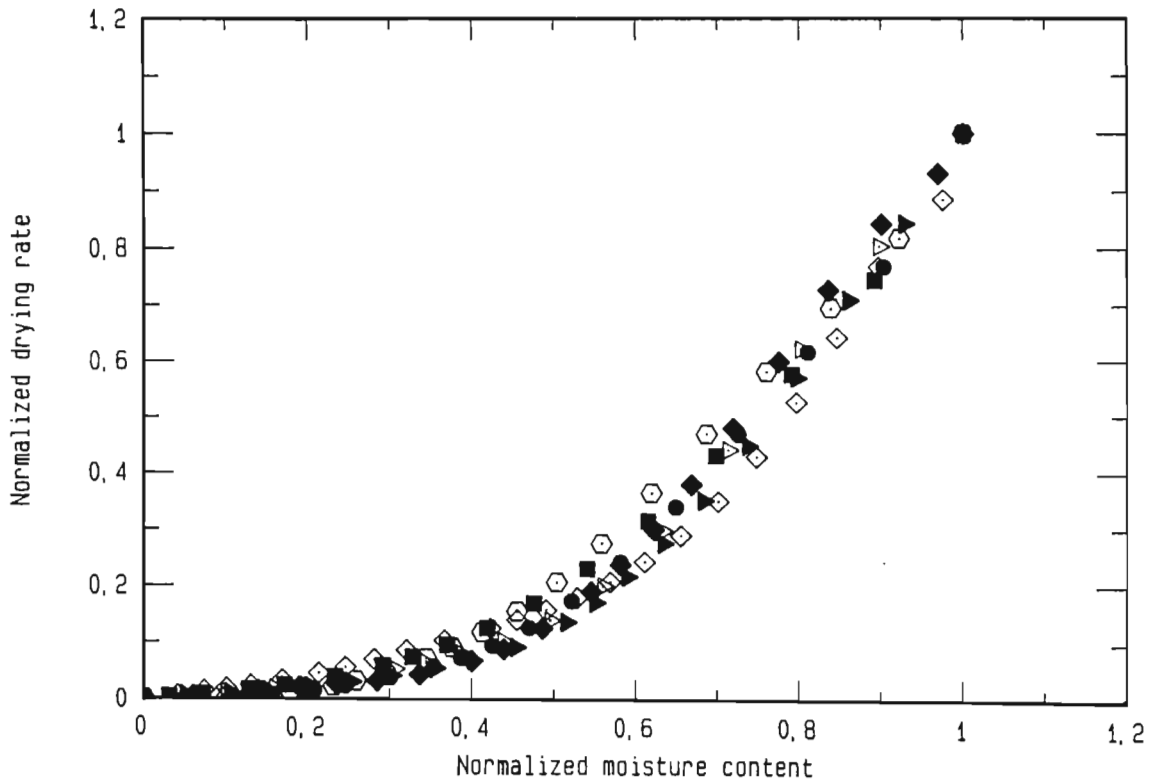


Figure 70: Normalized drying rates of molecular sieve in steam  
at a steam flow rate of 24,41 kg h<sup>-1</sup>  
(see Nomenclature for symbols)



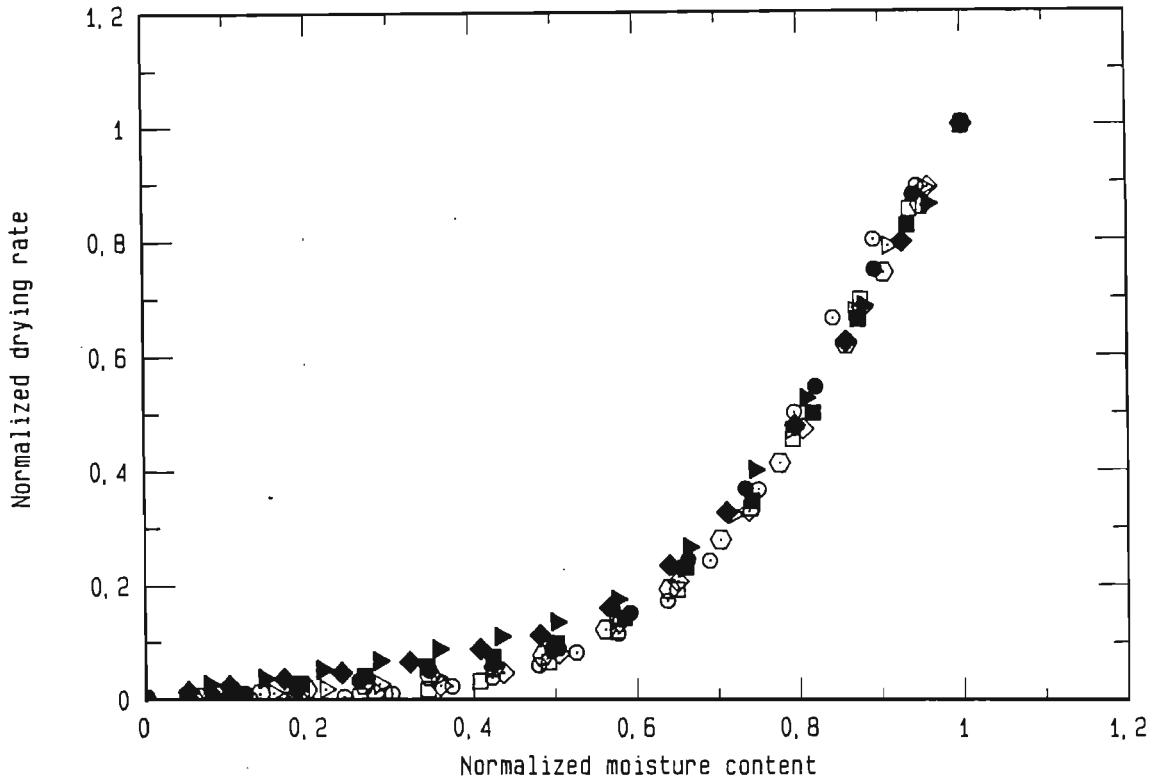


Figure 71: Normalized drying rates of molecular sieve in air  
at an air flow rate of  $25,96 \text{ kg h}^{-1}$   
(see Nomenclature for symbols)

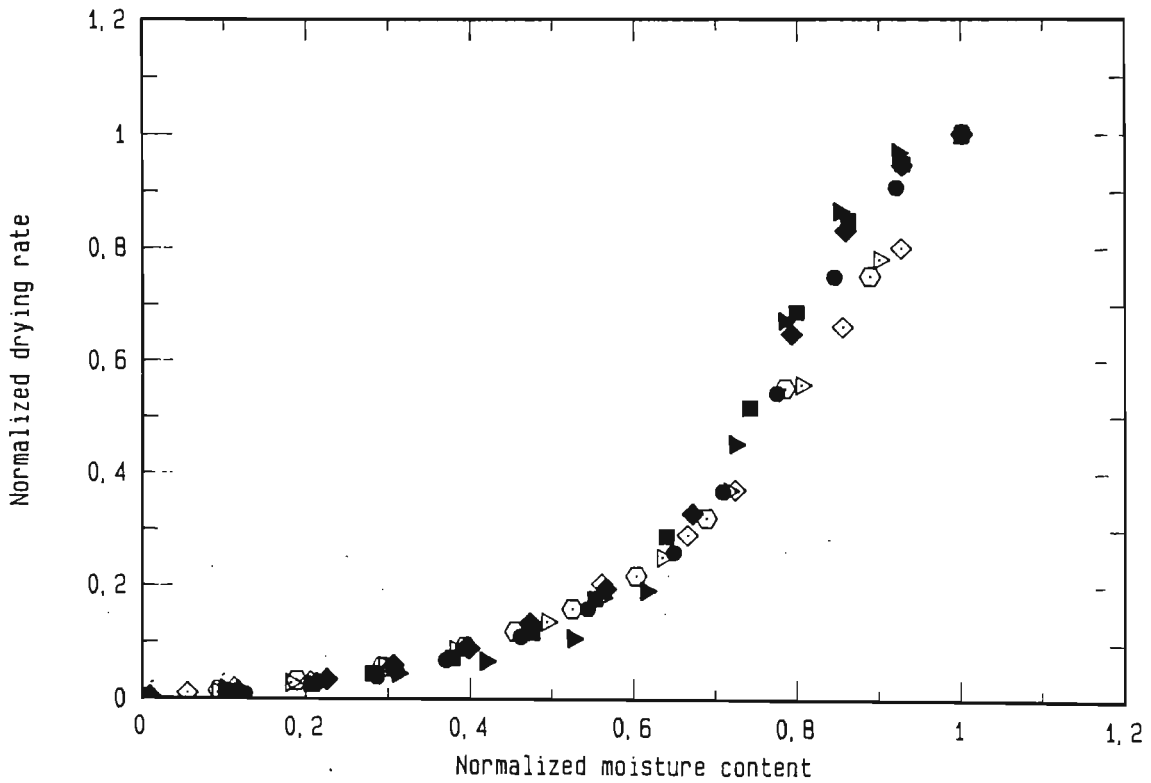


Figure 72: Normalized drying rates of molecular sieve in steam  
at a steam flow rate of  $25,96 \text{ kg h}^{-1}$   
(see Nomenclature for symbols)

In steam drying, the normalized drying rates are more scattered for normalized moisture contents higher than 0,6. The reason herefore lies in the experimental setup. The critical moisture content of the material was determined by the temperature rise in the fluidized bed. This temperature rise was indicated by a thermocouple. In steam, condensation took place on the thermocouple, which made it difficult to determine exactly the critical moisture content. As a result some inaccuracy was introduced which explains the slight scatter of the data in steam.

In Figure 73, the normalized drying rates of molecular sieve are plotted for air and for steam at two temperatures (125 °C and 275 °C). At 125 °C, the normalized drying rates in steam are higher than those in air and at 275 °C the opposite is true. The normalized drying rate curves of molecular sieve are not very temperature-sensitive and lie close together. Therefore it is difficult to draw any conclusions from this figure.

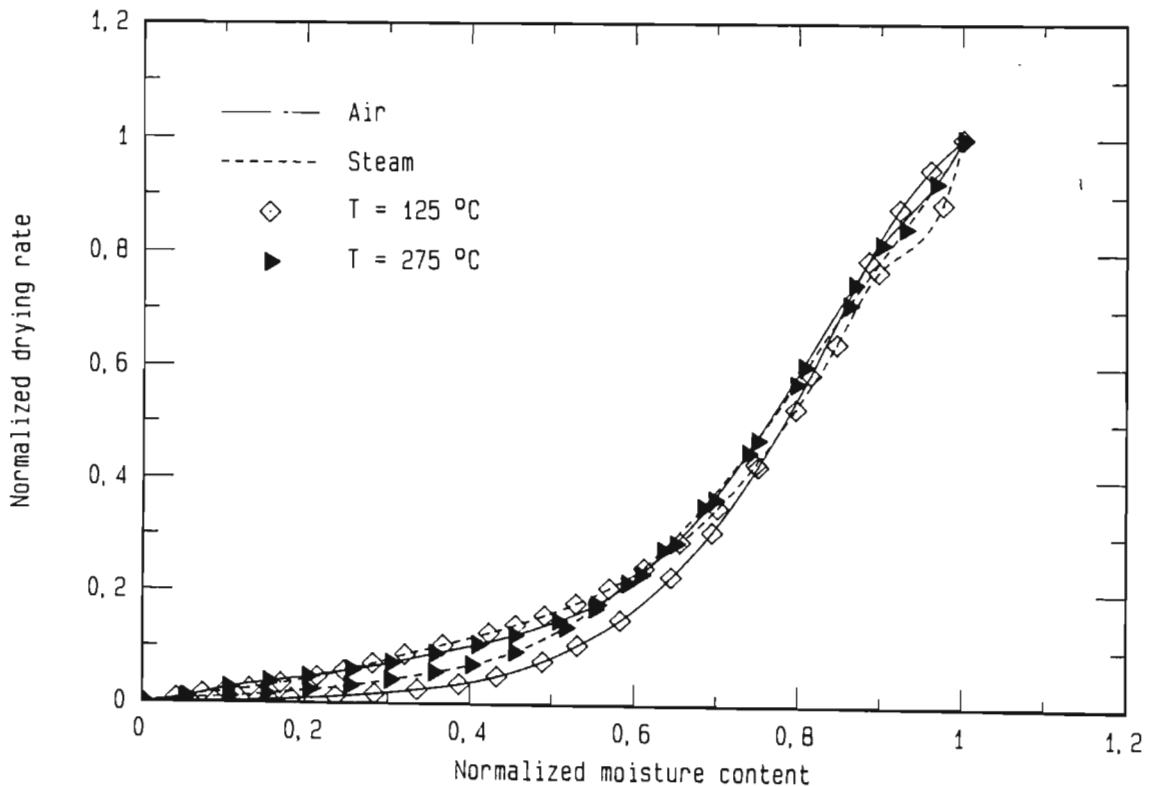


Figure 73: Normalized drying rates of molecular sieve in air and in steam at various temperatures (mass flow rate of 24,41 kg h<sup>-1</sup>)

#### 4.7 Mathematical model for the drying rate in the falling drying rate period

The comparison between air drying and steam drying during the falling drying rate period requires the development of a mathematical drying model. As stated in Section 2.3.6, mathematical drying models become very complex if the drying process is to be described accurately and are of little importance in the practical design of dryers. Therefore it is more appropriate to develop a simplified model that describes the major differences between air drying and steam drying. Such a model must be based on assumptions that neglect certain phenomena and it is clear that it can never describe the drying process accurately. In the context of this thesis, it was considered that such a simplified model would be satisfactory, especially as no temperature or moisture content profiles inside of the material could be measured, and so a complex model could anyway not have been verified on experimental data.

The principal mechanisms of moisture movement in the gaseous and in the liquid phase are discussed in Appendix I together with the differences in moisture movement in air drying and in steam drying.

##### 4.7.1 Mathematical model for air drying

The mathematical model that was developed to describe the drying of the testing materials is based on the receding plane model proposed by Krischer [K9] and extended by Schlünder [H3]. The model is described below.

During the constant drying rate period, heat is brought to the surface of the material by convection and is used for evaporation of the moisture. The mass transfer occurs by diffusion through the boundary layer around the material. The moisture content of the material decreases uniformly over the diameter of the particle, until it reaches the critical moisture content and the falling drying rate period starts.

During the falling drying rate period, the evaporative front withdraws into the body. Below this evaporative front, the local moisture content of the material is equal to the critical moisture content. Above the evaporative front, the material is considered to be partially wet, contrary to the classical receding plane model where the material above the evaporative interface is completely dry. The moisture movement takes place in both the vapour phase and the liquid phase. To warrant the assumption of liquid moisture flow, a moisture content gradient must exist in the partially dried layer. At the outer surface of the material, the local liquid moisture content is given by the sorption isotherm. Between the evaporative interface and the surface of the material, the moisture content decreases according to an arbitrary function. Heat is brought to the outer surface of the material by convection and then moves to the evaporative interface by conduction.

The kinetic formulas governing the drying process are presented below.

During the constant drying rate period, the transfer of moisture is given by:

$$\dot{m}_{ev,I} = \rho \beta \ln \left( 1 + \frac{y_{O,t}^* T_{O,t} - y_{\infty}}{1 - y_{O,t}^* T_{O,t}} \right) \quad (76)$$

The kinetic expression for the heat transfer is:

$$q = h \frac{\Delta h_v T_{O,t}}{c_{ps}} \ln \left( 1 + \frac{c_{ps} (T_{\infty} - T_{O,t})}{\Delta h_v T_{O,t}} \right) \quad (77)$$

During the falling drying rate period, the moisture moves in the inside of the material by capillarity according to following equation:

$$\dot{m}_l = \rho_{dp} \kappa \frac{(X_u - X_O)}{R \left( \frac{R}{r} - 1 \right)} \quad (78)$$

and by diffusion through the pores according to following equation:

$$\dot{m}_v = \frac{\tilde{M}_v}{R T} D_{eff} \frac{(p_{v,u} - p_{v,o})}{R \left( \frac{R}{r} - 1 \right)} \quad (79)$$

The mass transfer on the outside of the particle can be written as follows:

$$\dot{m}_e = \frac{\beta \rho_e}{p_t} (p_{v,o} - p_{v,\infty}) \quad (80)$$

The heat transfer on the inside of the material is by conduction according to following equation:

$$\dot{q}_i = \frac{\lambda_{dp}}{R \left( \frac{R}{r} - 1 \right)} (T_u - T_o) \quad (81)$$

and on the outside heat is brought to the material by convection according to following formula:

$$\dot{q}_e = h (T_o - T_\infty) \quad (82)$$

The Equations for the mass transfer on the inside and on the outside of the material can all be written as the product of a transfer coefficient and a driving potential as follows:

$$\dot{m}_i = B_i (X_u - X_o) \quad (83)$$

$$\dot{m}_e = B_e (X_o - X_\infty) \quad (84)$$

$$\dot{q}_i = h_i (T_o - T_u) \quad (85)$$

$$\dot{q}_e = h_e (T_\infty - T_o) \quad (86)$$

with following transfer coefficients:

$$B_i = \frac{\frac{\tilde{M}_v}{R T} D_{eff} + \rho_{dp} \kappa \frac{(X_u - X_o)}{(p_{v,u} - p_{v,o})}}{R \left( \frac{R}{r} - 1 \right)} \quad (87)$$

$$B_e = \frac{\beta \rho_e}{p_t} \quad (88)$$

$$h_i = \frac{\lambda_{dp}}{R \left( \frac{R}{r} - 1 \right)} \quad (89)$$

$$h_e = h \quad (90)$$

The transfer rates are divided into inner and outer transfer rates. The amount of moisture that is transported through the inside of the material to the external surface must be equal to the amount of moisture carried away from the external surface to the bulk of the drying medium.

$$\dot{m}_i = \dot{m}_e \quad (91)$$

The same applies to the transfer of heat. The amount of heat that reaches the surface of the material must be equal to the amount of heat conducted through the material to the evaporative interface.

$$\dot{q}_e = \dot{q}_i \quad (92)$$

The mass transfer on the inside and on the outside of the particle are set in series. The resulting mass transfer from the evaporative interface to the bulk of the drying medium,  $\dot{m}_{ev}$ , can be written as follows:

$$\dot{m}_{ev} = \frac{1}{\frac{1}{B_e} + \frac{1}{B_i}} (p_V^*(T_V) - p_\infty) \quad (93)$$

The resulting heat transfer from the drying medium to the evaporative interface can be written as follows:

$$\dot{q} = \frac{1}{\frac{1}{h_e} + \frac{1}{h_i}} (T_\infty - T_V) \quad (94)$$

Equations 93 and 94 represent the basic equations for heat and mass transfer. If the drying process is not too fast, then a third equation is formed by writing that the heat transferred to the evaporative interface is used for evaporation of moisture (Equation 95). The heating up of the particle is neglected.

$$\dot{q} = \dot{m}_{ev} \Delta h_v \quad (95)$$

The unknowns in the system are the temperature at the evaporative interface, as well as the temperature, the moisture content and the vapour pressure at the surface of the material.

A fourth equation is given by the sorption isotherm determined in Section 3.3.2, which gives a relation between moisture content, temperature and vapour pressure at the external surface of the material.

The external heat transfer coefficient,  $h_e$ , is determined from the Nusselt-type equation for convective heat transfer in fluidized beds presented in Section 4.3.2.

$$Nu = 0,03 Re^{1,3}$$

The external mass transfer coefficient,  $\beta_e$ , is determined from the heat transfer coefficient by using the Lewis equation (Equation 15).

The vapour pressure at the evaporative interface is equal to the saturation pressure at the interface temperature.

The thermal conductivity through the dry skeleton is used for describing the heat conduction inside the material. The thermal conductivity is assumed to be constant (independent of temperature or moisture content).

The diffusion coefficient on the inside of the material is calculated according to Equation 197. The capillary coefficient is calculated according to Equation 191. The constants  $a$  and  $b$  are varied until the calculated normalized drying rates agree with the measured ones. The same applies for the diffusion resistance factor.

The liquid moisture content profile on the inside of the material was calculated according to an arbitrary function. This function was chosen so that a sharp decrease in the moisture occurred at the interface and has following mathematical form:

$$u(r) = C_1 - C_2 r^{C_3} \quad (96)$$

The constants  $C_1$  and  $C_2$  are determined from the liquid moisture content at the surface of the material and from the critical moisture content. The constant  $C_3$  was fixed at 0,1.

#### 4.7.2 Mathematical model for steam drying

The mathematical model for drying in steam is, in principle, analogous to the model for drying in air. However, some alterations, had to be made. During the constant drying rate period, the heat transfer alone determines the drying rate, as there is no resistance to the transfer of moisture on the outside of the material.

$$\dot{m}_{ev,I} = \frac{h_e (T_\infty - T_o)}{\Delta h_v} \quad (97)$$

During the falling drying rate period, the moisture moves on the inside of the material by capillarity according to Equation 80 and by viscous flow on the basis of a total pressure gradient according to following Equation:

$$\dot{m}_s = \rho_s \frac{K_s (p_{s,u} - p_{s,o})}{\eta_s R \left( \frac{R}{r} - 1 \right)} \quad (98)$$

The kinetic expression for mass transfer is:

$$\dot{m}_{ev} = B_i (p_{s,u} - p_{s,o}) \quad (99)$$

In the case of steam drying, the steam pressure at the surface of the material is equal to the total pressure in the system. The inner mass transfer coefficient can be written as:



$$B_i = \frac{\rho_s \frac{K_s}{\eta_s} + \rho_{dp} \kappa \frac{(X_u - X_o)}{(p_{s,u} - p_{s,o})}}{R \left( \frac{R}{r} - 1 \right)} \quad (100)$$

The kinetic expression for heat transfer is given by:

$$q = \frac{1}{\frac{1}{h_e} + \frac{1}{h_i}} (T_\infty - T_u) \quad (101)$$

The unknowns in this system are the temperature at the surface of the material and the temperature at the evaporative interface. The moisture content at the surface is calculated over the sorption isotherm and is dependent only on the temperature of the surface, as the system pressure is fixed.

For steam drying, the same form of the moisture content profile was assumed as in air drying.

#### 4.7.3 Simulation of the drying of alumina

In Figures 74 to 79, the normalized drying rate curves of alumina in air and in steam are presented. The continuous lines indicate the model calculations and the symbols represent the measured data.

The following expressions for the capillarity coefficient were used for alumina (see Appendix I):

$$\text{Air drying:} \quad \kappa = 1,5 \cdot 10^{-9} \left( \frac{T}{273} \right)^{4,5} \quad (102)$$

$$\text{Steam drying:} \quad \kappa = 8,3 \cdot 10^{-11} \left( \frac{T}{273} \right)^{7,5} \left( \frac{X}{0,23} \right)^4 \quad (103)$$

The arithmetic average between the temperatures at the evaporative interface and the surface of the particle was used in the calculation of the capillarity coefficient.

The capillarity coefficient in air is independent of moisture content, whereas in steam drying it is strongly dependent on moisture content.

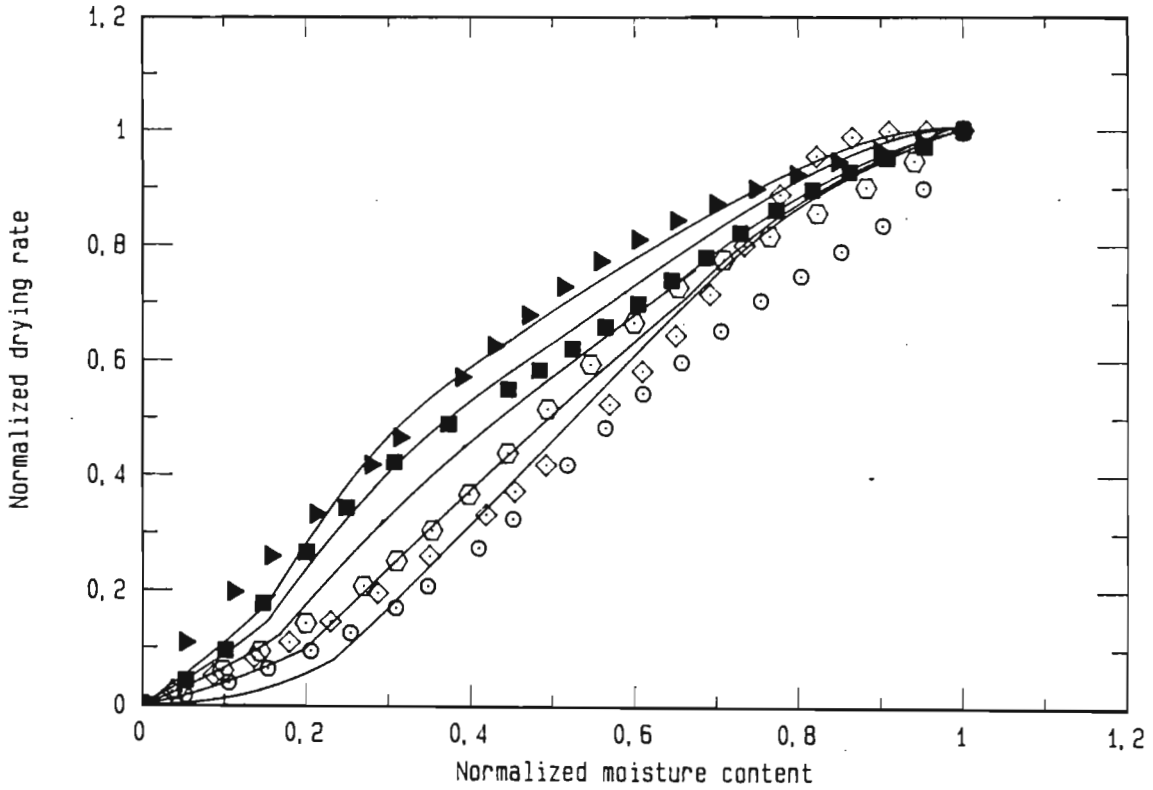


**Figure 74:** Simulation of the normalized drying rates of alumina in air at an air flow rate of 16,70 kg h<sup>-1</sup> (see Nomenclature for symbols)

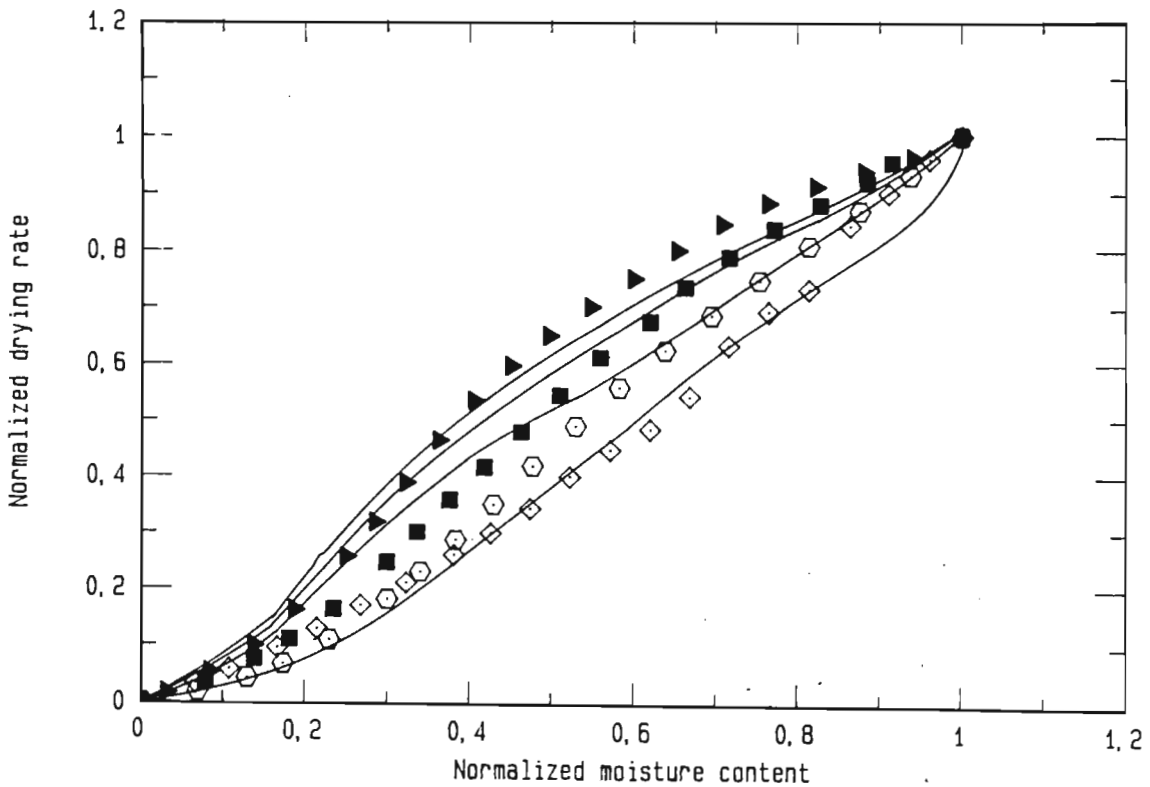


**Figure 75:** Simulation of the normalized drying rates of alumina in steam at a steam flow rate of 16,70 kg h<sup>-1</sup> (see Nomenclature for symbols)

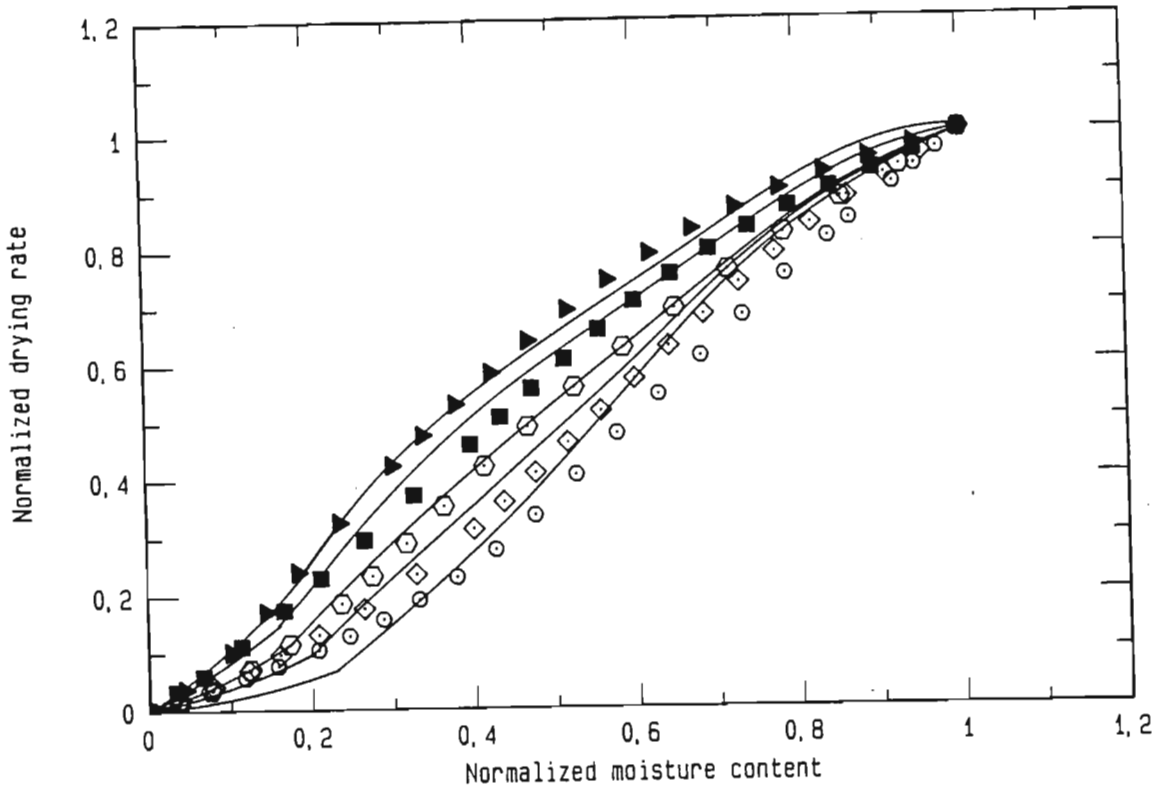


Figure 76: Simulation of the normalized drying rates of alumina in air at an air flow rate of  $19,27 \text{ kg h}^{-1}$  (see Nomenclature for symbols)

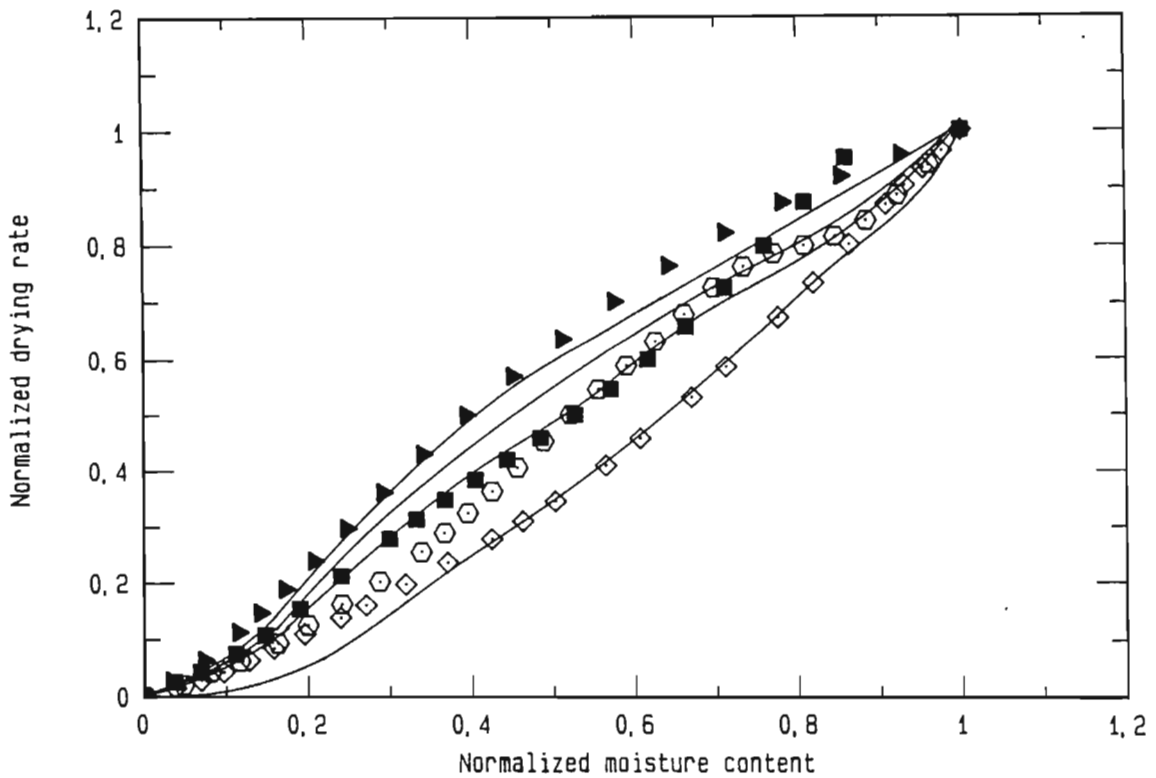
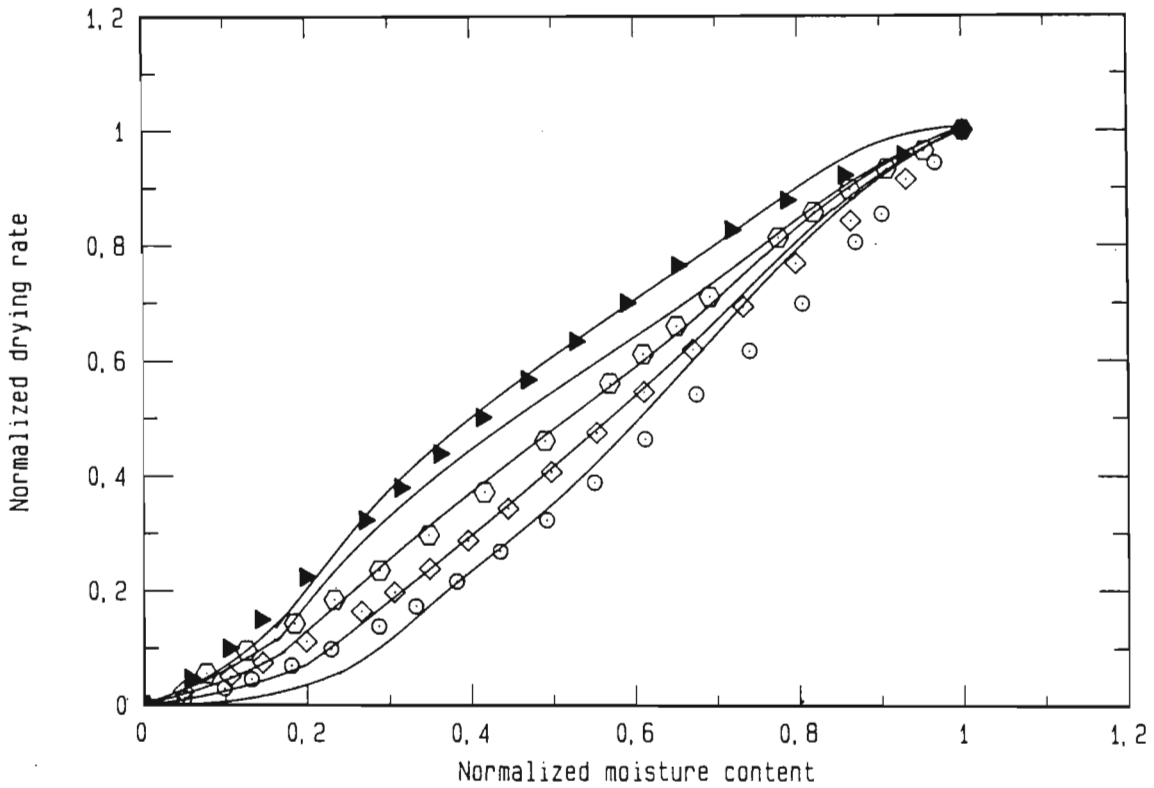
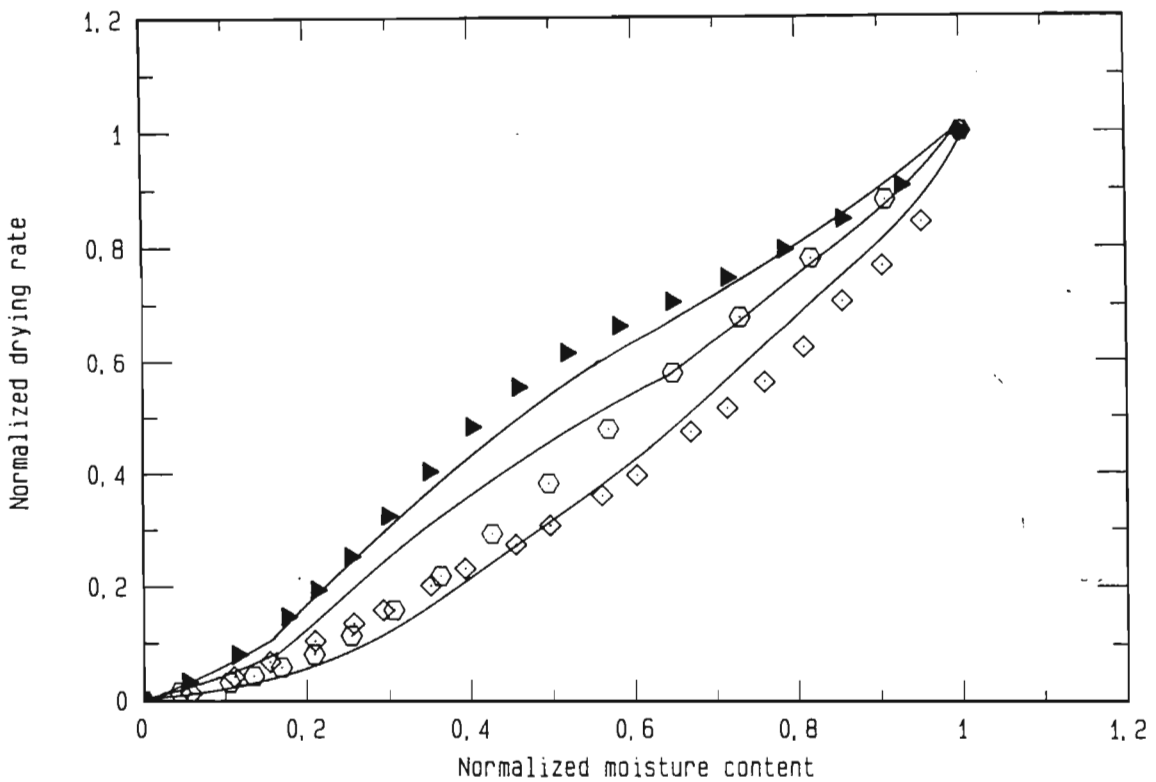


Figure 77: Simulation of the normalized drying rates of alumina alumina in steam at a steam flow rate of  $19,27 \text{ kg h}^{-1}$  (see Nomenclature for symbols)



**Figure 78:** Simulation of the normalized drying rates of alumina in air at an air flow rate of  $22,76 \text{ kg h}^{-1}$  (see Nomenclature for symbols)



**Figure 79:** Simulation of the normalized drying rates of alumina in steam at a steam flow rate of  $22,76 \text{ kg h}^{-1}$  (see Nomenclature for symbols)

The constant in the capillarity of steam is an order of magnitude lower than the constant in air drying. This would suggest that capillarity in air is much higher than in steam. However, the smaller value of the constant in steam is somewhat counterbalanced by the higher exponent in the temperature-dependence.

The resistance factor to vapour diffusion was 2 in air drying and 0,03 in steam drying. A resistance factor smaller than 1 is not logical and means that the 'real' vapour transfer process is speeded up compared with the theoretically expected transfer process. This seems also to indicate, what was said in Section 4.6, that in steam drying additional moisture transfer mechanisms may be acting.

For air drying the calculated normalized drying rates fit well for the higher temperatures. For the low temperatures one finds a discrepancy which is especially pronounced for high normalized moisture contents (i.e. close to the critical moisture content). This can be due to an overestimation of the capillary water movement at low temperatures. In general, however, the model fits the experimental data well.

For steam drying, the model does not fit the data as well. Whereas the experimental normalized drying rate curves are equally spaced for each temperature rise of 25 °C, the model values increase quickly for temperature rises at a low temperature level and increase slower at a high temperature level. This can be attributed to the simplified model, which uses a fixed moisture content profile inside the material. It is conceivable that the moisture content profile in air drying is different from the moisture content profile in steam. Furthermore the shape of the moisture content profile may change with the kinetics of the drying process and be different at low temperatures than at high temperatures. The moisture content profile that was chosen is very close to the moisture content profile of a receding plane model. The receding plane model, however, is not applicable to all materials [H3]. A different moisture content profile was not tried, as the model simulations were satisfactory.

The thermal conductivity of the material was not measured and an arbitrary value of  $\lambda_{dp} = 0,25 \text{ W m}^{-1} \text{ K}^{-1}$  was used [H3].

#### 4.8.4 Simulation of the drying of molecular sieve

In Figures 80 to 85, the normalized drying rate curves of molecular sieve in air and in steam are presented. The continuous lines indicate the model calculations and the symbols represent the measured data.

The following expressions for the capillarity coefficient were used for molecular sieve (see Appendix I):

$$\text{Air drying: } \kappa = 1,0 \cdot 10^{-9} \left(\frac{T}{273}\right)^{0,5} \left(\frac{x}{0,12}\right)^4 \quad (104)$$

$$\text{Steam drying: } \kappa = 2,5 \cdot 10^{-9} \left(\frac{T}{273}\right)^{0,5} \left(\frac{x}{0,05}\right)^{0,7} \quad (105)$$

The constant in the capillarity of steam is higher. The temperature-dependence is the same in air and in steam. The moisture content influence is more pronounced in air drying. In summary, the capillarity coefficients are of the same order of magnitude and are higher in steam than in air.

The resistance factor to vapour movement was 50 in air drying and 18 in steam drying. These are very high resistance factors and indicate that the moisture moves inside of the material mainly by capillarity.

For air drying the model fits the experimental data better than for steam drying. For normalized moisture contents bigger than 0,6 the model calculates normalized drying rates that are wider spaced than found experimentally. This is especially true for steam drying. For air drying, the calculated normalized drying rates open further up for lower normalized moisture contents, whereas for steam drying they converge for lower normalized moisture contents.

The presented drying model describes the drying behaviour qualitatively well. In the effort to keep the mathematical work in the solution of a drying model at a minimum, certain simplifying assumptions had to be made (e.g. fixed shape of the moisture content profile in the inside of the material). These simplifying assumptions do not allow the use of the model to investigate in detail the different drying mechanisms. The model must more be seen as a tool to generally describe the overall drying behaviour.

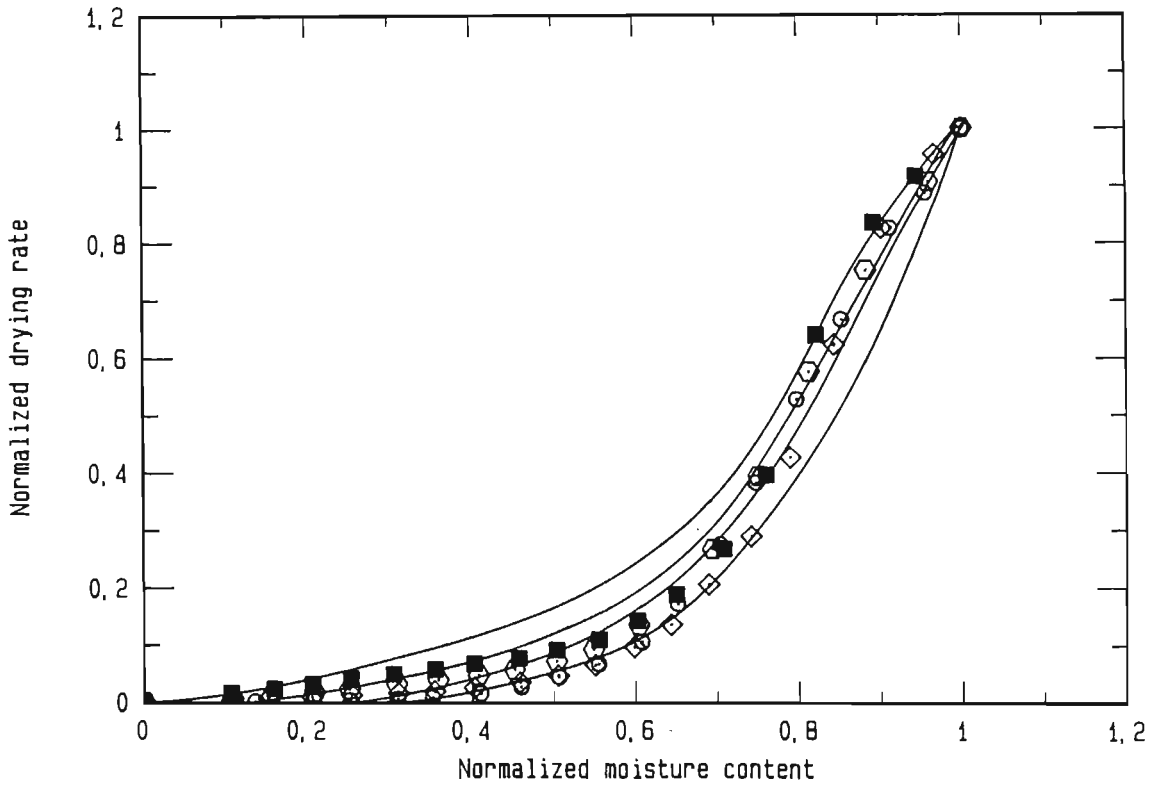


Figure 80: Simulation of the normalized drying rates of molecular sieve in air at an air flow rate of 21,06 kg h<sup>-1</sup> (see Nomenclature for symbols)

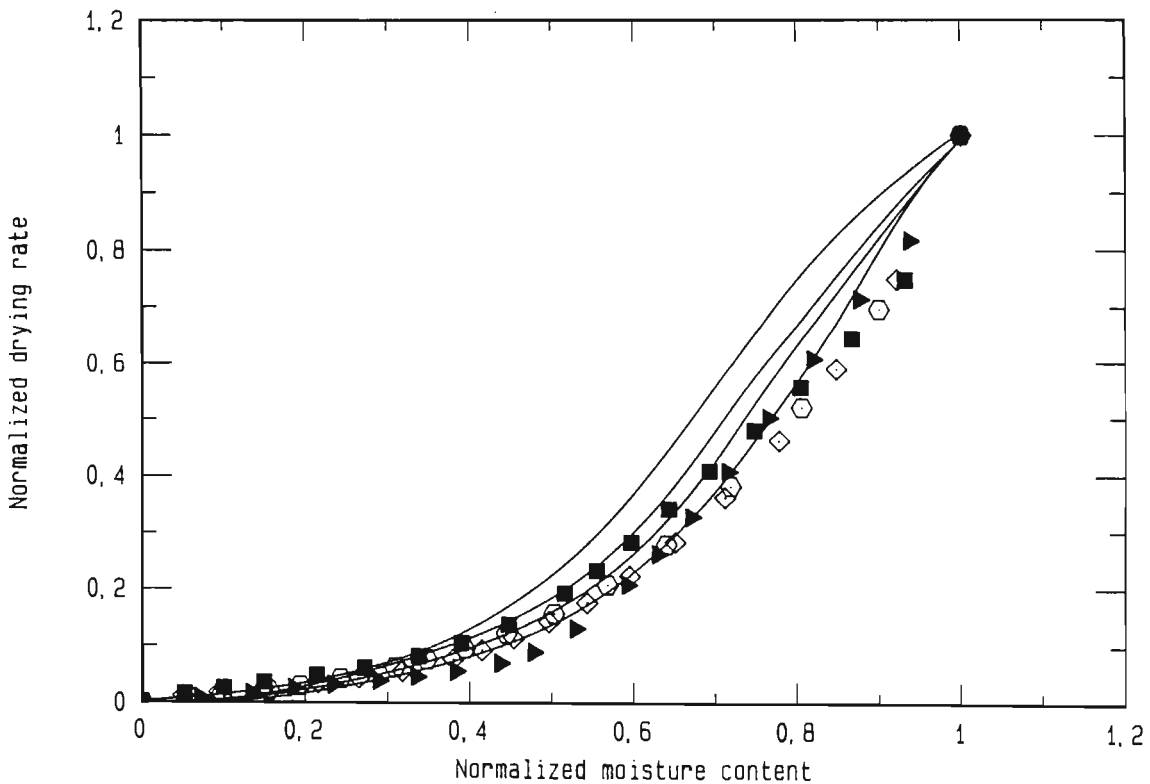


Figure 81: Simulation of the normalized drying rates of molecular sieve in steam at a steam flow rate of 21,06 kg h<sup>-1</sup> (see Nomenclature for symbols)

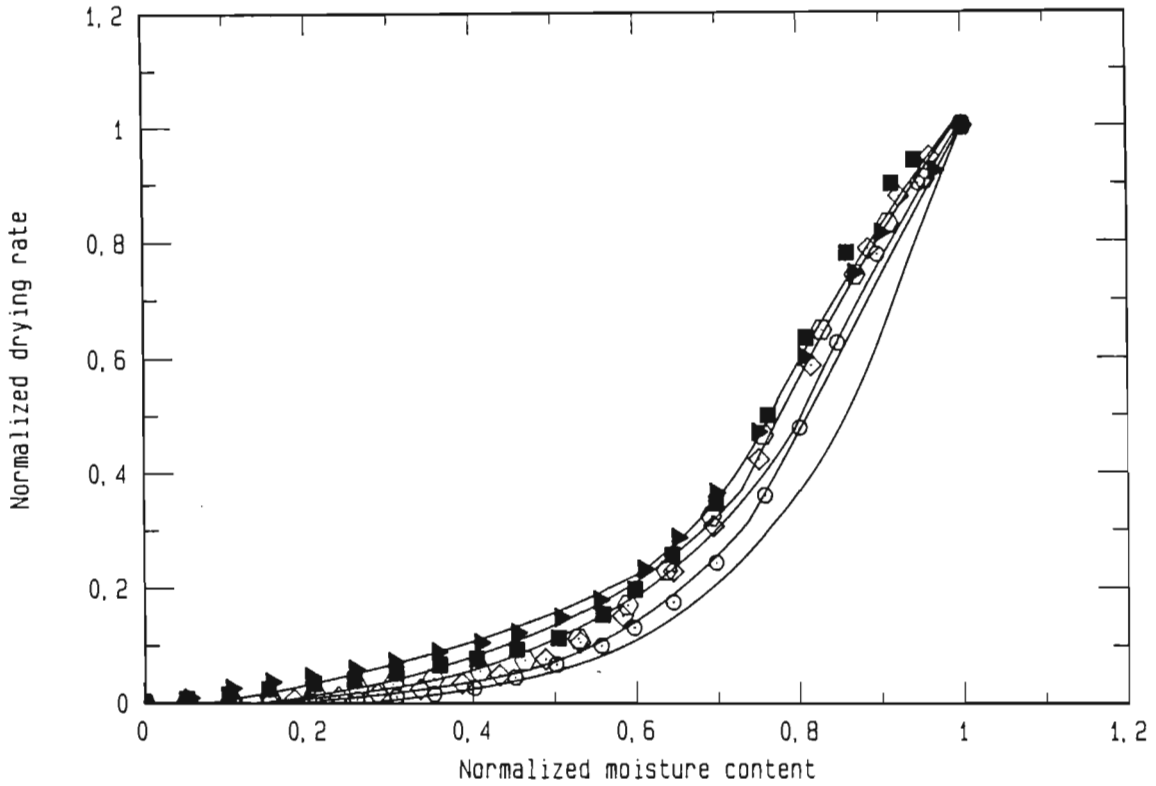


Figure 82: Simulation of the normalized drying rates of molecular sieve in air at an air flow rate of  $24,41 \text{ kg h}^{-1}$  (see Nomenclature for symbols)

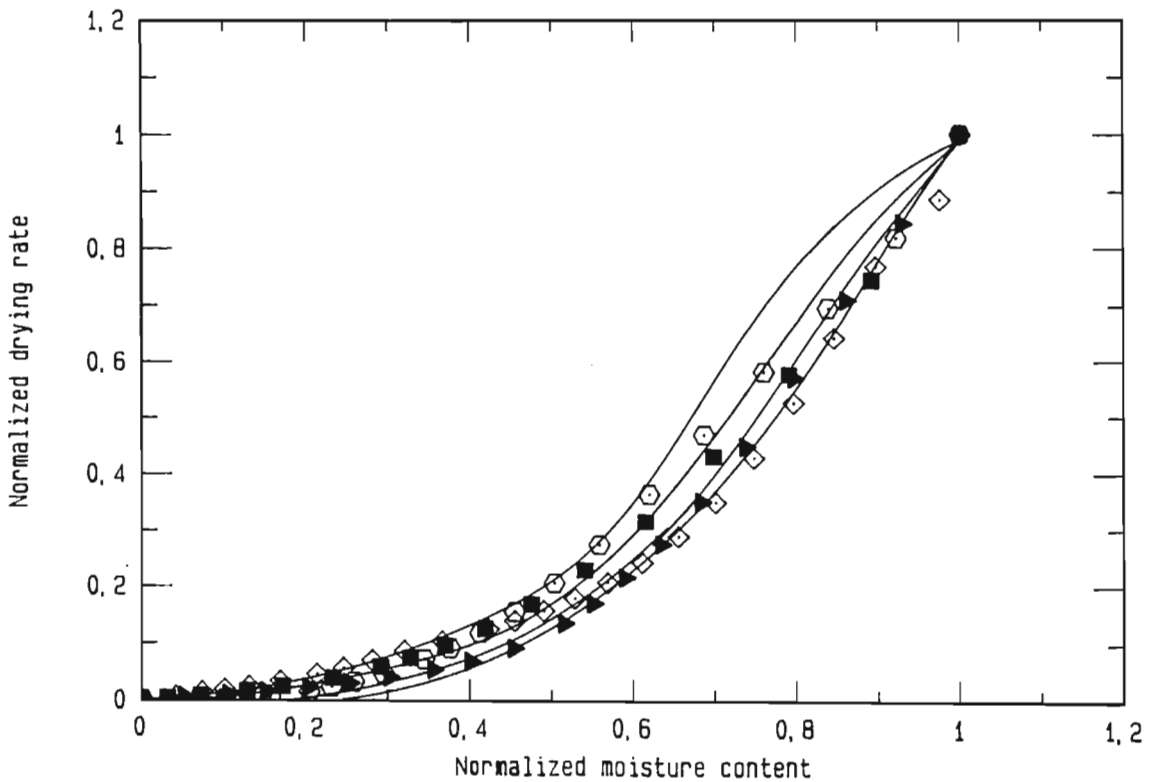


Figure 83: Simulation of the normalized drying rates of molecular sieve in steam at a steam flow rate of  $24,41 \text{ kg h}^{-1}$  (see Nomenclature for symbols)



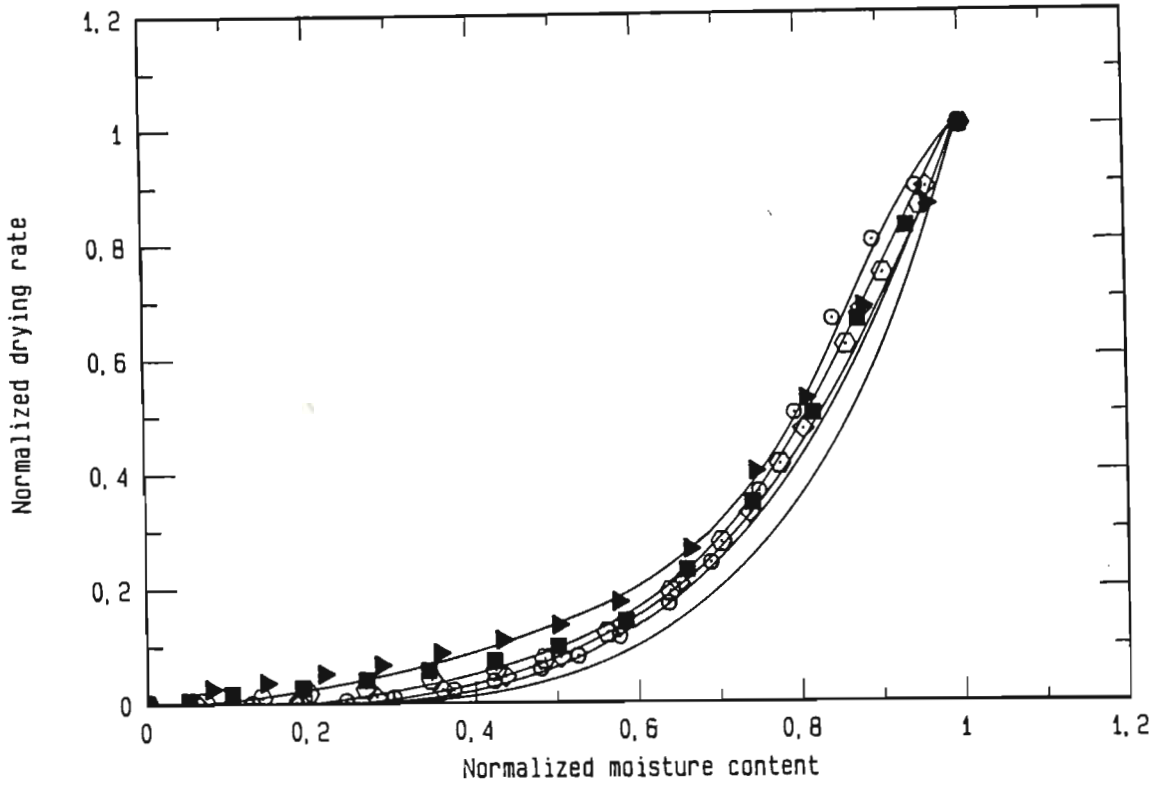


Figure 84: Simulation of the normalized drying rates of molecular sieve in air at an air flow rate of  $25,96 \text{ kg h}^{-1}$  (see Nomenclature for symbols)

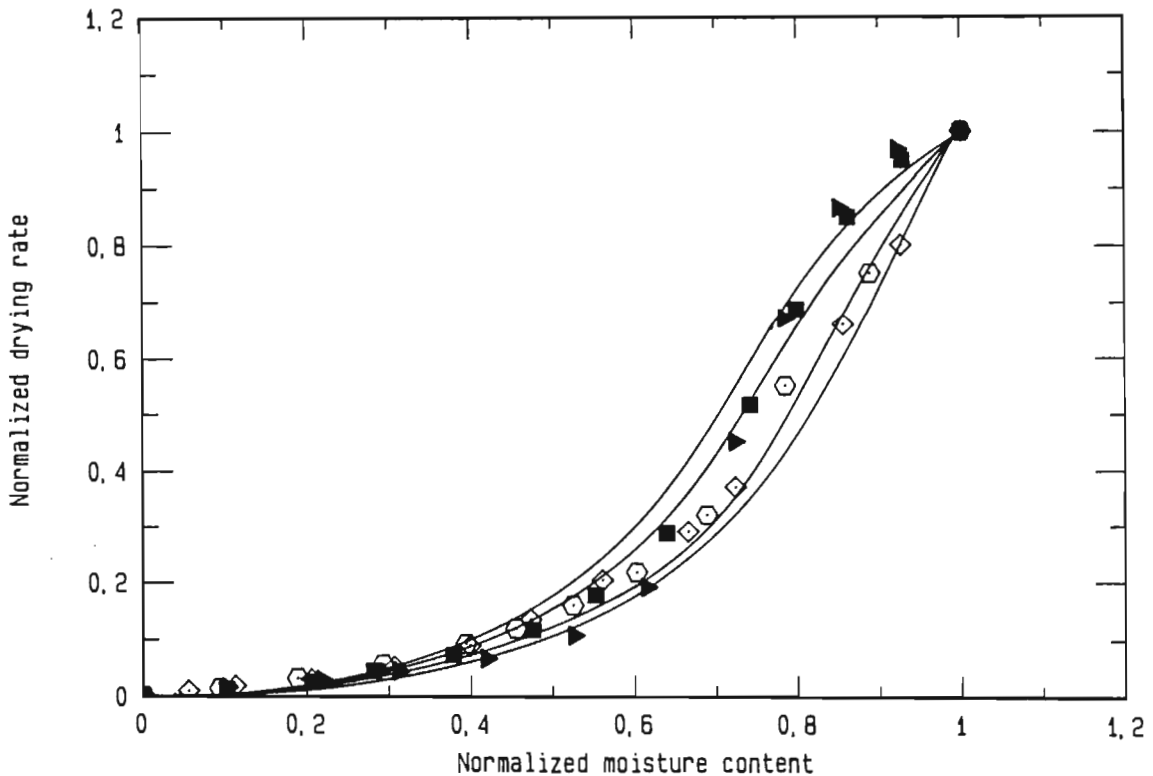


Figure 85: Simulation of the normalized drying rates of molecular sieve in steam at a steam flow rate of  $25,96 \text{ kg h}^{-1}$  (see Nomenclature for symbols)

## 5. ECONOMIC COMPARISON BETWEEN AIR DRYING AND STEAM DRYING IN A FLUIDIZED BED

An objective economic comparison between air drying and steam drying must be based on optimized drying systems for air and steam. In this thesis, only indirectly heated drying systems are considered. The schematic procedure for the economic analysis is presented in Figure 86.

The economic analysis is based on the running and capital costs of the drying system. These costs can be determined only once the drying system has been designed. The drying system consists of a blower, a heat exchanger, a dryer and a gas cleaning device. All this equipment is dimensioned according to the heart of the system, which is the dryer itself. Therefore the dryer must be designed first. For the design of the dryer, certain drying data on the material must be available. These data are the drying rate curve, which indicates how quickly the material dries, and the sorption isotherm, which indicates to what remaining moisture content the material can be dried.

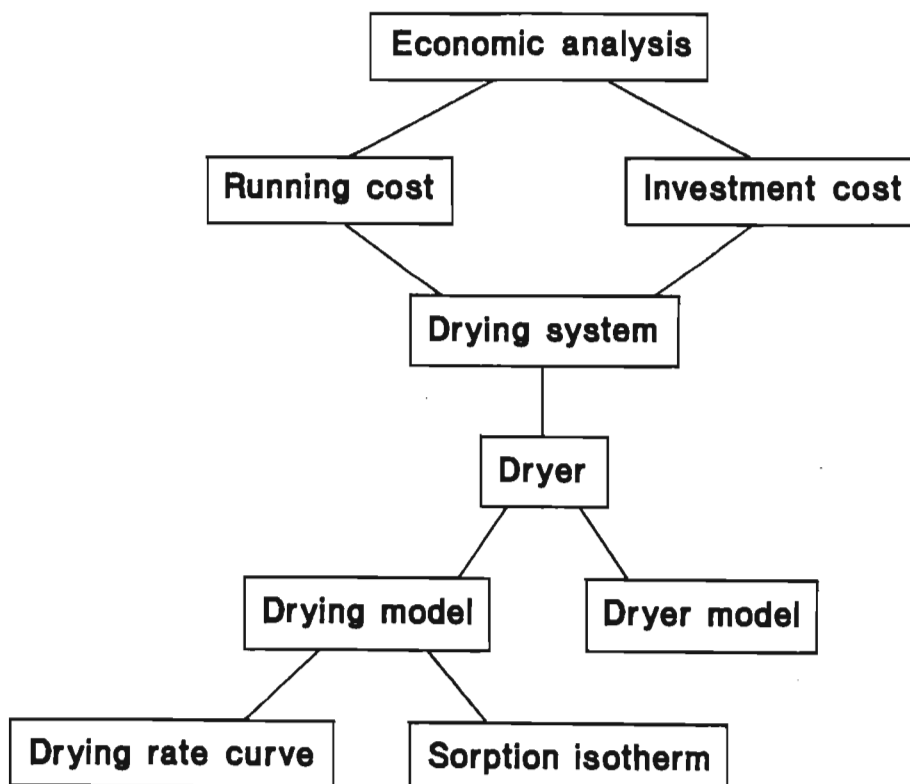


Figure 86: Schematic procedure for the economic analysis

The drying data are recorded at specific conditions (temperature, pressure, humidity, flow rate, etc.). Therefore a drying model is required to extrapolate the data recorded at a certain set of conditions to a different set of conditions. If the drying rate curve was recorded in a dryer of the same type as the dryer to be designed, then the drying rate curve can be used directly in the design procedure. If the drying rate curve was recorded in a different type of dryer to the one to be designed, then the recorded drying rate curve must be modified with the help of a dryer model in order to represent the expected drying rate curve in the dryer to be designed.

### 5.1 Design of fluidized-bed dryers

The practical design methods that are normally used by manufacturers are based on continuous drying tests in pilot plants. However, these continuous drying tests are time-consuming, require large amounts of material and are very expensive. Therefore attempts have been made to develop design methods based on the one hand on batch tests using smaller equipment and on the other hand on the available knowledge of the drying mechanisms.

Such a design method was first proposed by Vanecek *et al.* [V4]. The mean moisture content of the product was expressed by:

$$X = \int_0^{\infty} E(t) X(t) dt \quad (106)$$

$E(t)$  is the residence time distribution of the particles in the dryer and  $X(t)$  is the moisture content of the particles as a function of the time. For well mixed fluidized beds, the residence time distribution of the material can be expressed by [V4]:

$$E(t) = \frac{1}{t_m} \exp \left( -\frac{t}{t_m} \right) \quad (107)$$

The moisture loss as a function of time differs between batch tests and continuous tests. The reason is that in batch tests all the particles have the same moisture content and are at the same temperature.

In continuous tests, however, the particles that have been in the dryer for a long time are relatively dry and hot, whereas the particles that have been in the dryer for a short time are still wet and cold. Therefore heat is exchanged not only between gas and particles, but also between hot and cold particles [C6,V1-3]. For the same gas inlet temperature, the moisture loss recorded in continuous dryers is faster than the moisture loss recorded in batch dryers. Vanderschuurén [V3] found that for small particles of 0,685 mm, the contribution of the interparticle heat exchange to the total heat exchange with the drying particles was in the order of 65 % and for large particles of 2,145 mm in the order of 15 %. Therefore the moisture loss curve recorded in a batch test cannot be used directly in the design of a continuous dryer. Vanecek *et al.* [V4] devised a recording technique termed "batch simulated continuous run" (BSC) which simulates the drying of material in a continuous dryer by performing a batch drying test. A weighed amount of wet material is added to a fluidized bed of dry particles and is dried isothermally. The recorded drying rate curve is then put into a mathematical form and used in Equation 106. The temperature-dependence of the moisture loss curve is also taken into account.

In Vanecek *et al.*'s method [V4], the drying kinetics of the material have to be determined at a constant bed temperature, which is experimentally difficult to realize. Reay and Allan [R1] devised a design procedure based on the results of batch tests recorded at a constant inlet temperature. The drying curve is then divided into small segments and each segment is converted to a corresponding segment of drying curve that would exist in a continuous dryer. This method was successfully tested for zerolite, iron ore and wheat.

Reay and Allan found that for zerolite and iron oxide, the total amount of water that is evaporated is linearly proportional to the mass flow rate and independent of the bed height. For wheat, the total amount of water that is evaporated is dependent on bed height, but is independent of fluidizing velocity. The explanation for the different behaviour of the materials can be found in their inner structure. Iron ore and zerolite present weak resistance to the internal migration of moisture. As a result the drying medium left the dryer close to equilibrium with the particles. The drying rate is

controlled by a total energy balance and the total amount of moisture removed is independent of the bed height, but proportional to the mass flow rate. Wheat presents a high resistance to the internal migration of moisture. The drying medium that leaves the dryer is not in equilibrium with the material. The drying rate is kinetically controlled by the heat and mass transfer processes inside the material. Therefore the total amount of moisture that is evaporated is independent of the external mass flow rate of the drying medium, but depends of the bed height of the material.

In order to convert the recorded drying rate curve to a different temperature, Reay and Allan made certain assumptions. During the constant drying rate period, the moisture loss over time is proportional to the driving potential for mass transfer, which is the difference between the vapour pressure at the surface of the particle and the vapour pressure of the inlet air. For the falling drying rate period, this proportionality is corrected by the free moisture content to take into account the limiting moisture migration mechanism inside the particle. This method was used equally for materials with high internal resistance and with low internal resistance.

Milota [M5] gave an explanation as to why the temperature conversion method worked for both types of material. The temperature-dependence of the saturation pressure of water (materials with low internal resistance) derived from the Clapeyron equation is of the same type as the temperature-dependence of the coefficient for internal moisture migration (materials with high internal resistance), which for highly hygroscopic materials can be expressed by an Arrhenius-type equation (creeping flow).

A criticism of the method given by Reay and Allan is that they used the difference between vapour pressure at the surface of the material and vapour pressure in the drying medium at the inlet into the dryer as the driving potential. In a well-mixed fluidized bed, the particles are at the same temperature and the same moisture content throughout the bed. The humidity of the drying medium however, increases as it flows upwards through the dryer. As a consequence, the driving force for mass transfer decreases with increasing height. Therefore Reay and Allan should have used the mean vapour pressure of

the drying medium as the driving force for moisture transfer and not the vapour pressure at the inlet into the dryer. Why the difference of the vapour pressure on the surface of the particle and at the inlet of the dryer is the correct one to be used in the conversion of the drying rate curve will be explained below.

In the drying of materials with a low resistance to internal migration, the drying medium leaves the dryer in equilibrium with the material. The dryer is an equilibrium system. The rate of drying is not controlled by kinetic effects inside or outside the particle, but by the total mass and energy balance around the dryer. Therefore the drying rate can be expressed by the moisture uptake of the drying medium, which is given by the product of the mass flow rate of the drying medium and the difference in humidity between the outlet (given by  $p_v^*$ ) and inlet of the dryer (given by  $p_{v,in}$ ). As the drying medium leaves the dryer in equilibrium with the material, the humidity at the outlet of the dryer is given by the sorption isotherm. During the constant drying rate period, the humidity is equal to the saturation humidity and during the falling drying rate period it is equal to the saturation humidity corrected by a factor smaller than one. If the sorption isotherm is a linear function of the free moisture content, Reay and Allan's method is valid. It is however important to note the difference between the vapour pressure at the surface of the drying material and that in the drying medium at the inlet, which is used in the conversion by Reay and Allan, does not result from a kinetic driving force as claimed by Reay and Allan, but from the total moisture mass balance over the dryer.

For materials with a high internal resistance to moisture migration the kinetics of the internal moisture transfer can govern the total drying rate. This can also be the case for materials with low resistance to internal moisture migration in the falling drying rate period. The drying kinetics are governed by internal processes of heat and mass transfer. The internal rate of drying may then decrease so much that the drying medium cannot be saturated any more as it flows through the bed, and the assumption of equilibrium at the outlet of the dryer is no longer valid. This is why Reay and Allan's conversion method did not work so well any more for moisture contents deep into the falling drying rate period.

Milota [M5] found that the method proposed by Reay and Allan could not be successfully applied to the drying of wood particles in a fluidized bed. Milota's explanation was that the mechanisms which govern the drying of wood are different from those for the drying of wheat, iron ore or zerolite. Moisture moves inside the timber on the basis of a combination of pore diffusion, free water movement and bound water diffusion. Milota adopted the principle of the conversion method proposed by Reay and Allan, but adapted it to the drying of wood particles. He divided the mechanisms governing the drying rate into external and internal moisture movement. Then he developed a function describing the temperature-dependence of these mechanisms and calculated the relative importance of these mechanisms by forming the Biot number for each segment of the drying curve. After that he converted the segments using the weighted influences of the internal and external mechanisms.

From the works of Reay and Allan and of Milota, one can conclude that the batch tests used to determine the moisture content evolution with time in a fluidized bed can be divided into three major groups:

- 1) equilibrium systems (iron ore, zerolite),
- 2) non-equilibrium systems with kinetic control of both the outside and inside of the material (timber), and
- 3) non-equilibrium systems with kinetic control inside of the material (wheat).

To which category the test belongs is determined by the mass flow rate of the drying medium, the nature of the material and the drying rate period of the drying process. It is important to know into which category the drying test falls, as the conversion method must be chosen accordingly.

Lately, efforts have been made to incorporate the bubbling behaviour of fluidized beds into design models [H9,P1]. These studies are of interest for the determination of the drying mechanisms involved in fluidized-bed drying, but are much more complex and hence of less practical value.

It must, however, be emphasized that the bubbling behaviour influences the heat and mass transfer processes in a fluidized bed. In small-scale beds the bubbling behaviour is different than in large-scale beds. In small-diameter beds, the bubbles coalesce on their rise through the fluidized mass and can reach diameters that equal the diameter of the experimental equipment. As a consequence slugging occurs, which presents different heat and mass transfer characteristics than a bubbling fluidized bed. In the present experimental equipment slugging could not be observed. However, because the experimental particles are large and the experimental equipment small, the scale-up must be treated with care. In any case it is always safer to perform pilot-plant tests before commissioning an industrial unit.

## 5.2 Design method for steam fluidized-bed dryers

No design procedure is available in the literature for steam-operated fluidized-bed dryers. Therefore a new design method had to be developed.

The basic principle of the design method by Reay and Allan was used. Batch drying rate curves are recorded, transformed and used for the design of steam-operated fluidized beds. In the original method by Reay and Allan, the transformation of the drying rate curve is done over the mass transfer and the correction factor is formed by the difference in saturation pressure and vapour pressure at the inlet into the dryer. In steam drying, the vapour pressure is equal to the total pressure and is constant over the height of the dryer. Therefore the transformation cannot be done over the mass transfer.

For steam dryers, the transformation is done over the heat transfer to the material. During the constant drying rate period the moisture that is evaporated can be expressed by following energy balance:

$$\dot{m}_{ev,I} = \frac{\dot{M}_s c_{ps} (T_{s,in} - T_{s,out})}{\Delta h_v + T_{p,I}} \quad (108)$$

During the falling drying rate period, the evaporation rate is corrected by the free moisture content.



The conversion technique that is used for steam dryers is described below.

- 1) The moisture loss of the material is recorded with time in a batch test performed at constant inlet temperature and gas flow.
- 2) The inlet temperature into the dryer, the bed temperature and the outlet temperature are recorded as functions of time.
- 3) The drying curve is divided into segments of 15 seconds. The mean moisture content and the mean temperature of the drying material are determined for these segments.
- 4) The segments are corrected to the fluidizing velocity, bed height and bed temperature that will be used in the continuous dryer. The time interval needed for drying the material by a certain amount is converted to the design conditions. This conversion is described in Appendix J. The physical properties that are needed for the conversion are determined at the arithmetic mean temperature during the test interval. Finally, taking all the effects into consideration, the drying time in the isothermal inlet test can be related to the drying time in the isothermal bed dryer. This conversion is also described in Appendix J.
- 5) The converted drying rate curve is then inserted into Equation 106 and the mean product moisture content is determined.

This design method was put into a computer program used for the economic analysis. The algorithm is presented in Figure 87.

First the duty of the dryer and the material properties have to be defined. The dryer duty is given by the mass flow rate and the inlet and outlet moisture contents of the material:

$$\dot{M}_{ev} = \dot{M}_p (x_{p,in} - x_{p,out}) \quad (109)$$

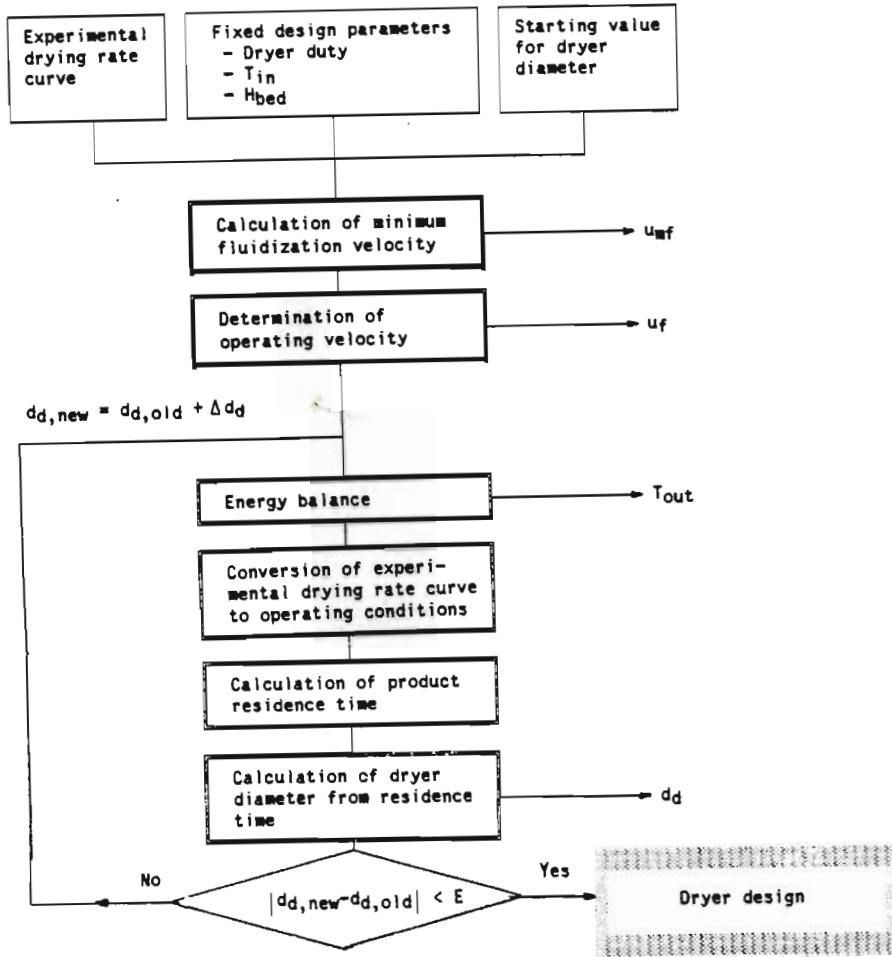


Figure 87: Algorithm for the economic analysis

The physical properties of the material are needed to calculate the minimum fluidizing velocity and the bulk density of the fluidized bed. According to Khokhar and Mujumdar [K6], the operating fluidizing velocity is between two to five times the minimum fluidizing velocity. In this thesis, a multiplication factor of 4 was chosen.

In general, the most economical temperature to use is the highest temperature possible that does not damage the material. Therefore the inlet temperature into the dryer was specified. The outlet temperature of the dryer was then calculated by making an energy balance around the dryer. The heat that is given off by the drying medium is used to evaporate moisture from the material, to heat the material up to bed temperature and to superheat the evaporated moisture.

For the energy balance, the diameter of the dryer must be known. Therefore a first approximation of the dryer diameter was specified. Once the bed temperature is known, the recorded batch curve can be converted to the given conditions of velocity, bed height and bed temperature. The batch drying curve recorded at 225 °C was used in all the conversions. The mean product moisture content was calculated according to Equation 106. The mean residence time was varied until the mean product moisture content was equal to the specified product moisture content. From the mean residence time and the mass flow rate of material, the volume of the dryer was determined. As the bed height is fixed, the bed diameter can be calculated. This calculated bed diameter is then compared with the initially guessed bed diameter. If the difference between these diameters is below a certain error, the fluidized-bed design is completed. Otherwise, the guessed diameter is changed and the whole procedure is repeated until the calculated and guessed values are close enough.

Once the dryer has been designed, the flow rate of the drying medium, the inlet and outlet temperatures of the drying medium and the thermal energy requirements of the dryer are known. The drying system that is considered is presented in Figure 88.

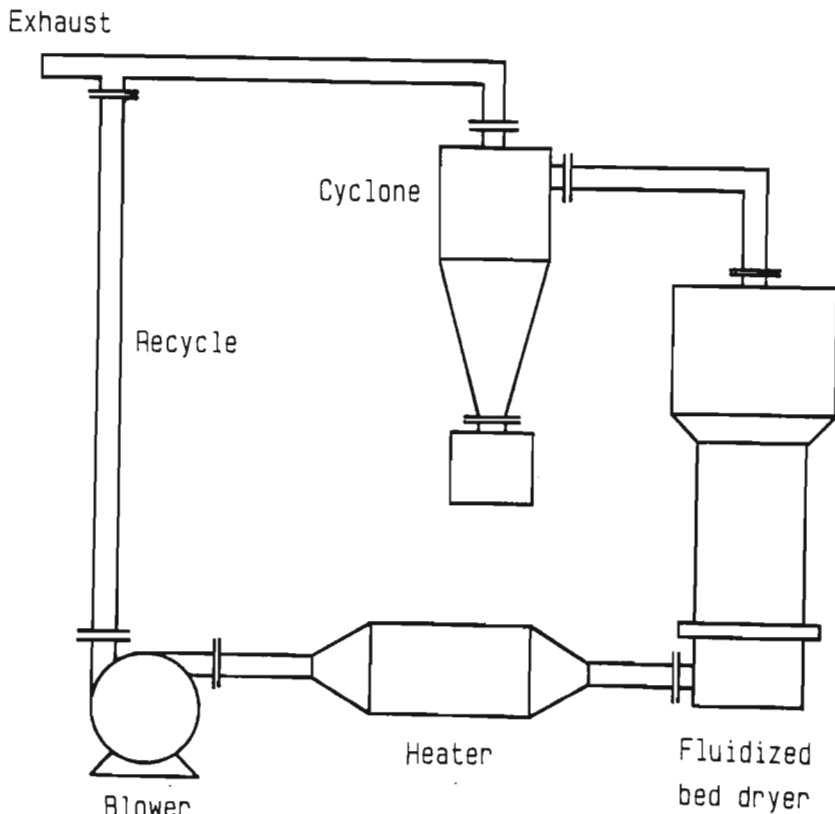


Figure 88: Drying system for the economic analysis

In the air case, ambient air is sucked into the system by a blower and pushed through a heat exchanger. The drying medium is brought to the required inlet temperature into the dryer. After passing through the dryer, the drying medium is cleaned in a cyclone before being discharged to the atmosphere. In the steam case, the equipment used is the same, except that the loop is closed and part of the steam leaving the cleaning equipment enters the blower again. The inlet temperature into the blower is then higher than the boiling point and special care must be taken of this part of the equipment.

Once the drying system has been designed, the running costs and capital costs can be calculated. In this thesis, the running costs are made up of only the energy costs. The reason is that no information was available for the maintenance costs of steam drying. The economic analysis should be seen as a comparative study. Therefore this comparison should be based on data that are verifiable and not falsified by speculative assumptions. The energy costs consist of the electrical costs for the blower and the thermal energy costs for the heat exchanger. Energy prices are based on 1986 prices on the Witwatersrand for large industries.

Energy requirements for the blower were determined by the volume flow rate of the drying medium and the pressure increase needed to overcome the pressure drop in the system. The total efficiency of the blower was taken as 75 %, whereas the efficiency of the electric drive was taken as 90 %. These efficiencies are conservative. The thermal energy requirements of the system were determined from the flow rate of drying medium and the temperature increase in the heat exchanger. No economic value was attributed to the purged steam from the closed system. Consideration of the purged steam would drastically reduce the running costs of steam drying and increase its economic attractiveness. However, as the purged steam is at a low pressure, there may be no use for it in the factory. It is therefore omitted from this study.

The capital costs of the drying equipment are calculated according to data obtained from manufacturers and according to literature data [F3].

### 5.3 Results of the economic analysis

The results of the economic analysis are now presented. In particular the changes in capital and running costs as a function of the inlet temperature into the dryer, as a function of the product moisture content and as a function of the production rate are investigated. The base data for the economic analysis are a production rate of dry particles of  $2\,000\text{ kg h}^{-1}$ , a product moisture content of 7 %, an inlet temperature into the dryer of  $275\text{ }^{\circ}\text{C}$  and a bed height of 0,2 m.

In Figures 89 and 90, the capital costs of the air and steam drying systems are presented as a function of temperature for alumina and molecular sieve.

An increase in temperature produces an increase in the drying kinetics. The residence time of the particles in the dryer is reduced and the dryer becomes smaller. Therefore the capital costs of the drying systems decrease with an increase in temperature. The capital costs of the steam-drying system are higher than the capital costs of the air-drying system. At lower temperatures, the advantage of air drying is more pronounced. At the boiling point, the drying rate in steam is nil, as there is no driving force for the transfer of heat. Consequently, the drying equipment must be infinitely large to fulfil the drying duty. Therefore the capital costs of the drying system in steam become infinity. With increasing temperature, however, the capital costs decrease rapidly and approach those for air drying.

For the drying of alumina, the advantage of air drying is more pronounced than it is for the drying of molecular sieve. The reason lies in the different drying behaviour of these materials. Alumina exhibits a relatively short falling drying rate period, both in air and in steam. Molecular sieve, however, exhibits a long falling drying rate period in air and a short one in steam. Therefore steam has a larger kinetic advantage for drying molecular sieve.

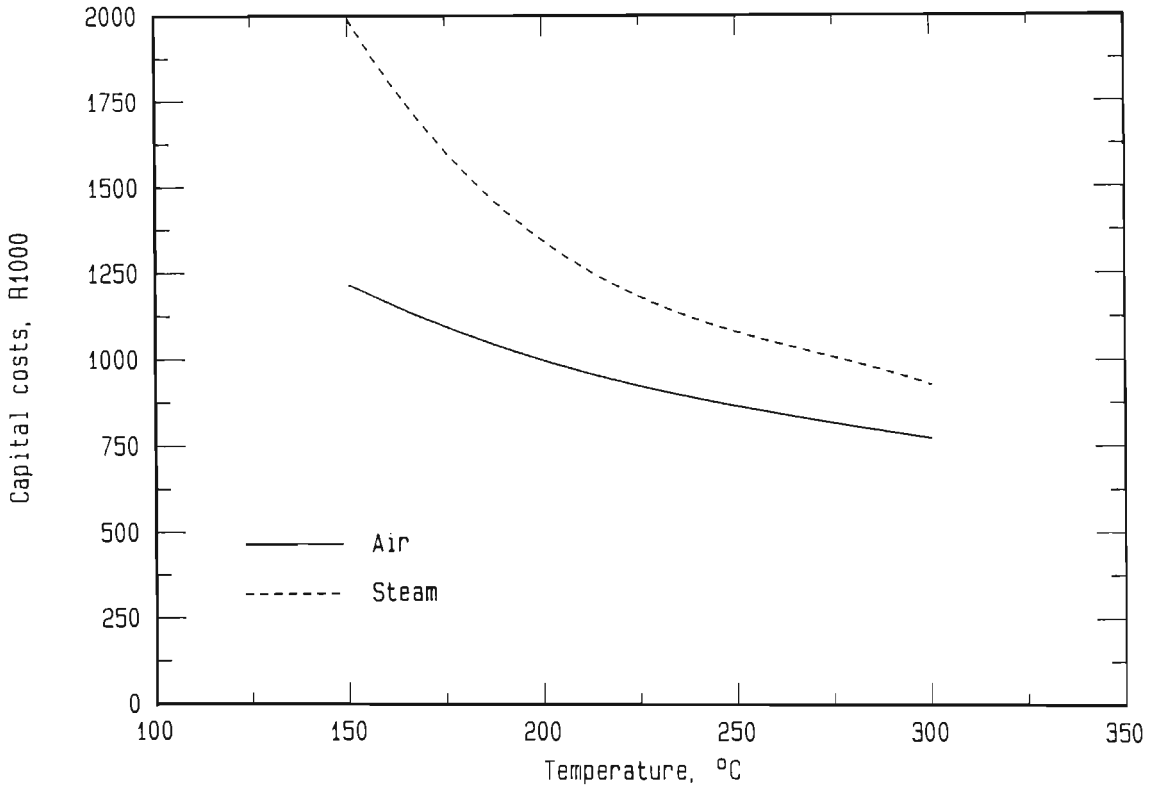


Figure 89: Comparison of the capital costs of an air-drying system and a steam-drying system for alumina as function of the inlet temperature into the dryer

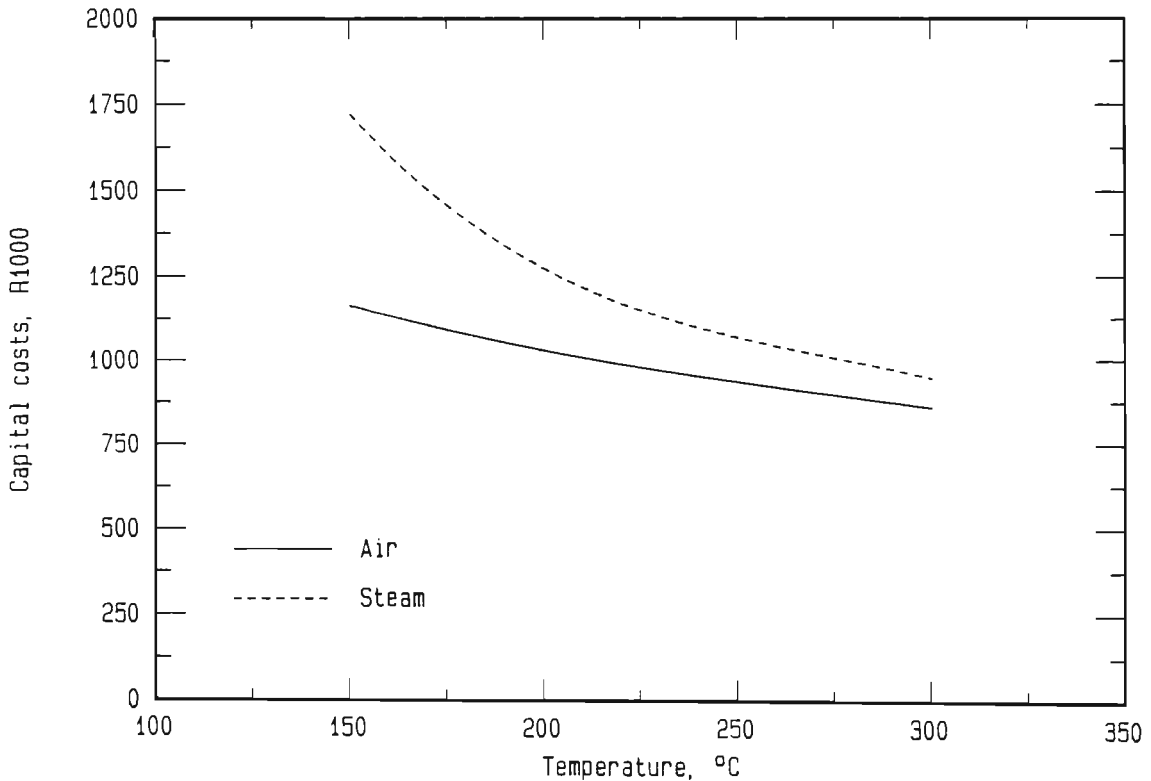


Figure 90: Comparison of the capital costs of an air drying system and a steam drying system for molecular sieve as function of the inlet temperature into the dryer

In Figures 91 and 92, the running costs for the drying system are given for alumina and molecular sieve. The evolution of the drying costs differs for the drying of the two materials. For alumina, the drying costs decrease in both drying media with an increase in temperature. For molecular sieve, drying costs first increase in air and then decrease at higher temperatures and in steam they increase for the whole temperature range.

The running costs of the drying system are made up mainly of the thermal energy input into the heat exchanger. This energy input depends on two factors, namely the amount of exhaust gas and the temperature of the exhaust. In a well-mixed fluidized-bed dryer, the moisture content of the product particles is widely spread due to the wide residence time distribution. Some particles remain in the dryer for a very short time and are still in the constant drying rate period. Others are in the dryer for a long time and are deep into the falling drying rate period. On the one hand, an increase in the gas inlet temperature increases the temperature of the particles that are in the falling drying rate period. As a result, the temperature of the exhaust gas increases as well. On the other hand, an increase in inlet temperature increases the drying kinetics. The residence time of the particles can then be shortened and the diameter of the dryer reduced. In a fluidized bed, the velocity of the drying medium must be above the minimum fluidizing velocity and is fixed in this analysis to four times the minimum fluidizing velocity. A reduction in the dryer diameter therefore reduces the amount of drying medium that is needed and hence the amount of energy that must be put into the system by means of the heat exchanger. These two mechanisms, a change in energy input into the system (due to a change in mass flow of drying medium) and a change in energy loss of the system (due to a change of exhaust temperature), determine the shape of the curve for the running costs.

There is a difference in the energy loss from the system in air drying and in steam drying. In air drying, the total amount of drying medium is blown off to atmosphere and the energy loss is made up of the amount of drying medium and the temperature of the exhaust. In steam drying, only an amount of steam equal to the evaporated moisture is purged from the system. This amount is fixed by the drying

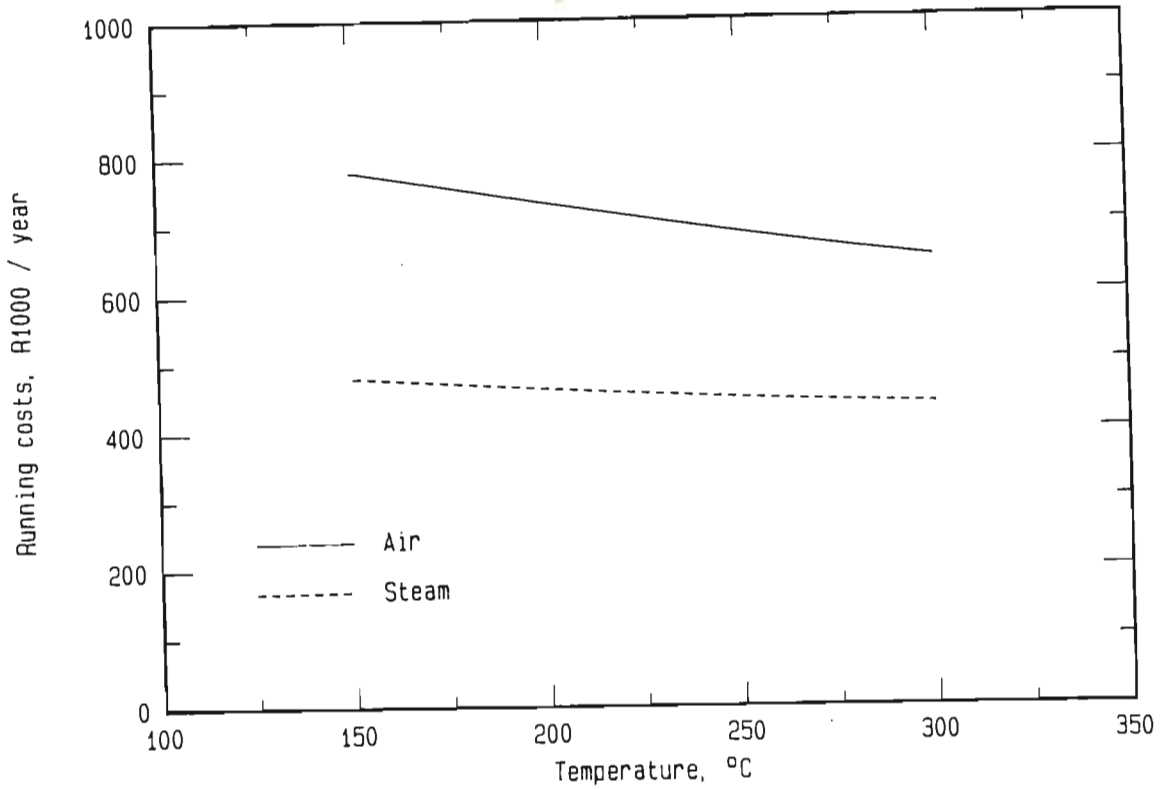


Figure 91: Comparison of the running costs of an air drying system and a steam drying system for alumina as function of the inlet temperature into the dryer

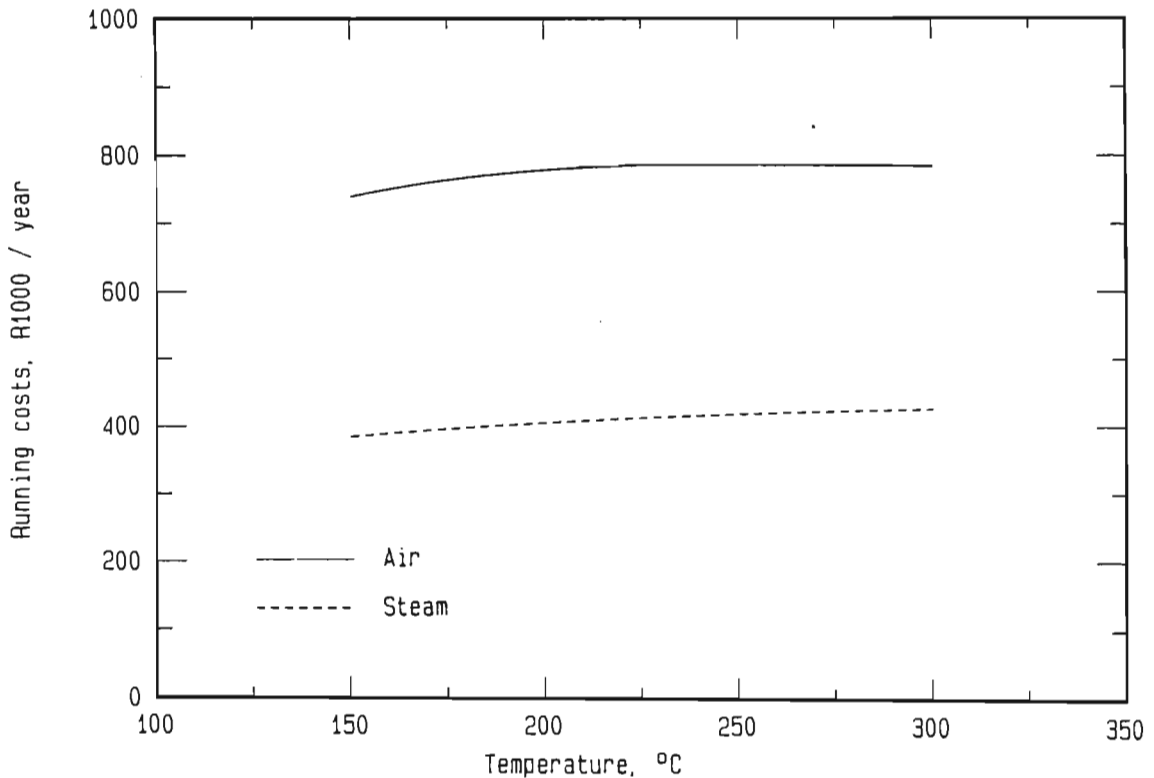


Figure 92: Comparison of the running costs of an air drying system and a steam drying system for molecular sieve as function of the inlet temperature into the dryer



duty. Therefore the energy loss of the steam system depends only on the temperature at which this steam is purged.

As was said earlier, alumina exhibits a short falling drying rate period in air and in steam. A relatively large amount of the particles are in the constant drying rate period, where the particle temperature is not affected by an increase in the inlet temperature. As a result, the exhaust temperature is not increased much by an increase in the inlet temperature. The drying kinetics, however, are heavily affected by an increase in temperature. Therefore the decrease in energy input outweighs the increase in energy loss, and the running costs decrease with increasing temperature.

Molecular sieve exhibits a long falling drying rate period in air.

A relatively large amount of particles are in the falling drying rate period. Therefore, the exhaust temperature is very sensitive to changes in the inlet temperature. At low temperatures, the increase in energy loss outweighs the decrease in energy input, and the running costs increase with increasing inlet temperature. At higher temperatures, the increase in exhaust temperature is no longer so pronounced and the decrease in energy input is larger than the increase in energy loss.

For steam drying, the increase in energy loss is larger than the decrease in energy input for the whole of the temperature range. The reason is that the particles that are in the constant drying rate period are more sensitive to temperature changes in the drying medium, whereas the particles that are in the falling drying rate period exhibit a drying rate that is governed mainly by internal processes and is not so sensitive to external temperature changes. In air, the energy loss decreases as a result of the decrease in the amount of exhaust. In steam, only the temperature of the purged steam determines the energy loss. This is why the running costs in steam increase over the whole temperature range, whereas in air they decrease for higher temperatures.

In Figures 93 and 94, the normalized drying costs, that is the ratio of costs in steam to the costs in air, are given as a function of the temperature. This figure does not give any new information, but the percentage decrease in running costs and increase in capital costs can be more easily seen.

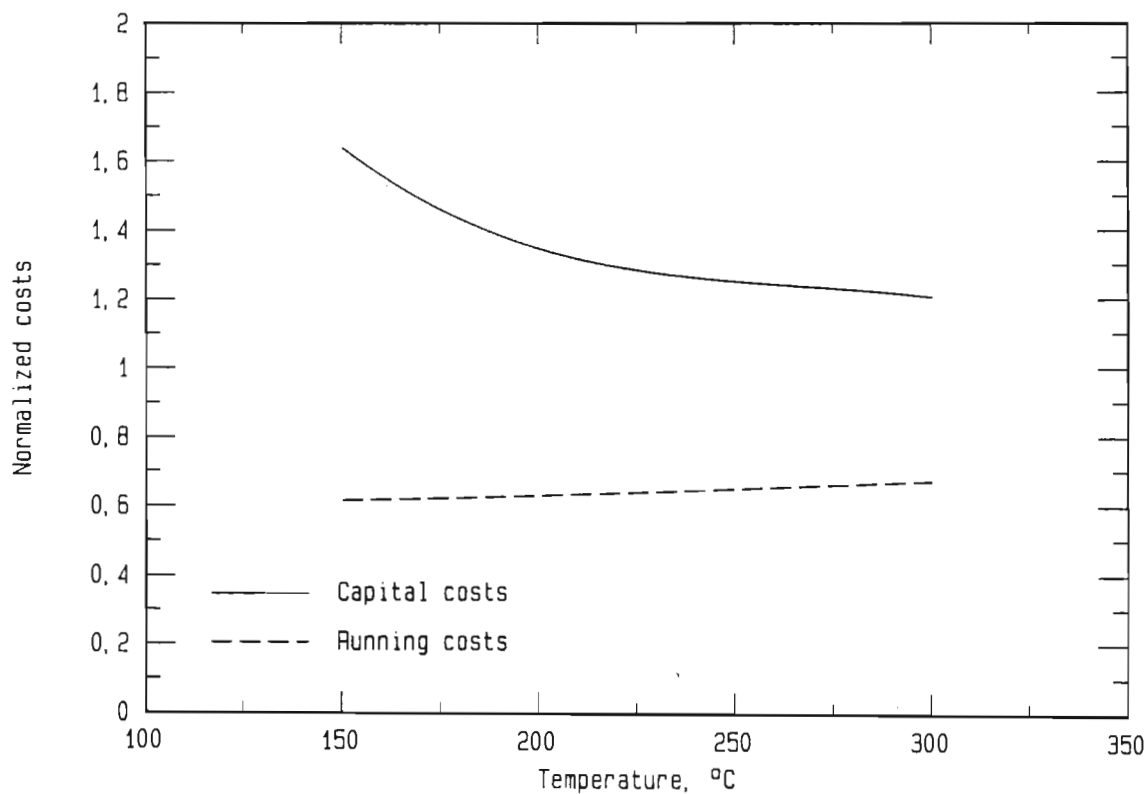


**Figure 93: Normalized costs for a drying system for alumina as function of the inlet temperature into the dryer**

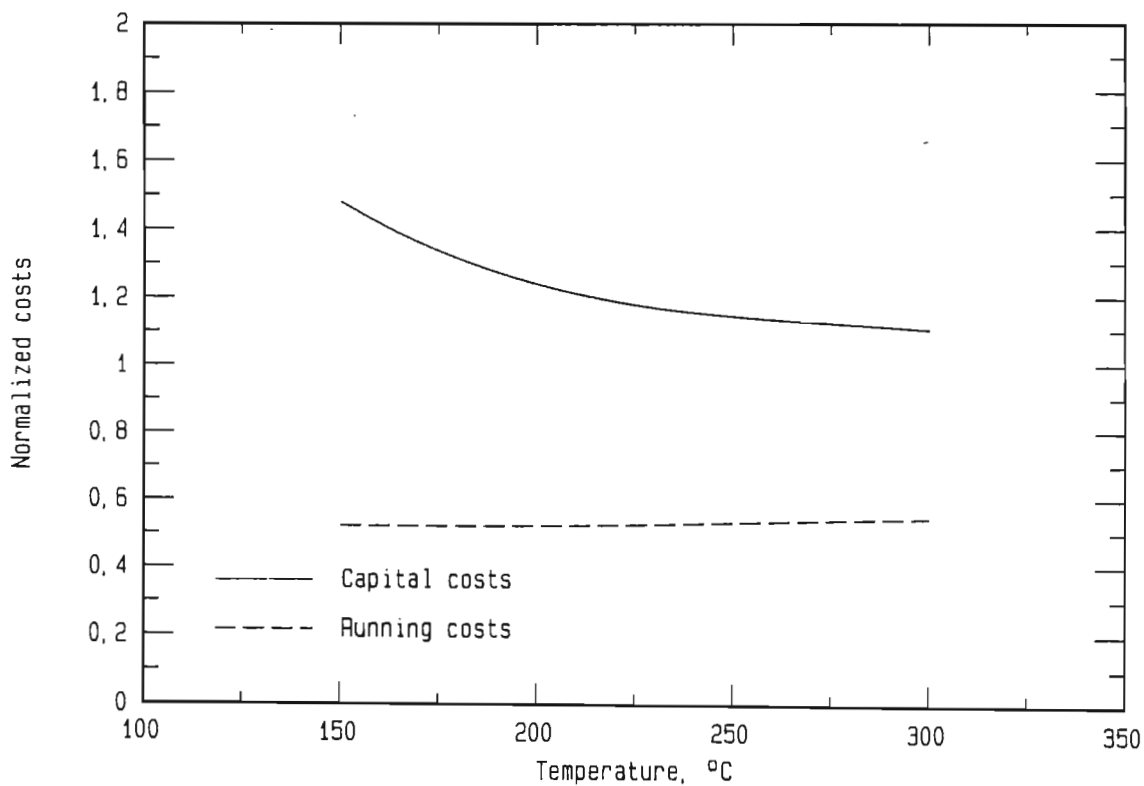


**Figure 94: Normalized costs for a drying system for molecular sieve as function of the inlet temperature into the dryer**

In Figures 95 and 96, the capital costs of the drying systems for the two materials are presented as a function of the product moisture content.

The capital costs of the drying system decrease sharply with an increase in the product moisture content. The residence time distribution in a well-mixed fluidized-bed dryer is widely spread. Some particles are removed from the dryer after very short residence times. The moisture content of such particles is close to the moisture content of the feed. For each such particle that by-passes the drying process, relatively many particles must leave the dryer at very low moisture contents (below the specified product moisture content). The lower this specified product moisture content, the more product particles must be very dry for each particle that is very wet. As the particle becomes dryer, the drying kinetics are reduced and the required mean residence time of the particles is drastically increased. This explains why the capital costs decrease sharply with an increase in product moisture content.

The capital costs for air drying are lower over the whole range of product moisture contents. The advantage of air is more pronounced for alumina than for molecular sieve.

In Figures 97 and 98, the running costs are presented as a function of the product moisture content. The running costs decrease sharply with an increase in the product moisture content for both materials. If the product moisture content is decreased, then the exhaust temperature is increased, because relatively more particles must be in the falling drying rate period. On top of that, the required residence time of the material is increased drastically. This means that both the energy loss and the energy input increase and therefore the running costs increase sharply. Steam drying has the greatest advantage for molecular sieve.

In Figures 99 and 100, the normalized costs are presented as a function of the product moisture content. The normalized capital costs for alumina and for molecular sieve are not very sensitive to changes in the remaining moisture content. For the drying of alumina, a steam-drying system is around 25 % more expensive than an air-drying

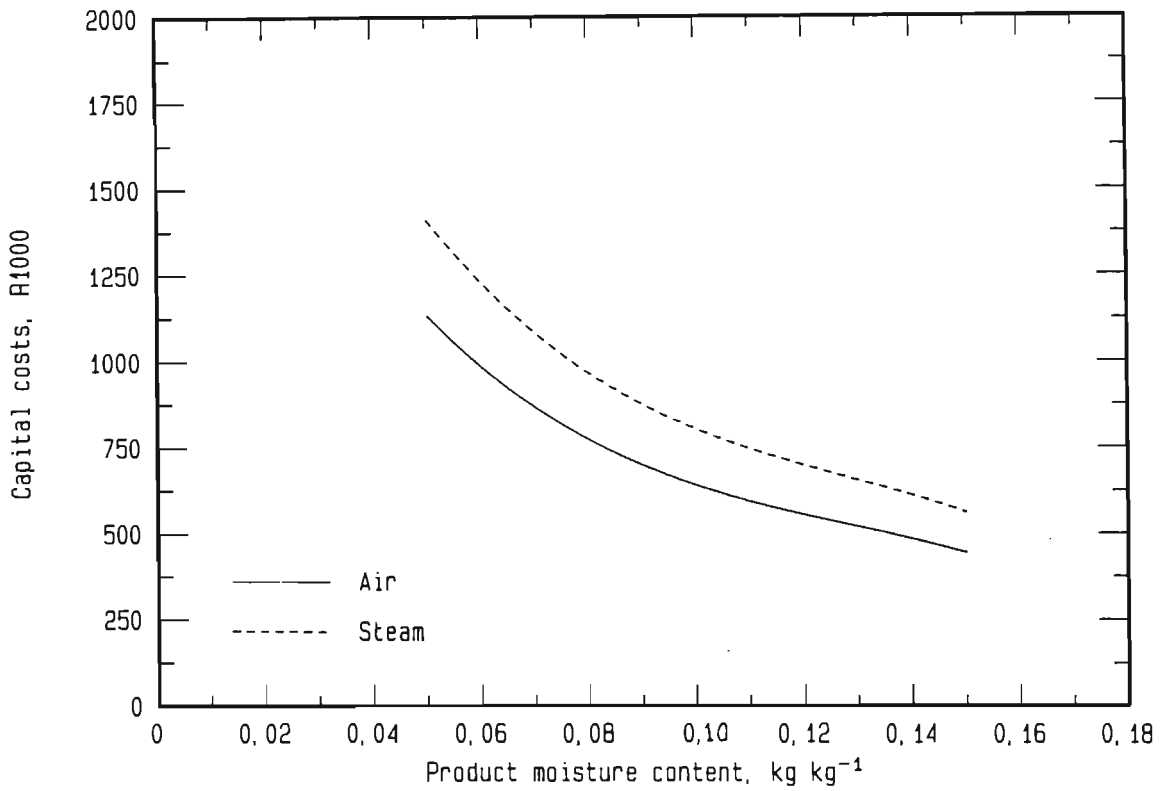


Figure 95: Comparison of the capital costs of an air-drying system and a steam-drying system for alumina as function of the product moisture content

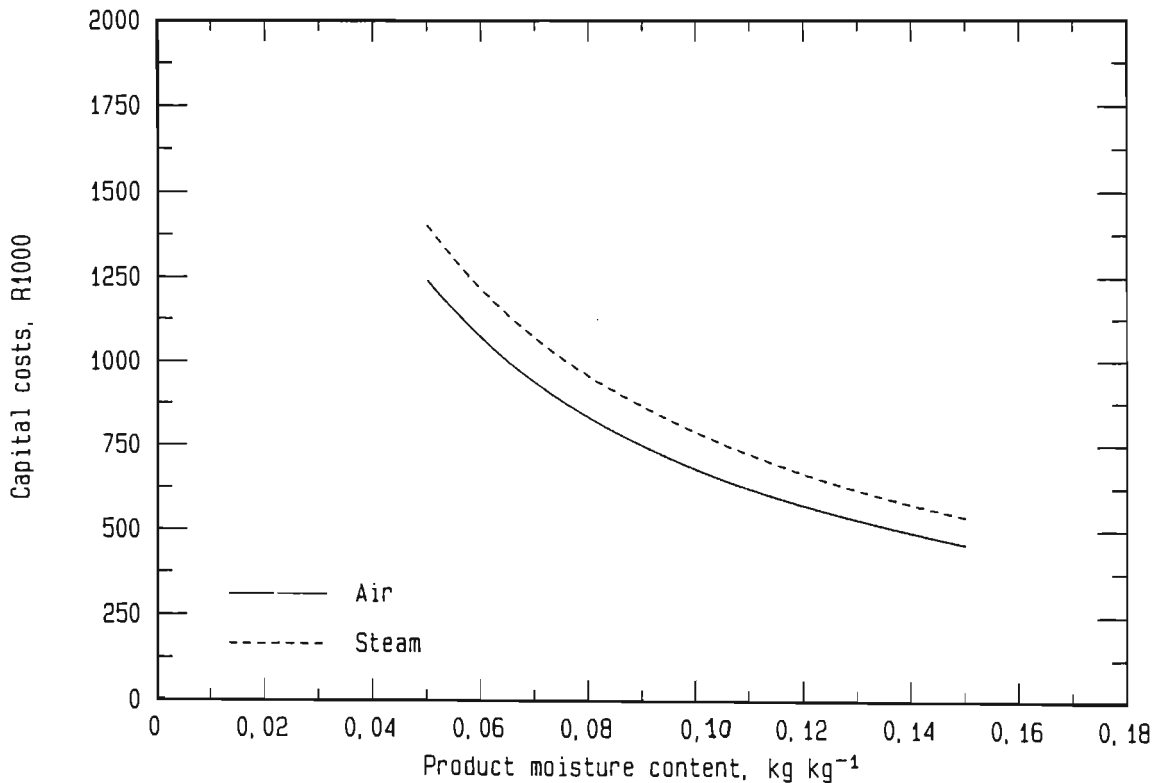
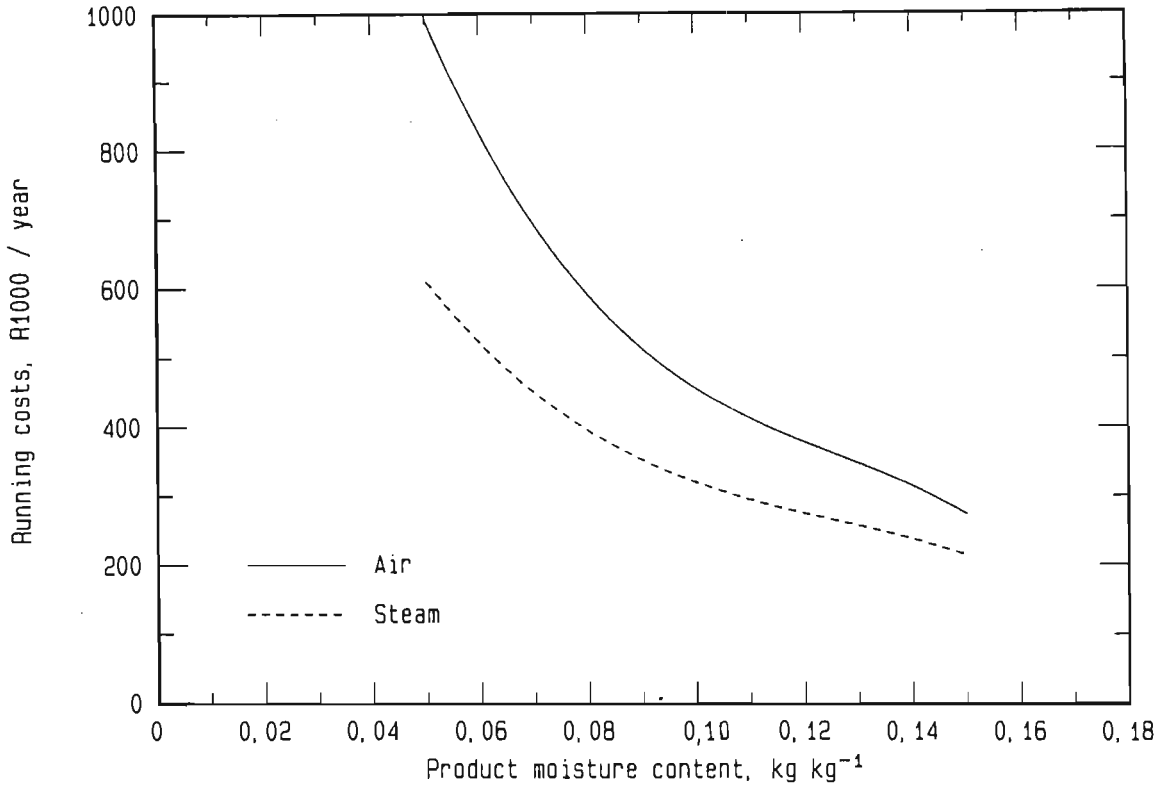
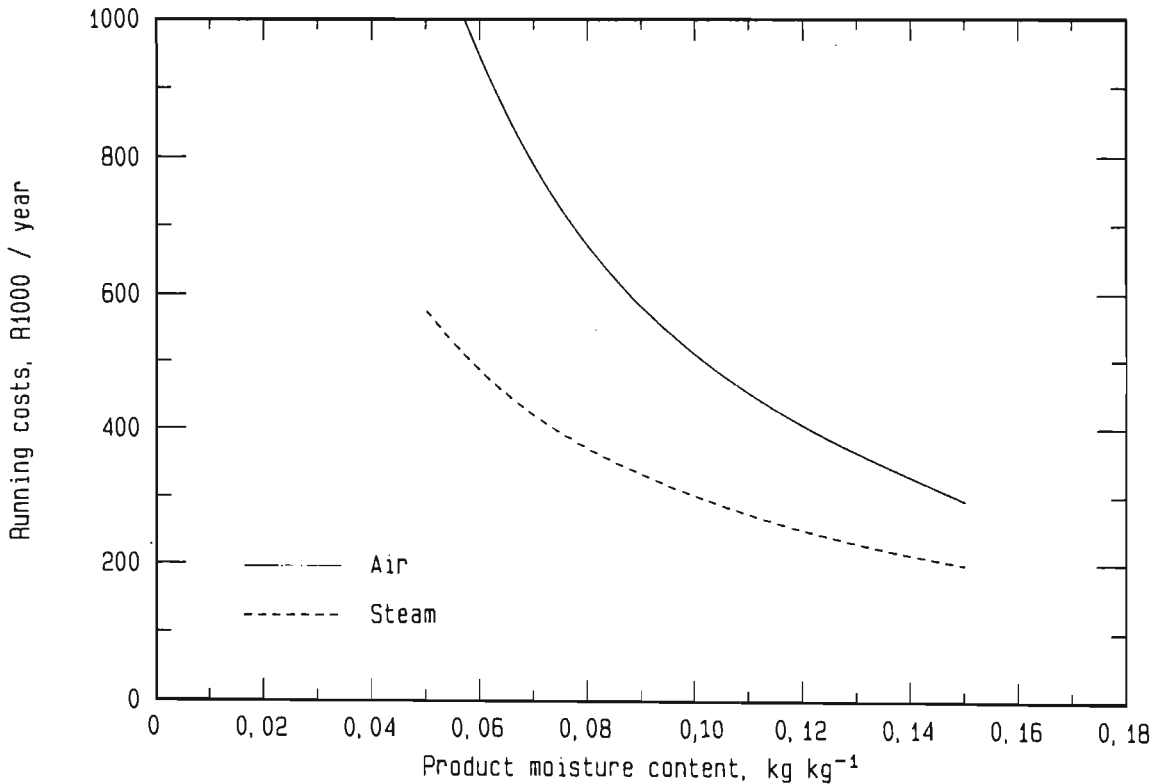


Figure 96: Comparison of the capital costs of an air-drying system and a steam-drying system for molecular sieve as function of the product moisture content



**Figure 97: Comparison of the running costs of an air-drying system and a steam-drying system for alumina as function of the product moisture content**



**Figure 98: Comparison of the running costs of an air-drying system and a steam-drying system for molecular sieve as function of the product moisture content**

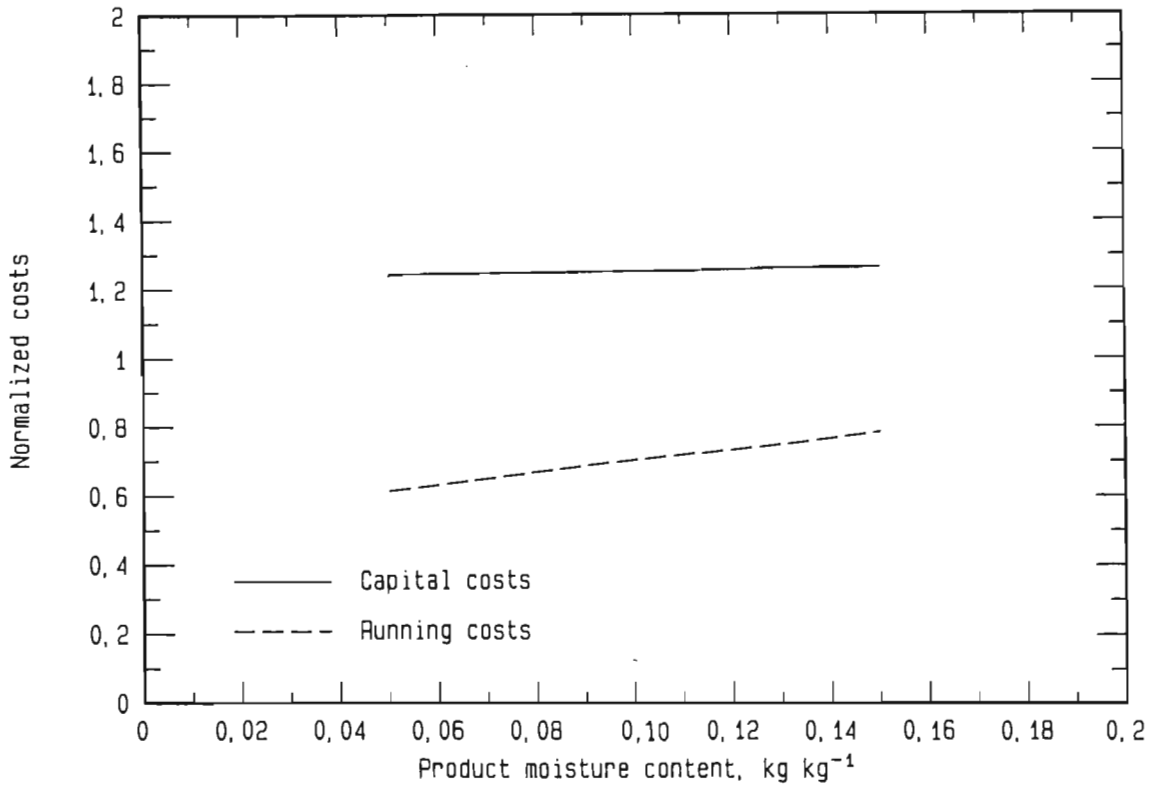


Figure 99: Normalized costs for a drying system for alumina as function of the product moisture content

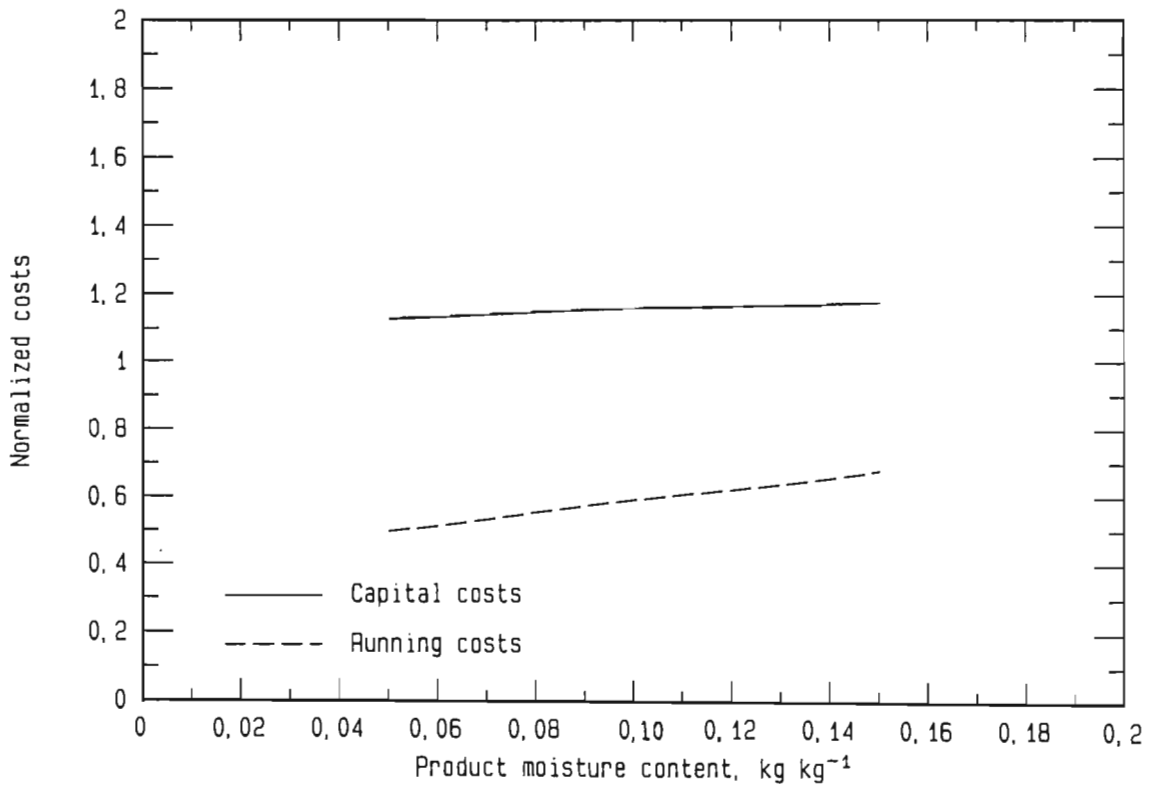


Figure 100: Normalized costs for a drying system for molecular sieve as function of the product moisture content

system. For the drying of molecular sieve, this percentage decreases to around 17 %. The normalized running costs for alumina and molecular sieve increase with an increase in product moisture content. This means that steam drying has a greater advantage if products have to be dried to a low remaining moisture content. On average, over the range investigated, the running costs in steam are 30 % lower for the drying of alumina and 40 % lower for the drying of molecular sieve.

In Figures 101 and 102, the capital costs of the drying systems for the two materials are presented as a function of the mass flow rate of dry feed.

The capital costs for steam lie above those for air and both increase with an increase in production rate, as is to be expected. At low production rates, the system capital costs increase more sharply because of the greater increase in the capital costs of the dryer. Indeed, for a small fluidized bed, the entrainment disengaging height is a function of the diameter of the dryer, whereas for a large fluidized bed, the entrainment disengaging height is a constant and therefore independent of the bed diameter.

In Figures 103 and 104, the running costs are presented as a function of the production rate. For both materials, the running costs increase linearly with the production rate.

In Figures 105 and 106, the normalized costs for the drying of alumina and molecular sieve are presented as a function of the production rate. Both the normalized capital and normalized running costs are independent of the mass flow rate. For alumina, the capital costs of a steam-drying system are around 25 % higher than for an air-drying system. For molecular sieve this difference is reduced to 14 %. The running costs of a steam-drying system are 34 % lower for the drying of alumina and 47 % lower for the drying of molecular sieve.

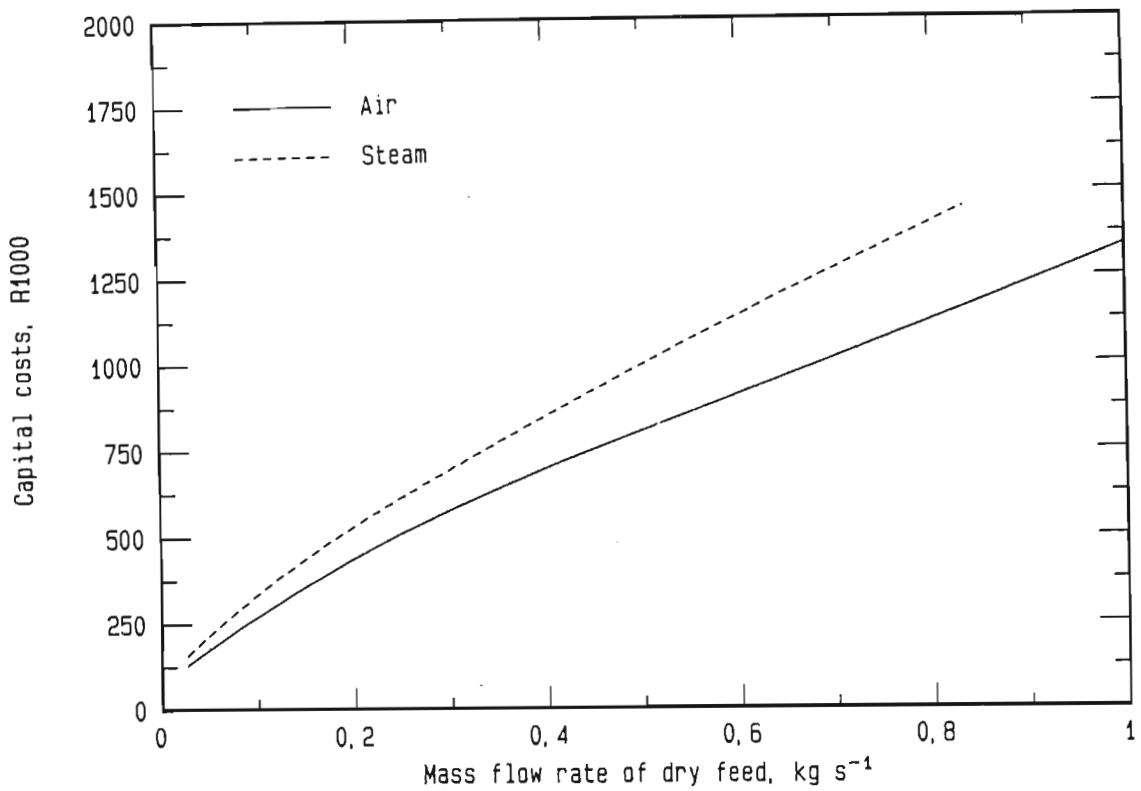


Figure 101: Comparison of the capital costs of an air-drying system and a steam-drying system for alumina as function of the product flow rate

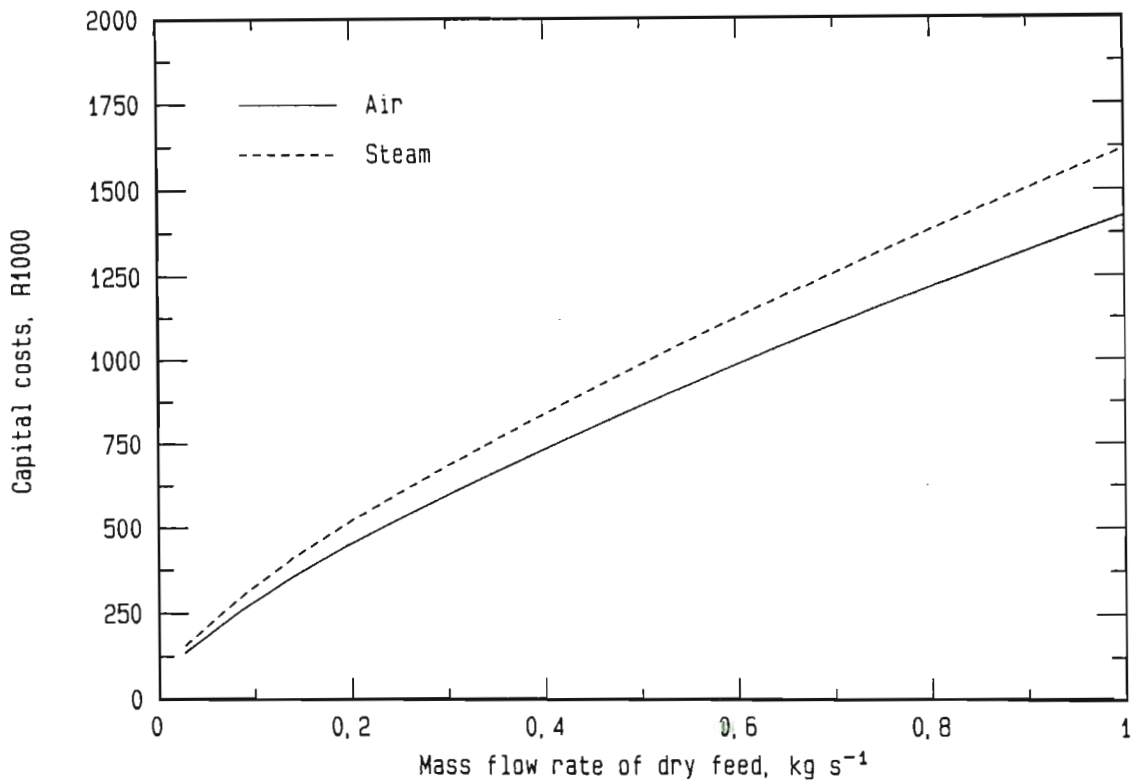


Figure 102: Comparison of the capital costs of an air-drying system and a steam-drying system for molecular sieve as function of the product flow rate



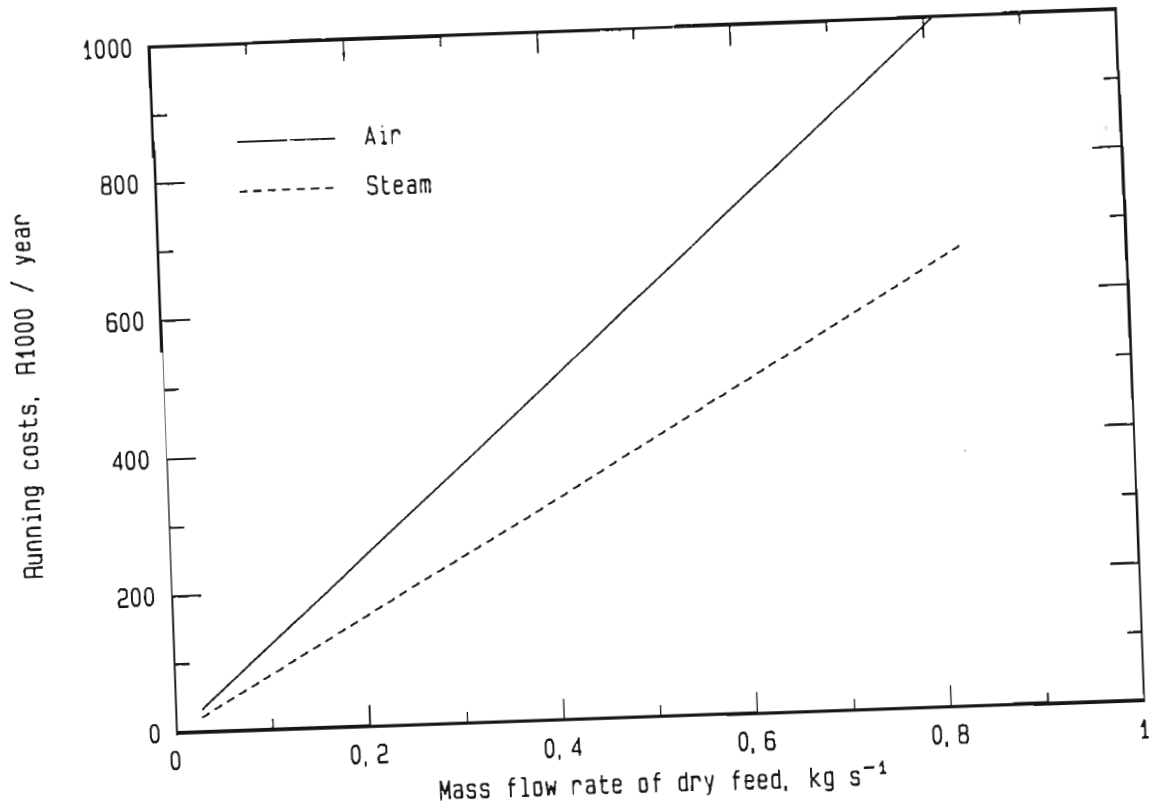


Figure 103: Comparison of the running costs of an air-drying system and a steam-drying system for alumina as function of the product flow rate

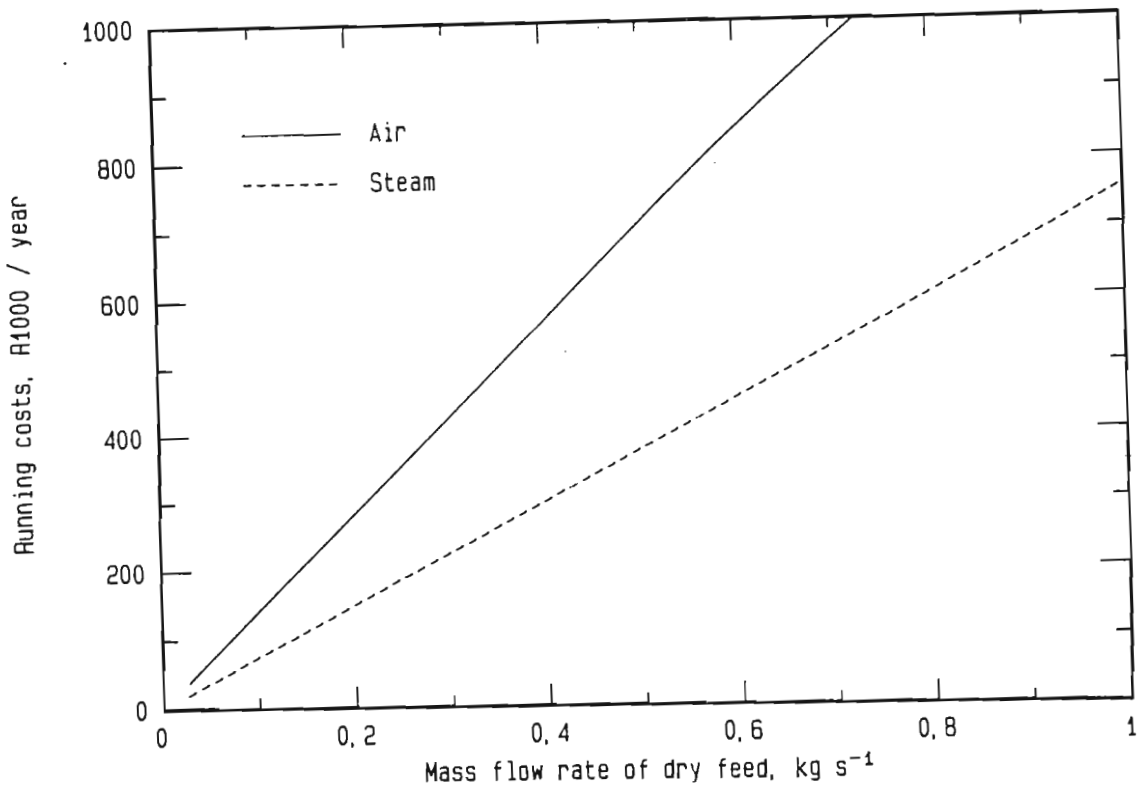


Figure 104: Comparison of the running costs of an air-drying system and a steam-drying system for molecular sieve as function of the product flow rate

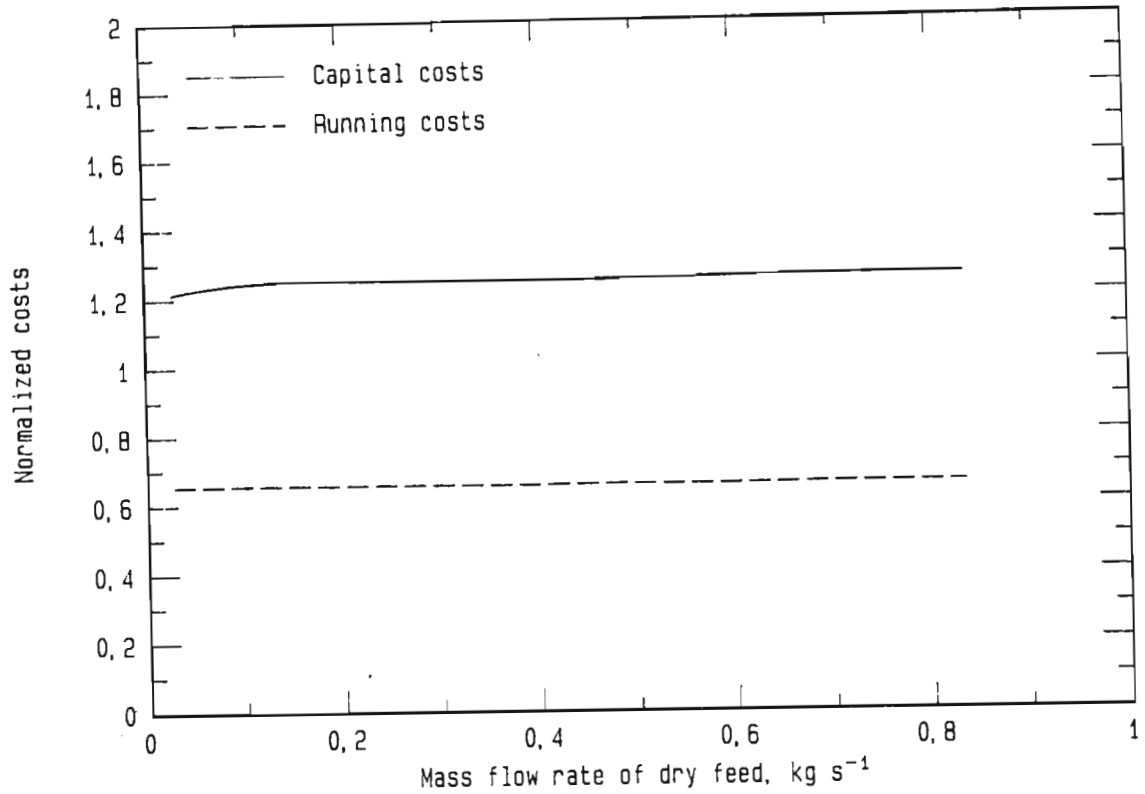


Figure 105: Normalized costs for a drying system for alumina as function of the product flow rate

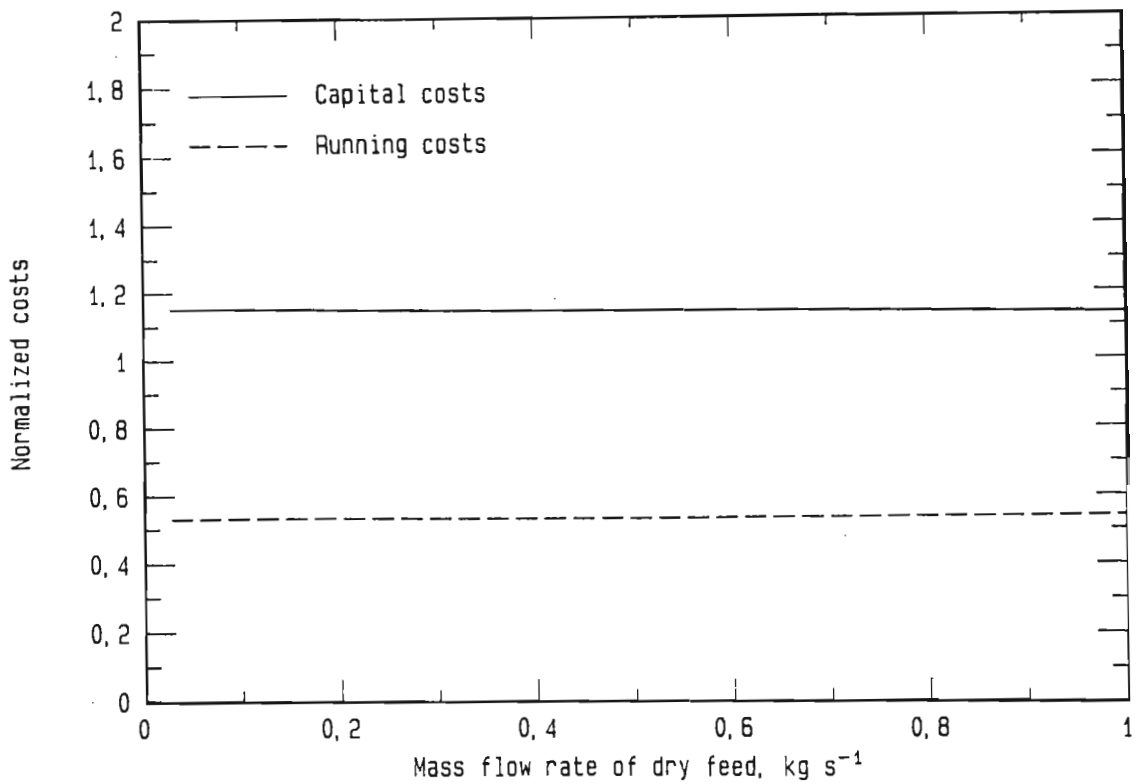


Figure 106: Normalized costs for a drying system for molecular sieve as function of the product flow rate

## 6. CONCLUSIONS

Superheated-steam drying has been advocated as an attractive alternative to conventional air drying. However, the market-penetration of steam dryers has been low. The reason herefore is the lack of understanding of steam drying and the absence of sound economic data. Until today, an economic analysis of steam-operated fluidized bed dryers was not possible. In the present thesis a method and equipment was developed that enable the engineer to gather the necessary information to make an objective choice between air drying and steam drying.

In particular, novel drying equipment was developed to determine the drying kinetics in a steam-operated fluidized bed. The measuring principle consists in recording the weight loss of the equipment with time. Experimental problems resulting from the weight fluctuations that are inherent to fluidization were solved by applying software filtering techniques. The measured data are converted into drying rate curves of the material. This technique is the only one available for measuring drying rate curves in steam fluidized beds without taking samples of the material.

Drying tests were carried out on two materials exhibiting different drying behaviour, namely a weakly hygroscopic alumina and a highly hygroscopic molecular sieve. Both materials show a distinct constant drying rate period and falling drying rate period in air and in steam. However, alumina exhibits a short falling drying rate period in air and in steam, whereas molecular sieve shows a long falling drying rate period in air and a short falling drying rate period in steam.

For the constant drying rate period, the existence of an inversion temperature was confirmed. Below the inversion temperature, drying rates are higher in air than in steam, and above it drying rates are higher in steam than in air. The existence of the inversion temperature was shown theoretically for a non-equilibrium system and both experimentally and theoretically for an equilibrium system. In a non-equilibrium system, the inversion temperature is determined by the kinetics of the heat transfer to the wet material. In an equilib-

rium system, the inversion temperature is determined by a total energy balance around the system. The reason for the existence of the inversion temperature is basically the same for the two systems and lies in the increase of the wet-bulb temperature with increasing drying temperature. For a fluidized-bed dryer (which is normally operated as an equilibrium system), the theoretical inversion temperature has a value of 154 °C for a pressure of 87 kPa (pressure in Pretoria).

It is experimentally shown that the air-to-solid and the steam-to-solid heat transfer coefficients in a fluidized bed can be described by an equation proposed by Kothari [K14]. However, attention must be paid to the evaluation of the experimental results. It was found that in steady state experiments using the evaporation of liquids to keep the temperature of the fluidizing material constant, the gas-to-solid heat transfer coefficient must be evaluated by taking into account the humidity increase of the drying medium over the height of the dryer.

For the falling drying rate period, the drying rate curves for alumina have a similar shape in air and in steam, whereas the drying rate curves for molecular sieve are different in the two drying media. For both materials, the critical moisture content is shifted to lower values in steam drying. However, this shift is much more pronounced for molecular sieve than for alumina. As a result the total drying time of molecular sieve was notably shorter in steam even for temperatures below the inversion temperature.

In order to investigate more deeply the different drying behaviour in the falling drying rate period, a mathematical model was developed. This model takes into account the main moisture transfer mechanisms in air and in steam. The model avoids the use of complicated computer hardware and software and yet describes the drying behaviour of the investigated materials qualitatively well. The model can, however, not be used for a detailed study of the individual moisture transfer mechanisms, as simplifying assumptions led to erroneous physical results (e.g. transfer resistances < 1).

The recorded drying rate curves are used as input data for an economic analysis. Investment costs and running costs are determined after the dryer has been designed. Conventional design methods cannot be used to dimension fluidized-bed dryers operated with steam. Therefore a new design method based on the principle of the design method by Reay and Allan [R1] was developed. The design method uses heat transfer expressions and is the only existing method for designing steam-operated fluidized bed dryers.

To make more universal use of the drying rate curve recorded in the fluidized bed, this one is normalized with respect to the constant conditions at the inlet into the dryer. This normalized drying rate curve is equivalent to the normalized drying rate curve of a single particle and can be used to design any type of dryer (provided a model describing the contacting between drying medium and material is available). The principle of this normalization technique was first introduced by Zabeschek [Z1] for non-equilibrium drying systems in air. In the present thesis this technique is extended to equilibrium systems and newly developed for steam-operated dryers.

The economic study of the fluidized bed system shows that the advantages of steam drying are more apparent for the highly hygroscopic molecular sieve which exhibits a long falling drying rate period in air than for the weakly hygroscopic alumina.

The capital costs of a steam system are higher than those for an air system. The amount by which the steam system is more expensive depends on the operating conditions and on the drying characteristics of the feed material, mainly operating temperature, required remaining product moisture content and extent of the falling drying rate period. The base conditions that were chosen for the economic analysis were a mass flow rate of dry particles of  $2\,000\text{ kg h}^{-1}$ , a product moisture content of 7 %, a bed height of the material of 0,2 m and a temperature of the drying medium of  $275\text{ }^{\circ}\text{C}$ . The difference in capital costs decreases with an increase in temperature, with a decrease of the remaining moisture content of the product and with an increase of the falling drying rate period of the feed material. For alumina the capital costs for a steam drying system were between

20 and 35 % higher than the capital costs for an air drying system and for molecular sieve this difference was between 10 % and 24 %.

The running costs of a steam system are lower than the running costs of an air system. The running costs do not depend as much on the temperature as do the capital costs. In steam the running costs increase with an increase in the operating temperature because of an increase in heat losses through the exhaust. In air the running costs decrease at higher temperatures because of an increase in the drying kinetics. This means that for the running costs, the economic advantage of steam is reduced by increasing the temperature of the drying system, whereas for the capital costs the economic advantage is increased. At the base conditions and a temperature of 200 °C, the running costs in steam were 37 % lower for alumina and 48 % lower for molecular sieve. Another factor that influences greatly the difference in running costs between air drying and steam drying is the remaining product moisture content. With a decrease in product moisture content, the difference in running costs increases. At the base conditions and a product moisture content of 15 %, the running costs in steam were 20 % lower for alumina and 33 % lower for molecular sieve. By decreasing the product moisture content to 4 %, the running costs in steam were 40 % lower for alumina and 53 % for molecular sieve.

## 7. RECOMMENDATIONS

- (i) Building of a pilot-scale fluidized-bed dryer that can be operated with air or with steam

Industrial applications of steam drying are still limited. The major reasons are lack of knowledge about steam drying, misunderstanding about the steam-drying process and a general resistance to 'new', unestablished processes. Therefore it is of vital importance to build a pilot-scale fluidized-bed dryer that can be operated with air or with steam. Such a unit would serve many purposes.

First of all it should be used as a demonstration unit to prove to industry the practical feasibility of steam drying.

Secondly, it would assist in investigating practical operating problems, such as feeding material into the dryer, product removal from the dryer, condensation on cold spots, corrosion and erosion of the construction materials, fouling of the heat exchanger, product degradation and requirements for the blower.

Thirdly, it would be used to verify the design procedure that has been developed in this thesis and it would yield important data for the scale-up of dryers.

Fourthly, it would yield operating data that would make the economic comparison between air drying and steam drying more realistic, as the study would then be based on actual measured data. Such data are the energy requirements and the maintenance costs of the system.

- (ii) Changes to the experimental equipment

The changes on the experimental equipment should make it more universal. To limit the effects of material loss, the experimental drying section should be followed by an entrainment disengaging section and, before leaving the dryer, the drying medium should be screened by a fine wire mesh. For materials that exhibit a high material loss by entrainment, blockage of the wire mesh and subsequent pressure build-

up inside the dryer can occur. Therefore it is recommended that both the height and the diameter of the entrainment disengaging section be increased. Furthermore the filtering action of the screens can be improved and the danger of blockage can be reduced by using a series of increasingly finer screens.

(iii) Development of a mathematical drying model for steam drying

A simplified drying model is always based on assumptions that do not reflect the real situation during the drying process, but that approximate it. As a consequence, the applicability of such models is limited and empirical functions may have to be used to describe the measured results. Therefore it is of interest to develop a rigorous drying model, based on the underlying fundamental mechanisms of heat and mass transfer, and which describes the drying process realistically. This will be of scientific interest, as will further the understanding of the transfer mechanisms involved in drying in general, and in steam drying in particular. Some of these complex models are available for air drying but cannot be used directly for steam drying. Therefore they must be modified and applied to the steam-drying process.

(iv) Performance of drying tests on more materials and on different sizes

It is recommended that drying tests be performed on various sizes of a hygroscopic material. These data can then be used to test the design procedure for the various sizes. This is of interest, especially for small-diameter particles in which the interparticle heat transfer may play an important role in the design of a continuous fluidized-bed dryer.



(v) Investigation of pressure or vacuum operation for steam-operated fluidized beds

It was suggested that an increase in pressure could drastically reduce the size of the drying equipment. In steam drying, the system must in any case be very well sealed off from the environment. Therefore it may be advantageous to operate the steam system under pressure. It is recommended that a rough paper study be performed on the economic implications of a pressure increase of the steam system before embarking on the development of experimental equipment to record drying curves in steam under pressure. By increasing the pressure of the system, the danger of degradation of the material is increased, as the material temperature will increase.

The major limitation of steam drying is the heat-sensitivity of the material. By reducing the pressure in the system to below atmospheric, the material temperature can be reduced as well. Therefore, steam drying can theoretically be applied to materials that under normal pressure would be degraded in steam. Again it is recommended that a rough paper study be carried out first on vacuum-operated steam dryers before experimental equipment is developed.

(vi) Investigation of the economic viability of steam compression drying

In countries where heat-recovery systems are subsidized by the government or where electricity is relatively cheap compared with coal, steam compression drying may be of interest. In these countries, electricity is produced by nuclear or hydroelectric power stations and is therefore not dependent on the coal price. The application of steam compression drying leads to an increase in capital costs, which may be partially carried by the government, and to a further reduction in running costs. Therefore the option of steam drying should be kept in mind, because the economic environment may change.

## APPENDICES

### APPENDIX A: MEASUREMENT ERRORS

#### A1. Measurement errors in the sorption isotherm

##### - Determination of the pressure in the container

Measurement errors in the relative pressure may originate in the measuring inaccuracy of the Bourdon gauge and/or in a temperature measurement error.

The measuring accuracy of the Bourdon pressure gauge is 0,5 % of the measured pressure. The pressure can be read with an accuracy of  $\pm 0,25$  kPa. The relative error is highest for low pressures. In the experiments, the lowest pressure that was used was 2,37 kPa. This leads to a maximum relative error of 10,6 %. Most of the data were measured at pressures higher than 9,5 kPa. This means that the relative error for most of the data is lower than 2,6 %.

Pressure readings may be falsified by a shift in the zero point. This shift may be due to a fluctuation in the height of the water column in the capillary connecting the gauge to the container. These variations are less than 5 mm. This height corresponds to an absolute error of 0,05 kPa, which leads to a relative error of 0,5 % for most of the measuring points.

The temperatures were measured with two calibrated thermocouples. They did not differ by more than 0,6 °C. The arithmetic average of these two measurements was taken as the temperature in the container. One can assume that the total error in the temperature readings was less than 0,6 °C. Such a temperature difference leads to a maximum change in saturation pressure of 1,1 kPa. As a result, the relative pressure will be falsified by a relative error of 2,4 %.

Air leaking into the system can increase the total pressure that is measured. As no evidence of such a leakage was found, the error introduced by this source was not investigated.

In summary, the maximum relative error in the measurement of the pressure in the container is 5,5 %.

- Determination of the moisture content

The error that is introduced in the measurement of the moisture content of the material inside the sorption isotherm container is due to the resolution of the balance and to convective air currents acting on the equipment.

Convective air currents are created around the measuring container due to the temperature difference with the surrounding air. The influence of these convective air currents is difficult to quantify. It was, however, found that the difference in balance reading between the hot container and the cold container was in the order of 8 g. As the moisture content measurements were all carried out at the same temperature of the container, the absolute error was considered to be less than 0,5 g. The mass of dry material in the container was roughly 300 g. At moisture contents higher than 2,5 %, the relative error introduced by the convective currents was then less than 6,7 %.

The resolution in the balance reading was 0,1 g. Therefore the error introduced by this source was less than 1,3 % for moisture contents higher than 2,5 %.

This leads to a maximum relative error in the measurement of the moisture content of the material of 8 %.

A2 Measurement errors in the heat transfer coefficient

- Height of the thermocouples

The temperature profile of the drying medium in the fluidized bed is measured with a series of bare thermocouples inserted at different heights in the bed (see Figure 107). The heights above the distributor plate are 0,5; 2,5; 5,0; 7,5; 11,5 and 24 mm. The thermocouple wires are soldered together and the measuring tip is formed by a more or less spherical piece of solder of 0,25 mm diameter (see Figure 108). Even though the height of the tip of the thermocouple above the

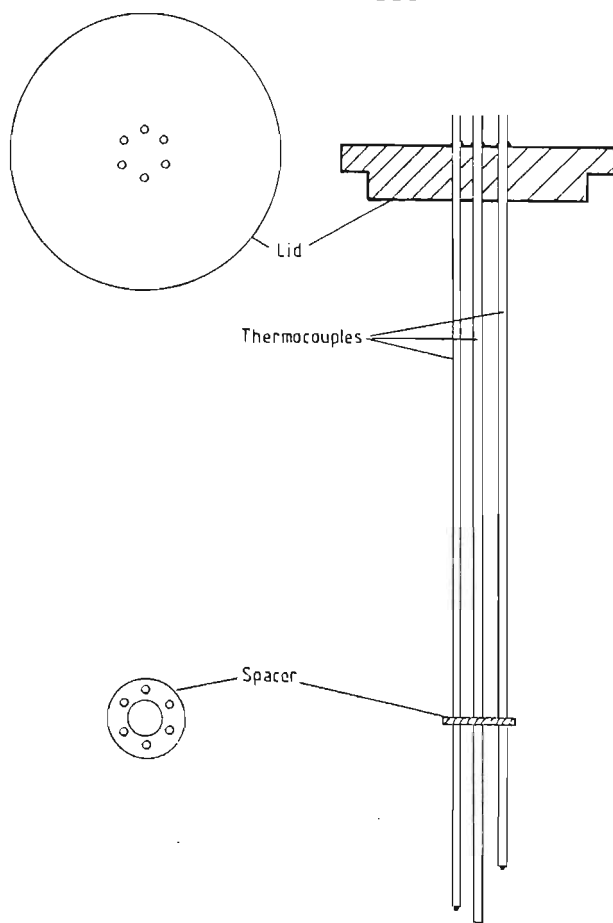


Figure 107: Thermocouple assembly

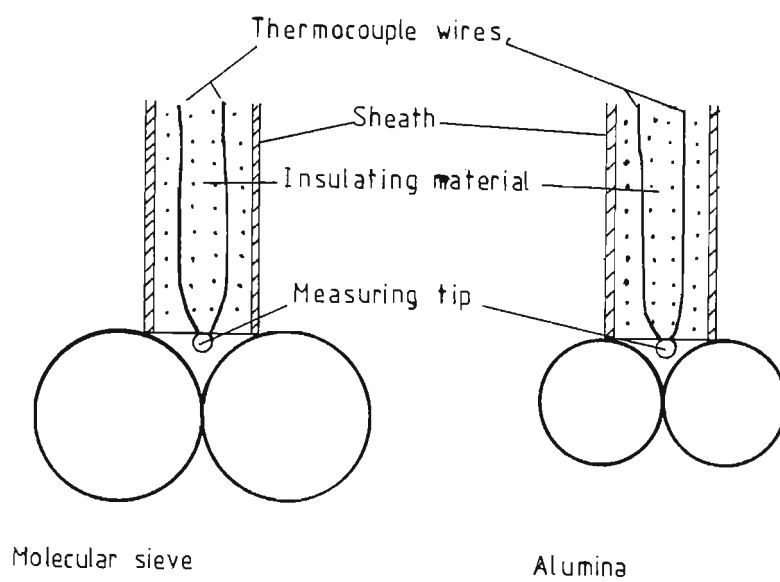


Figure 108: Measuring tip of a thermocouple

distributor plate is known, the actual measuring place is difficult to define and is somewhere inside the piece of solder. Furthermore it is difficult to define the temperature that is measured. The drying medium cools down very rapidly as it flows through the bed. Even though the piece of solder is kept small (<0,25 mm), the temperature of the drying medium changes over the height of this piece.

According to Equation 160, the local heat transfer coefficient is determined by:

$$h = - \frac{\dot{M}_a (c_{pa} + Y c_{ps})}{z a \Phi} \ln \left( \frac{T_z - T_p}{T_{in} - T_p} \right)$$

If one assumes that the height of the measuring tip can be determined to within 0,25 mm, then the relative error, RE, in the measurement of the heat transfer coefficient is given by:

$$RE = 1 - \frac{z_1}{z_1 + \Delta z} \quad (111)$$

For a height of 3 mm this leads to a relative error of 7,7 %.

The error becomes less important with increasing height in the bed and for a height of 15 mm is only 1,6 %.

#### - Determination of the temperature of the drying medium

The gas temperature is measured by bare calibrated thermocouples that are inserted into the fluidized bed. The tip of a thermocouple is represented in Figure 108. The stainless steel sheath of the thermocouple has a diameter of 1,6 mm. The spherical measuring tip protrudes into the gas stream. The thermocouple wires are embedded in an insulating mass that fills the stainless steel sheath and prevents the thermocouple wires from touching the walls of the sheath or each other.

The tip of the thermocouple is exposed to various heat sources and heat sinks that can falsify the temperature measurement. These are:

- 1) Heat transfer by conduction to the cold particles.
- 2) Heat exchange by radiation between the tip of the thermocouple and the fluidized mass
- 3) Heat exchange by radiation between the tip of the thermocouple and the distributor plate.
- 4) Heat transfer by conduction through the thermocouple wire.
- 5) Heat transfer by gas radiation to the tip of the thermocouple (only applicable in steam drying)

Of these influences, the most important one is the heat transfer to the wet, cold particles during the impact between particles and measuring tip. In the constant drying-rate period, in which the measurement of the heat transfer coefficients is realized, the particles are at the wet-bulb temperature in air and at boiling temperature in steam. On impact with the measuring tip, heat is transferred by conduction from the measuring tip through the dividing gas film to the wet particles. The fluidized particles that are used in the tests are much larger than the measuring tip. Therefore the heat transfer can be described by the heat transfer between a sphere and a flat surface. Schlünder [S8] determined the heat transfer coefficient that is obtained for short-contact times ( $<0,01$  s) between a sphere and a flat surface:

$$h_c = 4 \frac{\lambda_g}{d_t} \left\{ \left( \frac{2\sigma}{d_t} + 1 \right) \ln \left( \frac{d_t}{2\sigma} + 1 \right) - 1 \right\} \quad (112)$$

with

$$2\sigma = 4 \Lambda \left( \frac{2}{\gamma} - 1 \right) \quad (113)$$

Here  $\gamma$  is the accommodation coefficient which describes the incomplete energy exchange between gas molecule and the heat exchanging surface, and  $d_t$  is the diameter of the thermocouple tip. According to VDI [V5], the accommodation coefficient can be determined by Equation 114.

$$\log \left( \frac{1}{\gamma} - 1 \right) = 0,6 - \frac{\frac{1000}{T_g} + 1}{C_a} \quad (114)$$

The constant  $C_a$  has a value 2,8 for air and 3,62 for steam. The temperature  $T_g$  must be expressed in K.

$\Lambda$  is the mean free path of the gas molecules and can be determined by Equation 115.

$$\Lambda = \frac{16}{5} \cdot \frac{R T}{2 \pi \tilde{M}} \frac{\eta}{p} \quad (115)$$

According to Martin [M1] the contact time between a sphere and a flat surface is proportional to the flying time of one particle diameter. In our case, the diameter of the tip must be used, as this is the smallest.

$$t_c = \frac{4 d_t}{w_p C_k} \quad (116)$$

Martin determined the constant  $C_k$  as 3 for glass beads of various diameters. The velocity of the particles  $w_p$  can be determined by following equation [M1]:

$$w_p = g d_p \frac{(\Psi - \Psi_1)}{5 (1 - \Psi) (1 - \Psi_1)} \quad (117)$$

Here  $\Psi_1$  is the voidage of the bed at incipient fluidization and  $\Psi$  is the voidage of the bed at fluidizing conditions.

These values result in a contact time between the particles and the thermocouple tip of  $5 \cdot 10^{-3}$  s.

The radiative heat transfer coefficient between the tip of the thermocouple and the fluidized mass can be described by the following equation [M1]:

$$h_r = 4 \epsilon C_s T_m^3 \left\{ 1 + \left( \frac{T_t - T_p}{T_t + T_p} \right)^2 \right\} \quad (118)$$

Here  $T_m$  is the mean temperature between tip and particle,  
 $T_t$  is the temperature of the tip of the thermocouple,

$T_p$  is the temperature of the particles,  
 $\epsilon$  is an effective emissivity number and  
 $C_s$  is the Stefan-Boltzman constant and has the value  
 $5,67 \cdot 10^{-8} \text{ W m}^{-2} \text{ K}^{-4}$ .

The radiative heat transfer is then described by:

$$\dot{Q}_r = h_r A_p (T_t - T_p) \quad (119)$$

The radiative heat transfer between the distributor plate and the tip can be described by:

$$\dot{Q}_{r,d} = \Phi \epsilon_1 \epsilon_2 A_p \sigma (T_1^4 - T_2^4) \quad (120)$$

Here  $\Phi$  is the radiation number,  
 $\epsilon_1$  is the emissivity of the distributor plate,  
 $\epsilon_2$  is the emissivity of the tip,  
 $A_p$  is the projection surface of the tip,  
 $T_1$  is the temperature of the distributor plate, and  
 $T_2$  is the temperature of the tip.

The conductive heat transfer through the two thermocouple wires can be described by:

$$Q_{cd} = \frac{\lambda_w}{l} 2 A_w (T_t - T_\infty) \quad (121)$$

Here  $\lambda_w$  is the conductivity of the thermocouple wire,  
 $l$  is the length of the thermocouple,  
 $2$  is a factor that takes into account the number of thermocouple wires,  
 $A_w$  is the cross section of one wire, and  
 $T_\infty$  is the ambient temperature.

The gas radiative heat transfer in the case of steam drying may be neglected because of the low temperature level and the low temperature difference between the gas and the measuring tip.



For the lowest thermocouple (distance between the thermocouple tip and the distributor is 0,5 mm) the particles cannot impact onto the tip because of their large diameter (alumina 1,6 mm, molecular sieve 2,2 mm). The tip is exposed only to the radiative heat transfer from the distributor plate, the radiative heat transfer from the fluidized particles and the heat sink due to the conductive heat transfer through the thermocouple wires.

The remaining thermocouples are exposed to the conductive heat transfer to the particles, the radiative heat transfer from the fluidized particles and the heat sink due to the conductive heat transfer through the thermocouple wires. The thermocouple tips are shielded by the fluidized particles from the radiative influence of the distributor plate. The radiative heat transfer from the distributor plate to the tip is therefore neglected for these thermocouples. The contact time between particles and thermocouple tip was evaluated at 5 milliseconds. During this contact time the thermocouple tip transfers heat by conduction to the fluidized particle and by radiation to the fluidized mass. In the evaluation of the influence of the heat sinks and sources on the heat transfer coefficient it was assumed that the time between two impacts is a multiple of the contact time. For a flat surface the time between two impacts can be related to the voidage of the bed. If a row of particles passes the thermocouple tip at the velocity  $w_p$  determined by Equation 117, then the multiplication factor for the time between two impacts is given by the ratio of tip diameter and the diameter of the particle minus the tip diameter. For alumina this leads to a multiplication factor of 5,4 and for molecular sieve of 7,8. The voidage fraction of the fluidized bed increases this factor, so that in the calculation a multiplication factor of 10 was assumed for both alumina and molecular sieve. Between two impacts the tip is exposed to the convective heat transfer by the fluidizing medium and the radiative heat transfer to the fluidized mass.

The relative error in the heat transfer, resulting from an error in the temperature reading, is calculated below:

$$\frac{\Delta h}{h} = \left[ \ln \frac{T_z - T_p}{T_{in} - T_p} - \ln \frac{T_z + \Delta T_z - T_p}{T_{in} - T_p} \right] \div \ln \left( \frac{T_z - T_p}{T_{in} - T_p} \right) \quad (122)$$

$$= 1 - \frac{\ln \left( \frac{T_z - T_p}{T_{in} - T_p} + \frac{\Delta T_z}{T_{in} - T_p} \right)}{\ln \left( \frac{T_z - T_p}{T_{in} - T_p} \right)} \quad (123)$$

With following assumption:

$$T_z = T_p + K (T_{in} - T_p) \quad (124)$$

the relative error is given by

$$\frac{\Delta h}{h} = 1 - \frac{\ln \left( K + \frac{\Delta T_z}{T_{in} - T_p} \right)}{\ln K} \quad (125)$$

For large values of K, i.e. low heights of the thermocouple or small differences between the gas inlet temperature and the particle temperature, the relative error is highest. The results of the calculations are presented in Table 9.

In Table 9 the error in the determination of the heat transfer is calculated for the five lowest thermocouples (under the test conditions the temperature difference between gas and particles was too low to use the sixth thermocouple reading in the determination of the heat transfer coefficient). The error is calculated for alumina at an inlet temperature of 275 °C in air and in steam and at an inlet temperature of 200 °C in air, as well as at an air inlet temperature of 275 °C for molecular sieve. The individual error diminishes with increasing thermocouple height. The average value between the five thermocouple readings is taken in the determination of the heat transfer coefficient. This lowers the error and for all the cases the error lies around 9 %. The multiplication factor for the time between two impacts was increased to 20 to study its influence. The average error dropped to 5,3 %.

#### - Determination of the mass flow rate of the drying medium

The volumetric flow rate of the drying medium is measured by a rotameter with an accuracy of 1,5 %. This rate is multiplied by the density

Table 9 Error in the heat transfer coefficients by  
ignoring measurement errors in the gas temperature

$T_{in}$ °C	Mult	Gas	Mat	$h_{th}$ mm	$T_g$ °C	$T_{th}$ °C	Error %	Average error, %
275	10	Air	Al	0,5	248,9	248,3	2,4	8,9
				2,5	171,5	155,3	20,3	
				5,0	115,6	106,8	10,3	
				7,5	85,5	80,7	7,0	
				11,5	63,4	61,5	4,7	
275	10	Steam	Al	0,5	257,0	256,5	3,2	8,6
				2,5	201,4	190,1	19,2	
				5,0	158,1	151,3	9,7	
				7,5	132,5	128,5	6,6	
				11,5	111,7	109,9	4,5	
200	10	Air	Al	0,5	181,8	181,4	2,5	9,1
				2,5	127,8	116,2	20,7	
				5,0	88,6	82,3	10,5	
				7,5	67,4	63,9	7,1	
				11,5	51,7	50,4	4,7	
275	10	Air	MS	0,5	252,1	251,6	2,4	9,1
				2,5	181,7	166,3	20,7	
				5,0	127,2	118,0	10,5	
				7,5	95,2	89,8	7,1	
				11,5	69,3	67,0	4,7	
275	20	Air	Al	0,5	248,9	248,3	2,4	5,3
				2,5	171,5	162,6	11,4	
				5,0	115,6	110,8	5,8	
				7,5	85,5	82,8	4,0	
				11,5	63,4	62,3	2,7	

of the drying medium to get the mass flow rate. The density is determined over the ideal gas law. The temperature of the drying medium is measured by a calibrated thermocouple. The error resulting from the deviation from the ideal gas law is neglected. The error resulting from the effect of an inaccurate temperature measurement on the density is less than 0,03 % and can be neglected as well.

The relative error in the determination of the mass flow rate is then the same as that for the measurement of the volumetric flow rate, which is 1,5 %.

- Determination of the surface area of the particles

The surface area of the particles is determined over the bulk density of the fluidized mass and the mean diameter of the particles. It is difficult to determine the bulk density of the fluidized mass accurately. In this thesis it was taken as the bulk density of the material poured with a free fall into a measuring cylinder. The mean diameter of the material could not be determined by a sieve analysis, as the size distribution was very narrow. Therefore the mean diameter of a sample of 300 particles was determined with a micrometer.

If the relative error in the surface area determination is 10 %, then the relative error in the determination of the heat transfer coefficient is 9,1 %.

- Determination of the particle temperature

The temperature profile of the drying medium is determined by means of several thermocouples. The lowest temperature recorded is then taken as the particle temperature.

If the accuracy of the measured particle temperature is 0,1 °C, then the relative error in the heat transfer coefficient is below 1 %.

A3 Measurement errors in the determination of the normalized drying rate

The absolute error that is introduced in the evaluation of the drying kinetics by using the temperature normalization procedure is discussed below.

The temperature of the particles is measured by a thermocouple inserted into the bed. The thermocouple needs a certain relaxation time before it can follow the temperature change. Therefore the temperature that is recorded by the thermocouple lags behind the true temperature. As a consequence, the normalized drying rate that is calculated overestimates the actual drying rate. At high inlet temperatures, the drying rates are fast and so are the changes in particle temperature. Here the error is largest.

As was mentioned in Section 2.3.2.2, the temperature recorded by a bare thermocouple lies in between the temperature of the material and the temperature of the drying medium. Because the particle temperature is measured in the upper layers of the bed where equilibrium between drying medium and material has been reached, this influence is neglected.

In the normalization procedure, heat losses from the drying medium to the environment are neglected. Even though these heat losses can never be eliminated completely, special care was taken in the design of the experimental equipment to limit these losses to a minimum. Again, the error introduced by neglecting the heat losses is largest at high temperatures and tends to overestimate the normalized drying rate.

In the later stages of drying, the moisture content of the material is locally lower than the critical moisture content given by the sorption isotherm. Therefore the energy needed to change liquid moisture into vapour is given by the sorption energy, which is higher than the latent energy. In the normalization procedure presented, only the latent heat was considered. Therefore the normalized drying rates are overestimated.

In Figure 109, the normalized drying rate curves with respect to the average drying rate during the constant drying rate period are plotted for the normalization over the mass transfer and the normalization over the heat transfer.

#### A4 Measurement errors in the drying rates

In the data acquisition, 25 respectively 50 weight readings are averaged and recorded as 1 point. This averaged value is taken as the weight reading at the time of the last point (25th respectively 50th). A more accurate recording would be to position the averaged weight at the middle point. However, one is only interested in the drying rate, i.e. the loss of weight with moisture content, it is not important where the averaged weight is positioned as long as the drying rate and the moisture content correspond.

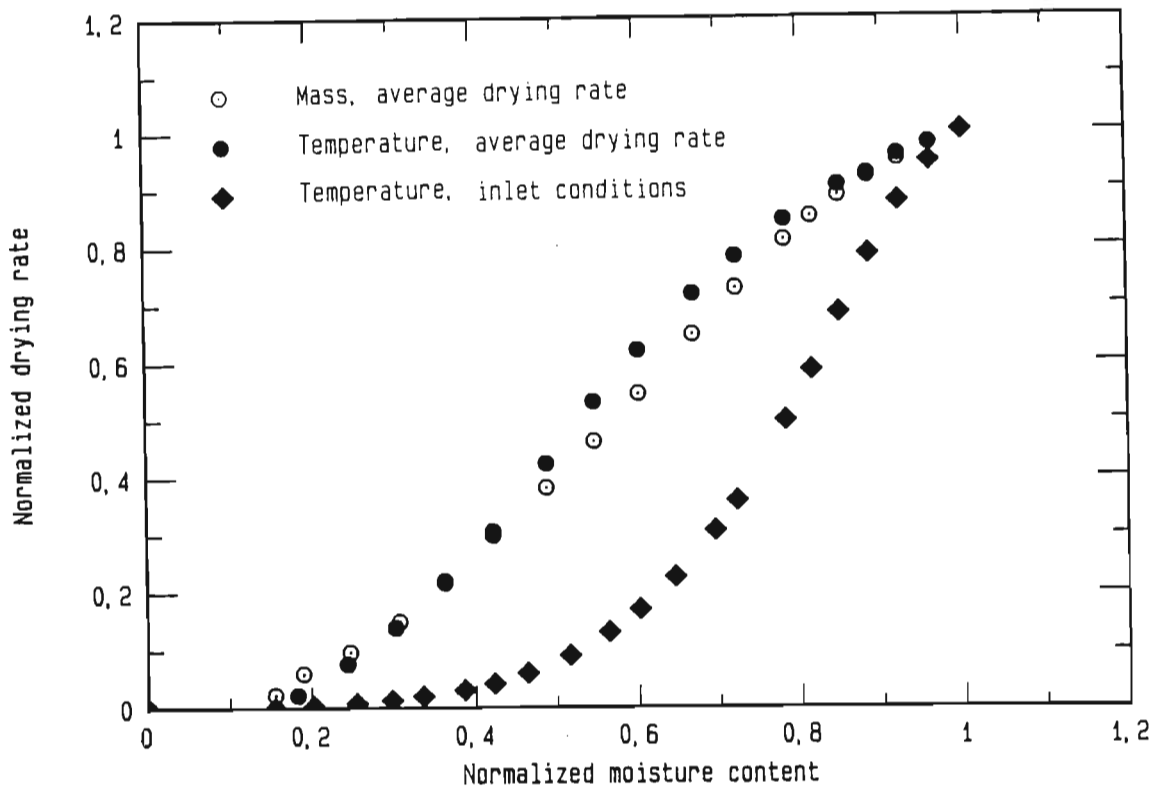


Figure 109: Comparison of the normalized drying rate curves with respect to the averaged drying rate with normalization over mass transfer and over heat transfer

A further error in the drying rate curves may be introduced by the smoothing technique that is used to evaluate the recorded weight readings. In general, smoothing techniques tend to stabilize the curve and no signs of distortion of the original curve could be found in this thesis.

Several curve fittings were tried to describe the smoothed curve of the weight readings vs time. Fittings using simple equations such as third-order polynomial or exponentials were not satisfactory at all. More complex fittings, using up to eight free parameters were more useful. The free parameters were determined by computer using an optimization procedure. The computing time was, however, excessively long (up to 12 hours) and it was decided to determine the drying rate by dividing the curve into small linearized segments as described in Section 3.2.6. Some error is introduced by this linearization close to the critical moisture content, where the change in the slope of the recorded weight curve is greatest, but the extent of this error is neglected.

## APPENDIX B: PHYSICAL PROPERTIES OF THE DRYING MEDIA AND OF THE MOISTURE

The physical properties of the drying media and of the moisture are described by the following equations [H3]:

Specific heat in  $\text{J kg}^{-1} \text{K}^{-1}$ :

$$c_{pa} = 1006 (1 + 5 \cdot 10^{-7} (T - 273,15)^2) \quad (126)$$

$$c_{ps} = 1880 (1 + 2,2 \cdot 10^{-4} (T - 273,15)) \quad (127)$$

$$c_{pl} = 4178 + 9 \cdot 10^{-6} (T - 308,15)^2 \quad (128)$$

$$c_{pwa} = \frac{(Y c_{ps} + c_{pa})}{(1 + Y)} \quad (129)$$

Dynamic viscosity in  $\text{kg m}^{-1} \text{s}$ :

$$\eta_a = 17,2 \cdot 10^{-6} \left(\frac{T}{273,15}\right)^{0,7} \quad (130)$$

$$\eta_s = 8,1 \cdot 10^{-6} \left(\frac{T}{273,15}\right)^{1,25} \quad (131)$$

$$\eta_{wa} = Y \eta_s + (1 - Y) \eta_a \quad (132)$$

Latent heat in  $\text{J kg}^{-1}$ :

$$\Delta h_v(T) = \Delta h_v(273,15) - (c_{pw} - c_{ps}) (T - 273,15) \quad (133)$$

The temperature is given in Kelvin for all of these equations.

## APPENDIX C: CURVE FITTING FOR THE SORPTION ISOTHERM

For molecular sieve, Henderson's equation [K3] was used as the basis for the development of an empirical equation to describe the sorption isotherm. The vapour pressure exerted by the moisture is expressed by the following equation:

$$p_v = [1 - \exp(-C_1 T X^{C_2})] p_s^* \quad (134)$$

$p_v$  is the vapour pressure,  $p_s^*$  is the saturation pressure and  $C_1$  and  $C_2$  are constants.

It was found that too-high values of the relative pressure were obtained for moisture contents higher than 0,16 kg/kg, if Henderson's equation was used without modifications. Therefore Equation 134 was corrected by an arbitrary empirical function. This correction function was modified until the graphical representation of the resulting function was visually judged to be in satisfactory agreement with the measured data. The final equation used to describe the sorption isotherm of molecular sieve reads as follows:

$$p_v = [1 - \exp(-60000 (X + f(T))^{5,3}) - 0,08 \exp(-(25 (X - 0,16 - f(T))^2)] \quad (135)$$

For alumina, Langmuir's equation for the adsorption of a monomolecular layer onto the solid skeleton was used as the basis for the development of an equation to describe the sorption isotherm.

$$\frac{X}{A} = \frac{c p_v}{1 + c p_v} \quad (136)$$

$c$  is a constant and  $A$  is the amount of vapour necessary for a complete monomolecular layer of adsorbed moisture.

With this equation, the vapour pressure can be expressed by:

$$p_v = \frac{1}{c} \frac{X}{(A - X)} \quad (137)$$



This equation was then modified by an empirical equation so as to describe the sorption isotherm of alumina as accurately as possible.

The final equation is written as:

$$p_v = f(T) \frac{X - g(T)}{h(T) + X - g(T)} \quad (138)$$

The functions  $f(T)$ ,  $g(T)$  and  $h(T)$  were determined by fitting the equation to the isotherms recorded at three different temperatures. Equation 137 was used as the starting point and, by trial and error, empirical equations were superimposed on the basic equation until the resulting curve agreed with the measured data.

$$f(T) = \text{INT}(1 + X - 0,0454 + 0,000262 T) \left( 1 + \frac{0,0567 - 0,000333 T}{1,56 - 0,00762 T} \right) \quad (139)$$

$$g(T) = 0,0454 - 0,000262 T \quad (140)$$

$$h(T) = 0,0567 - 0,000333 T \quad (141)$$

APPENDIX D: INFLUENCE OF THE SYSTEM GEOMETRY AND  
THE MASS FLOW RATE OF THE DRYING MEDIUM  
ON THE LOCUS OF THE INVERSION TEMPERATURE

The system geometries that are considered are a plate, a tube and a sphere. The model described in Section 4.1.1 is used to determine the inversion temperature for the various system geometries and mass flow rates. The results are presented in Figures 110 to 112. The evaporation rate in dry air and in pure steam is plotted against the inlet temperature of the drying medium for various mass flow rates of the drying medium. The length of the plate was taken as 0,2 m, because experimental equipment of this length can easily be built for experimental verification of the calculations. The dimensions of the tube were taken as being identical to those of the tube used by Yoshida. The sphere was considered to have a diameter of 1 mm, as this is in the size range that was used by Trommelen and Crosby [T2] in their tests. The mass flow rates that were used corresponded to linear velocities of air of  $1 \text{ m s}^{-1}$  to  $64 \text{ m s}^{-1}$ , a range that covers the velocities used in the various types of dryer.

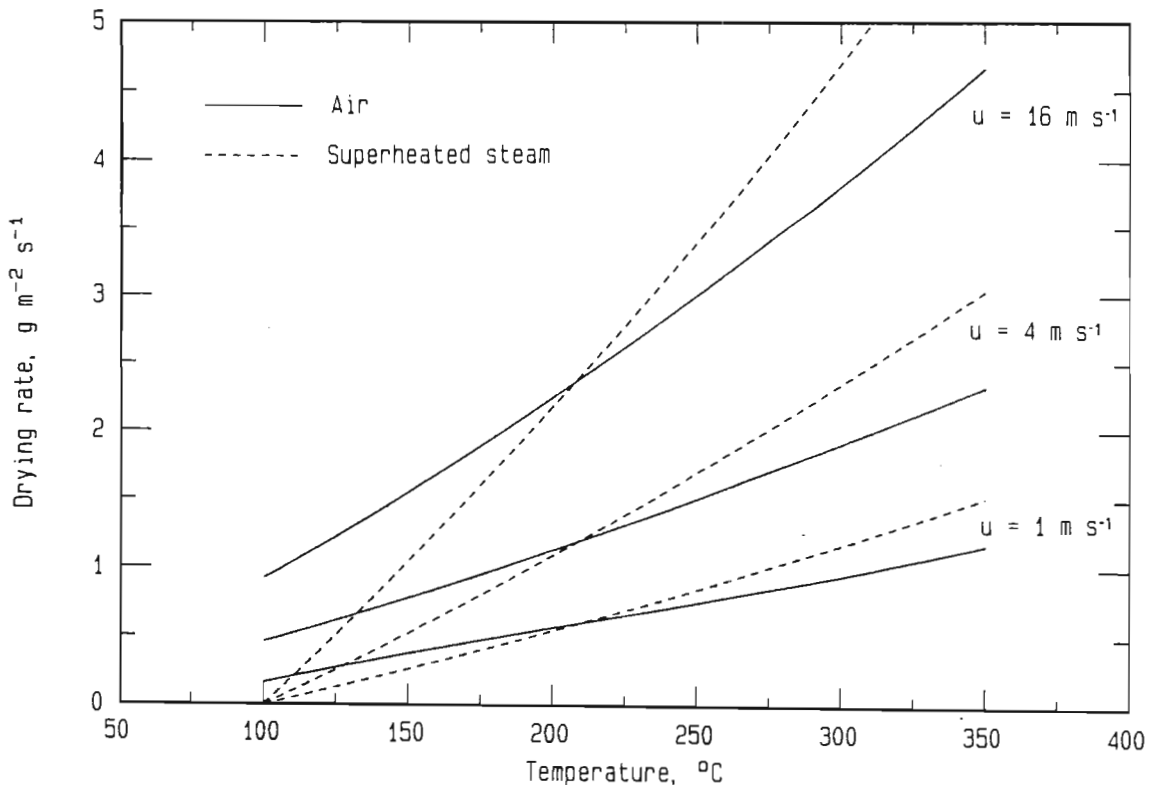


Figure 110: Inversion temperature for a plate (l = 0,2 m)

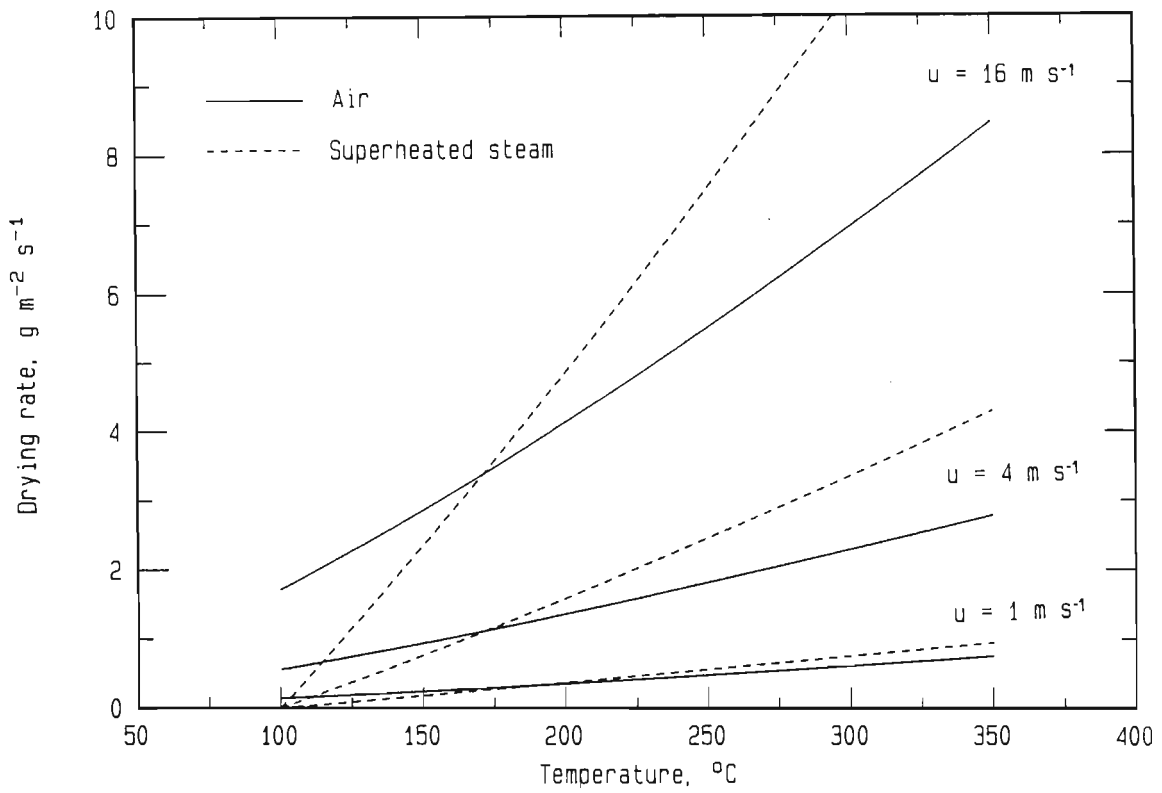


Figure 111: Inversion temperature for a tube ( $l = 1 \text{ m}$ ;  $d = 0,0288 \text{ m}$ )

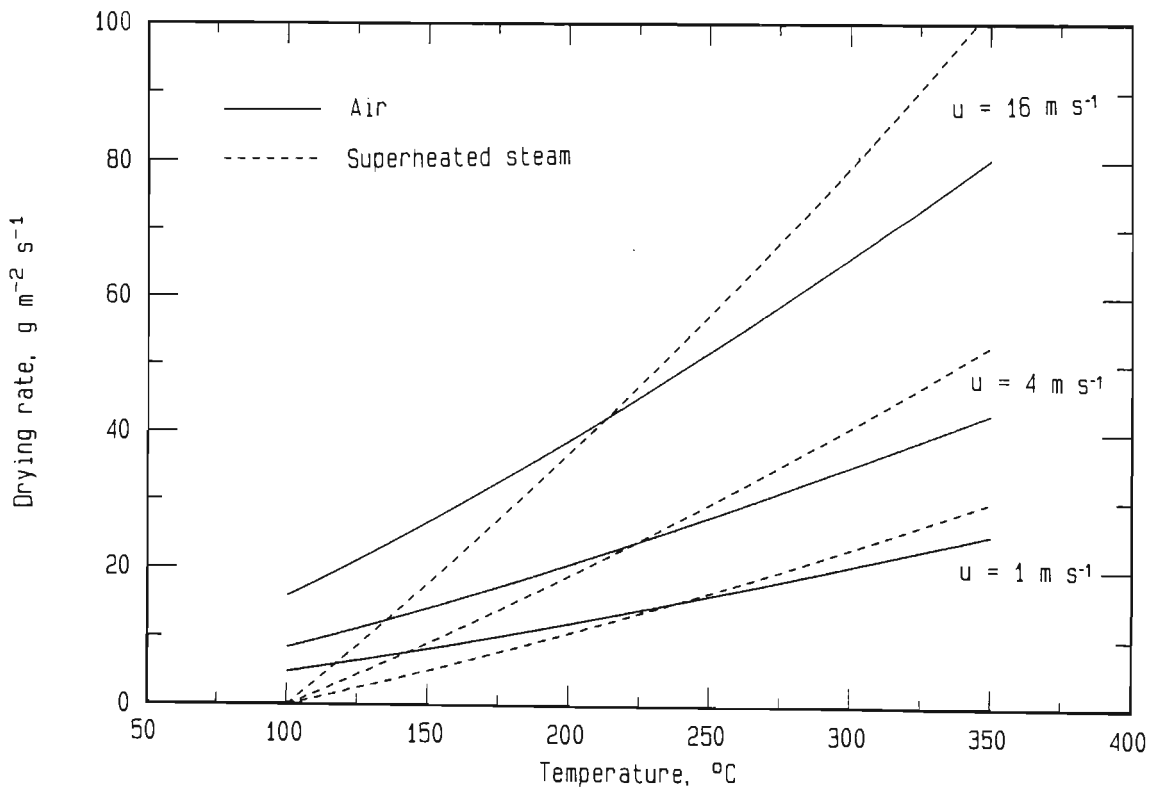


Figure 112: Inversion temperature for a sphere ( $d = 0,001 \text{ m}$ )

The inversion temperature depends on the system geometry. For a plate, an inversion temperature of 210 °C is found. For a tube it lies between 170 and 185 °C, and for a sphere between 210 and 245 °C. With the plate, the inversion temperature is independent of the mass flow rate of the drying medium, whereas with the tube and the sphere, it decreases with increasing mass flow rate.

For a given set of drying conditions (temperature, humidity and mass flow rate of the drying medium), the normalized temperature driving force and the normalized latent heat are identical for all configurations. The normalized heat transfer coefficient, however, varies from one configuration to another.

The heat transfer correlations used to determine the heat transfer coefficients in Equations 16 and 17 are listed in Appendix E.

In Figure 113 the normalized heat transfer coefficient of steam is plotted for the different configurations as a function of the temperature. The coefficient increases slightly with increasing temperature

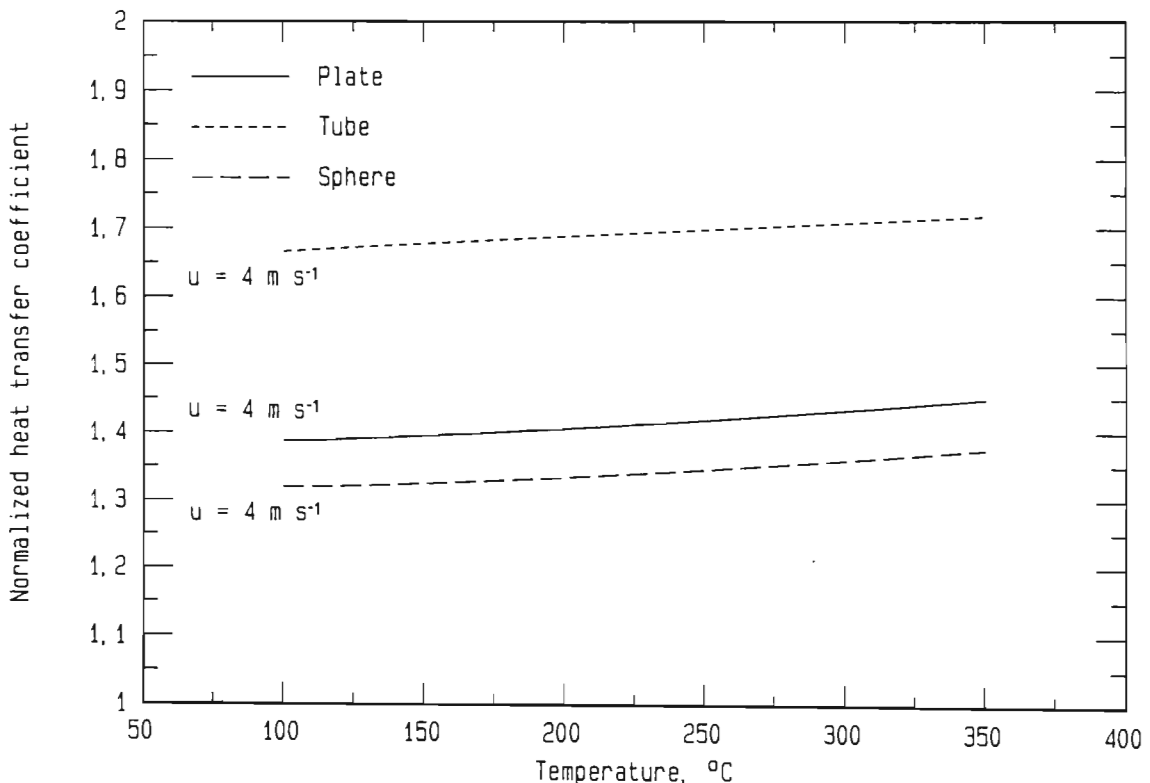


Figure 113: Normalized heat transfer coefficient for various configurations

for all geometries and is highest for the tube and lowest for the sphere. This means that the inversion temperature is also lowest for the tube and highest for the sphere, which is in accordance with the results shown in Figures 110 to 112.

The influence of the mass flow rate of the drying medium on the normalized heat transfer coefficient is investigated below for the various system geometries.

### Plate

In Figure 114 the normalized heat transfer coefficient of steam for flow over a plate is plotted against the temperature for various mass flow rates. The coefficient is seen to be independent of the mass flow rate. This explains the constant inversion temperature of 210 °C found in Figure 110. For all the velocities that are considered, the flow is in the laminar regime.

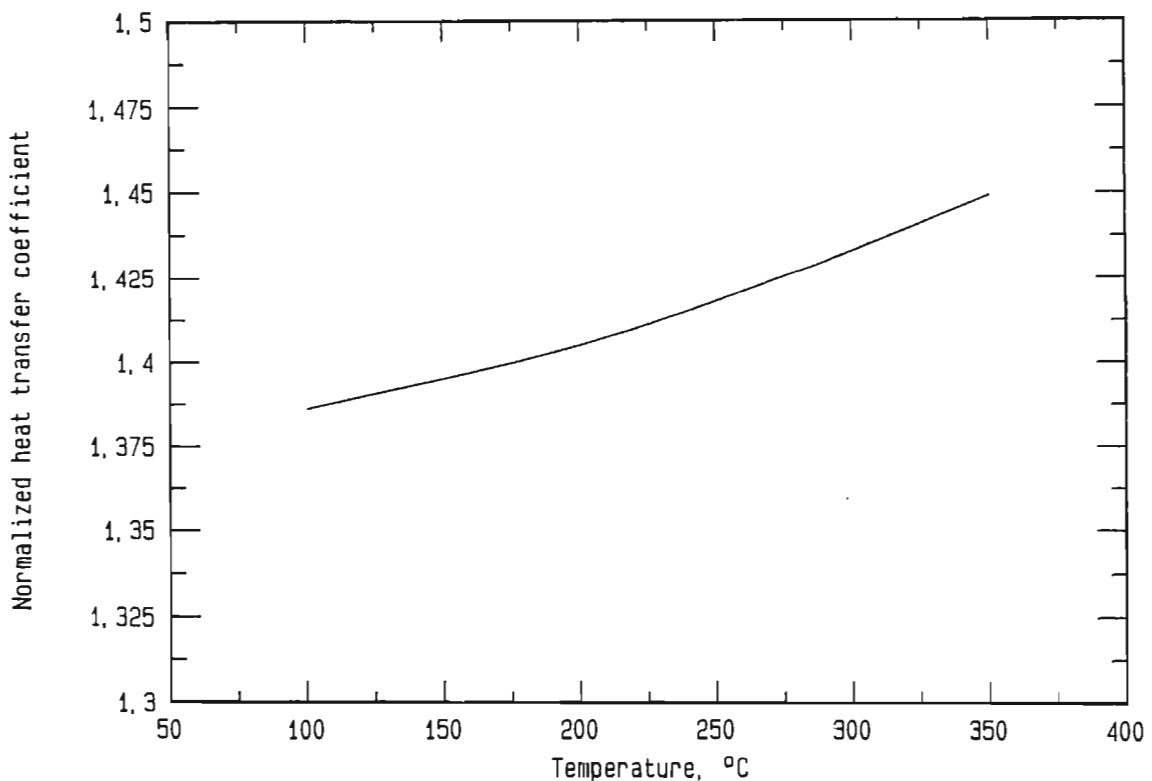


Figure 114: Normalized heat transfer coefficient of a plate as function of temperature for various mass flow rates

## Tube

In Figure 115 the normalized heat transfer coefficient of steam for flow through a tube is plotted against the temperature for various mass flow rates. The coefficient varies considerably with the mass flow rate of the drying medium. Each line of constant mass flow rate is labelled with the linear velocity ( $u$ ) of completely dry air through the empty tube at the given conditions.

For low flow rates ( $u_1$  to  $u_3$ ), air flow and steam flow are both in the laminar regime over the whole temperature range. The normalized heat transfer coefficient increases with increasing flow rate and increasing temperature.

For medium flow rates ( $u_4$  to  $u_5$ ), the air flow is in the laminar regime, but the steam flow is in the turbulent regime for low temperatures and in the laminar regime for high temperatures. Heat transfer coefficients are higher in the turbulent regime than in the laminar regime. The normalized heat transfer coefficient of steam decreases with increasing temperature, but continues increasing with increasing flow rate.

At flow rate  $u_6$  the normalized heat transfer coefficient again increases with increasing temperature. The reason is that the steam flow is turbulent over the whole temperature range, whereas the air flow is laminar. At this point, the normalized heat transfer coefficient reaches its maximum, and the inversion temperature is at its minimum.

At high flow rates ( $u_7$  to  $u_8$ ), the normalized heat transfer coefficient decreases with an increase in mass flow rate. The air flow now enters the turbulent regime, and the advantage of steam begins to decrease.

At very high flow rates ( $u_9$ ), air and steam are both in the turbulent regime over the whole temperature range, and the normalized heat transfer coefficient again increases with an increase in the mass flow rate.

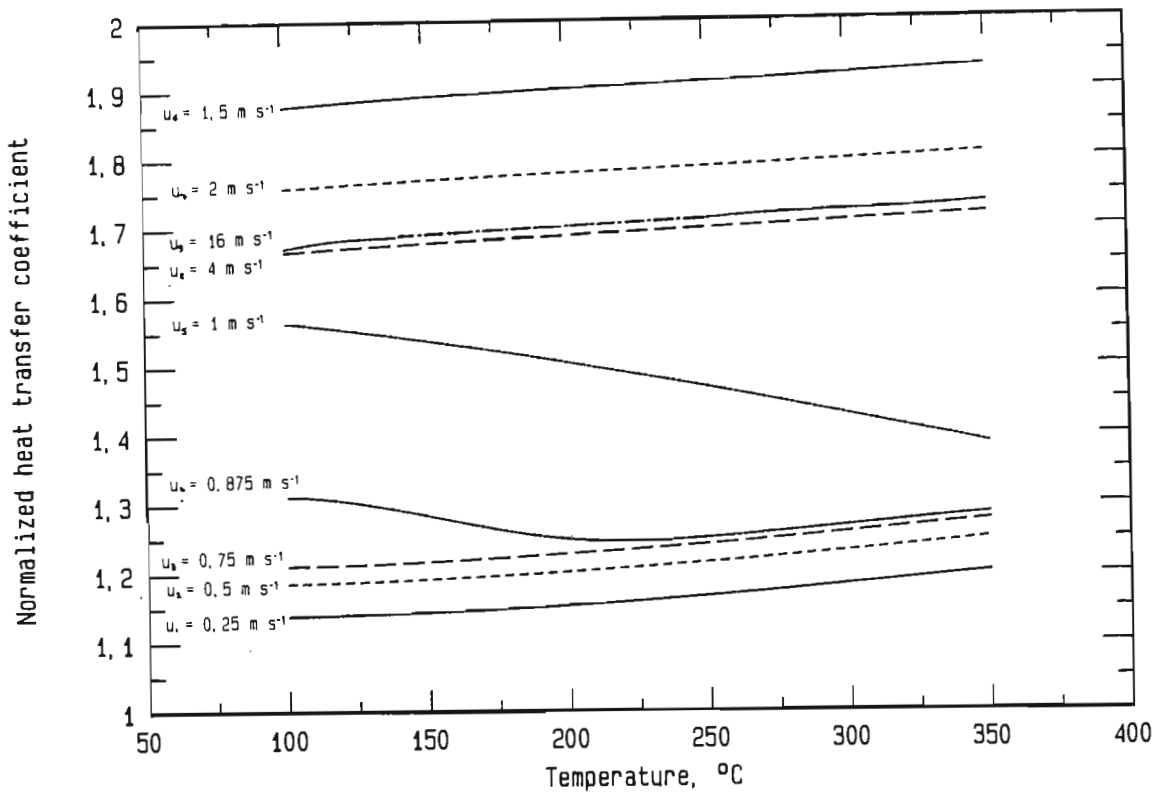


Figure 115: Normalized heat transfer coefficient of a tube as function of temperature for various mass flow rates

This behaviour shows the important effect of the flow regime on the inversion temperature.

### Sphere

In Figure 116 the normalized heat transfer coefficient of steam for flow over a sphere is plotted against the temperature for various mass flow rates. The coefficient increases with both increasing temperature and increasing mass flow rate. In this case the flow was in the laminar regime for both drying media.

For all configurations, plate, tube and sphere, there is a change in the normalized heat transfer coefficients with temperature. This change can be explained by the change in the physical properties of the drying media.

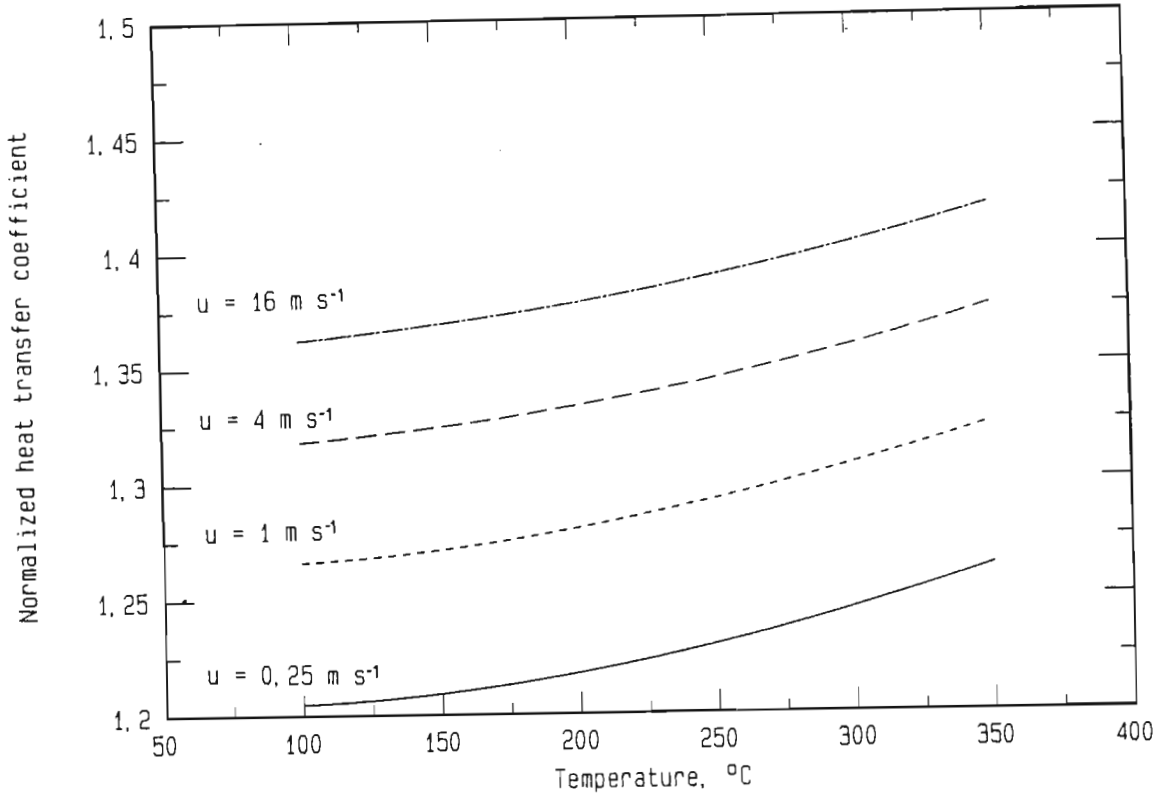


Figure 116: Normalized heat transfer coefficient of a sphere as function of temperature for various mass flow rates

For the sake of simplicity, the heat transfer correlation can be written as a function of the Reynolds number and the Prandtl number in following form:

$$Nu = C_1 Re^{C_2} Pr^{C_3} \quad (142)$$

From this correlation the relative heat transfer coefficient of steam can be written as a function of the physical properties of the drying medium as follows:

$$\frac{h_s}{h_a} = \left( \frac{\lambda_s}{\lambda_a} \right)^{(1-C_3)} \left( \frac{\eta_s}{\eta_a} \right)^{(C_3-C_2)} \left( \frac{c_{ps}}{c_{pa}} \right)^{C_3} \quad (143)$$

In Table 10 the normalized physical properties are listed as functions of the temperature.



The change in the normalized heat transfer coefficient with mass flow rate cannot be explained by the use of Equation 142, as the dependence on mass flow rate is cancelled when the relative heat transfer coefficient is formed. For a plate, the heat transfer correlation that was used (see Appendix E) has the basic form of Equation 142. Therefore, for a plate, the normalized heat transfer coefficient is independent of the mass flow rate. For a tube or a sphere, the heat transfer correlation has a more complex form and the mass flow dependence is not cancelled when the normalized heat transfer coefficient is formed.

Table 10: Normalized physical properties for various temperatures

Temperature °C	$\lambda_s/\lambda_a$	$c_{ps}/c_{pa}$	$\eta_s/\eta_a$
125	0,8526	1,9084	0,5638
150	0,8507	1,9104	0,5706
175	0,8498	1,9123	0,5769
200	0,8495	1,9139	0,5838
225	0,8504	1,9154	0,5907
250	0,8515	1,9167	0,5972
275	0,8537	1,9178	0,6032
% change	0,13	0,49	6,99

In the example of flow through a tube, it was found that the flow regime of the drying medium is important for the normalized heat transfer coefficient. At the same mass flow rate, the Reynolds numbers are higher for steam than for air. The normalized Reynolds number can be expressed by the normalized dynamic viscosity :

$$\frac{Re_s}{Re_a} = \left( \frac{\eta_s}{\eta_a} \right)^{-1} \quad (134)$$

In Table 10 the relative dynamic viscosity is given for various temperatures. The mean value of the relative viscosity is 0,5837. This means that the Reynolds number for steam is, on average, 1,71 times ( $1/0,5837$ ) higher than the Reynolds number for air. As a consequence, the steam is in the transition or turbulent regime, while the air flow is still in the laminar regime. The heat transfer characteristics are more favourable in the turbulent regime. Therefore, for the same mass flow rate, steam has a kinetic advantage over air.

# APPENDIX E: HEAT TRANSFER CORRELATIONS FOR VARIOUS GEOMETRICAL CONFIGURATIONS

Configuration      Reynolds number      Heat transfer correlation

Plate       $0 < Re < 500000$       
$$Nu = \frac{0,664 \sqrt{Re Pr}}{Pr^{1/6}}$$

$Re > 500000$       
$$Nu = \frac{\chi Re Pr}{(1 + 12,7 \chi (Pr^{0,66} - 1))}$$

$$\chi = 0,037 Re^{-0,2}$$

Cylinder      
$$Nu = \max (Nu_1, Nu_2, Nu_3)$$

$$Nu_1 = (49,03 + 4,25 Gz)^{0,33}$$

$$Nu_2 = \frac{0,664 \sqrt{Gz}}{Pr^{1/6}}$$

$$Nu_3 = \frac{\left\{ \frac{\chi}{8} (Re - 1000) Pr \left( 1 + \left( \frac{d}{L} \right)^{0,66} \right) \right\}}{\left\{ 1 + 12,7 \sqrt{\frac{\chi}{8}} (Pr^{0,66} - 1) Re^{-0,1} \right\}}$$

$$\chi = (0,7904 \ln(Re) - 1,64)^{-2}$$

Sphere      
$$Nu = 2 + \sqrt{Nu_{lam}^2 + Nu_{turb}^2}$$

$$Nu_{lam} = 0,664 Pr^{0,33} Re^{0,5}$$

$$Nu_{turb} = \frac{0,037 Re^{0,8} Pr}{(1 + 2,44 (Pr^{0,66} - 1) Re^{-0,1})}$$

APPENDIX F: SOLUTION OF DIFFERENTIAL EQUATION 36  
FOR THE HEAT TRANSFER COEFFICIENT

The differential Equation 36 for the temperature profile in a drying fluidized bed can be written as:

$$\frac{(T_a - T_p) (\Delta h_v + c_{ps} T_a - c_{ps} T_p + c_{ps} T_a)}{\Delta h_v + c_{ps} T_a - c_{ps} T_p} \frac{dT_a}{dz} = - \frac{h a \Phi}{M_a (c_{pa} + Y c_{ps})} dz \quad (145)$$

After development, the left side of this equation can be written as:

$$\frac{c_{ps} T_a + (\Delta h_v - c_{ps} T_p)}{2 c_{ps} T_a^2 + (\Delta h_v - 3 c_{ps} T_p) T_a - T_p (\Delta h_v - c_{ps} T_p)} dT_a \quad (146)$$

This temperature differential is of the form:

$$\frac{c_1 T_a + c_2}{c_3 T_a^2 + c_4 T_a + c_5} dT_a \quad (147)$$

with :  $c_1 = c_{ps}$

$$c_2 = \Delta h_v - c_{ps} T_p \quad (148)$$

$$c_3 = 2 c_{ps} \quad (149)$$

$$c_4 = \Delta h_v - 3 c_{ps} T_p \quad (150)$$

$$c_5 = - T_p (\Delta h_v - c_{ps} T_p) \quad (151)$$

Equation 146 can be transformed to:

$$\left( c_1 \frac{T_a}{c_3 T_a^2 + c_4 T_a + c_5} + c_2 \frac{1}{c_3 T_a^2 + c_4 T_a + c_5} \right) dT_a \quad (152)$$

With following abbreviations :

$$X = c_3 T_a^2 + c_4 T_a + c_5 \quad (153)$$

and

$$\Delta = 4 c_3 c_5 - c_4^2 \quad (154)$$

the integrated form of the equation is as follows [B9]:

$$\frac{c_1}{2 c_3} \ln (X) - \left( \frac{c_1 c_4}{2 c_3} + c_2 \right) \frac{1}{\sqrt{-\Delta}} \ln \left( \frac{2 c_3 T_a + c_4 - \sqrt{-\Delta}}{2 c_3 T_a + c_4 + \sqrt{-\Delta}} \right) \quad (155)$$

# APPENDIX G: COMPARISON OF THE GAS-TO-SOLID HEAT TRANSFER COEFFICIENT IN A FLUIDIZED BED EVALUATED WITH AND WITHOUT DRYING

The gas-to-solid heat transfer in a drying fluidized bed can be evaluated in two ways:

- 1) by assuming no drying of the material (i.e. no change in the humidity of the fluidizing medium with height), and
- 2) by assuming drying of the material (i.e. a change in the humidity of the fluidizing medium with height).

In Section 4.3.1 the evaluation of the heat transfer coefficient with drying of the material was presented. For the evaluation without drying, Equations 27 to 29 are valid. Equation 30 of the derivative of the enthalpy with height in the dryer, is reduced to:

$$\frac{dH}{dz} = \dot{M}_a (c_{pa} + Y c_{ps}) \frac{dT_a}{dz} \quad (156)$$

The humidity of the air is considered to be independent of the height of the fluidized bed and the arithmetic humidity average between outlet and inlet is used in Equation 156. The specific heat of the air and of the steam are determined at the arithmetic average temperature between outlet and inlet. By placing Equations 28 and 156 in the energy balance (Equation 27), an expression for the temperature gradient is obtained.

$$\dot{M}_a (c_{pa} + Y c_{ps}) \frac{dT_a}{dz} + h a \Phi (T_a - T_p) = 0 \quad (157)$$

By separating the variables, following expression is obtained:

$$\frac{dT_a}{(T_a - T_p)} = - \frac{h a \Phi}{\dot{M}_a (c_{pa} + Y c_{ps})} dz \quad (158)$$

Because of the well-mixed behaviour of the particles in the fluidized bed the particle temperature is constant over the height of the

dryer. Integration of Equation 158 leads to the temperature of the drying medium at any height  $z$  in the bed:

$$\frac{(T_{az} - T_p)}{(T_{in} - T_p)} = \exp \left( - \frac{h a \Phi}{\dot{M}_a (c_{pa} + Y c_{ps})} z \right) \quad (159)$$

If the temperature  $T_{az}$  and the height  $z$  are known, then the heat transfer coefficient can be determined by:

$$h_{a,z} = - \frac{\dot{M}_a (c_{pa} + Y c_{ps})}{z a \Phi} \ln \left( \frac{T_{az} - T_p}{T_{in} - T_p} \right) \quad (160)$$

In the case of steam, Equation 160 is also valid. Instead of the expression  $\dot{M}_a (c_{pa} + Y c_{ps})$ , the expression  $\dot{M}_s c_{ps}$  is used.

The gas-to-solid heat transfer coefficients were evaluated, based on the assumption of no humidity increase of the drying medium with height in the dryer in this Appendix and with humidity increase of the drying medium with height in the dryer in Section 4.3.1. The results are plotted in Figures 117 and 118. For all tests, the data with drying are closer to Equation 37 and those without drying lie below. For the same Reynolds number, the difference in Nusselt number using the two evaluation methods lies between 26 and 44 %, with an arithmetic average of 32,9 %. This shows that data gathered from an experiment in which the temperature of the bed is kept constant by evaporation of moisture cannot be evaluated in the same way as data gathered from an experiment in which no evaporation takes place and the bed temperature is kept constant by some other means (cooling, feeding of cold material, etc.). This fact may explain some of the divergent results of other authors.

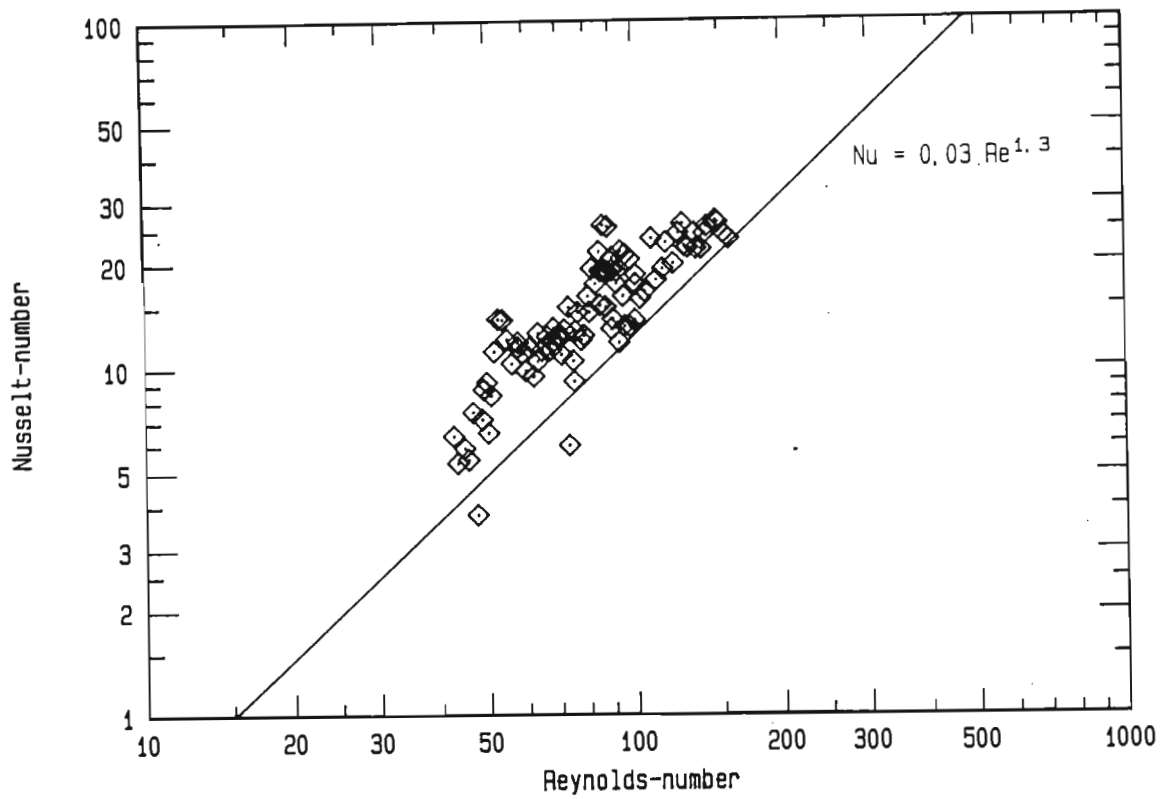


Figure 117: Heat transfer coefficient in a fluidized bed evaluated without drying

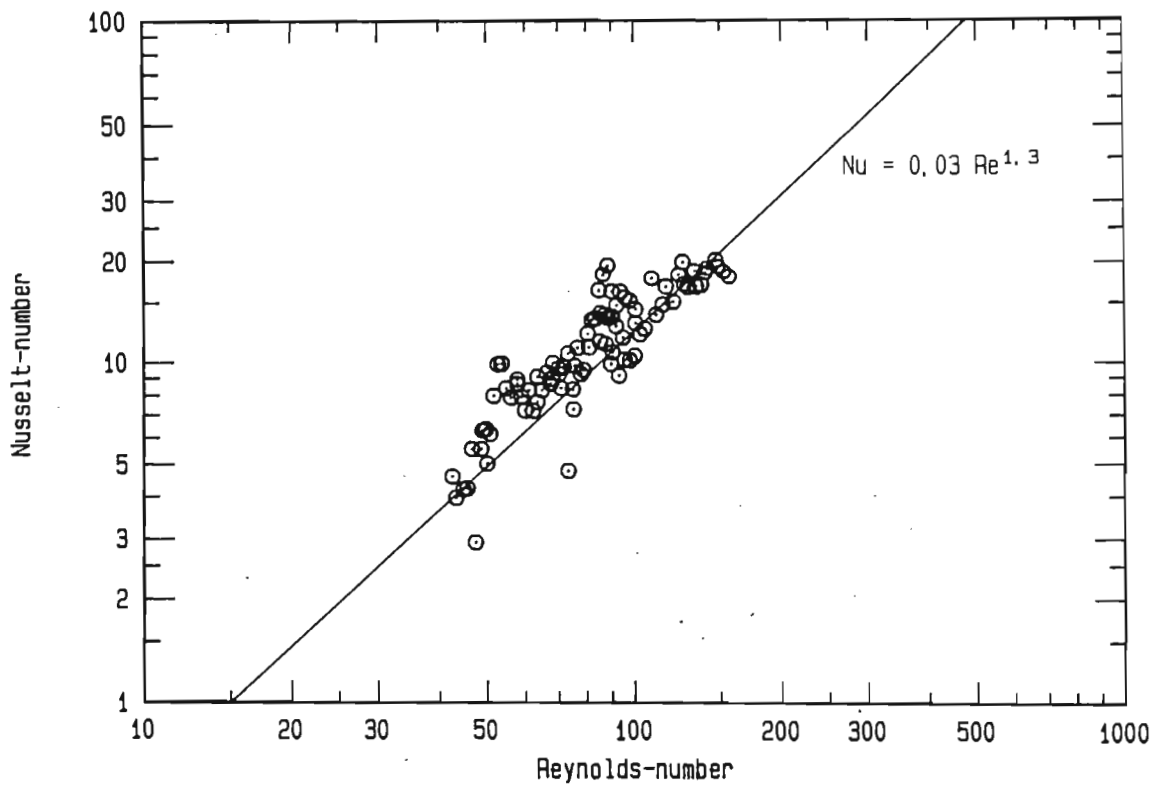


Figure 118: Heat transfer coefficient in a fluidized bed evaluated with drying

## APPENDIX H: NORMALIZATION METHODS

Two types of normalization method are investigated below, as represented in Figure 119. The first is the normalization with respect to the average drying rate during the constant drying rate period. This is used in systems where the conditions of the drying medium do not change during their flow through the material (e.g. single particles, a monolayer of particles, high flow rates, etc). The second method is the normalization with respect to the constant conditions at the inlet into the dryer. It is used if the state of the drying medium changes over the length of the dryer.

Both normalization procedures will be presented for both equilibrium and non-equilibrium systems. For each normalization procedure and each drying system, the normalization is presented using mass transfer and heat transfer equations.

For all normalizations, the moisture content is normalized with respect to the critical moisture content.

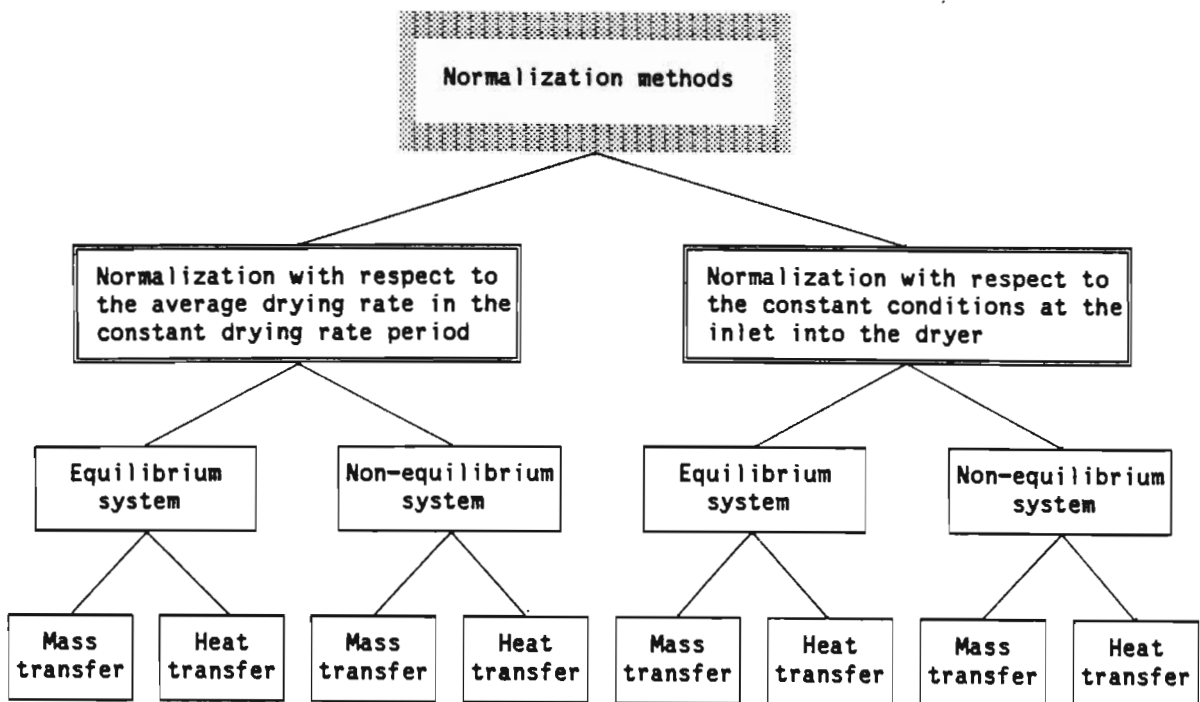


Figure 119: Normalization methods



H.1 Normalization with respect to the averaged drying rate during the constant drying rate period

A. Equilibrium system

(a) *Mass transfer*

The graphical representation of a measured drying rate curve gives the drying rate of the material as a function of the moisture content. The constant drying rate and the critical moisture content can be read off directly from the diagram and the normalized drying rate curve can be determined.

If the inlet and outlet humidities, as well as the mass flow rates of the drying medium, are known, then the drying rates can be determined from the mass balance over the dryer according to following formula:

$$\dot{m}_{ev} = \frac{\dot{M}_g (Y_{g,out}(t) - Y_{g,in})}{A} \quad (161)$$

The drying rate during the constant drying rate period is determined from:

$$\dot{m}_{ev,I} = \frac{\dot{M}_g (Y_{g,out,I} - Y_{g,in})}{A} \quad (162)$$

The normalized drying rate  $v$  can then be written as:

$$v = \frac{(Y_{g,out}(t) - Y_{g,in})}{(Y_{g,out,I} - Y_{g,in})} \quad (163)$$

(b) *Heat transfer*

For the constant drying rate period, the total energy balance can be written as:

$$\dot{M}_g c_{pg} (T_{g,in} - T_{g,out,I}) = \dot{m}_{ev,I} \Delta h_v A \quad (164)$$

For the falling drying rate period, the drying rate can be written as:

$$\dot{M}_g c_{pg} (T_{g,in} - T_{g,out}(t)) = \dot{m}_{ev} \Delta h_v A + M_p c_{pp} \frac{dT_p}{dt} \quad (155)$$

In the equilibrium case, the temperature of the exhaust is equal to the temperature of the particles, i.e.  $T_{g,out}(t) = T_p(t)$ .

Using the dimensionless numbers defined in Section 4.5, the normalized drying rate can be written as follows:

$$v = 1 - \xi_p^* \tau_{out}^* \frac{d\xi_p^*}{d\tau^*} \quad (166)$$

## B. Non-equilibrium system

### (a) *Mass transfer*

The normalization by mass transfer in the non-equilibrium system is done analogous to the normalization in the equilibrium system.

### (b) *Heat transfer*

Equations 164 and 165 are also valid for the non-equilibrium system. The outlet temperature  $T_{g,out}(t)$ , however, is not equal to the particle temperature  $T_p(t)$ . The normalized drying rate can then be written, using the previously defined dimensionless numbers, as:

$$v = \frac{1 - \xi_{g,out}^* - \tau_{out}^* \frac{\partial \xi_p^*}{\partial \tau^*}}{1 - \xi_{g,out,I}^*} \quad (167)$$

This is the general equation for the normalized drying rate by heat transfer. Indeed, in the equilibrium case,  $\xi_{g,out,I}^* = 0$  and  $\xi_{g,out}^* = \xi_p^*$  and Equation 167 becomes identical with Equation 166.

## H.2 Normalization with respect to the inlet conditions of the drying medium

This normalization procedure is partly described in Section 4.5. In the following the main steps of this normalization are repeated for the sake of completeness.

### A. Non-equilibrium system

#### (a) *Mass transfer*

The normalized drying rate with respect to the inlet conditions can be determined by integrating the differential mass balance over the height of the dryer.

The differential mass balance can be written as follows:

$$- \dot{M}_g \frac{\partial Y_g}{\partial z} dz + d\dot{m}_{ev} A \frac{dz}{L} = 0 \quad (168)$$

The differential evaporation rate can be written as follows:

$$d\dot{m}_{ev} = v \rho_g \beta (Y_{p,T_p,I}^* - Y_g) \quad (169)$$

In dimensionless form the differential mass balance can be written as follows:

$$\frac{d\xi_g^0}{\xi_g^0} = - v d\zeta^0 \quad (170)$$

If this differential equation is integrated over the height of the bed, this leads to:

$$v = - \frac{\ln(\xi_{g,out}^0)}{\zeta_{out}^0} \quad (171)$$

This form represents the normalized drying rate with respect to the inlet conditions into the bed, i.e. the normalized drying rate of a single particle exposed to the constant drying conditions at the inlet to the fluidized-bed dryer.

(b) Heat transfer

In this case the normalized drying rate can be determined by integrating the differential energy balance over the height of the fluidized bed.

The differential energy balance for the drying medium is :

$$\dot{M}_g c_{pg} \frac{\partial T_g}{\partial z} dz + \dot{m}_{ev} \Delta h_v A + M_p c_{pp} \frac{dz}{L} \frac{\partial T_p}{\partial t} = 0 \quad (172)$$

The differential evaporation rate during the falling drying rate period can be written as follows:

$$\dot{m}_{ev} = v \dot{m}_{ev,I} \quad (173)$$

The drying rate during the constant drying rate period can be expressed as follows:

$$\dot{m}_{ev,I} = \frac{h (T - T_{p,I})}{\Delta h_v} \frac{dz}{L} \quad (174)$$

With Equations 173 and 174, Equation 172 can be written in the dimensionless form as follows:

$$\frac{d\xi_g}{dz} + v \xi_g + \frac{\partial \xi_p}{\partial \tau} = 0 \quad (175)$$

Integration over the bed height leads to

$$v = - \frac{\ln \left[ \frac{v \xi_{g,out} + \frac{\partial \xi_p}{\partial \tau}}{v + \frac{\partial \xi_p}{\partial \tau}} \right]}{\xi_{out}} \quad (176)$$

The normalized drying rate can then be determined by iteration.

If the dimensionless temperature change of the particles with time is small compared with the dimensionless temperature at the outlet, then Equation 176 can be written as follows:

$$v = - \frac{\ln(\xi_{g,out}^{\circ})}{\xi_{out}^{\circ}} \quad (177)$$

This equation is the direct equivalent to Equation 171 for the normalization by mass transfer.

## B. Equilibrium case

### (a) *Mass transfer*

The normalized drying rate is determined by the total mass balance around the dryer:

$$\dot{M}_g (Y_{g,out} - Y_{g,in}) = \int_0^L v \rho_g \beta A (Y_p^* - Y_g) \frac{dz}{L} \quad (178)$$

The outlet humidity of the drying medium is equal to the saturation humidity on the surface of the particles:

$$Y_{g,out} = Y_p \quad (179)$$

The dimensionless form of Equation 178 is as follows:

$$1 = v \int_0^{\xi_{out}^{\circ}} \frac{\xi_g^{\circ}}{1 - \xi_p^{\circ}} d\xi^{\circ} \quad (180)$$

Before integration, the humidity potential must be expressed as a function of the dimensionless height. For the falling drying rate period, the mass balance over a differential element of the dryer is as follows:

$$- \dot{M}_g \frac{\partial Y_g}{\partial z} dz + \rho_g \beta (Y_p - Y_g) A \frac{dz}{L} = 0 \quad (181)$$

$Y_p$  is the humidity at the surface of the material. It is a function of the moisture content and the temperature of the particles and therefore not dependent on the bed height. Rearrangement leads to:

$$\frac{dY_g}{(Y_p - Y_g)} = \frac{\rho_g \beta A}{\dot{M}_g} \frac{dz}{L} \quad (182)$$

The integration of Equation 182 can be written in the dimensionless form as follows:

$$\xi_g^{\circ'} = \exp(-\zeta^{\circ}) \quad (183)$$

From Equation 62 following equation is derived:

$$\xi_g^{\circ} = (1 - \xi_p^{\circ}) \xi_g^{\circ'} + \xi_p^{\circ} \quad (184)$$

With Equation 183 into Equation 184, the dimensionless humidity potential is expressed as a function of the dimensionless height:

$$\xi_g^{\circ} = (1 - \xi_p^{\circ}) \exp(-\zeta^{\circ}) + \xi_p^{\circ} \quad (185)$$

Using Equation 176 in Equation 180 and integrating leads to:

$$\nu = \frac{(1 - \xi_p^{\circ})}{1 - \xi_p^{\circ} + \xi_p^{\circ} \zeta_{out}^{\circ} - (1 - \xi_p^{\circ}) \exp(-\zeta_{out}^{\circ})} \quad (186)$$

#### (b) Heat transfer

The total energy balance around the drying system can be written as follows:

$$\dot{M}_g c_{pg} (T_{g,in} - T_{g,out}) = \int_0^L \nu h A (T_g - T_{p,I}) \frac{dz}{L} + \dot{M}_p c_{pp} \frac{\partial T_p}{\partial t} \quad (187)$$

The energy that the drying medium gives to the particles is used for evaporating moisture and to heat up the particles. The part of the energy that is used for evaporation is expressed by the heat transferred to the particles in the constant drying rate period corrected by the normalized drying rate.

Equation 187 can be written in the dimensionless form as follows:

$$1 = v \int_0^{\tau_{out}^*} \frac{\xi_g^*}{(1 - \xi_p^*)} d\tau^* - \tau_{out}^* \frac{d\xi_p^*}{d\tau^*} \quad (188)$$

The temperature potential as a function of the height is as follows:

$$\xi_g^* = (1 - \xi_p^*) \exp(-\tau^*) + \xi_p^* \quad (189)$$

The normalized drying rate can then be expressed by:

$$v = \frac{1 - \xi_p^* + (1 - \xi_p^*) \tau_{out}^* \frac{\partial \xi_p^*}{\partial \tau^*}}{1 - \xi_p^* + \xi_p^* \tau_{out}^* - (1 - \xi_p^*) \exp(-\tau_{out}^*)} \quad (190)$$

### H.3 Summary of the normalization methods

Normalization with respect to the average drying rate in the constant drying rate period:

#### Equilibrium system

##### *Mass Transfer*

$$v = \frac{(Y_{g,out}(t) - Y_{g,in})}{(Y_{g,out,I} - Y_{g,in})}$$

##### *Heat transfer*

$$v = 1 - \xi_p^* \tau_{out}^* \frac{d\xi_p^*}{d\tau^*}$$

#### Non-equilibrium system

##### *Mass transfer*

$$v = \frac{(Y_{g,out}(t) - Y_{g,in})}{(Y_{g,out,I} - Y_{g,in})}$$

Heat transfer

$$v = \frac{1 - \xi_{g,out}^{\circ} - \zeta_{out}^{\circ} \frac{\partial \xi_p^{\circ}}{\partial \tau^{\circ}}}{1 - \xi_{out,I}^{\circ}}$$

Normalization with respect to the inlet conditions into the dryer

Equilibrium system

Mass transfer

$$v = \frac{(1 - \xi_p^{\circ})}{1 - \xi_p^{\circ} + \xi_p^{\circ} \zeta_{out}^{\circ} - (1 - \xi_p^{\circ}) \exp(-\zeta_{out}^{\circ})}$$

Heat transfer

$$v = \frac{1 - \xi_p^{\circ} + (1 - \xi_p^{\circ}) \zeta_{out}^{\circ} \frac{\partial \xi_p^{\circ}}{\partial \tau^{\circ}}}{1 - \xi_p^{\circ} + \xi_p^{\circ} \zeta_{out}^{\circ} - (1 - \xi_p^{\circ}) \exp(-\zeta_{out}^{\circ})}$$

Non-equilibrium system

Mass transfer

$$v = - \frac{\ln(\xi_{g,out}^{\circ})}{\zeta_{out}^{\circ}}$$

Heat transfer

$$v = - \frac{\ln \left[ \frac{v \xi_{g,out}^{\circ} + \frac{\partial \xi_p^{\circ}}{\partial \tau^{\circ}}}{v + \frac{\partial \xi_p^{\circ}}{\partial \tau^{\circ}}} \right]}{\zeta_{out}^{\circ}}$$



## APPENDIX I: MATHEMATICAL DESCRIPTION OF THE HEAT AND MASS TRANSFER MECHANISMS IN CAPILLARY POROUS BODIES

For a thorough analysis of the normalized drying rate curves in air and in steam, the heat and mass transfer processes inside the material must be described by the physical principles from which they originate. The differences in the internal transfer processes between air and steam can then be used to explain the differences in the falling drying rate periods.

### I.1 Moisture flow in the liquid phase

The strength and nature of the bonding of the liquid to the material determines the mobility of the liquid phase. The various categories of liquid moisture were discussed in Section 3.3.1.

In the early stages of drying, the moisture evaporates from the outside of the particle and the rate of drying is not influenced by the moisture mobility inside the material. Therefore the bonding of the surface water is negligible. At the other extreme, the chemically bound water is so strongly fixed to the solid that its mobility can be neglected. The capillary water and the adsorbed water must be considered in a mathematical drying model.

Phenomenologically, the capillary water moves on the basis of a gradient in liquid pressure (capillary flow) [K9] and on the basis of the gravity field, whereas the adsorbed water moves on the basis of a gradient in adsorbed water content (surface flow) [I1].

To describe the capillary water movement by a physical formula, Krischer [K9] chose a gradient in liquid moisture content as the driving force. This is phenomenologically wrong [B8], but was proved to be an acceptable assumption, especially as it simplifies the drying problem from a mathematical point of view. The transfer coefficient is not a constant, but depends on the liquid moisture content and on the temperature. It must be determined experimentally.

The temperature gradient as the driving force for the capillary water movement was introduced by Luikov [L5]. In his model, the influence of the temperature gradient on the moisture movement originates in the Sorret effect. Other authors [I1,H1+2] derive this influence from the temperature-dependence of the capillary pressure. In recent publications [C2,K13], the influence of the temperature gradient on the moisture movement is discussed. This effect is often included in the general development of drying models but is then omitted from the actual solution of the model. The major difficulty is determining a thermal mass transfer coefficient for the moisture movement. In the present model, the influence of the temperature gradient is neglected.

The adsorbed water is relatively strongly bound to the solid and its mobility is very limited. In the early stages of drying, capillary water movement is dominant and the adsorbed water flow can be neglected. In the later stages of drying, however, the adsorbed water flow can outweigh the capillary water movement.

The driving force for the flow of adsorbed water is the liquid moisture content [I1]. It is therefore convenient to include this flow in the mathematical expression for the capillary water flow as this is also assumed to move on the basis of a liquid moisture content. As the capillary transfer coefficient is determined over semi-empirical correlations, this approach is valid.

Gravitational effects on the movement of the liquid moisture are neglected in the present model, as small particles with narrow pores were used in the experiments.

In general, the liquid water flow can be influenced by a gradient in total vapour pressure. Imakoma et al. [I1] estimated the contribution of the total vapour pressure gradient to the movement of the capillary water. They concluded that the contribution of the capillary pressure gradient far exceeds the contribution of the total pressure gradient. Therefore this effect is neglected.

It can be concluded from the above that, the transfer coefficient for the liquid moisture movement (moisture conductivity) that is used in

the present model is a strong function of moisture content and temperature. Haertling [H3] groups these influences into two separate functions. A general form of the moisture conductivity can be written as:

$$\kappa = \kappa_0 \left(\frac{\eta}{\eta_0}\right)^a \left(\frac{T}{T_0}\right)^b \quad (191)$$

The constants a and b must be determined experimentally.

The moisture conductivity for capillary movement is proportional to the ratio of the surface tension to the dynamic viscosity [K9]. If the temperature-dependences of the surface tension and the dynamic viscosity are taken into account, then "a" lies between 6,5 and 7,5. For "b" Haertling chose a value of 0,5.

The liquid moisture moves in the inside of the material according to following equation:

$$\dot{m}_l = - \rho_{dp} \kappa \frac{\partial X}{\partial z} \quad (192)$$

## I.2 Moisture flow in the vapour phase in air drying

The flow of moisture in the vapour phase can be divided into diffusive flow and viscous flow. In the isothermal case, the diffusive flow occurs on the basis of a concentration gradient or partial pressure gradient, while the viscous flow occurs on the basis of a total pressure gradient. In the non-isothermal case, the vapour moisture is also moved by a temperature gradient. For the same reasons that the influence of the temperature gradient was neglected in the discussion of the capillary water movement, this influence is also neglected in the vapour movement.

The diffusion of vapour or gas through a network of capillaries can occur by two limiting diffusion mechanisms [E2,S5]:

- 1) Knudsen diffusion and
- 2) normal or Fickian diffusion

In Knudsen diffusion, the limiting mechanism is the collision of the molecules with the walls of the solid matrix. The mean free path of the molecules exceeds the diameter of the pores. The collision of molecules with each other is of minor importance. Therefore the diffusion of each species through the porous medium is independent of all other species in the gas phase.

In normal or Fickian diffusion the limiting factor is the collision of the molecules with each other. The mean free path of the molecules is smaller than the pore diameter. The diffusion of one species depends on the other species in the gas phase.

Obviously there is an interim regime in which the collisions between molecules and with the wall are both important. This regime is called the intermediate diffusion regime.

As the criterion for determining which diffusion regime applies, the ratio of pore diameter to mean free path of the molecules is used. This ratio is called the Knudsen number (Kn).

For $Kn > 10$	Normal or Fickian diffusion occurs
For $0,1 < Kn < 10$	Interim diffusion occurs
For $Kn < 0,1$	Knudsen diffusion occurs

For most gases at ordinary temperatures and pressures, the intermediate diffusion regime extends from pore diameters of  $5 \cdot 10^{-9}$  m up to  $5 \cdot 10^{-7}$  m. This diameter occurs in a number of materials and is of practical interest [S5].

Diffusion through porous media is formally analogous to diffusion through tubes [S5].

$$\dot{m}_i = - \rho_i D_{eff} \frac{\partial y_i}{\partial z} \quad (193)$$

The effective diffusion coefficient can be expressed by the diffusion coefficient divided by a diffusion resistance factor. The diffusion resistance factor may be divided into two parts [K9]. The first part,  $q$ , represents the ratio of the length of a straight tube with equiva

lent diameter having the same pressure drop as the material, to the thickness of the material. This part includes the detours a molecule must take compared with a straight path, as well as the geometry of the pores (dilatation, contraction, sharp edges, etc.). The second part,  $\Psi$ , is the ratio of the free area to the total area of the material.

$$\mu = \frac{\Psi}{q} \quad (194)$$

For normal diffusion, the diffusion coefficient of water vapour in air can be expressed by the following empirical correlation [S1]:

$$D_{no} = 2,263 \cdot 10^{-5} \left( \frac{p_0}{p} \right) \left( \frac{T}{T_0} \right)^{1,81} \quad (195)$$

For Knudsen diffusion, the diffusion coefficient can be described by the following equation [L4].

$$D_{Kn} = \frac{97}{2} \left[ \frac{T}{1000 \bar{M}} \right]^{0,5} d_{por} \quad (196)$$

In the intermediate diffusion regime, the diffusion coefficient may be determined by the Bosanquet interpolation formula [E2]:

$$D^{-1} = (D_{no})^{-1} + (D_{Kn})^{-1} \quad (197)$$

In the normal diffusion regime, the diffusion coefficient is inversely proportional to the pressure, whereas for Knudsen diffusion it is independent of pressure.

If there is a total pressure gradient in the porous medium, vapour moves by viscous flow, expressed by Darcy's law:

$$\dot{m}_i = - \rho_i \frac{K_g}{\eta_g} \frac{\partial p}{\partial z} \quad (198)$$

Wheeler [S5] showed that there must be appreciable total pressure gradients in pores of 10 to 1 000 Å if Poiseuille flow is of importance for the mass transfer. The pore sizes of the materials that are

used in this thesis fall in this region. Therefore in air drying, the diffusion mechanism is the prevalent mode of vapour transport.

At the beginning of drying, the pores are filled with water. The free diameter of the pores is small and Knudsen diffusion should prevail. At the end of drying, it will depend on the pore geometry as to which diffusion type prevails. In the early period, mass transfer based on vapour diffusion is small compared with mass transfer in the liquid phase. Therefore the real pore diameter (as opposed to the free pore diameter) can be chosen to determine the type of diffusion.

### 1.3 Moisture flow in the vapour phase in steam drying

In steam drying, diffusion does not exist. Steam moves through the pores of the medium under the influence of a total pressure gradient. In principle the flow of steam can occur in the laminar or turbulent regime.

For laminar flow, the vapour flux can be expressed by Darcy's law:

$$\dot{m}_s = - \rho_s \frac{K_s}{\eta_s} \frac{\partial p}{\partial z} \quad (199)$$

Applied to a tube and assuming the Hagen-Poiseuille velocity distribution, the following expressions for the steam flux are obtained:

$$\dot{m}_s = - \rho_s \frac{d_{por}^2}{32 \eta_s} \frac{\partial p}{\partial z} \quad (200)$$

or

$$\dot{m}_s = - \frac{d_{por}^2}{32 v_s} \frac{\partial p}{\partial z} \quad (201)$$

For gases,  $v$  increases only slightly with temperature. Therefore the mass flux is influenced mainly by the pressure gradient. Analogous to the diffusion transfer coefficient, the permeability can be corrected by a resistance factor including the tortuosity.

For turbulent flow, Darcy's law is not applicable. In the drying processes of porous media, only small Reynolds numbers are expected. The laminar region extends up to Reynolds numbers of 2 300. At 100 kPa, the viscosity of steam is  $1,2 \cdot 10^{-5}$  Pa s and the density  $0,6 \text{ kg m}^{-3}$ . This means that for pores smaller than  $10^{-3} \text{ m}$ , the steam velocity has to be higher than  $46 \text{ m s}^{-1}$  to reach turbulent flow. Therefore we can assume that in capillary porous bodies laminar flow exists.

Another possibility of movement is the molecular flow [L4], which is analogous to the Knudsen diffusion and occurs in very narrow pores. In this case, the transfer coefficient can be expressed by:

$$m_s = - \dot{\rho}_s \frac{97}{2} \sqrt{\frac{T}{1000 M_s}} d_{\text{por}} \frac{1}{p} \frac{\partial p}{\partial z} \quad (202)$$

#### 1.4 Heat transfer in capillary porous bodies

Heat is transferred through wet porous materials by conduction through the different phases (solid, liquid, gas), by convection in the mobile phases (liquid, gas) and by radiation.

Luikov [L5] defines an equivalent thermal conductivity that incorporates all these effects.

Krischer and Kroll [K9] include a mechanism based on evaporation-condensation sequences in his description of the heat transfer. Although the thermal conductivity of the solid, liquid and gas phases varies only slightly with temperature, the thermal conductivity due to evaporation-condensation increases exponentially with temperature.

By dividing the wet body into two regions, the first containing the previously mentioned manners of heat transfer in parallel, and the second containing them in series, Krischer was able to determine the thermal conductivity of bricks as a function of temperature and moisture content.

At low temperatures, the evaporation-condensation mechanism can be neglected and the thermal conductivity of the wet body falls between the thermal conductivities of the completely wet and completely dry bodies. As temperatures increase, the evaporation-condensation mechanism gains in importance and the thermal conductivity of the wet body first increases with decreasing moisture content and then decreases to the thermal conductivity of the completely dry body. At higher temperatures ( $>80^{\circ}\text{C}$ ), the influence of the temperature on the thermal conductivity increases considerably. Although Krischer attributes this to the increased activity of the evaporation-condensation mechanism, Luikov [L5] attributes it to the increasing importance of the radiative heat transfer.

The convective component of heat transfer is small in comparison with the conductive component, provided that the equivalent Reynolds number is smaller than 20 [L5]. In most cases of mass transfer in capillary porous bodies,  $Re_{eq} \ll 1$ . Therefore the convective heat transfer is neglected compared with the conductive heat transfer. If the pore diameter is small ( $d < 10^{-5} \text{ mm}$ ), the radiative component may be neglected as well [L5]. Therefore we can assume that in the materials being tested here, heat transfer occurs mainly by conduction.

At the early stages of drying, the material is very wet and the heat conductivity is high. The rate-limiting step for drying is the external heat and mass transfer. In the later stages of drying, the heat conductivity through the dried material is the limiting factor. Therefore, according to Krischer [K9], it is not necessary to know the exact thermal conductivity through partially wet materials as this is never the limiting step.

In summary, the heat conducted through the wet skeleton can be described by Fourier's law:

$$\dot{q} = - \lambda_{\text{eff}} \frac{\partial T}{\partial z} \quad (203)$$

$\lambda_{\text{eff}}$  is the effective heat conductivity of the wet material and depends on the temperature and strongly on the moisture content.



## I.5 Comparison of the transfer coefficients in air and in steam

The magnitude of the transfer coefficients in air and in steam is compared below. It is assumed that vapour moisture moves on the basis of a partial pressure gradient in air (diffusion) and of a total pressure gradient in steam (molar flow). Diffusion is divided into normal diffusion and Knudsen diffusion, whereas molar flow is divided into viscous flow and molecular flow. The liquid moisture moves in both media on the basis of a moisture content gradient.

In Table 11, the transfer coefficients are presented as functions of the temperature and the pore diameter. The density of the moving species is included in these transfer coefficients, so that they only need to be multiplied by the driving force to give the mass transfer rate. This simplifies the comparison.

The transfer coefficients for air are determined at the wet-bulb temperature, whereas the transfer coefficients for steam are determined at the boiling point. During the constant drying rate period, these temperatures will be the particle temperatures. Even though the internal moisture movement is not the limiting mechanism at that stage, it still determines the critical moisture content and is therefore of importance.

The boiling point is only a function of the pressure in the system and does not change with the temperature of the drying medium. This is why the transfer coefficients in steam do not change with an increase in external temperature.

For the first two pore diameters (15 and 100 Å), diffusion occurs in the intermediate regime, whereas for the last one (1000 Å), normal diffusion prevails. Therefore the Knudsen diffusion term and the molecular flow term are not valid at the high diameter.

The Knudsen diffusion and molecular diffusion terms decrease with increasing temperature. The reason is that the transfer coefficients in this regime are proportional to the square root of the temperature. As, in this comparison, the transfer coefficients were multiplied by the density, which is inversely proportional to the temperature, the resulting term decreases with an increase in temperature.

Table 11: Comparison of the transfer coefficients in air and in steam

Temperature			Pore dia- meter	Normal diffu- sion	Viscous flow	Knudsen diffu- sion	Molecu- lar flow	Capillary flow	
Gas	Particle			Air	Steam	Air	Steam	Air	Steam
	Air	Steam							
°C	°C	°C	nm	s 10 <sup>+10</sup>	s 10 <sup>+10</sup>	s 10 <sup>+10</sup>	s 10 <sup>+10</sup>	kg/(ms)	kg/(ms)
100	28,5	96	15	2,191	0,003	0,214	0,193	2,78 10 <sup>-8</sup>	11,4 10 <sup>-8</sup>
			100	2,191	0,135	1,425	1,288	2,78 10 <sup>-8</sup>	11,4 10 <sup>-8</sup>
			1000	2,191	13,509	14,251	12,885	2,78 10 <sup>-8</sup>	11,4 10 <sup>-8</sup>
150	36,0	96	15	2,236	0,003	0,211	0,193	3,31 10 <sup>-8</sup>	11,4 10 <sup>-8</sup>
			100	2,236	0,135	1,407	1,288	3,31 10 <sup>-8</sup>	11,4 10 <sup>-8</sup>
			1000	2,236	13,509	14,075	12,885	3,31 10 <sup>-8</sup>	11,4 10 <sup>-8</sup>
200	42,3	96	15	2,272	0,003	0,209	0,193	3,80 10 <sup>-8</sup>	11,4 10 <sup>-8</sup>
			100	2,272	0,135	1,393	1,288	3,80 10 <sup>-8</sup>	11,4 10 <sup>-8</sup>
			1000	2,272	13,509	13,935	12,885	3,80 10 <sup>-8</sup>	11,4 10 <sup>-8</sup>
250	47,7	96	15	2,304	0,003	0,207	0,193	4,29 10 <sup>-8</sup>	11,4 10 <sup>-8</sup>
			100	2,304	0,135	1,382	1,288	4,29 10 <sup>-8</sup>	11,4 10 <sup>-8</sup>
			1000	2,304	13,509	13,817	12,885	4,29 10 <sup>-8</sup>	11,4 10 <sup>-8</sup>
300	52,6	96	15	2,332	0,003	0,206	0,193	4,76 10 <sup>-8</sup>	11,4 10 <sup>-8</sup>
			100	2,332	0,135	1,371	1,288	4,76 10 <sup>-8</sup>	11,4 10 <sup>-8</sup>
			1000	2,332	13,509	13,713	12,885	4,76 10 <sup>-8</sup>	11,4 10 <sup>-8</sup>

A similar temperature effect is expected for the viscous flow. As the temperature for determining the coefficients in steam was fixed (boiling point), the temperature-dependence of this term cannot be seen. The viscous flow coefficient is inversely proportional to the dynamic viscosity. With increasing temperature, the dynamic viscosity of gases increases and the viscous flow coefficient decreases. In addition, a temperature increase results in a density decrease. The density decrease is however weakened, as an increase in temperature would also induce an increase in the total pressure (at least above the critical moisture content), which would counter the decreasing influence of the temperature.

One error that was made in Table 11 is that the normal diffusion coefficient was used instead of the effective diffusion coefficient, which is corrected for the influence of the inner structure of the material on the transfer of moisture. Therefore it appears that the effective normal diffusion term is independent of the pore diameter, which it is not. In general, the diffusion resistance is determined experimentally, therefore it was not included in these calculations.

The term for viscous flow is proportional to the square of the pore diameter. This explains the large variation with the pore diameter. For large pore diameters, the normal diffusion term is smaller than the viscous flow term.

In the Knudsen diffusion regime, the molecular flow is smaller than the Knudsen diffusion term. This is a result of the higher temperature in steam.

The term for capillary movement of moisture is much higher in steam than in air and it can be expected that it is this influence, that increases the drying rate and also reduces the critical moisture content in steam drying.

APPENDIX J: CONVERSION OF EXPERIMENTALLY RECORDED  
DRYING RATE CURVES TO DESIGN CONDITIONS

(i) Influence of the fluidizing velocity

The fluidizing medium transfers heat to the particles only in a shallow layer close to the distributor plate. If the fluidizing velocity is increased, then the size of this layer increases, but the outlet temperature of the fluidizing medium remains the same. The amount of heat transferred to the particles, and hence the drying rate, is therefore proportional to the fluidizing velocity. The drying curve is recorded as moisture content versus time. The curve recorded at a given fluidizing velocity  $u_0$  can be converted to a different fluidizing velocity  $u_1$  by multiplying the time scale by the factor  $u_0/u_1$ .

(ii) Influence of the bed height

The fluidizing medium transfers the same amount of heat to the material irrespective of the bed height. Therefore the rate of drying in unit mass per time is constant. As the surface area of the particles is proportional to the height of the bed, the drying rate in unit mass per time is inversely proportional to the bed height. Therefore the drying rate curve recorded at a bed height  $H_0$  can be converted to a bed height  $H_1$  by multiplying the time scale by the factor  $H_1/H_0$ .

(iii) Influence of the bed temperature

As was mentioned earlier, the fluidizing medium transfers all its heat to the particles in a shallow layer close to the distributor plate. At the outlet of the bed, the drying medium is in thermal and mass equilibrium with the material.

In steam drying, the drying rate is determined from the heat transfer. The temperature of the steam at the outlet of the dryer is equal to the temperature of the material. During the constant drying rate

period, this temperature is equal to the boiling point. All the heat transferred to the material is used for drying. During the falling drying rate period, the temperature of the material is higher than the boiling point. The heat lost by the steam is then used only partially for drying.

Analogous to the method by Reay and Allan, it is assumed that the amount of heat used for evaporation is proportional to the free moisture content of the material. For the whole drying cycle in steam, the drying rate is proportional to the following ratio:

$$\frac{(T_{in} - T_{out})_1 (X - X_e)_1 (\Delta h_v)_2}{(T_{in} - T_{out})_2 (X - X_e)_2 (\Delta h_v)_1} \quad (204)$$

$T_{in}$  is the inlet temperature of the steam into the dryer,  $T_{out}$  is the outlet temperature of the steam and  $\Delta h_v$  is the heat of evaporation. This ratio is used to multiply the time scale on the drying rate curve.

(iv) Conversion from batch data to data for continuous operation

In a continuous operation, the bed temperature is constant. In a batch operation, the bed temperature is constant only during the constant drying rate period; it increases during the falling drying rate period. If the temperature increase of the bed with time is known, the batch data can be converted to continuous data. For this, the batch drying curve is divided into small time increments. It is assumed that during an incremental time step  $t_1$  the bed temperature in the batch test is constant and equal to the arithmetic mean temperature. Then, for each incremental time step, the batch curve is converted in the manner described in the previous paragraph.

(v) Determination of the mean moisture content of the product in a fluidized-bed dryer

In a continuous fluidized-bed dryer, the bed temperature remains constant. The residence time of the individual particles in a well-mixed fluidized bed is different for each particle.

As the residence time of individual particles varies, the moisture content varies as well. The particles that remain in the bed for a short time are still wet and the particles that remain in the bed for a long time are drier than average. It is reasonable to expect that such particles will have different temperatures. Particles with a moisture content higher than the critical moisture content are at the wet-bulb temperature and particles with a moisture content lower than the critical moisture content are at a higher temperature, as determined by their free moisture content according to:

$$T = T_{wb} \frac{x}{x_{cr}} + T_{out} \frac{(x_{cr} - x)}{x} \quad (205)$$

$T_{wb}$  is the wet-bulb temperature which is equal to the particle temperature during the constant drying rate period, and  $x_{cr}$  is the critical moisture content.

The bed temperature of the dryer is preset. The inlet temperature of the drying medium is then determined from an energy balance around the dryer. The recorded drying rate curve is converted to the given bed temperature.

The mean residence time of the material is increased until the mean moisture content determined by Equation 106 is lower than the specified remaining moisture content of the material.

In Figures 120 and 121, the conversions with respect to temperature are shown for the moisture content evolution for the drying of molecular sieve in air and in steam.

In the constant drying rate period (i.e. low drying times), the conversion works very well and the data for the three temperatures fall together. In the falling drying rate period, there is a slight discrepancy. For the two low temperatures (125 and 200 °C), there is agreement, but for the high temperature, the drying time is underestimated. The reason herefore is probably the calculation of the drying time over the energy balance, where no consideration of the sorption energy is taken. The same pattern can be seen for air and for steam, but it is more apparent for air. As basis for the conversion, the

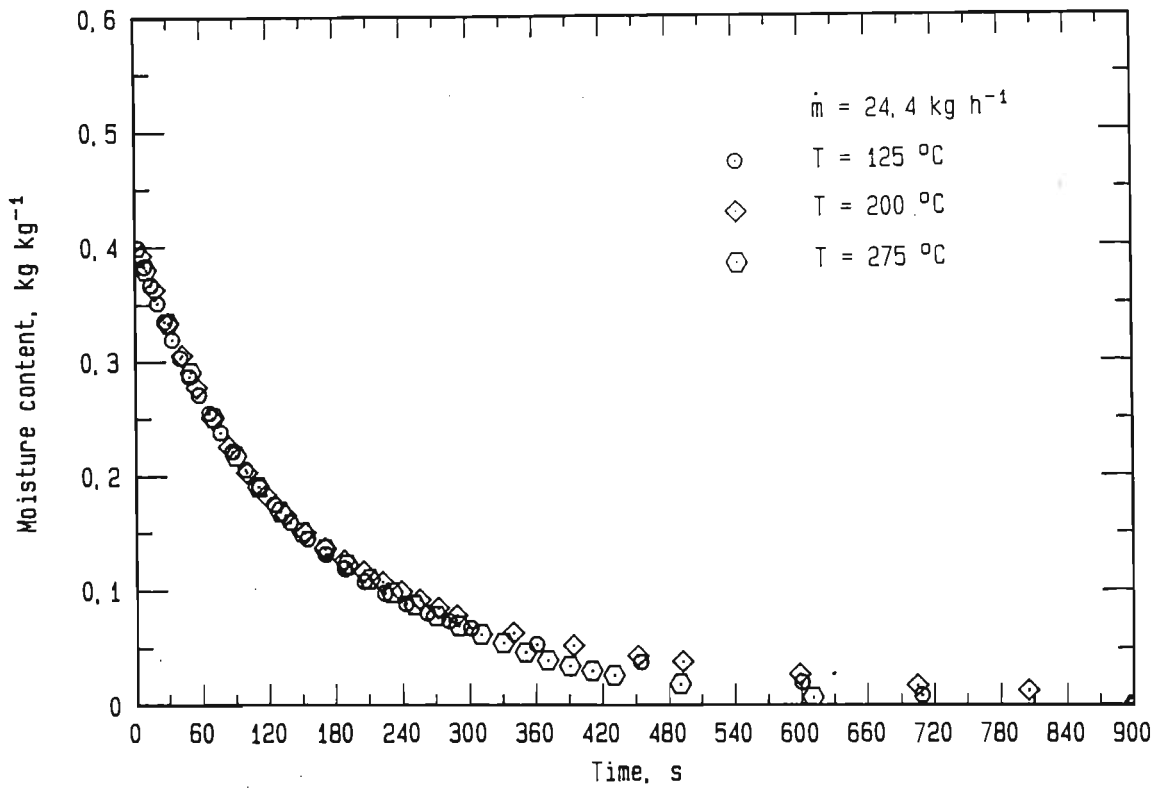


Figure 120: Drying rate conversion over temperature for molecular sieve in air

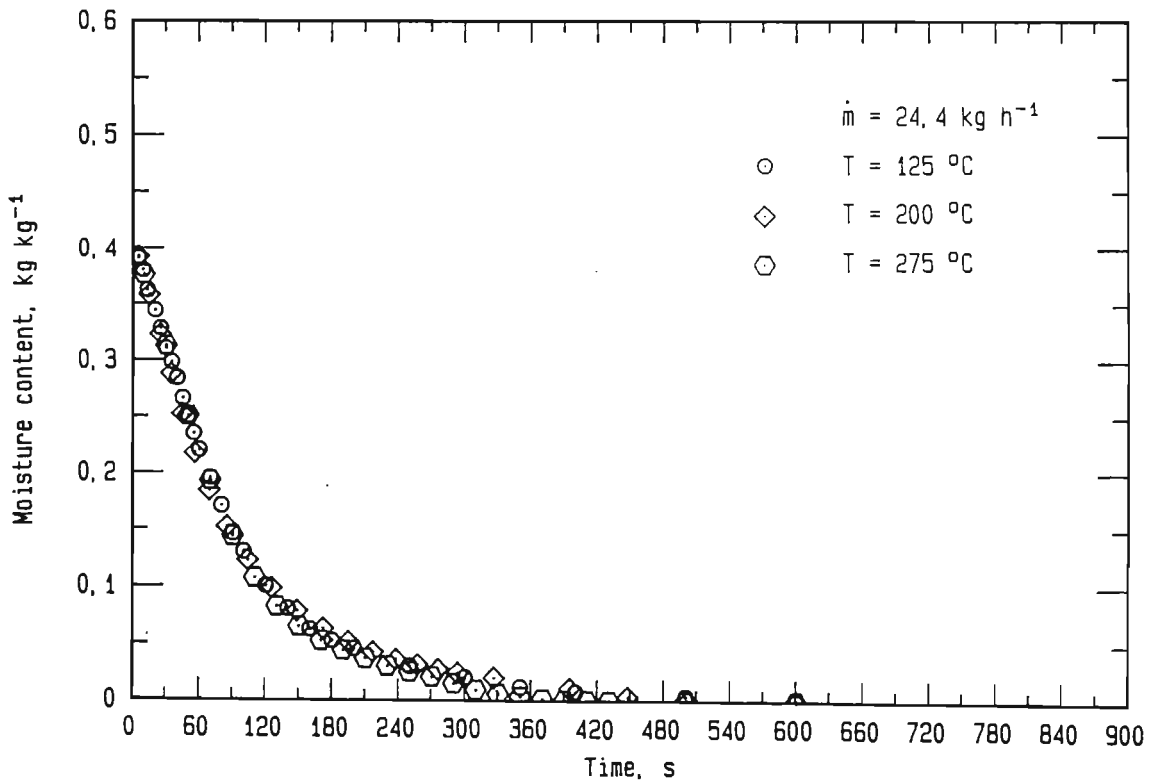


Figure 121: Drying rate conversion over temperature for molecular sieve in steam

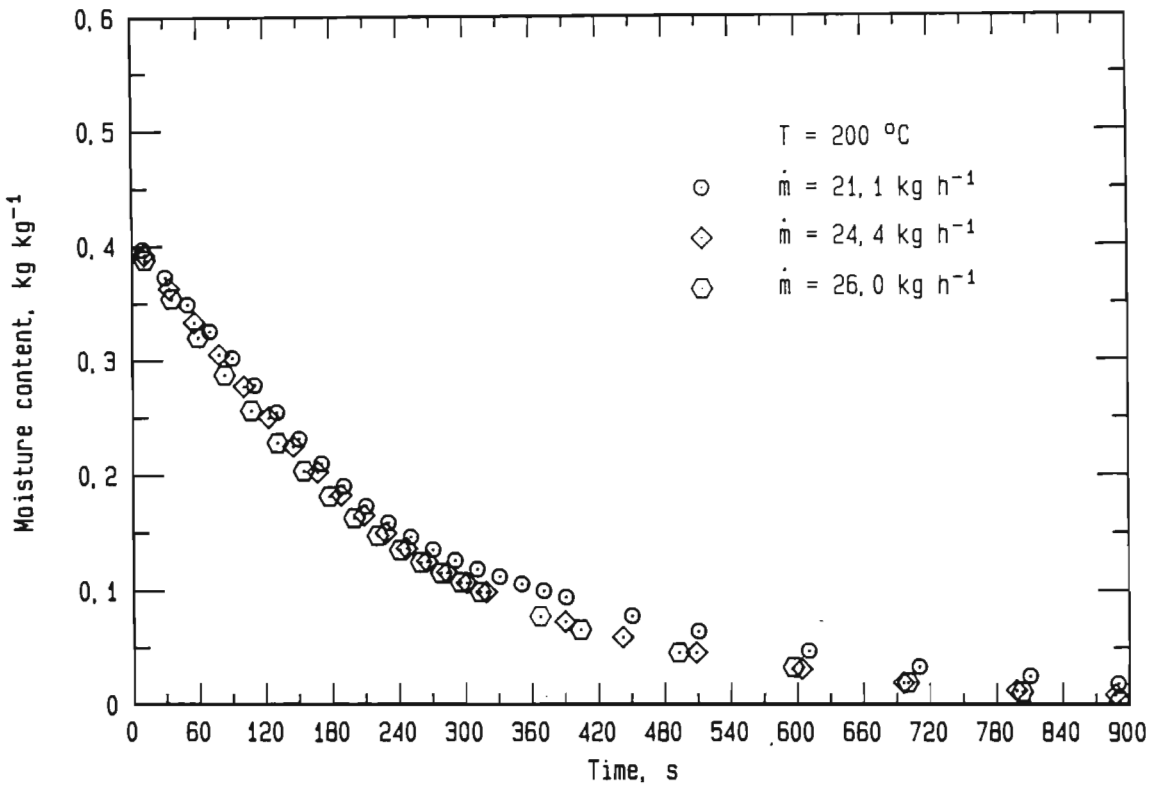


Figure 122: Drying rate conversion over mass flow rate for molecular sieve in air

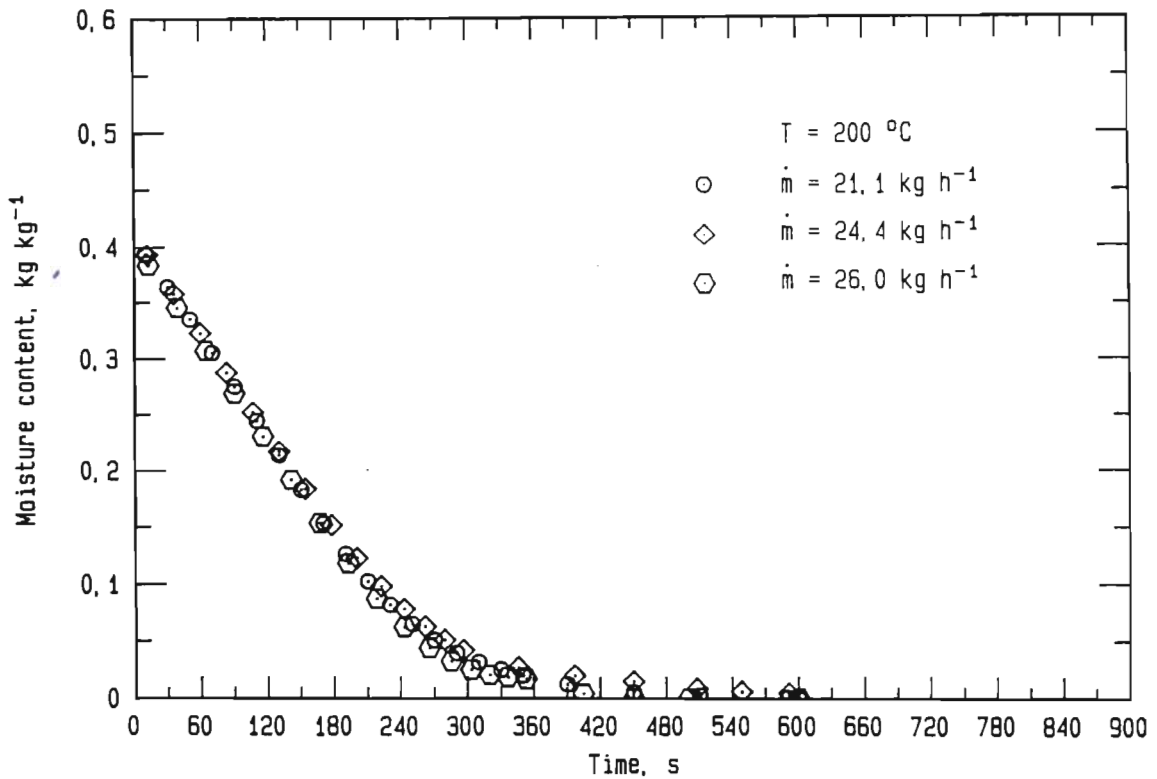


Figure 123: Drying rate conversion over mass flow rate for molecular sieve in air



drying rate at 225 °C was taken. The extrapolation from this temperature stretches over 100 °C. For such a high conversion range, the agreement between the calculated data is extremely good.

In Figures 122 and 123, the conversions with respect to flow rate of the drying medium are shown for the moisture content evolution for the drying of molecular sieve in air and in steam.

Again, for steam the conversion data agree better than for air. The conversion with respect to mass flow rate does however not produce such good results as the conversion for temperature. The reason may be the inaccuracies in the mass flow rate measurement or the increase in the by-pass flow rate with increasing temperature.

In general, however, the conversion method using the heat transfer is a satisfactory basis for an economic analysis.

## APPENDIX K:

In this appendix, the forces acting on the fluidized bed dryer during a drying test are discussed. For a better understanding, the dryer is divided into 3 parts and for each part the forces that act on the flow of gas are marked as shown in Figure 124. The walls of the reactor are not included in this description.

The first part comprises the bottom section of the dryer, the second part the distributor plate and the fluidized bed and the third part the top section of the dryer.

The forces that act in the vertical direction on the gas in the top and in the bottom sections are:

- the impulse forces  $F_{i,1}$  and  $F_{i,2}$  and
- the pressure forces  $F_{p,1}$  and  $F_{p,2}$ .

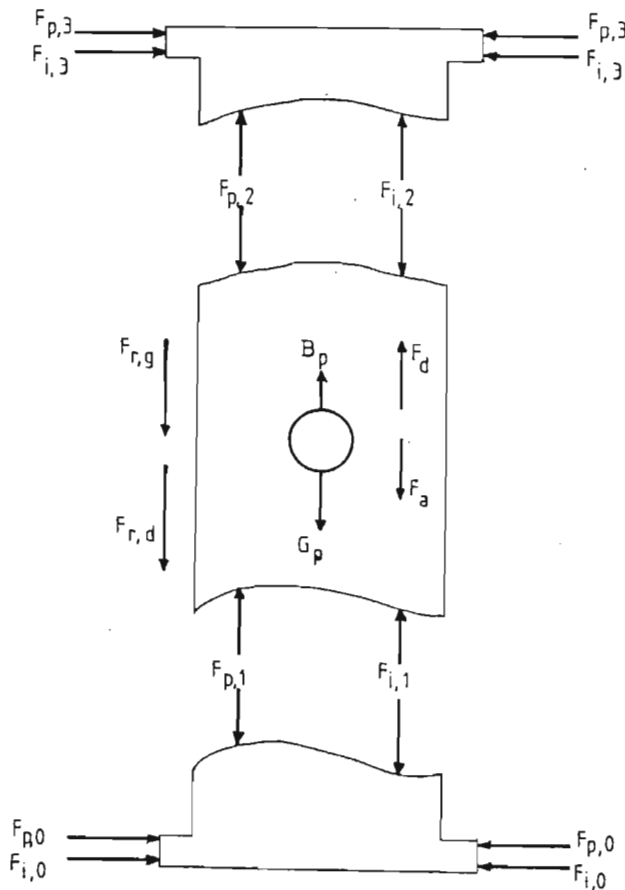


Figure 124: Forces acting on the flow of gas in a fluidized bed

In the top section and the bottom section, the friction forces from the walls of the reactor and the weight of the gas volume are neglected.

The impulse forces can be written as the product of the mass flow rate of gas and the velocity:

$$F_i = \dot{m}_i u_i \quad (206)$$

The pressure forces can be written as the product of the pressure and the area:

$$F_p = p A \quad (207)$$

An equal amount of gas enters or leaves the dryer from opposite sides. As a result the horizontal components of the acting forces counterbalance.

In the bottom part, a downwards directed force pushes onto the flowing gas. This force is equal to the sum of the pressure force  $F_{p,1}$  and the impulse force  $F_{i,1}$ . The impulse force does not change during a drying test, as the mass flow rate and the velocity are kept constant. The pressure force varies as drying proceeds.

In the top section of the dryer, an upwards directed force acts on the flowing gas. This force is equal to the sum of the pressure force  $F_{p,2}$  and the impulse force  $F_{i,2}$ . The impulse force changes during drying, as the mass flow of gas changes with a change in drying rate. The pressure force,  $F_p$ , changes only slightly during drying due to a change in friction force in the top section of the dryer with a change in mass flow rate.

In the middle section of the fluidized bed, the forces that act on the top and bottom surfaces are the impulse forces,  $F_{i,1}$  and  $F_{i,2}$ , the pressure forces  $F_{p,1}$  and  $F_{p,2}$ . Due to the friction force  $F_{r,d}$  that the distributor plate exerts onto the flow of gas, a pressure drop is recorded over the distributor plate.

Above the distributor plate the flow of gas fluidizes the particles. The forces that act on the mixture of gas and solids are:

- the weight of the wet particles  $G_p$ ,
- the weight of the gas  $G_g$ ,
- the buoyancy of the particles  $B_p$ ,
- the friction forces of the walls of the dryer onto the flow of gas,  $F_{r,g}$  and the moving solids  $F_{r,p}$ ,
- the acceleration force,  $F_a$ , that accelerates the evaporated moisture to the velocity of the main gas stream, and
- the deceleration force,  $F_d$ , that decelerates the volume flow of gas.

The phenomenon of friction force  $F_{r,p}$  of the walls onto the particles is a very complex one. Small bubbles are created at the distributor plate. On their way upwards through the bed they coalesce to bigger bubbles and burst at the surface. As a consequence of the bubbling of the bed, the bed height is not constant and fluctuates around an average value. At one time there are therefore more particles flowing upwards than downwards and at the next time the opposite holds. Therefore the friction force of the walls of the dryer onto the particles is not constant over time. It is however reasonable to assume that this force fluctuates around an average value which is zero.

The evaporated moisture is accelerated to the velocity of the main gas stream. This is done by the acceleration force  $F_a$ . As drying proceeds,  $F_a$  changes with a change in evaporation rate.

On its flow through the bed of particles, the fluidizing medium cools down. As a result the volume flow is decelerated. This is taken into account by the deceleration force  $F_d$ .

In this discussion the pressure loss due to turbulence is neglected. If one assumes that this pressure loss is constant during the drying test, then it does not influence the drying rate measurement.

The momentum equation around the fluidized bed can be written as:

$$p_1 A_1 + \dot{m}_1 u_1 + B_p - p_2 A_2 - \dot{m}_2 u_2 - G_p - G_g - F_{r,d} - F_{r,g} - F_a + F_d = 0 \quad (208)$$

In Figure 125 the forces that act in the vertical direction on the fluidized bed dryer itself are marked.

On the bottom and top surfaces of the dryer act the pressure forces  $F_{p,b}$  and  $F_{p,t}$  and the impulse forces  $F_{i,b}$  and  $F_{i,t}$ . On the walls of the dryer act the friction forces  $F_{r,g}$  and on the distributor plate the forces  $F_{r,d}$ . The friction forces that the gas exerts onto the dryer walls and the distributor plate are equal and opposite to the friction forces of the dryer walls and distributor plate onto the gas. On the outside of the dryer acts the atmospheric pressure force,  $F_{p,a}$ . Obviously the weight of the dryer,  $G_d$ , pushes also onto the balance.

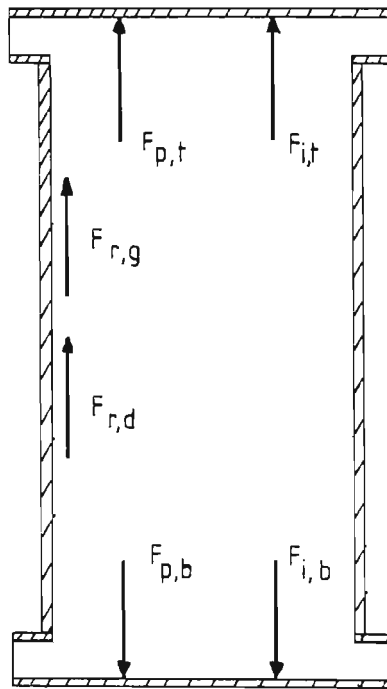


Figure 125: Forces acting on the fluidized bed

The sum of these forces is counterbalanced by the reaction force of the balance.

This can be written by Equation 209:

$$R = G_d + p_b A_b + \dot{m}_b u_b - p_t A_t - \dot{m}_t u_t - F_{r,d} - F_{r,g} \quad (209)$$

Here  $R$  is the resultant force acting on the balance

$G_d$  is the weight of the dryer and the distributor plate

$p_b$  is the over-pressure on the bottom of the dryer

$p_t$  is the over-pressure on the top of the dryer

$A_b$  is the area of the bottom of the dryer

$A_t$  is the area of the top of the dryer

$\dot{m}_b$  is the mass flow rate of gas at the bottom of the dryer

$\dot{m}_t$  is the mass flow rate of gas at the top of the dryer

$u_b$  is the gas velocity at the bottom of the dryer

$u_t$  is the gas velocity at the top of the dryer

$F_{r,d}$  is the friction force onto the distributor plate

$F_{r,g}$  is the friction force onto the walls of the dryer

With Equation 208 where subscript 1 means the bottom and subscript 2 means the top of the dryer, Equation 209 can be simplified to:

$$R = G_d + G_p + G_g - B_p + F_a - F_d \quad (210)$$

The acceleration force can be written as :

$$F_a = \dot{m}_{ev} u_t \quad (211)$$

The deceleration force can be written as :

$$F_d = \dot{m}_b u_b - \dot{m}_b u_t \quad (212)$$

The difference between the acceleration force and the deceleration force is equal to the change of momentum of the flowing gas.

The reaction force of the balance can then be written as:

$$R = G_d + G_p + G_g - B_p + \dot{m}_b u_b - \dot{m}_t u_t \quad (213)$$

In the evaluation of the experimental drying tests the change of the reaction force with time was taken as the drying rate. From Equation 213 it becomes apparent that an error is introduced in the drying rate by making this assumption. In the following, this error is evaluated.

During the constant drying rate period, the only force that changes as function of time is the weight of the particles  $G_p$  and the drying rate is equal to the change in the balance reading with time. During the falling drying rate period, all the forces, except the weight of the dryer  $G_d$ , change with time. In order to evaluate the effect of this change on the drying rate, the various forces are evaluated in Table 12 for alumina and molecular sieve at the highest mass flow rate and the highest temperature used in the experiments. Under these conditions the changes are highest. The forces are given in gp (gramme-power) at the beginning of the falling drying rate period (subscript 0) and at the end of drying (subscript f). The difference between impulse force on the bottom and on the top is marked by  $d(\dot{m} u)$ .

Table 12 Evaluation of the time variable forces at the beginning and at the end of a drying test  
(forces in gramme-power)

Test	$G_g, 0$	$G_g, f$	$B_p, 0$	$B_p, f$	$d(\dot{m} u)_0$	$d(\dot{m} u)_f$
Alumina Air, 275°C	4,152	2,594	0,351	0,207	0,233	0,000
Alumina Steam, 275°C	2,284	1,610	0,191	0,128	0,114	0,000
Mol. sieve Air, 275°C	4,230	2,640	0,273	0,161	0,319	0,000
Mol. sieve Steam, 275°C	2,326	1,639	0,148	0,100	0,151	0,000

The change in the weight of the gas with time results in the change of the temperature drop between inlet and outlet of the dryer. At the start of the falling drying rate period, the temperature falls from the inlet temperature to the wet-bulb temperature in air or the boiling temperature in steam. At the end of drying, there is virtually no temperature difference between inlet and outlet of the dryer.

The change of buoyancy with time results from the change of the density of the drying medium in the fluidized bed with a change in temperature and, for air, also in humidity.

The change of the impulse force with time results in the change of the drying rate and of the temperature drop over the dryer.

The change of buoyancy or of impulse force is small compared to the change in gas weight.

Table 13 Error in the drying rate due to  
the change of gas weight with time

Test	Constant dr. rate g s <sup>-1</sup>	Moisture content %	Error %
Alumina Air, 275°C	0,745	27,5 6,5 1,5 0,2	1,1 2,3 4,6 11,6
Alumina Steam, 275°C	1,069	27,5 6,0 1,3 0,2	0,3 0,7 1,4 3,5
Mol. sieve Air, 275°C	0,770	27,5 13,0 7,5 1,0	1,1 2,3 4,6 11,5
Mol. sieve Steam, 275°C	1,290	25,0 9,0 5,0 1,0	0,5 1,0 2,0 4,9



If the change of gas weight is spread evenly over three minutes (the duration of the falling drying rate period at the test conditions), then the influence of this change on the drying rate can be evaluated. The error in the drying rate due to the change of gas weight is given in Table 13 for the drying of alumina and molecular sieve in air and in steam.

The relative error increases as drying proceeds. For alumina the error is relatively small ( $<4,6\%$ ) until very low ( $1\%$ ) moisture contents. For the largest part of the falling drying rate period (until  $6\%$  moisture content) the error is less than  $2\%$  in air drying and less than  $1\%$  in steam drying. This error can be neglected.

For molecular sieve the error is higher. But still, in steam drying of molecular sieve the error is less than  $2\%$  until moisture contents of  $5\%$ . In air drying of molecular sieve the error is less than  $4,6\%$  until moisture contents of  $7,5\%$ . The falling drying rate period starts at  $27,5\%$  moisture content, so that it is only for the last quarter of this period that higher errors occur. However, during this quarter the drying rates are small and it is doubtful whether more information can be gained by converting the drying rates for this period.

In the economic analysis between air drying and steam drying, recorded drying rate curves at the temperature of  $225\text{ }^{\circ}\text{C}$  were used for the dimensioning of the dryer. The errors resulting from the use of these curves are roughly halve the ones presented in Table 13.

## LITERATURE

- [A1] Akao, T.  
Fukurawa, T. and  
Watanabe, H. "Superheated steam drying for deodorization"; Proc. Third Int. Drying Symp., vol. 1, pp. 285-294, Birmingham, 1982.
- [A2] Allardice, D.J.  
and Evan, D.G. "The brown coal/water system: Part 1. The effect of temperature on the evolution of water from brown coal"; pp. 201-210, Fuel, vol. 50, 1971.
- [B1] Baker, C.G.J.  
and Reay, D. "Energy usage for drying in selected U.K. industrial sectors"; Proc. Third Int. Drying Symp., vol. 1, pp. 201-209, Birmingham, 1982.
- [B2] Basel, L. and  
Gray, E. "Superheated solvent drying in a fluidized bed"; Chem. Eng. Prog., vol. 58, no. 6, pp. 67-70, 1962.
- [B3] Beeby, C. and  
Potter, E. "Steam drying"; Proc. Fourth Int. Drying Symp., vol. 1, pp. 51-68, Kyoto, 1984.
- [B4] Benstead, R. "Steam compression drying"; Proc. Third Int. Drying Symp., vol. 1, pp. 274-294, 1982.
- [B5] Berger, D.  
and Pei, D.C.T. "Drying of hygroscopic capillary porous solids. A theoretical approach"; Int. J. Heat Mass Transf., vol. 16, pp. 293-302, 1973.
- [B6] Bixler, N.E.  
Eaton, R.R. and  
Russo, A.J. "Drying analysis of a multiphase, porous-flow experiment in fractured volcanic tuff"; ASME/JSME/ISES Solar Energy Conf., vol. 87, no. 20, Honolulu, 1987.
- [B7] Brakel, J. van "Mass transfer in convective drying"; Advances in drying, vol. 1, pp. 217-267, Hemisphere/McGraw-Hill, Auckland, 1980.
- [B8] Brakel, J. van "Pore space models for transport phenomena in porous media"; Powder Technology, no 11, pp. 205-236, 1972.
- [B9] Bronstein, I.N. and  
Semendjajew, K.A. "Taschenbuch der Mathematik", 13. Auflage, Verlag Harri Deutsch, Zurich, 1973.
- [B10] Buckingham, E. U.S. Dept. Agr., Bur. Soils, Bull., vol. 38, 1907.
- [B11] Bennet, K.F. "Energy utilization in South Africa", Department of Planning and Environment.

- [B12] British Institution of Chemical Engineers, Solids Drying Group "Research development priorities for solids drying and related heat treatment operations", 1982.
- [C1] Cairns, R.C. and Roper, G.H. "Heat and mass transfer at high humidities in a wetted wall column"; Chem. Eng. Sci., vol. 3, pp. 97-109, 1954.
- [C2] Cary, J.W. and Taylor, S.A. "Thermally driven liquid and vapour phase transfer of water and energy in soil"; Soil Sci. Soc. Am. Proc., vol. 26, pp. 417-420, 1962.
- [C3] Ceaglske, N.H. and Hougen, O.A. "Drying granular solids"; Eng. Chem., vol. 29, no. 7, pp. 805-813, 1937.
- [C4] Chazal, M. de Chi Leung, P. Rosen, H.N. and McGinnes Jr., E.A. "Corrosion studies in pressure steam drying of lumber." Proc. Fourth Int. Drying Symp., vol. 1, pp. 668-673, Kyoto, 1984.
- [C5] Chemical Engineering Research Group "Energy conservation in the South African process industry by drying with superheated steam"; CERG Memo 85/11, CSIR, Pretoria, July 1985.
- [C6] Chen, C.C. "Effect of particle to particle heat transfer on continuous fluidized bed dryers"; Proc. Nat. Sci. Council, no. 8, part 3, Taiwan, May 1975.
- [C7] Chow, L.C. and Chung, J.N. "Evaporation of water into a laminar stream of air and superheated steam". Int. J. Heat Mass Transf., vol. 26, no. 3, pp. 373-380, 1983.
- [C8] Chu, J.C. Lane, A.M. and Conklin, D. "Evaporation of liquids into their superheated vapors"; Ind. Eng. Chem., vol. 45, no. 7, pp. 1586-1591, 1953.
- [C9] Chu, J.C. Finnelt, S. Hoerrner, W. and Lin, M.S. "Drying with superheated steam-air mixtures"; Ind. Eng. Chem., vol. 51, no. 3, vol. 1, pp. 275-280, 1959.
- [C10] Crowe, C.T. Chow, L.C. and Chung, J.N. "An assessment of steam operated spray dryers"; Proc. Fourth Int. Drying Symp. pp. 369-377, Kyoto, 1984.
- [C11] Covington, R.O. "Steam stream drying"; Drying Technology, vol. 3, no. 4, pp. 501-515, 1985.
- [C12] Cui, W.K. Douglas W.J.M. and Mujumdar, A.S. "Impingement steam drying of paper"; Drying Technology, vol. 3, no. 2, pp. 307-320, 1985.

- [D1] Danilov, O.L. and Leonchik, B.I. "Advantages of using superheated steam at atmospheric pressure in drying processes"; J. Eng. Phys., vol. 13, no. 3, pp. 283-288, 1967.
- [D2] Davidson, J.F. and Harrison, D. "Fluidization"; Academic Press, London, 1971.
- [E1] Emmett, R.C. Jr and Dahlstrom, D.A. "Steam drying of filter cake", Chem. Eng. Prog., vol. 68, no. 1, pp. 51-55, January 1972.
- [E2] Evans, R.B. Watson, G.M. and Mason, E.A. "Gaseous diffusion in porous media at uniform pressure"; J. Chem. Phys., vol. 35, no. 6, pp. 2076-2083, December 1961.
- [E3] Evans, R.B. Watson, G.M. and Mason, E.A. "Gaseous diffusion in porous media. II. Effect of pressure gradients"; J. Chem. Phys., vol. 36, no. 7, pp. 1894-1902, 1962.
- [F1] Faber, E.F. "Superheated steam drying. A literature review"; CSIR Report CENG 570, Pretoria, July 1985.
- [F2] Faber, E.F. Heydenrych, M.D. Seppä, R.U.I. and Hicks, R.E. "A techno-economic comparison of air and steam drying"; Proc. Fifth Int. Drying Symp., vol. 2, p. 588, Boston, 1986.
- [F3] Faber, E.F. and Heydenrych, M.D. "Techno-economic comparison of drying with steam or air in fluidized beds"; CSIR Report CENG 653, Pretoria, 1987.
- [F4] Feuga, J.R. and Massot J.C. "Sechage a la Vapeur d'Eau Surchauffee avec C.M.V. - Application a la Luzerne et a la Pulpe de Betterave. Version 3.", EDF Direction des Etudes et Recherches, HE 142 W 2161, 1984.
- [F5] Frame, G.B. Galland, K.V. and Svensson, C. "Steam drying of industrial and agricultural products and wastes"; Energy Progress, vol. 3, no. 1, pp. 36-39, March 1983.
- [G1] Gauvin, W.H. and Costin, M.H. "Spray drying in superheated steam. A techno-economic study"; Drying 80, vol. 1, pp. 320-331, Ed. A S Mujumdar, 1980.
- [G2] Gupta, S.N. Chaube, R.B and Upadhyay, S.N. "Fluid-particle heat transfer in fixed and fluidized beds." Chem. Eng. Sci., vol. 29, pp. 839-843, 1972.
- [H1] Hadley, G.R. "Theoretical treatment of evaporation front drying"; Int. J. Heat Mass Transf., vol. 25, no. 10, pp. 1511-1522, 1982.

- [H2] Hadley, G.R. "Numerical modelling of the drying of porous materials"; Proc. Fourth Int. Drying Symp., vol. 2, pp. 151-158, Kyoto, 1984.
- [H3] Haertling, M. "Messung und Analyse von Trocknungsverlaufskurven als Grundlage zur Vorausberechnung von Trocknungsprozessen"; Ph.D. thesis, University of Karlsruhe, 1978.
- [H4] Harmathy, T.Z. "Simultaneous moisture and heat transfer in porous systems with particular reference to drying"; Ind. Eng. Chem. Fund., vol. 8, no 1, pp. 92-103, February 1969.
- [H5] Hausbrand, E. "Drying by means of air and steam"; Third revised English edition, Scott, Greenwood & Son, London, 1924.
- [H6] Heertjes, P.M.  
de Boer, H.G.J. and  
de Haas van  
Dorsser, A H. "Temperature and humidity measurements in a drying fluidized bed"; Chem. Eng. Sci., vol. 2, no. 3, pp. 97-107, June 1953.
- [H7] Heertjes, P.M. and  
McKibbins, S W. "The partial coefficient of heat transfer in a drying fluidized bed"; Chem. Eng. Sci., vol. 5, pp. 161-167, 1956.
- [H8] Hilmart, S. and  
Gren, U. "Steam drying of wood residues - An experimental study"; Paper presented at the Sixth International Drying Symposium, Boston MA, 1986.
- [H9] Hoebink, J.H.B.H. "Drying granular solids in a fluidized bed", Ph.D. thesis, Technical University Eindhoven, 1977.
- [H10] Hyodo, T. and  
Yoshida, T. "An experimental study of a closed circuit dryer"; Mech. Eng. Trans., Inst. Eng. Australia, 1976.
- [I1] Imakoma, H.  
Okazaki, M. and  
Toei, R. "Mathematical model for drying of adsorptive porous materials"; Acta Polytechnica Scandinavica, Chemical Technology and Metallurgy, Series no. 160, Helsinki, 1985.
- [K1] Kaumann, W.G. "Equilibrium moisture content relations and drying control in superheated steam drying"; Forest Products Journal, pp. 328-332, September 1956.
- [K2] Keey, R.B. "Drying: Principles and practice"; Pergamon Press, 1972.

- [K3] Keey, R.B. "Progress towards understanding the drying behaviour of materials"; Proc. Third Int. Drying Symp., vol. 1, pp. 7-21, Birmingham, 1982.
- [K4] Keogh A.J. and Potter, O.E. "Drying high-moisture coals before liquefaction or gasification"; Fuel Process Technology, vol. 4, pp. 217-227, 1981.
- [K5] Kettenring, K.N. Manderfield, E.L. and Smith, J.M. "Heat and mass transfer in fluidized systems"; Chem. Eng. Prog., vol. 46, no. 3, pp. 139-145, 1950.
- [K6] Khokhar, M.I. and Mujumdar, A.S. "Fluid bed drying - Design considerations"; IE, Journal-CH, vol. 58, pp. 28-32, 1978.
- [K7] Klemm, H. Rogriguez-Giles, J. and Ruther, U. "Einflussgrossen bei der Trocknung von Druckerzeugnissen mit überhitztem Wasserdampf"; Das Papier, 38. Jahrgang, Heft 7, pp. 289-295, 1984.
- [K8] Knibbe, P.G. and Faber, E.F. "Energy-efficient drying with steam"; S.A. Journal of Science, vol. 83, no. 6, p. 331, June 1987.
- [K9] Krischer, O. and Kröll, K. "Die wissenschaftlichen Grundlagen der Trocknungstechnik"; Springer Verlag, Berlin, 1963.
- [K10] Krivsky, Z. and Vanecek, V. "The calculation of a fluid bed dryer by means of a computer"; Brit. Chem. Eng., vol 12, no. 12, pp. 1886-1889, December 1967.
- [K11] Kumada, T. Hirota, T. Tamura, N. and Ishiguro, R. "Heat and mass transfer with liquid evaporation into a turbulent air stream"; Letters in Heat and Mass Transfer, vol. 9, pp. 1-9, 1982.
- [K12] Kunii, D. and Levenspiel, O. "Fluidization engineering"; John Wiley and Sons Inc., New York, 1969.
- [K13] Kuramae, M. "On the vapour transfer rate in porous media under a temperature gradient", Proc. Fourth Int. Drying Symp., vol. 2, pp. 797-803, Kyoto, 1984.
- [K14] Kothari, A.K. M.S. Thesis, Illinois Institute of Technology, Chicago, 1967.
- [L1] Lane, A.M. and Stern, S. "Application of superheated-vapor atmospheres to drying"; Mech. Eng., vol. 78, no. 5, pp. 423-426, May 1956.
- [L2] Lee, K. and Ryley, D.J. Trans. ASME J. Heat Transf., vol. 90, pp. 445-451, 1968.

- [L3] Lebedev, P.D. "Heat and mass transfer during the drying of moist materials"; Int. J. Heat Mass Transf., vol. 1, pp. 294-301, 1961.
- [L4] Levenspiel, O. "Engineering flow and heat exchange."; Plenum, New York, 1984.
- [L5] Luikov, A.V. "Heat and mass transfer in capillary porous bodies"; Pergamon Press, Oxford, 1966.
- [M1] Martin, H. "Wärme- und Stoffübertragung in der Wirbelschicht"; Chem. Ing. Tech., vol. 52, no. 3, pp. 199-209, 1980.
- [M2] Massot, J.C. and Cardrain, L. "Essais de Séchage a la Vapeur d'Eau Surchauffée"; EDF Direction des Etudes et Recherches, HE 142 W 2257, 1985.
- [M3] Meel, D.A. van "Adiabatic convection batch drying with recirculation of air"; Chem. Eng. Sci., vol. 9, no. 1, pp. 36-44, 1958.
- [M4] Miller, W. "Energy conservation in timber-drying kilns by vapour recompression"; Forest Products Journal, vol. 27, no. 9, pp. 54-58, 1977.
- [M5] Milota, M.R. "Engineering study on the drying of wood particles in a fluidized bed"; Ph.D thesis, Oregon State University, February 1984.
- [M6] Moench, A.F. "An evaluation of heat transfer coefficients in moist porous media"; Ph.D. thesis, University of Arizona, 1969.
- [M7] Mosberger, E. "Über den Wärme- und Stoffaustausch zwischen Partikel und Luft in Wirbelschichten sowie über deren Ausdehnungsverhalten"; Ph.D. thesis, T.H. Darmstadt, 1964.
- [M8] Moyers Jr, C.G. "Drying of solution droplets in superheated vapor"; Proc. First Int. Drying Symp., pp. 224-229, Montreal, 1978.
- [M9] Moyne, C. and Degiovanni, A. "Importance of gas phase momentum equation in drying above the boiling point of water"; Proc. Fourth Int. Drying Symp., pp. 119-125, Kyoto, 1984.
- [M10] Menne, D.M. "Proposed action of the CERG in the field of drying", CERG Memo 77/20, 1970.

- [N1] Nomura, T. and Hyodo, T. "Behaviour of inversion point temperature and new applications of superheated vapour drying"; Proc. Fourth Int. Drying Symp., vol. 2, pp. 804-809, Kyoto, 1984.
- [N2] Novak, L.T. "Transport phenomena in porous media with emphasis on water movement in soils"; Ph.D. thesis, Michigan State University, 1972.
- [N3] Novak, L.T. and Coulman, G.A. "Mathematical models for the drying of rigid porous materials"; Can. J. Chem. Eng., vol. 53, pp. 60-67, 1975.
- [N4] Nuijens, P.G.J.M. "A simple digital filter for removing noise from data"; CERG Memo 86/18, CSIR, Pretoria, 1986.
- [P1] Palancz, B. "A mathematical model for continuous fluidized bed drying"; Chem. Eng. Sci., vol 38, no. 7, pp. 1045-1059, 1983.
- [P2] Phillip, J.R. and de Vries, D.A. "Moisture movement in porous materials under temperature gradients"; Trans. Am. Geophys. Union, vol. 38, no. 2, pp. 222-232, 1957.
- [P3] Poersch, W. "Wirbelschichttrockner. Schritte und Überlegungen zum Scale-up"; Aufbereitungstechnik, no. 4, pp. 205-218, 1983.
- [P4] Potter, O.E.  
Beeby, C.J.  
Fernando, W.J.N.  
and Ho, P. "Drying in steam heated steam fluidized beds"; Proc. Third Int. Drying Symp., vol 2, pp. 115-123, Birmingham, 1982.
- [P6] Prat, M. "Analysis of experiments of moisture migration caused by temperature differences in unsaturated porous medium by means of two-dimensional numerical simulation"; Int. J. Heat Mass Transf., vol. 29, no. 7, pp. 1033-1039, 1986.
- [R1] Reay, D. and Allen, R.W.K. "Predicting the performance of a continuous well-mixed fluidized bed dryer from batch tests"; Proc. Third Int. Drying Symp., pp. 130-140, Birmingham, 1982.
- [R2] Rosen, H.N. "Drying of lumber in superheated steam above atmospheric pressure"; AIChE Symp. Ser., vol. 77, p. 207, 1981.
- [S1] Schirmer, R. "Die Diffusionszahl von Wasserdampf-Luftgemischen und die Verdampfungsgeschwindigkeit"; Verfahrenstechnik, Beih. z. VDI, pp. 170-177, 1938.



- [S2] Schlünder, E.U. "Wärmeübertragung I"; Hochschulkurs, University of Karlsruhe, 1979.
- [S3] Schlünder, E.U. Chem. Ing. Tech., vol. 43, no. 11, pp. 651-654, 1971.
- [S4] Schlünder, E.U. "Fortschritte und Entwicklungstendenzen bei der Auslegung von Trocknern für vorgeformte Trocknungsgüter"; Chem. Ing. Tech., 48. Jahrgang, no. 3, pp. 190-198, 1976.
- [S5] Scott, D.S. and Dullien, F.A.L. "Diffusion of ideal gases in capillaries and porous solids"; AIChE Journal, vol. 8, no. 1, pp. 113-117, March 1962.
- [S6] Sherwood, T.K. "The drying of solids"; Ind. Eng. Chem., vol. 21, no. 1, January 1929.
- [S7] Svensson, C. "Steam drying of pulp"; Proc. Third Int. Drying Symp., vol. 1, pp. 301-307, Birmingham, 1982.
- [S8] Schlünder, E.U. "Wärmeübergang an bewegte Kugelschüttungen bei kurzfristigem Kontakt", Chemie. Ing.- Techn., no. 11, pp. 651-654, 1971.
- [T1] Toei, R.  
Imakoma, H.  
Tamon, H. and  
Okazaki, M. "Water transfer coefficient in adsorptive porous body"; J. Chem. Eng. Japan, vol. 16, no. 5, pp. 364-369, 1983.
- [T2] Trommelen, A.M. and Crosby, E.J. "Evaporation and drying of drops in superheated vapors"; AIChE Journal, vol. 16, no. 5, pp. 857-867, 1970.
- [T3] Tzimopoulos, C. and Sidiropoulos, E. "Coupled heat and moisture transfer in unsaturated porous bodies", Proc. Euro-mech. 143, pp. 169-172, Delft, 1981.
- [V1] Vanderschuren, J. and Delvosalle, C. "Bed-to-particle and interparticle heat transfer in the design of fluidized bed dryers"; Drying '82, Section II, pp. 48-54, Hemisphere Publishing Company, Montreal, 1982.
- [V2] Vanderschuren, J. and Delvosalle, C. "Particle-to-particle heat transfer in fluidized bed drying"; Chem. Eng. Sci., vol 35, pp. 1741-1748, 1980.
- [V3] Vanderschuren, J. "Batch simulation of continuous drying in fluidized bed"; Proc. Int. Drying Symp.,  
---

- [V4] Vanecek, V.R. Drbohlav, and Markvart, M. "Calculation of continuous fluidized bed drying equipment based on laboratory tests"; Symp. Interactions Fluid Particles, pp. 233-237, London, 1962.
- [V5] VDI VDI-Wärmeatlas, VDI-Verlag, Düsseldorf, 1974.
- [V6] Viannay, S. Bobleter, A. and Wintrebert, G. "Séchage a la vapeur d'eau surchauffée"; Int. Meeting Energy Savings in Drying Processes. Applications to Industry and Agriculture., pp. B3.1.-B3.7., Liège, 1983.
- [V7] Vivian, J.E. and Behrmann, W.C. "The effect of concentration level on the phase absorption coefficient"; AIChE Journal, vol. 11, no. 4, pp. 656-661, 1965.
- [W1] Walton, J.S. Olson, R.L. and Levenspiel, O. "Gas-solid film coefficients of heat transfer in fluidized coal beds"; Ind. Eng. Chem., vol. 44, no. 6, pp. 1474-1480.
- [W2] Wasan, D.T. and Wilke, C.R. "Role of concentration level of the non-diffusing species in turbulent gas phase mass transfer at ordinary mass transfer rates"; AIChE Journal, vol. 14, no. 4, pp. 577-583, 1968.
- [W3] Wenzel, L. and White, R.R. "Drying granular solids in superheated steam"; Ind. Eng. Chem, vol. 43, p. 1829, 1951.
- [Y1] Yoshida, T. and Hyodo, T. "Superheated vapor speeds drying of foods"; Food Engineering, vol. 38, no. 4, pp. 86-87, 1966.
- [Y2] Yoshida, T and Hyodo T. "Evaporation of water in air, humid air and superheated steam"; Ind. Eng. Chem., Proc. Des. Dev., vol. 9, no. 2, pp. 207-214, 1970.
- [Z1] Zabeschek, G. "Experimentelle Bestimmung und analytische Beschreibung der Trocknungsgeschwindigkeit rieselfähiger, kapillarporöser Güter in der Wirbelschicht"; Ph.D. thesis, University of Karlsruhe, 1977.